DEVELOPMENT OF A MODEL OF THE AEROBIC MEMBRANE BIOREACTOR TREATING ILLOVO WASTEWATER

By

Liam Grant Kay

In fulfillment of the academic requirements of Master of Science Degree in Chemical Engineering in the College of Agriculture, Engineering and Science, University of KwaZulu-Natal.

November 2014

Supervisor: Dr K. M. Foxon

Co-supervisor: Mr C. J. Brouckaert

Declaration

I, ……., declare that

1. The research reported in this thesis, except where otherwise indicated, is my original research.

2. This thesis has not been submitted for any degree or examination at any other university.

3. This thesis does not contain other persons' data, pictures, graphs or other information, unless specifically acknowledged as being sourced from other persons.

4. This thesis does not contain other persons' writing, unless specifically acknowledged as being sourced from other researchers. Where other written sources have been quoted, then:

a. Their words have been re-written but the general information attributed to them has been referenced

b. Where their exact words have been used, then their writing has been placed in italics and inside quotation marks, and referenced.

5. This thesis does not contain text, graphics or tables copied and pasted from the Internet, unless specifically acknowledged, and the source being detailed in the thesis and in the References sections.

Signed

……

As the candidate's Supervisor I agree/do not agree to the submission of this thesis

1) …… ……. …….

Name **Signature** **Date**

2) …… ……. …….

Name **Signature** **Date**

Acknowledgements

Dr K. Foxon	Thank you for introducing me to PRG, and for providing assistance when I needed it.
Mr C. Brouckaert	Your supervision and guidance throughout this study is much appreciated, as well as your willingness to assist at all times.
Mr C. Krüger	Thank you for making this study possible, and providing the resources at Sezela to perform the work.
Illovo Staff	Thank you to all the staff from Sezela that aided me in one way or another, Rob, Kumari and Thabo to name a few.
Wife	To my beloved Wife, thank you for your patient support throughout my studies, and for keeping me going.
Mother and Brother	To my Ma and Boet, your support got me to where I am today, and I am grateful for that.
PRG	Thanks to all the guys at PRG for the companionship, and keeping the work interesting.

Abstract

The Membrane Bioreactor (MBR) at Sezela, KwaZulu-Natal treats a process effluent emanating from a sugar industry by-products plant. Depending primarily on the effluent feed rate to the MBR as well as other less significant factors, the MBR tends to operate at a temperature that fluctuates between 40 and 50 °C. As a result of the temperature fluctuations the MBR may operate at either mesophilic or thermophilic temperatures. In an attempt to avoid the operational instability that accompanies the transition between temperature regimes, it would be conceivable to maintain mesophilic operation through either the removal of heat during feed increases or by continuously maintaining a low feed rate; alternatively to maintain thermophilic operation by providing auxiliary heat to the MBR when low feed rates are experienced, or by maintaining a high feed rate, possibly in conjunction with a buffer tank.

A solution to the problem was sought through the formulation of a coupled dynamic mass and energy balance model, with an attached speciation routine. Development of a simulation model allowed the prediction of key operating parameters, namely the temperature, pH, substrate concentration, and volatile suspended solids (VSS) concentration.

The sources of data used for modelling were laboratory experiments, historical MBR data, and literature data. Kinetic and stoichiometric coefficients of the model were determined from batch respirometric tests on the MBR furfural plant effluent feed and the activated sludge. The final model yielded a dynamic temperature (Root Mean Square Deviation (RMSD) of 1.61 and 1.34 °C) and pH (RMSD of 0.36 and 0.47) prediction over a continuous 69 day interval, where only the furfural plant effluent feed and sludge wasting rates were required as model inputs. The prediction of the substrate concentration and VSS concentration were found to be unreliable.

The results of the comparison of mesophilic to thermophilic operation, through the final calibrated model, indicated that thermophilic operation was advantageous, however a rigorous economic analysis is required to substantiate this outcome. Thermophilic operation at 50 °C can handle feed rates 2.2 times higher than mesophilic operation at 40 °C, but may be more susceptible to process upsets.

Table of Contents

List of Tables

List of Tables

List of Figures

List of Figures

Symbols		
A_l	Area of the reactor that surrounds the liquid phase	m^2
A_s	Surface area of the reactor contents in direct contact with the environment	m^2
B	Power of the aerator/compressor	W
b_i	Molality of component i	mol. kg^{-1}
C	Number of carbon atoms in the electron donor	-
C_c	cloud cover (tenths)	-
$C_{p.i}$	Heat capacity of component i	J. kg^{-1}. K^{-1}
$c(i)$	Concentration of component i	mol. m^{-3}
d	Day of the year (out of 366)	day
E	Fraction of energy transfer captured	-
F	Calibration factor	h^{-1}
$F_{x,act}$	Active fraction of biomass in MLVSS	-
f_e^0	True energy fraction	-
f_P	Fraction of inert COD generated by Lysis	kg. kg^{-1}
f_s^0	True synthesis fraction	-
ΔG_{ana}	Gibbs energy required for anabolism	J. eeq^{-1}
ΔG_c	Gibbs energy required to convert pyruvate to cells	J. eeq^{-1}
ΔG_{cata}	Gibbs energy available for catabolism	J. eeq^{-1}
$\Delta G_{f,i}$	Standard Gibbs energy of formation of Component i	J. mol^{-1}
ΔG_N	Free energy required to reduce nitrogen to ammonia	J. eeq^{-1}
ΔG_p	Gibbs energy required to convert ED to pyruvate	J. eeq^{-1}
ΔG_R	Gibbs energy released from 1 eeq of ED	J. eeq^{-1}
ΔG_{rxn}	Gibbs Energy of reaction	J. mol^{-1}
ΔG_x	Total Gibbs energy required for biomass production	J. mol^{-1}
ΔG_x^m	Gibbs energy required for new biomass	J. mol^{-1}
H_{CO_2}	Henry's law constant	Pa. kg. mol^{-1}
$\Delta H_{f,i}$	Standard enthalpy of formation of component i	J. mol^{-1}
ΔH_{rxn}	Enthalpy of reaction	J. mol^{-1}

$\Delta H_{rxn,i}$	Heat of reaction i	J. mol^{-1}
$H_{SR,0}$	Average daily absorbed solar radiation for clear sky conditions	W. m^{-2}
ΔH_{vap}	Latent heat of vapourisation	J. kg^{-1}
h_f	Exit air humidity factor	-
h_v	Convective transfer coefficient	m. s^{-1}
i	Component	-
j	Number of components	-
K_{ev,CO_2}	Rate constant for CO_2 evolution per unit liquid based on the partial pressures	mol. Pa^{-1}. m^{-3}. s^{-1}
K_{f,CO_2}	Formation constant for CO_2	Pa. mol^{3}. kg^{-3}
K_i	Surface conductance at the air-surface area inside the basin	W. m^{-2}. K^{-1}
K_o	Surface conductance at the air-surface area outside the basin	W. m^{-2}. K^{-1}
K_S	Half saturation constant	kg. m^{-3}
k_d	Specific death rate constant	h^{-1}
k_i	Thermal conductivity of material i	W. m^{-1}. K^{-1}
$k_{T_k i}$	Reaction rate coefficient at temperature i	-
k_w	Ionic product of water	mol^{2}. m^{-6}
l	Latitude of the reactor	°
M_i	Total mass of component i	kg
MM_w	Molar mass of water	kg. mol^{-1}
m	Constant	-
m_D	Rate of consumption of ED that is catabolised to generate the necessary Gibbs energy flow for maintenance	mol substrate. mol biomass^{-1}. h^{-1}
m_G	Gibbs energy required for biomass maintenance	J. mol biomass^{-1}.h^{-1}
$m_{i,j}$	Mass flow rate of component i and stream j	kg. s^{-1}
N_i	Moles of component i	mol
$n_{i,j}$	Molar flow rate of component i in Stream j	mol. s^{-1}
P	Pressure	Pa
P_{CO_2}	Partial pressure of CO_2 in the gas contacting liquid	Pa

$P_{CO_2,eq}$	Partial pressure of CO_2 in equilibrium with the actual solution composition	Pa
Q_i	Heat transfer rate of Mechanism i	W
q_i	Volumetric flow rate of component i	$m^3. s^{-1}$
q_G^m	Maximal rate of Gibbs energy made available per unit biomass	$J. mole^{-1}. h^{-1}$
q_m	Maximum specific substrate utilisation rate	h^{-1}
R	Universal gas constant	$J. mol^{-1}. K^{-1}$
r_h	Relative humidity percentage	%
r_i	Mass reaction rate of component i	$kg. m^{-3}. s^{-1}$
$\dot{r}_i$	Molar reaction rate of component i	$mol. m^{-3}. s^{-1}$
S	Concentration of the limiting substrate for growth	$kg. m^{-3}$
S_O	Dissolved oxygen concentration	$kg. m^{-3}$
S_S	Readily biodegradable substrate concentration	$kg. m^{-3}$
T	Temperature	ºC
T_a	Ambient temperature	K
T_k	Temperature	K
U_i	Overall heat transfer coefficient for conduction	$W. m^{-2}. K^{-1}$
V	Volume of the system	m^3
v_a	Vapour pressure of water at ambient temperature	Pa
v_w	Vapour pressure of water at reactor temperature	Pa
W	Wind velocity	$m. s^{-1}$
X	Concentration of the micro-organisms	$kg. m^{-3}$
X_H	Active heterotrophic biomass concentration	$kg. m^{-3}$
X_P	Inert organic matter from decay	$kg. m^{-3}$
X_S	Slowly biodegradable substrate concentration	$kg. m^{-3}$
X_{VSS}	Volatile suspended solids concentration	$kg. m^{-3}$
x_i	Thickness of material i	m
Y_{obs}	Observed biological yield	$mg\ VSS. mg\ COD^{-1}$
Y	Biological yield	mg COD biomass. mg COD $soluble^{-1}$
Y_t^m	Maximal biological yield	mol biomass. mol $subtrate^{-1}$

Greek Symbols		
α_j	Kinetic rate equation for component j	-
β	Atmospheric radiation factor	-
γ	Degree of reduction	-
γ_i	Activity coefficients of component i	-
ϵ	Water-surface emissivity	-
η	Efficiency of the aerator/compressor	%
θ	Temperature-activity coefficient	-
λ	Water-surface reflectivity	-
μ	Biomass specific growth rate	h^{-1}
μ_m	Maximum specific growth rate	h^{-1}
υ_{ij}	Stoichiometric coefficients	-
ρ_i	Density of component i	kg. m^{-3}
σ	Stefan-Boltzmann constant	W. m^{-2}. K^{-4}

Subscripts	
A	Aeration
AR	Atmospheric radiation
a	Air
C	Convection
EV	Surface evaporation
e	Evaporation from MBR
g	Ground
l	Liquid
o	Feed to MBR
P	Compressor
p	Permeate from MBR
RX	Reaction
SR	Solar radiation
sw	Sludge wasting from MBR
TW	Tank wall/floor

ATAD	Autothermal Thermophilic Aerobic Digestion
ATP	Adenosine Triphosphate
CAS	Conventional Activated Sludge
COD	Chemical Oxygen Demand
DAF	Dissolved Air Flotation
DO	Dissolved Oxygen
ED	Electron Donor
EPA	Environmental Protection Agency
GUI	Graphical user interface
HACCP	Hazard Analysis and Critical Control Points
HRT	Hydraulic Retention Time
MBR	Membrane Bioreactor
MLSS	Mixed Liquor Suspended Solids
MLVSS	Mixed Liquor Volatile Suspended Solids
ODE	Ordinary Differential Equation
OTE	Oxygen Transfer Efficiency
OTR	Oxygen Transfer Rate
OUR	Oxygen Utilisation Rate
RMSD	Root Mean Square Deviation
SABS	South Africa Bureau of Standards
SBR	Sequenced Batch Reactor
SRT	Sludge Retention Time
SSE	Sum of Squared Error
TKN	Total Kjeldahl Nitrogen
TSS	Total Suspended Solids
uCOD	Unbiodegradable COD
VSS	Volatile Suspended Solids
WAS	Waste Activated Sludge

1. INTRODUCTION

1.1. Context of the study

The Sezela Mill Complex, operated by the Illovo group, consists of a sugar mill with an attached downstream products facility. The downstream site consists of a furfural production plant and a range of smaller plants that produce other organic chemicals. The furfural plant generates an acidic effluent, as a by-product of the process, that is pumped to a surf outfall and exits through a pipeline close to the shore (Gent, 2012). It is unlikely that Sezela will be permitted to discharge the untreated furfural plant effluent into the sea indefinitely, due to ever stricter environmental regulations. This places some pressure on finding an effective method for the treatment of the effluent. The discharge of effluent also has a negative effect on Sezela's water balance. Possible treatment of the effluent therefore provides an attractive opportunity for water recovery. A practical solution for the effluent would also increase the viability of a second furfural plant. These factors prompted the construction of a pilot aerobic Membrane Bioreactor (MBR) as a possible means of treating the effluent.

The MBR is a large open tank in which air is bubbled through diffusers situated along the bottom of the tank. There is a bank of flat sheet membranes submerged within the tank through which the permeate passes. Selection of the MBR technology was due to the presence of an unknown trace toxin in the process effluent which inhibits conventional aerobic and anaerobic treatments (Judd, 2011). The high mixed liquor suspended solids (MLSS) offered by the MBR overcomes this limitation.

The furfural plant effluent that is fed to the MBR has a high chemical oxygen demand (COD). The COD primarily consists of readily assimilable matter in the form of acetic acid, with minor amounts of formic acid and intermittent furfural concentrations (Judd, 2011). It was anticipated that the MBR would operate mesophilically in the region of 30 °C. However, with the consumption of COD being exothermic and a high feed temperature, it was found that the MBR could operate thermophilically, maintaining a temperature between 40 and 50 °C.

1.2. Problem statement

Due to the nature of the upstream processes and a sugarcane supply that is dependent on weather conditions, furfural plant effluent feed fluctuations to the MBR occur on a regular basis. During feed fluctuations the temperature of the MBR is observed to shift which often results in a transition between mesophilic and thermophilic temperature regimes. The transition period is marked by a dramatically reduced biomass activity which leads to operational instability. In order to avoid the operational instability it would be conceivable to either remove heat from the MBR during feed increases, or permanently maintain a low feed rate to maintain mesophilic operation

(40 °C); alternatively to provide heat during feed reductions, or maintain a high feed rate (through a buffer tank) and maintain thermophilic operation (50 °C).

1.3. Purpose of the study

The general aim of this study lies in a comparison of the two modes of operation, mesophilic and thermophilic. This will be achieved through the compilation of relevant literature, and the subsequent formulation of a mathematical model able to describe the fundamental processes occurring within the MBR, and predict the dynamic operation of the MBR. From the model an increased understanding of the underlying processes can be obtained, and through a critical evaluation of the different temperature regimes a detailed assessment between the modes of operation can be performed, from which a recommendation of which operational strategy to follow can be outlined.

1.4. Structure and presentation of the dissertation

The introduction provided a brief outline to the thesis, and the problem statement upon which this work was based. These topics will be further elaborated in the subsequent chapters.

Chapter 2 provides the relevant literature concerning the study: that is a background to the MBR; the fundamentals of aerobic biological wastewater treatment, with emphasis on the estimation of kinetic and stoichiometric parameters and the effect that varying temperatures have; and an introduction to basic mathematical modelling theory.

Chapter 3 provides context to the problem statement, giving a brief introduction to the Illovo group, and providing a background to wastewater treatment at the Sezela Mill Complex. A detailed description of the MBR specifications is provided, and the typical operating parameters and strategies outlined.

The primary objectives of the project are underlined in **chapter 4**, the hypotheses formed, and a breakdown of the approach that is taken listed.

In **chapter 5** the experimental methodology is discussed, and the procedure followed is detailed. The determination of the parameters for populating the mass and energy balance model are also elaborated on.

The combined model is outlined in **chapter 6**. The mass balance over the MBR is formed and the components in the mass balance are selected. A pH prediction capability to the model is also illustrated and linked to the mass balance. An associated energy balance is subsequently defined, and linked to the mass balance primarily through the heat of reaction.

Chapter 7 presents the experimental results that were obtained through respirometric techniques, and the subsequent determination of the kinetic and stoichiometric parameters. The experimental work is carried out at 40 and 50 °C.

The combined model is calibrated in **chapter 8** against historical MBR plant data, and where allowable parameters are altered within an acceptable range. A steady state calibration is performed first, after which a final unsteady state calibration is performed. A sensitivity analysis is additionally undertaken to examine the significance of energy balance parameters on the MBR temperature.

The outcome of the work performed is discussed in **chapter 9**. The scientific outcomes of the work are analysed and the hypotheses outlined in chapter 4 discussed. The full capability of the model is also tested in order to provide an in depth comparison of the mesophilic and thermophilic regime, with a summary of the advantages and disadvantages provided. Finally a recommendation is provided on the future operation of the MBR.

Chapter 10 is the concluding chapter of this study and summarises the pertinent results obtained. Recommendations are also provided to improve the operational performance and future designs of the Illovo MBR.

2. LITERATURE REVIEW

This chapter gives an introduction to biological treatment, a background to MBRs and thermophilic aerobic treatment, effect of temperature on biological performance, the mechanisms of aerobic operation which is required for modelling, as well as the bioenergetics of microbial growth which is required for modelling and comparison of experimental parameters. Lastly a background was given to bioprocess modelling, which was further elaborated upon in later chapters. This information is pertinent to the development of a model of the aerobic membrane bioreactor treating Illovo wastewater, which operates at temperatures between 40 and 50 °C.

2.1. Introduction to biological wastewater treatment

Biological wastewater treatment is the use of micro-organisms for the processing and cleansing of water. Biological treatment is an important and integral part of any wastewater plant that treats wastewater from either municipalities or industry having soluble organic impurities (Amy *et al.*, 2011).

Biological wastewater treatment may be classified into two distinct categories, i.e. treatment where conditions are either aerobic (presence of air) or anaerobic (absence of air). These two terms are directly related to the type of bacteria or micro-organisms that are involved in the degradation of organic impurities in a given wastewater and the operating conditions of the process (Eddy *et al.*, 2003).

Wastewater treatment can be further subdivided, from aerobic and anaerobic, into categories according to the specific temperature employed. The temperature of the process determines the kind of micro-organism present in the wastewater process. The range in which micro-organisms can be classified based on their temperature range for growth is illustrated in Fig. 2.1.

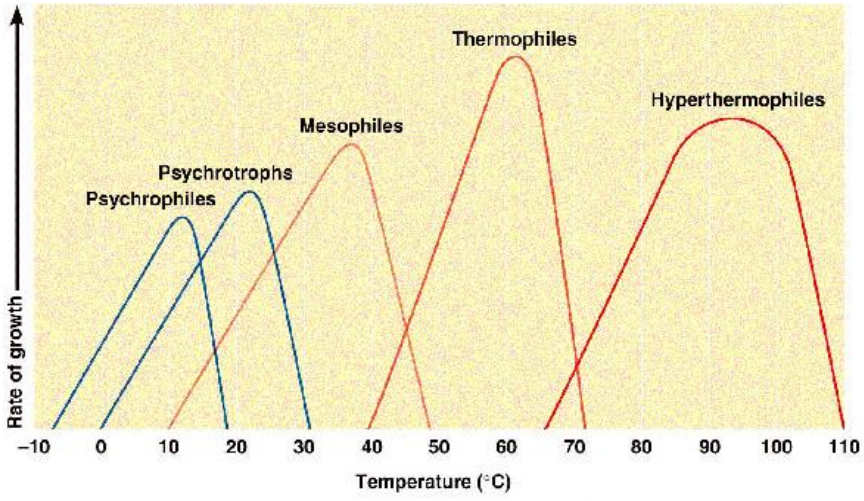

Figure 2.1. Representative ranges and optima for five types of micro-organisms, classification based on their temperature range for growth (Prescott et al., 2002).

All living organisms are limited to certain temperature ranges. Growth and metabolism of micro-organisms are constrained to certain temperature intervals within which an optimal temperature is found (Jamniczky-Kaszas, 2010). As a general rule of thumb the rate of reaction of the micro-organisms doubles with every increase of 10 °C. The optimal temperature for each interval is close to the maximum growth rate, above which denaturation of the enzymes catalysing the biochemical reactions becomes dominant.

Of interest to this investigative work are mesophilic and thermophilic organisms:

- Mesophiles: They have an optimum growth range between 20 and 45 °C. Most micro-organisms fall into this category. Their minimum temperature occurs between 15 and 20 °C, while their maximum occurs at about 45 °C or lower (Prescott *et al.*, 2002).
- Thermophiles: Their optimum is generally between 55 and 65 °C, however their minimum growth rate occurs at around 45 °C. These organisms flourish in many habitats including composts, self-heating hay stacks, hot water lines, and hot springs. Thermophiles differ from mesophiles in having a much more heat-stable enzyme and protein synthesis system able to function at high temperatures (Prescott *et al.*, 2002). The active microflora in aerobic thermophilic sewage sludge are highly homogenous and consists nearly exclusively of thermophilic neutrophilic *Bacilli* (Ponti *et al.*, 1995).

2.2. MBR background

2.2.1. Introduction

The implementation of membranes within the treatment steps of a wastewater plant was initially limited to tertiary treatment as well as polishing. The high capital costs, as well as a lack of knowledge on the applications of membrane technology in waste treatment limited the growth of this technology. However, with the appearance of less expensive and more efficient membrane modules and the implementation of ever-stricter water discharge standards, membrane systems regained popularity (Cicek, 2003).

Membrane modules have moved on from being used solely for tertiary wastewater treatment and polishing to being integrated into secondary wastewater treatment. These systems are commonly referred to as membrane bioreactors (MBRs) (Cicek, 2003).

The MBR process is similar to the conventional activated sludge (CAS) process, in that both have mixed liquor solids in suspension in a tank (Fig. 2.2). The difference between the two processes lies in the method of separation of bio-solids. In the MBR process, the bio-solids are separated by means of a polymeric membrane based on microfiltration or ultrafiltration, as against a gravity settling process in a secondary clarifier in CAS processes (Bérube, 2010). Primary clarifiers are commonly used prior to CAS processes to remove materials that can easily settle by gravity,

reducing contaminant load on these systems. However, as MBRs can sustain higher loading rates than CAS processes, primary clarifiers are normally not required. On the other hand, fine mesh screening is usually used prior to MBRs to remove large debris and fine materials, which can negatively affect the performance of the membrane component of these systems (Cicek, 2003).

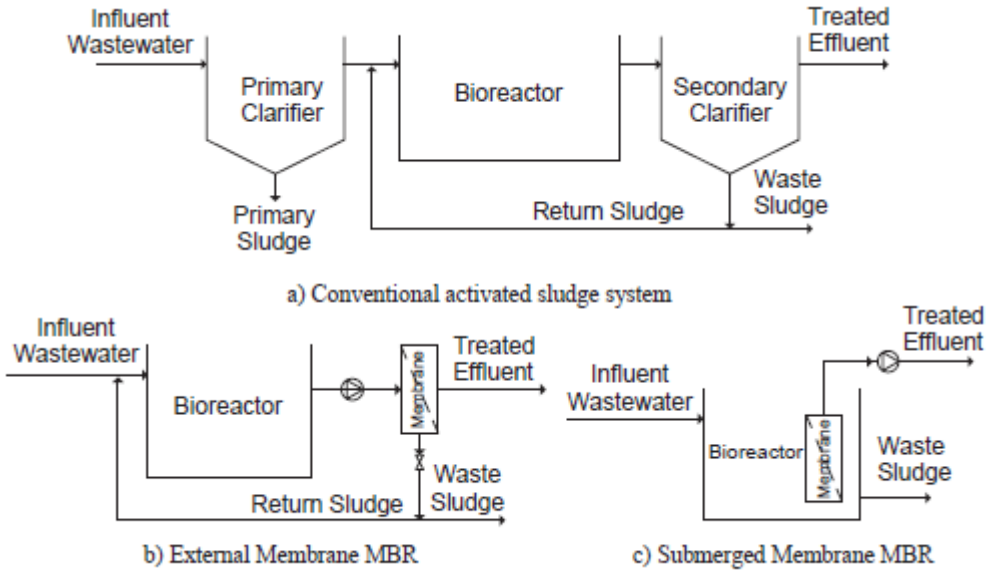

Figure 2.2. CAS and MBR process schematics (Bérube, 2010).

2.2.2. System configuration

MBRs are composed of two primary parts, the biological unit responsible for biodegradation of the wastewater, and the membrane unit for the physical separation of the treated water from the mixed liquor. Early designs of MBRs simply replaced the secondary clarifier of CAS processes with an external membrane, although most MBRs are now designed with the membrane submerged within the bioreactor component of the system (Bérube, 2010). The submerged MBR involves outer skin membranes that are located inside of the MBR. The driving force across the membrane is achieved by pressurizing the MBR or creating negative pressure on the permeate side (Cicek, 2003). The membranes require frequent cleaning which is achieved through permeate back-pulsing and occasional chemical backwashing. A diffuser is usually placed directly beneath the membrane module to facilitate scouring of the exposed membrane surface by the air bubbles and associated turbulence. Aeration and mixing may also be achieved by the same unit (Cicek, 2003).

2.2.3. Advantages and disadvantages

Although MBRs and CAS processes are relatively similar, their process configurations in wastewater reuse applications differ substantially. The advantages offered by MBRs over conventional bio-treatment processes are widely recognized, the most commonly accepted are:

- Production of high quality, clarified and largely disinfected permeate product in a single stage (Amy *et al.*, 2011). This is primarily due to the membrane component of the system, which can effectively retain particulate material, and associated organic material, within the bioreactor wherein it can degrade (Bérube, 2010).
- Since suspended solids are not lost in the clarification step, absolute and independent control of solids retention time (SRT) and hydraulic retention time (HRT) is obtained, parameters which are usually coupled in a CAS plant (Amy *et al.*, 2011).
- Operation at higher MLSS concentrations, which both reduces the required reactor size and cost (Amy *et al.*, 2011). An additional benefit of high MLSS concentrations are that higher strength wastewaters can be treated, and lower biomass yields are realized due to longer SRTs (Cicek, 2003).
- Operation at longer SRTs providing an opportunity to select for sensitive, slow-growing bacterial populations with possible enhanced treatment (Cicek, 2003).
- CAS processes are not as effective at removing the contaminants of concern present in wastewaters, and therefore the effluent from these systems may require further treatment before reuse applications (Bérube, 2010).
- MBRs allow more compact systems as compared to CAS processes, reducing the plant footprint (Cicek, 2003). MBRs effectively displaces three individual steps in a CAS treatment plant (primary settling, activated sludge system and disinfection), requiring that only the initial screening stage be upgraded to limit the damage to the membrane component (Amy *et al.*, 2011).
- High molecular weight compounds which are not readily biodegradable in conventional systems, are retained within the MBR, increasing their residence time and the possibility of oxidation (Cicek, 2003).
- MBRs are better able to handle fluctuations in nutrient concentrations due to extensive biological acclimation and retention of dying biomass (Cicek, 2003).

On the other hand MBRs are not without their disadvantages, these disadvantages are primarily related to cost:

- Greater aeration requirements for both biological and membrane fouling/clogging control (Cicek, 2003).
- MBRs have high capital costs due to expensive membrane units, and high operating costs due to the need for a pressure gradient and substantial aeration requirements (Cicek, 2003).
- Membrane fouling problems can lead to frequent cleaning of the membranes, which halts operation (Cicek, 2003).

- When operated at high SRTs, inorganic compounds may accumulate within the MBR and reach concentrations that are harmful to the microbial population or membranes (Cicek, 2003).
- The propensity for foaming is greater at the higher MLSS concentrations achieved in MBRs (Amy *et al.*, 2011).
- Since the MBR retains all suspended solids and most soluble organic matter, waste activated sludge (WAS) may exhibit poor filterability and settleability, leading to a less readily dewaterable sludge product (Cicek, 2003).

2.2.4. Operating parameters

2.2.4.1. MLSS concentration

Easily biodegradable substrates have a high maximum rate of substrate consumption. The substrate consumption rate is the product of the specific consumption rate (amount of substrate consumed per unit time per unit of biomass) and the concentration of the active biomass population (Eddy *et al.*, 2003). Therefore by maintaining a high biomass concentration in the bioreactor the less biodegradable substrates can be consumed rapidly.

Since membranes can retain virtually all of the biomass, relatively high substrate utilization rates are maintained, and therefore, relatively small bioreactor volumes may be used. Typical biomass concentrations, measured as MLSS, in MBRs range from 8 to 12 $g.L^{-1}$. By comparison the typical MLSS concentrations that can be maintained in CAS systems typically range from 2.5 to 4 $g.L^{-1}$ (Bérube, 2010). As a result, the HRT in MBRs, which is the ratio of the volume of the bioreactor to the hydraulic flow rate through the system, can be as low as 4 h. At MLSS concentrations greater than approximately 12 $g.L^{-1}$, oxygen transfer in the bioreactor may be limiting which can inhibit the growth of aerobic biomass. High MLSS concentrations can also negatively affect the permeate flux through the membrane component of MBRs (Bérube, 2010).

2.2.4.2. Aeration

Effective aeration is a crucial component to the successful operation of a submerged MBR. Due to the higher biomass concentrations employed in MBRs the oxygen transfer is somewhat less efficient than that of CAS systems. Most MBRs are run with intermittent aeration to reduce energy consumption as much as possible, although it is critical to provide sufficient air to the membrane module to suppress clogging of the membrane channels and fouling of the membrane surface. It has been generally acknowledged that permeability increases with membrane aeration up to some critical value, beyond which there is no further increase (Amy *et al.*, 2011).

The primary purpose of aeration concerns the demand of the mixed liquor for air required for agitation of the solids and dissolved oxygen (DO) for maintaining a viable aerobic micro-organism population for biological treatment. The oxygen requirements for the biological system

relates to the feed flow rate, substrate degradation, sludge production and concentration of Total Kjeldahl Nitrogen (TKN) that is oxidized to form nitrate (Amy *et al.*, 2011).

The oxygen is most commonly transferred to the micro-organisms by bubbling air, or in some cases pure oxygen, into the system by diffusers. Only a portion of the air or oxygen that enters the system is transferred to the mixed liquor. This is quantified by the oxygen transfer efficiency (OTE), defined as the amount of oxygen transferred to the mixed liquor per amount of oxygen injected into the vessel. The transfer efficiency is dependent on the type of diffuser used in addition to the specific system design (Amy *et al.*, 2011).

2.2.4.3. Membranes

Pressure driven membranes are typically classified based on the amount of material that they can retain. Microfiltration and ultrafiltration membranes, also commonly referred to as low-pressure membranes, are generally used for MBR applications. The membranes essentially function as sieves, retaining particulate material that is larger than the pore size of the material. Membrane pore sizes ranging from 0.04 to 0.4 μm are usually used for MBRs (Bérube, 2010).

A number of membrane geometries exist, although in general three predominate in existing commercial MBR technologies. These are flat sheet, hollow fibre and multitube type membranes.

2.2.4.4. Permeate quality

MBRs provide excellent treated water quality, achieving four to sixfold removal of pathogenic bacteria, almost complete removal of suspended solids, and often reducing ammonia or TKN levels to less than 1 $mg.L^{-1}$. Therefore only problematic particles significantly smaller than the effective membrane pore size and non-biodegradable dissolved materials present a challenge to the process (Judd, 2011).

2.3. Thermophilic aerobic wastewater treatment

Thermophilic aerobic wastewater treatment is a process of treating wastewater under aerobic conditions at temperatures that exceed 45 °C, sometimes reaching temperatures in excess of 70 °C (Staton *et al.*, 2001). The physical, chemical and biological characteristics of this process are so different from mesophilic processes that the knowledge base from conventional operation is unusable (LaPara and Alleman, 1999). A limiting factor preventing the widespread implementation of thermophilic biotechnology is due to the cost associated with raising the reactor temperature. There are two ways in which this can be overcome: 1) when wastewaters are produced hot; and 2) when wastewaters are highly concentrated such that the heat released during substrate biodegradation is sufficient for autothermal operation. Wastewater that is readily biodegradable has an improved potential for autothermal heat generation, due to increased degradation rates that occur from rapid microbial activity (LaPara and Alleman, 1999).

With an adequate supply of oxygen, micro-organisms, nutrients, and biodegradable organic material, autothermal aerobic digestion can degrade complex organic substances into end products that include carbon dioxide (CO_2) and water. Some of the energy released by microbial degradation is used in the formation new cellular material, however much of the energy is released as heat. Typical biological heat production values reported or assumed range from 14 190 to 14 650 kJ.(kg O_2)$^{-1}$ (USEPA, 1990). The carbonaceous oxygen requirements vary but are often considered to be 1.42 (kg O_2).(kg volatile suspended solids (VSS))$^{-1}$ oxidized (Amy *et al.*, 2011).

It has been illustrated by Sürücü *et al.* (1976) that a waste stream with a minimum COD of 7 500 mg.L^{-1} is sufficient for thermophilic operation to be self-sustaining with the heat produced by biological reaction. LaPara and Alleman (1999) showed through their energy balance model that the minimum amount of COD removal for autothermal thermophilic operation appears to be above 10 000 mg.L^{-1} with OTE fractions between 0.05 to 0.25, and an ambient temperature of 25 °C.

2.3.1. Development of autothermal thermophilic aerobic digestion processes

Autothermal thermophilic aerobic digestion (ATAD) was first developed in the late 1960's for the stabilisation of waste biological sludge. Khambu and Andrews (1968) performed the first research effort into ATAD technology, demonstrating through a computer simulation, that autothermal operation was possible with high efficiency aerators and influent Total Suspended Solids (TSS) levels ranging between 4 and 6 % solids.

ATAD was further studied during the next decade, particularly in Europe. Autothermal operation was empirically demonstrated by Matsch and Drnevich (1977) using high purity oxygen aeration, and by Jewell and Kabrick (1980) via self-aspirating aeration units using air. The first full-scale ATAD plant was commissioned in Germany in 1977, the technology was widely implemented in the 1980's in Germany. The United Stated Environmental Protection Agency (EPA) recognised ATAD as a technology capable of significantly reducing pathogens and produced a biosolid that was not restricted in terms of agricultural land usage. Today, this technology is widespread in Europe, especially Germany and Switzerland, and also Northern America. It is normally used in smaller treatment facilities providing a service to small and medium settlements (Jamniczky-Kaszas, 2010).

2.3.2. Benefits of ATAD

The advantages of thermophilic operation as compared to conventional mesophilic operation are:

- Increased substrate biodegradation rates. The maximum specific substrate utilisation rates (q_m) cited in literature are typically 3 to 10 times higher than those of analogous

mesophilic operation. The high biodegradation rates may improve process stability by allowing for a rapid recovery from a process upset (LaPara and Alleman, 1999).

- Low sludge yields, which stem from a high specific death rate constant (k_d). k_d is generally 10 times higher than those for analogous mesophilic operation (LaPara and Alleman, 1999).
- The biosolids that are produced in an ATAD reactor have less organic content and produce less odours, and are suitable for wasted sludge drying, and use in landfilling and composting (Jamniczky-Kaszas, 2010).
- Due to the high reaction rates and low retention times smaller reactors are required compared to other conventional processes, this in turn leads to lower capital costs (LaPara and Alleman, 1999).
- Thermophilic aerobic operation has the added benefit of a higher level of sludge hygienisation, the elevated temperature reaches a higher level of pathogen reduction, producing biologically stable and pathogen-free biosolids as an end product (Jamniczky-Kaszas, 2010).
- Thermophilic operation is particularly suited for wastewaters with toxicity concerns stemming from high salinity levels or the presence of hazardous compounds (LaPara and Alleman, 1999).

2.3.3. Disadvantages of ATAD operation

Disadvantages that are associated with thermophilic operation are:

- The increased cost for operating the aeration and mixing devices from a capital and operational cost perspective (Jamniczky-Kaszas, 2010).
- Thermophilic aerobic operation results in poor bacterial flocculation characteristics, this results from dispersed growing micro-organisms. As a consequence, biomass separation becomes exceptionally difficult and often limits the overall treatment efficiency (LaPara and Alleman, 1999).
- The air requirements for thermophilic aerobic operation are expected to be around 14 % higher than those of mesophilic operation (Sürücü *et al.*, 1976). This is a direct result of the lower sludge yields, in which more substrate is converted to CO_2 and water instead of cellular components (LaPara and Alleman, 1999).
- The higher reactor temperatures reduce the surface tension of the water which may lead to increased foaming. Foaming in thermophilic aerobic reactors is also associated with high cell concentrations (Rozich and Colvin, 1997); (LaPara and Alleman, 1999).

- There is a lack of consistent data available on thermophilic operation. The optimal values of such fundamental parameters as temperature, pH and DO concentration have yet to be found.

2.3.4. Operational issues

2.3.4.1. pH

It is expected that the pH plays a less significant role in thermophilic processes as nitrification is suppressed during digestion, and as a result the pH depression commonly experienced in nitrifying environments does not occur. The pH may be used as an indicator of autothermal conditions or as an early warning to unstable operation. Should the oxygen become limited due to organic overloading the pH may decrease, which is an indication of volatile fatty acids production during the fermentation of organics (Jamniczky-Kaszas, 2010). The pH levels typically observed within thermophilic systems tend to be slightly above neutral (Staton *et al.*, 2001).

2.3.4.2. Foam

Thermophilic systems inevitably produce foam as a consequence of increased biological activity which promotes a high rate of endogenous respiration. This results in the breakdown protein and the release of extracellular enzymes which tend to cause foam (Wynn *et al.*, 1997). In order to have an effective system the growth of the foam layer should be controlled rather than eliminated. Excessive foaming may be aesthetically unpleasing and lead to a loss of solids from the reactor. A controlled foam layer can be beneficial as it helps to insulate the tank, contributing to thermophilic operation (Jamniczky-Kaszas, 2010).

2.3.4.3. Microbial character

When temperatures are consistently elevated within an ATAD system, the viable microbial population is primarily composed of thermophiles, whose physiological nature and lifestyle have, as yet, not been fully established. In all likelihood, this bacterial consortium is similar to that which would be found within composting biomass (Staton *et al.*, 2001).

2.3.4.4. Operating DO and OUR

The properties that affect the oxygen transfer rate (OTR) are highly dependent on temperature. Changes in temperature alters the overall OTR within the reactor, which will therefore differ for mesophilic and thermophilic operation. In addition to this the elevated solids levels tend to complicate both oxygen transfer and mixing within the reactor. Typically thermophilic biomass are expected have a higher oxygen uptake rate (OUR) than other aerobic systems, although they are seemingly tolerant of low DO concentrations (Staton *et al.*, 2001).

2.4. Effect of temperature on biological wastewater treatment

Many of the physical parameters involved with wastewater treatment vary with temperature. The effect of temperature on some of the physical parameters is shown in Table 2.1.

Table 2.1. Physical-chemical parameters of water affected by high temperatures.

Property	Temperature °C				Effect	Reference
	25	30	47	60		
DO ($mg.L^{-1}$)	8.3	7.5	5.4	3.8	-Reduced OTR	Eddy *et al.* (2003), Tripathi and Allen (1999)
Viscosity 10^{-3} (Pa.s)	0.8998	0.7223	0.5663	0.4665	-Improved gas transfer efficiency -Improved mixing efficiency	Weast (1981)
Surface Tension 10^{-3} ($N.m^{-1}$)	71.9	70.4	68.2	66.2	-Improved gas transfer efficiency -Potentially increased foaming	
Diffusivity	Increase with temperature				-Improved gas transfer efficiency -Improved mixing efficiency	LaPara and Alleman (1999)
Solid-Liquid Solubility	Increase with temperature				-Higher possible concentrations of most organics and inorganics -Exceptions include the solubility of carbonate salts	
Gas-Liquid Solubility	Decrease with temperature				-Reduced gas transfer efficiency -Improved off-gas stripping efficiency	

2.4.1. Oxygen transfer efficiencies

DO saturation concentrations vary under differing temperatures, from 8.3 to 3.8 $mg.L^{-1}$ at 25 and 60 °C, respectively. The lowered DO saturation concentration has a negative effect on the OTR. However, several researchers have concluded that the overall effect of temperature on oxygen transfer within the system is negligible (Boogerd *et al.*, 1989); (Wynn *et al.*, 1997). The associated changes in the physical-chemical parameters of water, such as viscosity, surface tension and diffusivity enhance the overall oxygen transfer rate, so as to offset the decrease caused by the reduction in the oxygen saturation concentration.

Vogelaar *et al.* (2000) investigated the effect of temperature on the OTR in three different liquids: tapwater, anaerobically pretreated paper process water, in addition to thermophilic sludge that was grown on a mineral medium and volatile fatty acids as carbon source. The OTR was measured between temperatures of 20 to 55 °C for tap and process water. The OTR in the case of thermophilic sludge was measured at 55 °C. The OTR was observed to remain constant over the specified temperature range in the case of tapwater and showed a slight increase in the case of the process water. At a temperature of 55 °C the OTR in the thermophilic sludge was comparable

to both other liquids. It was concluded that the OTR for process water and thermophilic sludge were slightly lower compared to tapwater, this is caused by lower oxygen saturation concentrations in these mediums. The mass transfer coefficient values of these liquids did not differ significantly from those found for tapwater.

2.4.2. Kinetics

The kinetics of microbial growth govern the oxidation of substrate and the production and death of biomass, which contributes to the total suspended solids (TSS) concentration within the reactor. As wastewaters contain numerous substrates, the concentration of organic compounds is generally defined by the biodegradable or unbiodegradable COD, both of which are comprised of soluble, colloidal and particulate components. The biomass solids within the reactor is usually measured as TSS or VSS, and comprise of biomass, unbiodegradable VSS and inert organic TSS (Eddy *et al.*, 2003).

The most common and well known description for the oxidation of substrate and the production of biomass is the Monod equation:

$$r_g = \mu X = \mu_m \frac{SX}{K_s + S} \qquad (2\text{-}1)$$

Where:

r_g is the rate of growth of the micro-organisms (kg.m^{-3}.h^{-1}).

μ is the specific growth rate of the micro-organisms (h^{-1}).

μ_m is the maximum specific growth rate of the micro-organisms (h^{-1}).

S is the concentration of the limiting substrate for growth (kg.m^{-3}).

K_s is the half saturation constant (the value of S when μ/μ_m = 0.5) (kg.m^{-3}).

X is the concentration of the micro-organisms (kg.m^{-3}).

An alternate form of the Monod equation in terms of substrate utilisation is:

$$r_s = qX = q_m \frac{SX}{K_s + S} \qquad (2\text{-}2)$$

Where:

r_s is the rate of consumption of substrate (kg.m^{-3}.h^{-1}).

q is the specific substrate consumption rate (h^{-1}).

q_m is the maximum specific substrate consumption rate (h^{-1}).

The two equations are linked by the biological yield as follows:

$$\mu_m = Y q_m \qquad (2\text{-}3)$$

Where:

Y is the biological yield (kg COD biomass. kg COD soluble^{-1}).

The decay of the biomass may be modelled by first order kinetics as follows:

$$r_d = k_d X \qquad (2\text{-}4)$$

Where:

r_d is the rate of decay of the micro-organisms ($kg.m^{-3}.h^{-1}$).

As demonstrated in Table 2.2, q_m in thermophilic applications cited in literature are typically 3 to 10 times greater than those of analogous mesophilic systems. k_d is generally 10 times greater for thermophilic operation. μ_m was found to vary, although in general they increase by a factor of 2 for thermophilic operation as opposed to mesophilic operation.

Table 2.2. Comparison of stoichiometric and kinetic parameters at mesophilic and thermophilic temperatures.

Waste	***T*** **(°C)**	μ_m **(day^{-1})**	q_m **(day^{-1})**	***Y***	k_d **(day^{-1})**	**Reference**
Municipal	20	3	5	0.6*	0.06	Tchobanoglous and Burton (1991)
Industrial	25	0.6	1.95	0.31**	0.03	Kim *et al.* (1997)
Acetate	30	11.52	-	0.5**	0.096	Vogelaar *et al.* (2003)
Industrial	30	3.19	-	0.46**	0.037	Abeynayaka (2009)
Industrial	33	0.6	2	0.30*	0.08	Campbell and Rocheleau (1976)
Industrial	45	5.8	16.5	0.35*	0.52	Couillard and Zhu (1993)
Industrial	47	4.94	-	0.47**	0.304	Abeynayaka (2009)
Industrial	52	6	19.8	0.30*	0.32	Couillard *et al.* (1989)
Industrial	53	3.4	5.6	0.6***	0.52	Jackson (1983)
Acetate	55	17.04	-	0.5**	0.408	Vogelaar *et al.* (2003)
Glucose	58	5.2	15.4	0.34*	0.48	Sürücü *et al.* (1976)
Industrial	58	10.1	31.1	0.32*	0.78	Couillard *et al.* (1989)
Industrial	60	7.3	-	0.48**	0.325	Abeynayaka (2009)

*(mg TSS/mg COD), **(mg VSS/mg COD), ***(mg TSS/mg BOD_5)

2.4.3. Effect of temperature and reactor type on observed yield

The observed biological yield (Y_{obs}) is based on measurements of biomass production and substrate consumption from the process, as compared to the biological yield (Y) which is the amount of biomass produced immediately upon consumption of substrate. Y_{obs} will always be less than Y due to cell loss, concurrent with cell growth (Eddy *et al.*, 2003).

Abeynayaka (2009) performed aerobic tests on sugar molasses at 30, 47 and 60 °C for sequencing batch reactors (SBRs) and MBRs. The results of the different reactor configurations are shown in Table 2.3. A significant reduction in Y_{obs} at all three MBR temperatures was observed in comparison to the same loading rate for the SBR. The Y_{obs} value was found to substantially decrease with an increase in temperature for both reactor configurations.

Table 2.3. Observed yield comparison for SBR and MBR at 24.75 kg COD.m^{-3}.day^{-1} (Abeynayaka, 2009).

T	***Y*$_{obs}$**	
(°C)	**((mg VSS).(mg COD)$^{-1}$)**	
	MBR	SBR
30	0.36	0.46
47	0.10	0.49
60	0.08	0.38

2.5. Mechanisms and bioenergetics of aerobic operation

2.5.1. Mechanisms of aerobic operation

Metabolism is the sum of all chemical processes that take place in living cells. Although there are many chemical processes that are involved in the metabolism of living cells, three major processes can be identified that are applicable to the biological treatment of wastewater. These are ingestion, respiration, as well as growth and division. These processes are highly interrelated in that no one process can go quicker than the other. The significance of this is that if measuring the respiration rate, the rate of growth and the rate of carbon ingestion is subsequently indirectly measured (Davies, 2005). The respiration rate could be measured by the OUR, by the rate of CO_2 production or alternatively by the rate of heat liberation. CO_2 is difficult to measure in aqueous media. Heat production could be measured in a calorimeter, however the simplest and most commonly used method of measuring the respiration rate is by measuring the OUR with an activated sludge respirometric device (Davies, 2005).

Microbial metabolism requires energy for cell synthesis and may be divided into two categories: catabolism and anabolism. Catabolic reactions are the energy supply of the cell, while anabolic

reactions use this energy for the synthesis and maintenance of cellular components from carbon sources and other nutrients (Amy *et al.*, 2011). Cell growth is the driver as well as the rate-limiting step. Every living cell has a genetically programmed maximum rate of growth that can be attained under ideal conditions (Davies, 2005).

When the external substrate has become exhausted, the cells begin to metabolise cellular proteins and other structural molecules. Eventually the cell splits open and dies, releasing the residual internal contents, which becomes available as a potential food source (Davies, 2005). The respiration rate during this process is termed the endogenous respiration rate; which can be defined as the oxygen consumption rate of the micro-organisms in the absence of substrate from any external sources. Maintenance is an alternate concept from literature that is used to describe microbial behaviour, whereby the external substrate is oxidised to maintain the biomass in its current state. Substrate is only oxidised for energy generation, there is no generation of new biomass. Both of these concepts are capable of representing the specific process behaviour (Vanrolleghem, 2002). This process of endogenous respiration can be represented in stoichiometric form as:

$$C_5H_7O_2N + 5O_2 + 3H_2O \rightarrow 5HCO_3^- + NH_4^+ + 4H^+ \qquad (2\text{-}5)$$

Where the biomass is represented by $C_5H_7O_2N$.

The difference between endogenous respiration and the biodegradation of external substrate (exogenous respiration) is illustrated graphically in Fig. 2.3. The sum of endogenous respiration and exogenous respiration forms the total respiration rate.

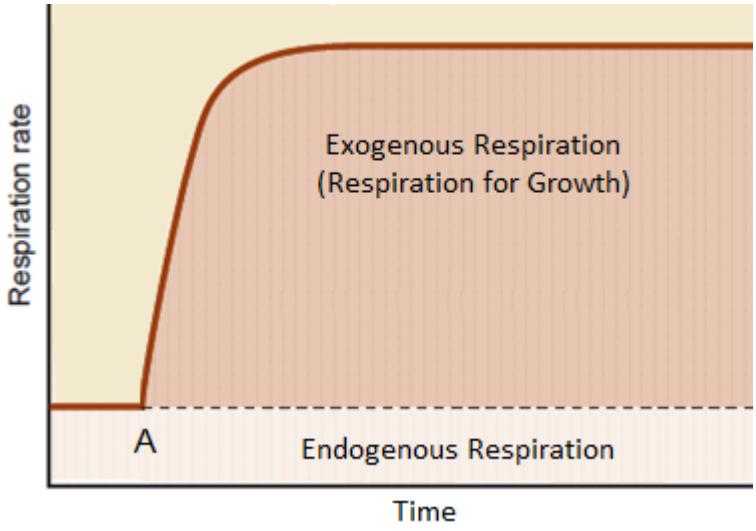

Figure 2.3. Exogenous and endogenous respiration form the total respiration rate, A represents the point of substrate addition (Davies, 2005).

In biochemistry terms respiration is defined as the adenosine triphosphate (ATP) generating metabolic process in which either organic or inorganic compounds serve as the electron donor

and inorganic compounds such as O_2, NO_2^-, NO_3^-, etc. serve as the final electron acceptor (Vanrolleghem, 2002). If oxygen is the final electron acceptor, the process is termed aerobic respiration.

Respirometry is the experimental measurement and interpretation of the oxygen consumption rate of the micro-organisms (Vanrolleghem, 2002). Respirometry can be seen from two aspects, the analysis of the activated sludge without the addition of a wastewater effluent sample, and the analysis of a specific wastewater effluent sample injected into the activated sludge.

Oxygen is directly associated with aerobic biomass growth and death, as well as substrate consumption. The OUR is therefore a measure of biological activity within a system. ATP is generated as the electrons that are removed from the substrate are transferred along the electron transport chain from one metabolic carrier to the next and, finally, to oxygen. In this way the biomass can convert the energy of intramolecular bonds in the substrate to the high-energy phosphate bonds of ATP (Vanrolleghem, 2002). The energy is then used to synthesize various molecular components required for cell growth and reproduction.

If the concentration of substrate is high the micro-organisms will grow at their maximum rate and the rate of oxygen consumption will approximate its maximum value, termed the maximum respiration rate. Like the endogenous respiration rate, the maximum respiration rate is practically independent of the substrate concentration when the substrate concentration is high enough, and is indicative of the active biomass concentration (Vanrolleghem, 2002).

2.5.2. Bioenergetics of microbial growth

Bioenergetics provides a theoretical tool to quantify the amount of energy that is available for various biological reactions which can then be used to determine Y of the reaction (Amy *et al.*, 2011). The stoichiometry of microbial growth is illustrated in Fig. 2.4. There are seven compounds that are required to provide the building elements to create biomass; these are a carbon source, biomass, electron donor, nitrogen source, H_2O, HCO_3^-, and H^+ (Heijnen and Kleerebezem, 2010). To convert the five compounds into biomass, a large amount of biochemical energy mediated by ATP is required. The amount of energy needed to make biomass depends on the type of carbon source used. The required energy, in the form of Gibbs energy, is delivered by the catabolic reaction between an electron donor and an electron acceptor.

The macro-chemical reaction containing all the stoichiometric information relating to the growth process is shown:

$$aCarbon\ Source + bNH_4^+ + cH^+ + dO_2 + eH_2O + 1C_5H_7O_2N + fHCO_3^- = 0 \qquad (2\text{-}6)$$

Where a - f are stoichiometric coefficients.

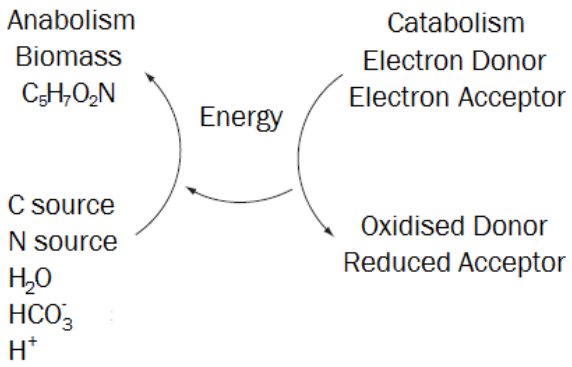

Figure 2.4. Schematic of bioenergetics (Heijnen and Kleerebezem, 2010).

The macro-chemical equation is a combination of the anabolic and catabolic reaction, the ratio of which is defined by Y. The macro-chemical reaction, along with the endogenous respiration reaction provide a complete stoichiometric description of the three major process that occur in biological treatment: ingestion, respiration, as well as growth and division. Therefore only Y is required for a complete description.

From Fig. 2.4 it can be observed that there are at least seven compounds involved in microbial growth. The conversion rates of these compounds are mathematically related by conservation equations for C, H, O, N and electric charge. These can be defined in five conservation equations giving five independent relations. To solve the macro-chemical equation the measurement of two rates are required, alternatively an experimentally determined Y value can be used, which gives the ratio of the biomass growth rate to substrate consumption rate.

As Y changes, as is expected with a change in temperature, so the stoichiometry of the macro-chemical reaction will change. From the macro-chemical reaction the Gibbs energy, and more importantly the heat of reaction can be determined.

The Gibbs energy and heat of reaction for the macro-chemical reaction are calculated following standard thermodynamic methods (Smith *et al.*, 2005):

$$\Delta G_{rxn} = a\Delta G_{f,C\ source} + b\Delta G_{f,NH_4^+} + c\Delta G_{f,H^+} + d\Delta G_{f,O_2} + e\Delta G_{f,H_2O} + \Delta G_{f,X} + f\Delta G_{f,HCO_3^-} \quad (2\text{-}7)$$

$$\Delta H_{rxn} = a\Delta H_{f,C\ source} + b\Delta H_{f,NH_4^+} + c\Delta H_{f,H^+} + d\Delta H_{f,O_2} + e\Delta H_{f,H_2O} + \Delta H_{f,X} + f\Delta H_{f,HCO_3^-} \quad (2\text{-}8)$$

Where:

$\Delta G_{f,i}$ is the standard Gibbs energy of formation for component i (kJ.mol^{-1}).

$\Delta H_{f,i}$ is the standard enthalpy of formation for component i (kJ.mol^{-1}).

2.6. Mathematical modelling

A model may be described as a purposeful representation or description of a system of interest (Amy *et al.*, 2011). Balance equations form the basis of any model description. These equations

describe the state variables in a reactor in time as the result of chemical and biological conversions, and of transport processes (Amy *et al.*, 2011).

The state of any physical system is in general dependent on four independent variables, time and spatial coordinates x, y, z. Mathematical models may be classified as lumped parameter models or alternatively distributed-parameter systems. Lumped parameter models are systems with which state does not depend on the spatial coordinates. At each point of such a system the conditions are identical (concentrations and temperature). Furthermore if the model did not depend on time then the system would be classified as steady state. As a result of this steady state lumped-parameter systems are described in terms of algebraic equations, while non-steady state lumped parameter systems are described in terms of ordinary differential equations (ODE's). Distributed-parameter models are systems which depend on the spatial coordinates, the conditions are a function of the position within the system. Steady state distributed-parameter systems may be described in terms of partial differential equations which contain neither time derivatives nor the time variable explicitly. Non-steady state distributed-parameter systems are described in terms of partial differential equations in their most general form (Cameron and Hangos, 2001). Only lumped parameter systems will be considered for the work undertaken.

2.6.1. Mass balance

2.6.1.1. Mass balance equations

General expressions are developed for both total and component mass balances in a process system.

An overall mass balance follows the basic principles of conservation of mass:

$$\left\{\begin{matrix}\text{rate of accumulation}\\ \text{of mass}\end{matrix}\right\} = \left\{\begin{matrix}\text{mass flow}\\ \text{in}\end{matrix}\right\} - \left\{\begin{matrix}\text{mass flow}\\ \text{out}\end{matrix}\right\}$$

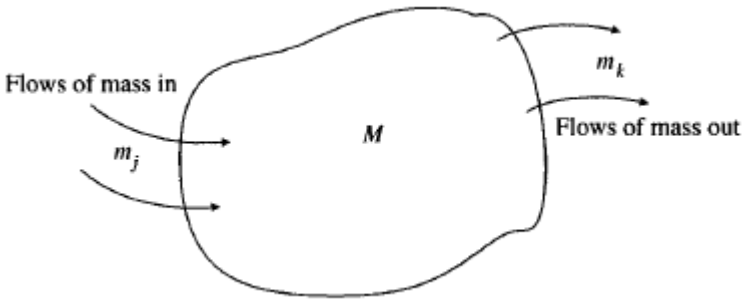

Figure 2.5.Graphical material balance (Cameron and Hangos, 2001).

Or expressed as an equation takes the following form, where p and q represent input and output streams respectively:

$$\frac{dM}{dt} = \sum_{j=1}^{p} m_j - \sum_{k=1}^{q} m_k \qquad (2\text{-}9)$$

Where:

$\frac{dM}{dt}$ is the rate of change of mass with time (kg.s^{-1}).

m_j and m_k is the mass flow rate into and out of the system respectively (kg.s^{-1}).

The general expression for the component mass balance takes the form:

$$\begin{Bmatrix}\text{rate of accumulation}\\ \text{of component i}\end{Bmatrix} = \begin{Bmatrix}\text{mass flow in of}\\ \text{component i}\end{Bmatrix} - \begin{Bmatrix}\text{mass flow out of}\\ \text{component i}\end{Bmatrix} + \begin{Bmatrix}\text{rate of formation or consumption}\\ \text{of component i}\end{Bmatrix}$$

Or in equation form for component i:

$$\frac{dM_i}{dt} = \sum_{j=1}^{p} m_{i,j} - \sum_{k=1}^{q} m_{i,k} + r_i V\,, \qquad i = 1, \dots \dots n \qquad (2\text{-}10)$$

Where:

n is the number of components under consideration.

r_i is the reaction rate of component i (kg.m^{-3}.s^{-1}).

V is the volume of the system (m^3).

The general and component mass balance can also be similarly written in molar terms.

2.6.1.2. Kinetic description

The kinetics of biological growth can be described by either the traditional modelling approach in which respiration is associated with the growth and decay of micro-organisms, or the death-regeneration approach where respiration is associated only with aerobic growth of micro-organisms (Vanrolleghem, 2002). Fig. 2.6 shows the main processes for growth and decay for the different approaches.

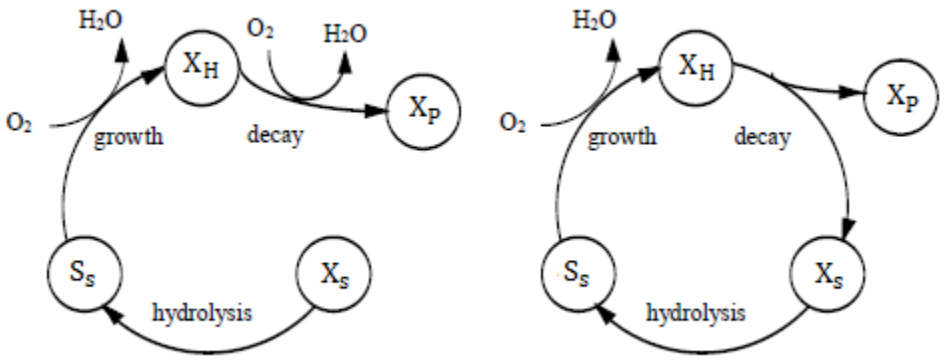

Figure 2.6. Activated sludge modelling approaches, traditional (left) and death-regeneration (right) (Vanrolleghem, 2002).

Both of the modelling approaches describe the growth of biomass as a process wherein oxygen is consumed. However, the traditional approach models biomass decay as an additional oxygen consuming step, in which decaying biomass is oxidised while inert matter is simultaneously formed. Therefore when the readily biodegradable substrate (S_S) and slowly biodegradable substrate (X_S) has been depleted, the remaining oxygen consumption is only associated with biomass (X_H) decay (Vanrolleghem, 2002).

In the death-regeneration approach the decaying biomass is split into two fractions, X_P and X_S. X_S is then hydrolysed to S_S. No oxygen is consumed during this process. The death-regeneration approach implies that when all external substrate is depleted, there remains an oxygen consumption that is associated with the growth on substrate released from decay and hydrolysis of the micro-organisms. The amount of new biomass generated from the internal substrate is always less than the amount of biomass decayed (Vanrolleghem, 2002).

Both models imply that in the absence of any external substrate the respiration rate will gradually decrease until all the biomass has depleted (endogenous respiration).

2.6.1.3. Presentation of activated sludge models-the Gujer Matrix

The International Water Association Activated Sludge Models, upon which the mass balance model is based, are presented in a format called the Gujer Matrix. It provides an efficient way to convey the maximum amount of information relating to the kinetic interactions between the model components. In the model, insoluble components are given the symbol *X* and soluble components are given the symbol *S*. Subscripts are used to specify individual components (Henze *et al.*, 2000).

Considering the situation where X_H is growing in an aerobic environment (in which S_O is consumed), and S_S is utilised for carbon and energy, the following example may be given. The two fundamental processes that are occurring are the biomass growth, and biomass decay. The simplest model of this situation must consider the concentrations of three components: X_H, S_S, and S_O. These components are linked to the processes through the system stoichiometry. The particular system is represented by the matrix shown in Table 2.4, with concentrations in units of $mg.L^{-1}$.

The index i is assigned to each component. In this case, i ranges from 1 to 3 for the three compounds in the model. The kinetic rate equations for the processes are recorded in the rightmost column of the matrix, and are denoted by α_j, where j corresponds to the process of concern. The elements within the matrix consist of the stoichiometric coefficients (v_{ij}) which give the mass relationships between the components in the individual processes. Stoichiometric coefficients are determined from experiment or predicted by applying the continuity equation

provided other coefficients are known. The sign of the stoichiometric coefficient corresponds to either utilisation or formation, represented by a negative and positive sign, respectively.

Table 2.4. Gujer matrix showing the aerobic growth and decay of heterotrophic biomass (Henze et al., 2000).

i	Components →	1	2	3	
j	Processes ↓	S_S	X_H	S_O	α_j
1	aerobic growth of biomass	$-1/Y$	1	$(1-Y)/Y$	$\frac{\mu_m S_S X_H}{K_S + S_S}$
2	biomass decay		-1	1	$k_d X_H$
		Readily biodegradable substrate	Active heterotrophic biomass	Oxygen uptake	

From the Gujer matrix the reaction rate pertaining to a particular component can be obtained. The system reaction term r_i of the component under consideration in the mass balance is determined from the matrix as the sum of the product of the stoichiometric coefficients, and the process rate expression. This is illustrated in mathematical form as:

$$r_i = \sum_j \nu_{i,j} \alpha_j \qquad (2\text{-}11)$$

Thus the reaction rate for X_H would be written as follows:

$$r_{X_H} = \frac{\mu_m S_S X_H}{K_S + S_S} - k_d X_H \qquad (2\text{-}12)$$

The reaction rates may for written for S_S and S_O in a similar manner.

2.6.2. Energy balance

Literature contains numerous heat balance models which are capable of describing active sludge processes ((Khambu and Andrews, 1968), (Argaman and Adams, 1977), (Jewell and Kabrick, 1980), (Vismara, 1985), (Messenger *et al.*, 1990), (Talati and Stenstrom, 1990), (Brown and Enzminger, 1991), (Sedory and Stenstrom, 1995)). The general energy balance over the system follows the conservation of energy, as shown in Fig. 2.7.

An energy balance may be formed that is based on the conservation of energy principles as follows:

$$\begin{Bmatrix}\text{rate of change}\\ \text{of total energy}\end{Bmatrix} = \begin{Bmatrix}\text{flow of energy}\\ \text{into the system}\end{Bmatrix} - \begin{Bmatrix}\text{flow of energy}\\ \text{out of system}\end{Bmatrix}$$

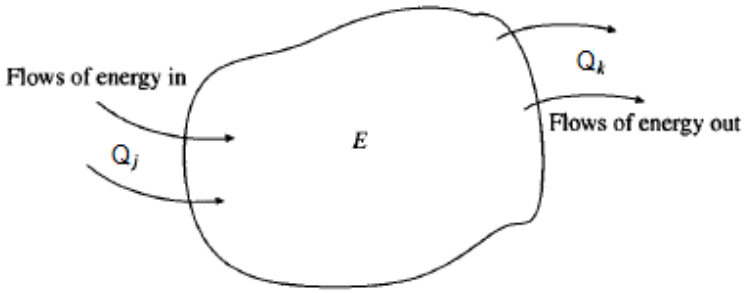

Figure 2.7. Graphical energy balance (Cameron and Hangos, 2001).

The energy balance may be expressed in simplified equation form:

$$V\rho C_p \frac{dT}{dt} = Input(H_{liq}) - Output(H_{liq}) + Q \qquad (2\text{-}13)$$

Where:

ρ is the density of the bulk fluid (kg.m^{-3}).

C_p is the heat capacity of the bulk fluid (J.kg^{-1}.K^{-1}).

$\frac{dT}{dt}$ is the rate of change of the temperature with time (K.s^{-1}).

Q is inclusive of all energy gained or lost from any reactions taking place, any shaft or expansion work as well as conductive and radiative terms (W).

$Input(H_{liq})$ and $Output(H_{liq})$ is the heat flow provided by the influent and effluent (W).

Assumptions that were made to obtain energy balance Eq. 2-13 are, (i) the kinetic and potential energy components have been neglected, (ii) internal energy is not dealt with but is assumed equivalent to the enthalpy, (iii) the specific enthalpy of the system and the specific enthalpy at the outlet are assumed equal (Cameron and Hangos, 2001).

2.6.3. pH

In acidic solutions there are more oxonium ions (H_3O^+) than hydroxide ions (OH^-) present, and vice versa for alkaline solutions. If the system is neutral then there are equal amounts of both ions. The product of the oxonium and hydroxide ion activities, ionic product of water, is constant. Acidic, alkaline and neutral solutions are thus defined as:

$\{H_3O^+\} > \{OH^-\}$ acidic

$\{H_3O^+\} = \{OH^-\} = \sqrt{k_w} = 1.0 \times 10^{-7}$ (25 °C) neutral

$\{H_3O^+\} < \{OH^-\}$ alkaline

Where:

k_w is the ionic product of water (mol^{-2}.dm^{-6}).

For practical reasons the logarithmic scale is used, the pH value is therefore defined as:

$$pH = -log_{10}\{H_3O^+\} \quad (2\text{-}14)$$

Therefore at 25ºC a pH above 7 would indicate an alkaline solution, and a pH below 7 would indicate an acidic solution.

The pH of the system is determined by its ionic speciation chemistry, which is a detailed distribution of the ionic species. The term components will be used to describe the model entities that define the material content of a system. Species may be defined as the material entities which are required to describe the physical state of the material. A single model variable may represent both a species and component, however in many important cases, such as equilibrium models, separate variables are needed. In general speciation may be defined as the calculation process by which a composition, expressed in terms of component masses, is transformed into one expressed in terms of species masses (Brouckaert and Brouckaert, 2014b). An example of speciation may be illustrated in the reaction equation for acetogenesis:

$$CH_3CH_2COOH + 2H_2O \rightarrow CH_3COOH + CO_2 + 3H_2 \ \textit{(Component Form)} \quad (2\text{-}15)$$

$$CH_3CH_2COO^- + 2H_2O \rightarrow CH_3COO^- + CO_3^{2-} + 2H^+ + 3H_2 \ \textit{(Speciated Form)} \quad (2\text{-}16)$$

The pH is calculated from the concentration of free, unassociated H^+ ions, in accordance with Eq. 2-14. To determine the pH of the system an external equilibrium speciation model can be used to handle aqueous phase ionic equilibria. A such model has been formulated by Brouckaert *et al.* (2010). Ionic equilibria pose a special problem for material balances in that the rates of the ionic speciation reactions in the aqueous phase are many orders of magnitude higher than other biological reactions occurring in a biological reactor. The fast reactions can be considered to always be in a state of chemical equilibrium. The speciated equilibrium composition of the solution is completely determined by the total concentrations, temperature and pressure. Therefore the model calculations are divided into differential mass balances which determine the composition in terms of total concentrations of components, followed by an equilibrium calculation which determined the ionic species concentrations from the total concentrations. The pH is subsequently determined from the ionic species concentrations (Brouckaert *et al.*, 2010).

2.7. Summary of literature

Biological wastewater treatment is a fundamental process in the treatment of many wastewaters. The temperature that the treatment takes place plays an important role in determining which micro-organisms are present in biological treatment, as well as their activity.

MBRs allow for the treatment of wastewaters with greater flexibility than CAS processes in that the SRT and HRT are uncoupled. This presents the opportunity for more sensitive, slow growing micro-organisms to be selected for which helps in the treatment of wastewaters with toxicity

concerns. An MBR also maintains higher MLSS concentrations which makes them more effective at treating high strength wastewaters. However they can be more costly than other treatment processes and add operational complexity.

Thermophilic operation is the result of wastewaters that are produced hot or have a high concentration of biodegradable substrate. The underlying concepts of thermophilic treatment is less understood than mesophilic treatment. However, thermophilic treatment is expected to present advantages over mesophilic in terms of higher substrate degradation rates and lower sludge yields.

There are 3 processes that play an important role in aerobic operation, namely ingestion, respiration, as well as growth and division. Through the measurement of the respiration rate these three processes may be quantified which would give a representative description of the system.

Mathematical models form the basis in forming a description or representation of a biological system. The model is made up of balance equations, primarily in the form of a mass and energy balance. A kinetic description is required to complete the mass balance, this is most commonly obtained from the Monod model.

3. ILLOVO SITE AND DESCRIPTION

3.1. Illovo core business

Illovo is the biggest producer of sugar within Africa and is a significant manufacturer of downstream products, Illovo has operations in 6 African countries. Furfural and its derivatives are produced at the Sezela Mill Complex which is located on the south coast of KwaZulu-Natal. High quality ethyl alcohol, from which various grades of alcohol are manufactured, are produced at the Merebank plant situated in Durban and at the Glendale distillery on the north coast. Lactulose is also manufactured at the Merebank factory (Illovo, 2014).

3.2. Wastewater treatment at Sezela Mill Complex

The Sezela site consists of a sugar mill with an attached downstream products facility. The downstream site has a large plant that produces furfural and a range of smaller plants that make furfuryl alcohol, diacetyl, 2,3-pentanedione and methanol. There are two wastewater treatment plants located at Sezela – a CAS process that treats the sugar mill effluent along with the local domestic sewage, and a second plant which consists of a MBR that treats a portion of the furfural plant effluent. Both effluent treatment plants treat wastewater by biological means. The conventional plant provides a key function of generating WAS which is used to seed the MBR; this is essential as the MBR operates for only eight to nine months of the year, during the sugar cane harvesting season.

3.3. Furfural effluent stream

The furfural plant (Fig. 3.1) produces roughly 100 tonnes per day of furfural at greater than 99.5 % purity. First the bagasse, a by-product of sugar production, is subjected to hydrolysis at a high temperature and pressure. The resulting vapour is condensed to give an aqueous stream that contains 3 % furfural and 1 % acetic acid. This stream is distilled in an azeotrope column to remove the majority of the water, which exits at the bottom of the column as the furfural plant effluent, and to concentrate the furfural up to 30 %. The furfural stream is then sent for further processing to achieve the desired purity. The furfural losses to the effluent bottoms are controlled to below 300 ppm. The acidic effluent from the column is sent to the cooling towers to reduce the temperature from 100 °C to 45 °C, the general properties of this stream are shown in Table 3.1. The acid stream is then sent to the dissolved air flotation (DAF) unit to reduce the wax and suspended solids. A portion of the furfural plant effluent (up to 25 %) from the DAF is then sent to the MBR and the remainder is pumped out to a surf outfall (Gent, 2012).

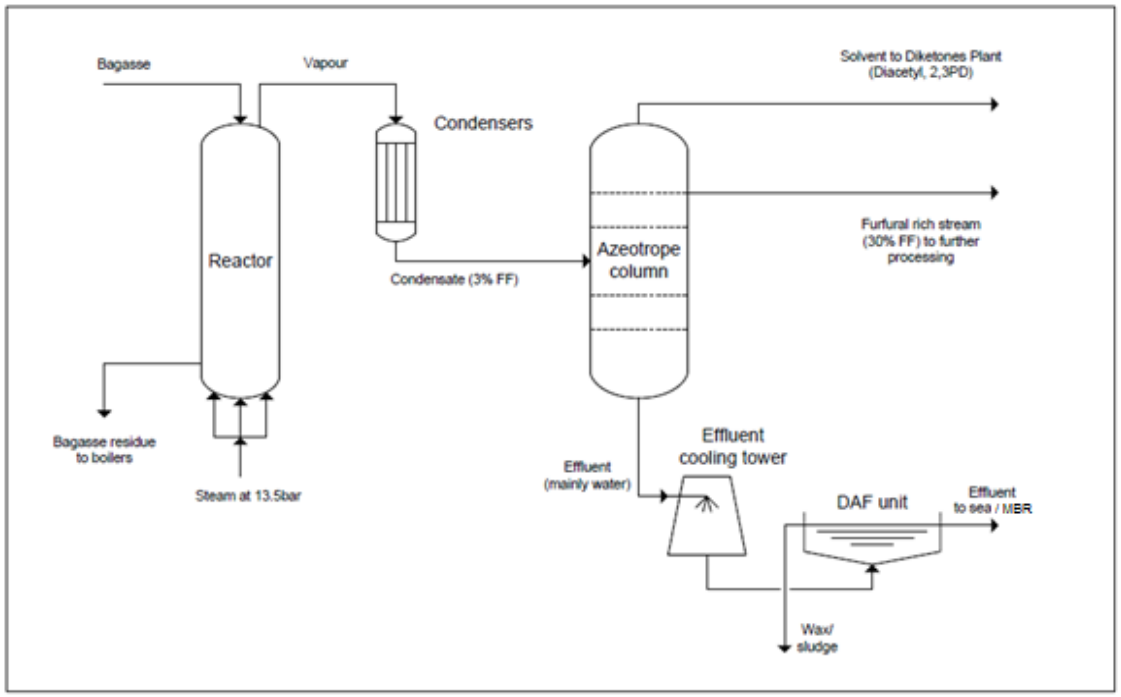

Figure 3.1. Simplified diagram of furfural production process (Gent, 2012).

Table 3.1. General properties of furfural plant effluent from azeotrope column (Gent, 2012).

Flow	$m^3.(ton\ FF)^{-1}$	30
pH		2.8
COD	$mg.L^{-1}$	17 500
Acetic Acid	wt %	1.2
Formic Acid	wt %	0.1
Furfural	$mg.L^{-1}$	200
Waxes	$mg.L^{-1}$	100

The furfural plant effluent that is pumped to the sea exits via a pipeline close to the shore in a very aerated area. It is unlikely Sezela will be permitted to discharge untreated furfural plant effluent into the sea indefinitely, and the possibility has always existed that the plant could be forced to close should the permit be refused (Gent, 2012). This places pressure on finding an effective solution for the treatment of the furfural plant effluent. The discharge of effluent also heavily affects Sezela's water balance as the steam fed to the reactors (typically 140 $tonnes.h^{-1}$) is essentially pumped out to the sea. If a practical solution were to be found to treat the effluent it would also open up the opportunity to build a second furfural plant (Gent, 2012). It would be ideal to be able to construct a furfural plant at a site with surplus bagasse. However, the most significant hurdle is the challenge of what to do with the effluent – it is unlikely that any site for a second furfural plant would have a point available where it would be permitted to discharge

untreated effluent. Economical effluent treatment is therefore a prerequisite for a second furfural plant.

These factors prompted the construction of a 4 600 m^3 MBR to treat the effluent. The MBR was constructed as a "pilot" plant to treat a third of the furfural plant effluent, although practically it has been found to satisfactorily treat up to 25 % of the effluent (Gent, 2012).

3.4. Illovo MBR

Sezela's MBR is an open top tank through which air is injected through fine bubble diffusers situated along the bottom of the tank in a grid pattern. The MBR was selected due to the suspected presence of a trace toxin which inhibits conventional aerobic and anaerobic treatments. The high MLSS offered by the MBR overcomes this limitation. The MBR has a hydraulic design capacity of 1 200 $m^3.day^{-1}$ but in practice treats a feed flow rate of no more than 1 000 $m^3.day^{-1}$. It comprises of a 29 m diameter, 7 m deep cylindrical tank, which is fitted with 12 EK400 Kubota membrane modules providing a total membrane area of 2 840 m^2 from 4 800 panels. Two 224 kW blowers, rated at 7 060 $Nm^3.h^{-1}$ at 740 mbar, supply air via the fine bubble diffusers along the floor of the tank. A third 61.5 kW blower, rated at 2 880 $Nm^3.h^{-1}$ at 500 mbar, also supplies air as course bubbles to scour and clean the membranes (Judd, 2011).

The plant is operated by controlling a number of parameters such as furfural plant effluent feed rate, MBR pH, DO and MLSS concentration. Sludge is wasted from the tank to maintain the MLSS concentration in the range of 12 000 to 16 000 $mg.L^{-1}$. Nutrients of nitrogen (urea) and phosphorus (phosphoric acid) are added to maintain a healthy microbial community. The nutrients are dosed manually to ensure a residual amount of nitrogen and phosphorus in the permeate. When operating in a stable manner, the MBR can achieve a 95 % COD removal (Judd, 2011). However, in practice the effluent COD is maintained below 1 000 $mg.L^{-1}$. The permeate colour remains high and if the water were to be reused, secondary treatment would be necessary as a polishing step.

The plant is challenged with a feed of 17 500 to 18 000 $mg.L^{-1}$ COD at a pH between 2.5 and 2.8, with very low TSS, thus requiring minimal screening (0.55 mm wedge wire). The COD mostly consists of readily assimilable organic matter in the form of ~1.2 % acetic acid, ~0.1 % formic acid, as well as intermittent furfural concentrations of no more than 400 $mg.L^{-1}$ (Judd, 2011). The flow of the furfural plant feed into the tank is controlled by monitoring the pH of the mixed liquor, which is continually maintained at a value above 6 by reducing the flow of the feed to the MBR when the pH decreases below this set point.

The MBR was constructed as a "pilot" plant and has been operational since 2005. The MBR was not specifically engineered for operation at thermophilic temperatures. It was assumed that the

MBR would operate in the mesophilic range at around 30 °C (Gent, 2012). However, with the furfural plant effluent entering the reactor at about 40 °C, and with the rapid consumption of the COD being exothermic, the reactor operates at between 40 and 50 °C, which results in the MBR reaching thermophilic temperatures.

The MBR operates on the furfural plant effluent for between eight to nine months of the year determined by harvesting of the sugar cane. The sugar cane harvesting season is between April and December each year, thus demanding the startup of the MBR in April each year. The MBR is seeded with sludge from the CAS plant, building up to a solids concentration of around 8 $g.L^{-1}$. The reactor is then fed with the furfural plant effluent and the temperature is gradually allowed to increase to its operating temperature. The WAS dosing to the MBR is required to maintain the required bioactivity, to ameloriate toxic shocks, and maintain the membrane permeability; there is a notable deterioration in the permeability below an MLSS of 10 $g.L^{-1}$ (Judd, 2011). Once the MBR reaches its operating temperature and MLSS concentration, the dosing of seed WAS is suspended. The addition of WAS seeding is resumed if there is a clear indication of reduced bioactivity in the MBR. The reduced bioactivity is often a result of the feed to the reactor being inconsistent, depending on the operation of the furfural plant. Another factor is thought to be ambient conditions, such as a cold front or high rainfall. This leads to instability within the reactor as the temperature drops and the culture fluctuates between mesophilic and thermophilic operation. The WAS from the CAS also provides essential nutrients for the MBR originating from domestic wastewater that it cannot obtain from the industrial effluent.

4. RESEARCH OBJECTIVES

4.1. Research question

The Illovo MBR regularly experiences process upsets, primarily as a result of an inconsistent feed, which has adverse effects on its stability, as explained in section 1.2. The feed interruptions cause fluctuations in the operating temperature of the MBR, and result in operation between a mesophilic temperature of 40 °C and a thermophilic temperature of 50 °C. The change between the two temperature regimes leads to reactor instability in terms of decreased biomass activity.

Any kind of temperature change concerning biological treatment must be approached carefully and cannot be applied without considering the nature of the processes involved. To aid in the elucidation of the processes, a better understanding of the underlying mechanisms occurring within the MBR has been sought. A better understanding in terms of the microbiological activity within the MBR, the effects of different heat transfer mechanisms on the temperature of the MBR, and additionally the effect of the pH on MBR operability. This study aims to develop a dynamic mathematical model of the mass and energy balances over the MBR, making use of the best available knowledge to describe the differences in microbial kinetics and stoichiometry at different temperatures, with the objective of simulating the transition between mesophilic and thermophilic operation. Should such a model be able to realistically describe plant behaviour, the model can be interrogated to investigate possible scenarios for managing process upsets, as well as assist in the future design of MBRs treating the Illovo effluent. In addition, the construction of a model that can describe plant behaviour should give insight on the factors that likely have a significant influence on the MBR operating temperature.

4.2. Presentation of research hypothesis

In order to predict the MBR performance key variables associated with its performance are required. These variables are the operating temperature (*T*), readily biodegradable substrate concentration (S_S), VSS concentration (X_{VSS}) (which is a function of the active biomass concentration (X_H) and the inert organic matter from decay concentration (X_P)), and pH. These variables provide a description of the MBR that can be related to measured parameters. They may be predicted through the formulation of a mass and energy balance model, with an attached speciation routine, which is based on kinetic data obtained experimentally, and modified through calibration against measured plant data.

It has been speculated by Illovo staff that there may be two different microbial populations involved in the operation of the MBR. This is supported by the reduction in biomass activity that occurs when the temperature changes between 40 and 50 ºC, possibly due to the transition to a more dominant micro-organism population. This is further evidenced by a colour change in the mixed liquor when thermophilic temperatures are reached to a maroon colour. However, these

alone are not sufficient to prove that the consortia are different under the different conditions. Therefore in maintaining good modelling practice, it was initially assumed that it was adequate to model only one micro-organism population.

The hypotheses are formulated as follows:

Hypothesis 1:

A mass and energy balance model of the MBR that explicitly considers the interactions of temperature and pH on the kinetics and stoichiometry of the furfural plant effluent degradation, will be able to simulate the key variables to agree with plant observations during transition from mesophilic to thermophilic conditions.

Hypothesis 2:

The transition from a mesophilic to thermophilic regime, or thermophilic to mesophilic regime, can be described by modelling a single biomass population, as opposed to separate biomass populations representing each temperature regime.

The two proposed hypotheses are closely linked in that they are both dependent on the successful outcome of the final calibrated model. If the first hypothesis is verified and the model can predict MBR performance by modelling a single biomass population, then the second hypothesis will be simultaneously verified, as it proves that the biomass population can successfully be modelled by a single population model. However, if the two or more biomass populations are required to model the MBR then the first hypothesis would be verified but the second hypothesis wouldn't.

4.3. Research plan

The following steps were identified as required to be undertaken to achieve the primary aims of this project:

- Mathematical models, in the context of biological wastewater treatment, were to be investigated from literature as a basis for developing a detailed dynamic model over the MBR.
    - A mass balance was to be performed over the MBR for the components of interest, a suitable kinetic description of the pertinent kinetic processes was to be formed.
    - The mass balance was to be extended by the addition of a speciation subroutine which allows the prediction of the pH of the MBR.
    - A detailed energy balance of the MBR system had to be formed, supported by literature, from which the temperature could be predicted.
- The integrity of the combined mathematical model required verification.

- A temperature dependent description of the kinetic parameters for the mass balance needed to be obtained experimentally, from laboratory scale tests, to describe the MBR operation between the two temperature regimes of interest. The experimental work had to be carried out at a mesophilic temperature of 40 °C and a thermophilic temperature of 50 °C.
- A model calibration from the parameters obtained from experimental work and literature was to be performed.
- The accuracy of the combined dynamic model was to be validated against an independent set of Illovo plant data.
- A sensitivity analysis to determine effects of various energy balance parameters on the temperature of the MBR was to be performed.
- The model would allow the prediction of the system behaviour for conditions that have not been experimentally tested, assisting in the preliminary selection of favourable scenarios, thereby reducing experimental effort.
- The model was to be simulated for various scenarios for both mesophilic and thermophilic operation, such that comparison of the two operating regimes could be performed.
- The accumulated results could be analysed in order that recommendations for which temperature regime to follow for enhanced MBR process design and operation be made.

5. EXPERIMENTAL METHODOLOGY

A kinetic model of a system such as the Sezela MBR requires quantitative descriptions of the relationships between process reaction rates and MBR conditions, and also stoichiometry and process conditions; where these are expected to change across the range of conceivable conditions. While some of these data can be inferred from historical data from the MBR, and from targeted measurements in the MBR, some of the measurements are more suited to determination under controlled laboratory conditions.

This chapter describes the outcomes of the experimental work performed in order to determine the kinetic and stoichiometric parameters required to complete the mass balance model, which the energy balance is partially dependent on. The model kinetic and stoichiometric parameters were determined from batch respirometric experiments involving mixed liquor samples obtained directly from the MBR, and in some cases composite furfural plant effluent samples.

5.1. Overview

An overview of the experimental work performed and the parameters that were obtained is shown in Fig. 5.1. The work initially involved the sampling of the mixed liquor containing the activated sludge from the MBR, as well as obtaining a representative furfural plant effluent sample. The substrate concentration (S_s) and the MLSS concentration, from which the active biomass concentration (X_H) was inferred, were then measured, and subsequently through experimental work the parameters Y and k_d were obtained. This allowed for the regression of the kinetic parameters, and the population of the mass balance.

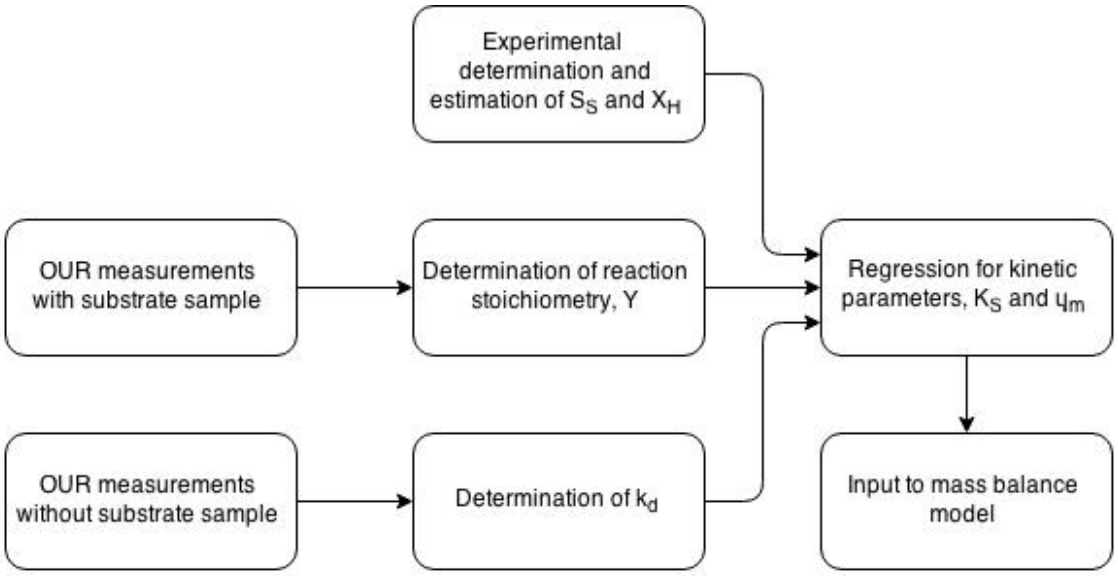

Figure 5.1. Overview of experimental work performed and information obtained from each experiment.

5.2. Experimental methods

5.2.1. Wastewater sample collection

The furfural plant effluent was collected from the Sezela Mill Complex by the Illovo staff. The wastewater influent was sampled daily from which weekly composite samples were formed to obtain a representative wastewater sample. The influent samples were drawn from a sampling point along the furfural plant effluent feed pipeline to the MBR. As the wastewater sample is at a pH of around 2.7 (Table 3.1), it was expected that negligible biological degradation of the influent sample occurred over the weekly sampling time, allowing storage of the samples at room temperature.

5.2.2. Activated sludge sample collection

The activated sludge (mixed liquor) was collected near the MBR surface. The sample was obtained from a 3 L sampling bucket, and was immediately transported to the respirometer to ensure negligible thermal shock occurred to the sample. The MBR operating temperature was between 40 and 50 °C; the temperature of the sample dropped by no more than 5 °C while being transported to the respirometer, where the temperature could be increased by the device to the original sampling temperature. Sampling of the activated sludge from the MBR was only performed when the blowers were operational, to ensure adequate homogeneity of the sampled sludge.

5.3. Respirometer description

A respirometer is a device for the measurement of the respiration rate, which is defined as the mass of oxygen consumed per (unit of volume) per unit of time. The Surcis S. L., model BM-EVO multifunction respirometer was utilised in the experimental work for the measurement of the respiration rate of the activated sludge. The measurement of the respiration rate was performed with a DO-sensor in the liquid phase.

The BM-EVO respirometer is a 1 L batch reactor, which includes an aerator, stirrer, DO probe, an internal integrated heater/cooler for temperature control, and a peristaltic pump for recirculation of the reactor contents (Fig. 5.2). The respirometer outputs the measured data to a computer, which is displayed on a graphical user interface (GUI) provided by the respirometer software. The tests on the respirometer are configured and performed through the GUI provided by the computer software.

The BM-EVO respirometer uses a novel design in which the glass reactor vessel is divided into two compartments by a dividing plate, the lower and upper part. The air diffuser is installed in the upper part and the DO probe is installed in the lower section. This is to avoid the interference that the air bubbles from the diffuser, as well as the air from the atmosphere (enhanced by the stirrer) would have on the DO probe. The dividing plate has a one-way valve, where the reactor

contents can only flow from the upper part to the lower part. This occurs only when the peristaltic pump is operational, which recirculates the reactor contents from the lower part to the upper part.

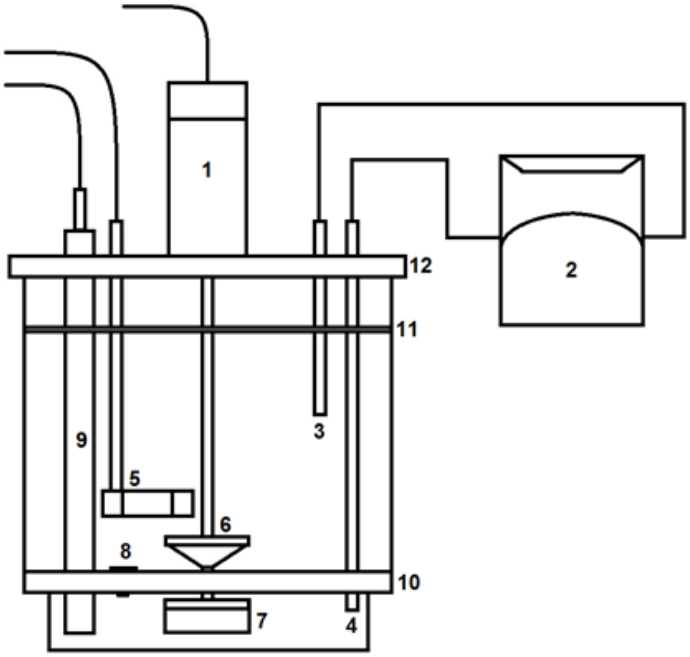

Figure 5.2. Schematic of glass reactor vessel located within BM-EVO respirometer device. 1. Stirrer motor, 2. Peristaltic pump, 3. Return tube, 4. Withdrawal tube, 5. Aerator sparger, 6. Upper stirring paddle, 7. Lower stirring paddle, 8. One-way valve, 9. DO probe, 10. Dividing plate, 11. Anti-splash sieve plate, 12. Top cover plate.

The respirometer can operate in a closed (static mode) or open system (dynamic mode), where three different modes of operation are possible. Static OUR, Cyclic OUR and Dynamic Response Test mode. Only two modes of operation will be considered for the experimental work, Cyclic OUR mode and Dynamic Response Test mode.

5.3.1. Cyclic OUR Test

Cyclic OUR mode involves setting a maximum (high-set) and minimum (low-set) DO concentration through the equipment software. The low-set-point will activate the aeration and peristaltic pump, and the high set-point will stop the aerator and peristaltic pump. The stirrer and temperature control operates continuously throughout the test. When the aeration and pumping has stopped at the high-set DO concentration, the DO concentration will gradually drop to the low-set DO concentration due to the oxygen consumption from the biomass. When the DO concentration reaches the low-set value the aerator and peristaltic pump is once again turned on and the sequence is repeated until the user halts the test. The DO concentration versus time plot that is generated by the equipment resembles Fig. 5.3.

From the generated data the equipment software automatically evaluates the gradient of the decreasing DO concentration line (air off), which is the OUR of the sludge sample. The down

slope is the rate of change of the oxygen concentration solely due to biological activity. Therefore, every cycle in which the DO concentration decreases from the high-set DO concentration to the low-set DO concentration will generate one OUR data point.

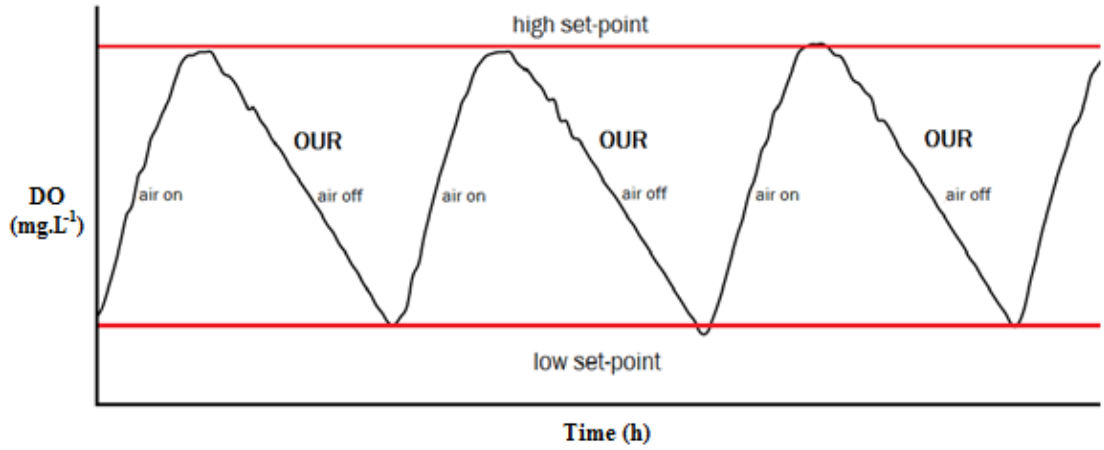

Figure 5.3. typical DO concentration profile during Cyclic OUR Test.

This method of determining the OUR can be used for estimating the respiration rate for samples that are undergoing endogenous respiration or exogenous respiration (resulting from substrate addition). However, in practice it has been found that this method is not effective for measuring the exogenous respiration rate due to the lengthy time intervals between each OUR data point measurement, which only occurs every cycle. The Cyclic OUR Test was therefore only used for measuring endogenous respiration. The exogenous respiration rate may be accurately measured by the Dynamic Response Test. A detailed experimental procedure for the Cyclic OUR Test may be found in Appendix F.

5.3.2. Dynamic Response Test

The Dynamic Response Test involves the continuous aeration of the mixed liquor in the respirometer, until conditions of endogenous respiration are achieved. Throughout the aeration, mixed liquor is pumped from the aerated upper chamber to the lower unaerated chamber. Once steady sate conditions have been reached within the glass reactor vessel the baseline DO concentration for the test is selected. The maximum steady state DO concentration that is measured under endogenous respiration for a preselected aeration rate is taken as the baseline DO concentration for the test; it is an assumption of the Dynamic Response Test that the baseline DO concentration is constant for the remainder of the test. This assumption implies that the biomass concentration within the respirometer is constant throughout the test. Once the baseline DO concentration has been determined, the furfural plant effluent sample is injected into the mixed liquor within the respirometer, and the corresponding drop in the DO concentration due to an increased OUR is recorded by the equipment. The aeration rate, peristaltic pump speed, stirrer and temperature are kept constant throughout the test.

From a predetermined calibration factor (section 5.3.3) the OUR resulting from exogenous respiration for the Dynamic Response Test can be determined by the difference in the baseline DO and current DO concentration as follows:

$$OUR = F(S_{o,s} - S_o) \qquad (5\text{-}1)$$

Where:

OUR is the exogenous respiration rate ((mg O_2).L^{-1}.h^{-1}).

F is the calibration factor (section 5.3.3) (h^{-1}).

$S_{o,s}$ is the baseline DO concentration, at saturation level, for the test ((mg O_2).L^{-1}).

S_o is the DO concentration for the test ((mg O_2).L^{-1}).

A typical response of the DO concentration to the addition of substrate, and the subsequent generation of a respirogram is shown in Fig 5.4.

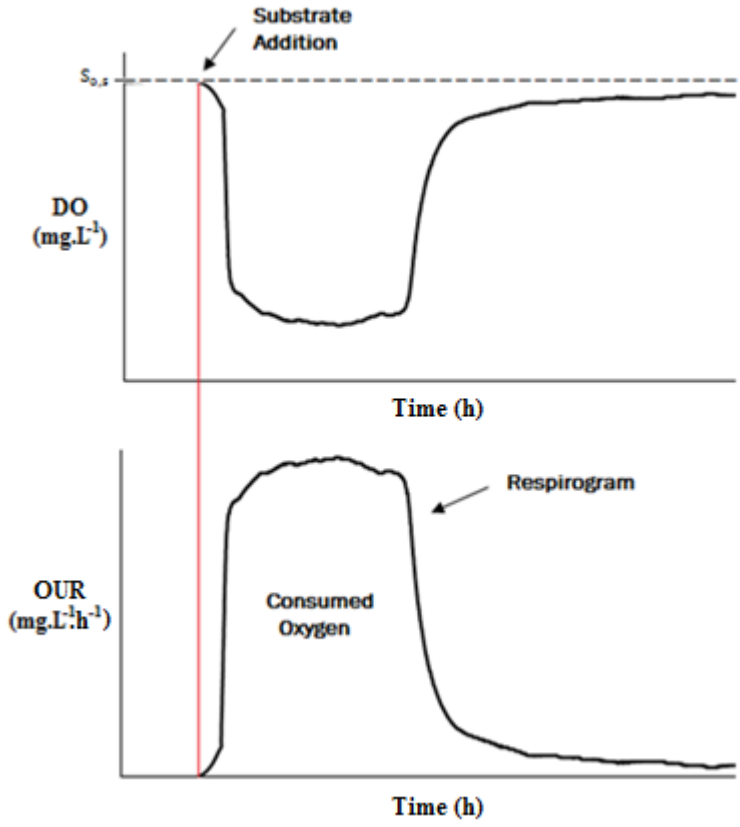

Figure 5.4. Relation between the measured DO concentration and the generated respirogram.

The Dynamic Response Test can only be performed for tests involving the addition of substrate (exogenous respiration), and therefore is not suitable for determining the OUR during endogenous respiration. The experimental procedure that was followed is detailed in Appendix F.

5.3.3. Equipment calibration

The Dynamic Response Test requires calibration before carrying out the test. The calibration calculates F, from which the OUR is generated. The method involves the addition of a known amount of sodium sulphite into the respirometer which contains distilled water. The amount of oxygen that is required to oxidise the sodium sulphite can be determined from:

$$Na_2SO_3 + 1/2\,O_2 \rightarrow Na_2SO_4 \qquad (5\text{-}2)$$

Thus for 1 mole of sulphite to be oxidised, half a mole of oxygen would be required.

The calibration factor is then determined automatically by the equipment from:

$$F = \Delta O_{2,sulphite} / \int (S_{o,s} - S_o) \qquad (5\text{-}3)$$

Where:

$\Delta O_{2,sulphite}$ is the mass of oxygen required to fully oxidise the sulphite (mg O_2).
$\int (S_{o,s} - S_o)$ is the integral of the DO profile (mg O_2.h).

Refer to Appendix E for the calibration data generated by the equipment.

5.4. Substrate and MLSS concentration determination

The substrate (furfural plant effluent) COD, acetic acid and formic acid content, as well as the MLSS concentration of the mixed liquor were measured by the Downstream Laboratory at Illovo, Sezela. The Downstream Laboratory has SABS and HACCP accreditation.

5.4.1. Substrate concentration

The substrate concentration was measured in terms of COD concentration. The COD of the furfural plant effluent fed to the MBR was determined from standard methods for the closed reflux, colorimetric method by the Illovo Laboratory. A suitable volume of the sample, as well as a blank, was measured into a tube or ampule. The samples were then prepared, with the addition of a strong acid and potassium dichromate, and digested, after which they were left to cool to room temperature. The absorption of each sample blank was measured at a selected wavelength. The digested blank was then subtracted from the sample COD to obtain the final COD (Rice, 2012). The COD measurements were checked against a standard to ensure accuracy of the test method. A 1 000 mg.L^{-1} potassium hydrogen phthalate solution was used as the standard which was tested monthly, with an allowable tolerance of 50 mg.L^{-1}. Only one replicate was performed for each of the furfural plant effluent samples. The test was performed once a week on a composite sample taken once a day.

The quantity of acetic acid and formic acid were also determined by the Illovo Laboratory. The total acidity of the furfural plant effluent was determined by a titrimetric method using 0.1 N

Sodium Hydroxide. The formic acid content in the effluent was found based on the reduction of Hg^{2+} to insoluble HgCl which is filtered, dried and weighed. The acetic acid content was found by the difference between the total acidity and formic acid content. The total acidity represents the majority of the furfural plant effluent, approximately 97 to 98 %, while the remaining undetermined fraction consists of low concentrations of furfural, waxes, suspended solids and total dissolved solids. For part of the 2013 Illovo plant data this unknown fraction tends to account for an average of 459 $mg.L^{-1}$ of the total measured COD, however with a high standard deviation of ± 475 $mg.L^{-1}$.

5.4.2. MLSS concentration

The MLSS concentration of the MBR was obtained following standard methods for TSS determination. The work was performed by the laboratory located at the Sezela Mill Complex. A well-mixed sample was filtered through a standard glass-fiber filter (106 µm) and the residue retained on the filter was dried to a constant weight at 103 to 105 °C. The increase in weight of the filter represents the TSS (Rice, 2012). One replicate was performed per mixed liquor sample, the MLSS concentration was measured for the MBR once a day.

5.5. Kinetic and stoichiometric parameters from respirometric tests

5.5.1. Specific death rate constant k_d

To determine k_d of the activated sludge, the Cyclic OUR Test was performed. Sufficient oxygen levels were continually provided throughout the test (> 2 (mg O_2).L^{-1}) to ensure that oxygen limited conditions did not occur. The test was run for an extended amount of time (> 24 hours), to ensure that any external substrate present in the sample was consumed, and endogenous respiration reached. The substrate is primarily readily biodegradable, therefore endogenous respiration for the MBR samples were reached timeously, within 8 hours.

k_d can be determined from the OUR versus time data that was generated by the respirometer during the Cyclic OUR Test. A plot of the natural logarithm of the OUR during endogenous respiration, as a function of time describes the exponential decay of biomass as a straight line with slope k_d, which refers to the traditional specific death rate constant.

5.5.2. Aerobic yield of heterotrophic biomass *Y*

Y can be estimated from the data that is generated from the Dynamic Response Test. The pre-programmed Dynamic Response Test generates a respirogram, which is a time series of respiration rates over the test interval. The integral of the respirogram gives the quantity of oxygen that is consumed over the test due to consumption of substrate.

The equipment manual states that the measured OUR from the Dynamic Response Test is solely due to the biodegradation of external substrate (exogenous respiration), although this statement

is reliant on an assumption of a constant biomass concentration during the test. The assumption implies that the net amount of biomass growth and death for the duration of the test is zero. As the experimental work was performed at high temperatures, where the k_d can be significant, the assumption was tested on selected experimental data to determine its validity (Appendix B).

Under the assumption that the respirogram only represents the exogenous respiration rate, *Y* can be easily found. *Y* may be determined from the numerical integration of the respirogram to determine the consumed oxygen due to exogenous respiration and the following calculation:

$$Y = 1 - \frac{CO}{\Delta COD} \qquad (5\text{-}4)$$

Where:

CO is the consumed oxygen during the test (mg O_2).
ΔCOD is the COD consumed by the micro-organisms (mg O_2).

The trapezoidal rule was used for all numerical integrations performed in this work.

5.5.3. Heterotrophic maximum growth rate μ_m and half saturation coefficient K_S

The kinetics were regressed by modelling the respirometer glass reactor vessel through a batch system mass balance. The mass balance was simulated through MATLAB R2010a, and using the built-in minimisation routine 'fmincon' to determine the best fit for the parameters. The MATLAB code that was written can be found in Appendix I. The kinetics for the mass balance are the same as those used in the MBR model, described in section 6.1.3. In the simulation k_d and Y were kept constant, the experimentally obtained values were used, and the kinetic parameters μ_m and K_S were found by regression. It was an assumption of the Dynamic Response Test that the active biomass concentration is constant throughout the test, therefore the respiration is solely due to exogenous respiration. This assumption was followed through in the mass balance to model the glass reactor vessel, and only exogenous respiration was modelled.

A dynamic mass balance model that calculates the OUR was fitted to the respirograms generated during the Dynamic Response Test, using an error minimisation routine in MATLAB 2010a. Only suitable respirograms could be effectively used in obtaining the kinetics. Suitable in terms of a respirogram that is long enough that the maximum OUR is achieved exhibited by a flat top, but not so long that substantial biomass growth would occur. Also a respirogram in which inhibition is not significant (Fig. 5.5). The predicted OUR was compared to the experimental OUR, and the error minimised through a minimisation routine on MATLAB R2010a. In the regression of μ_m only the OUR at maximum growth is required, and for K_S only the rate at which the OUR falls after the readily biodegradable substrate has been consumed is required. Therefore the initial 10-20 % of the respirograms were neglected, as the kinetic model does not account for

the lag that was experienced by the micro-organisms in initially reaching the maximum growth rate. The effect of the lag could be modelled with a first order function or the empirical equation of Kono (1968), but as the lag occurred over a relatively small time (<5 minutes) it was seen as negligible and was excluded from the mass balance model. The last portion of the respirogram where the OUR drops to the baseline value was also neglected in the regression. This is because the respirogram did not reach an OUR of zero at the end of the test, but tended to hover somewhere above. It was initially expected that this was due to the growth of new biomass during the test, although this was effectively disproven as shown in Appendix B. It is therefore likely that substrate (furfural plant effluent) has a small slowly biodegradable fraction, which is consumed at a much slower rate. The kinetic model does not account for this behaviour.

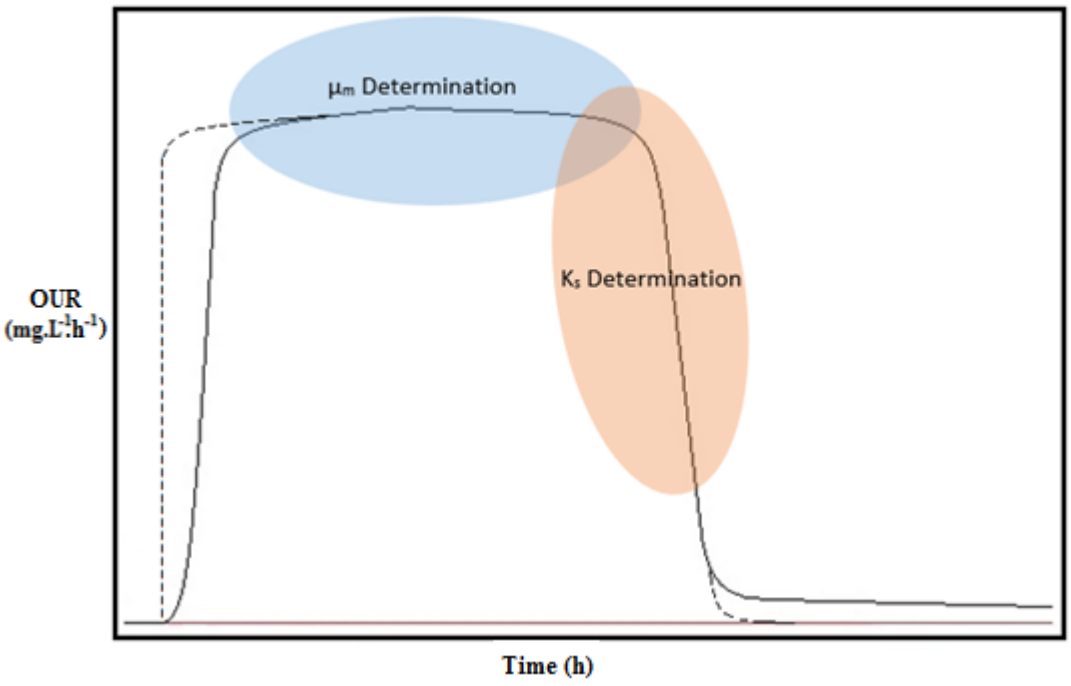

Figure 5.5. Portion of respirogram used for kinetic regression, ---- model, ——— experimental.

5.5.4. Summary of kinetic and stoichiometric parameters

The kinetic parameters which are determined experimentally are summarised as follows:

Symbol	Description	Method Used
Y	Biological yield	Dynamic Response Test
k_d	Specific death rate constant	Cyclic OUR Test
μ_m	Maximum specific growth rate	Curve fitting of predicted OUR data to measured OUR data
K_S	Half saturation coefficient	Curve fitting of predicted OUR data to measured OUR data

6. MODEL FORMULATION

The modelling approach adopted in this work was to start with the simplest model structure that could represent the principal observations, and to add complexity only when it was shown that the simple model structure could not adequately describe the observations.

The mass balance model consists of a kinetic and stoichiometric reaction model, and a digester hydrodynamic model. In section 5.5.3, the digester hydrodynamic model for the respirogram generated by the respirometer was modelled as a batch experiment of fixed volume, using the kinetics described in section 6.1.3 to predict the OUR. Subsequently the digester hydrodynamic model for the MBR was modelled as a continuous system, detailed in this chapter. The MBR hydrodynamic model is an expansion of the mass balance proposed by Gent (2012) which was limited to describing the substrate and biomass concentrations. The same kinetic and stoichiometric reaction model was used for both the batch and continuous modelled systems, however different boundary conditions were used. An energy balance was formulated around the MBR mass balance following the work of Sedory and Stenstrom (1995), to predict the reactor temperature as a function of various input variables. A dynamic pH prediction capability linked to the mass balance was also formed, which utilises the speciation routine of Brouckaert *et al.* (2010).

6.1.Mass balance model

The components under consideration for the mass balance were readily biodegradable substrate (S_S), active heterotrophic biomass (X_H), and inert organic matter from biomass decay (X_P). The rate of oxygen uptake due to biological processes (S_O) was included in the kinetic description for the purposes of modelling the OUR generated from the experimental work. X_P was included for the prediction of the VSS concentration within the MBR. A diagram of the mass balance is shown in Fig. 6.1.

6.1.1. Overall mass balance

The mass of the working fluid within the MBR fluctuates depending on the feed rate into the MBR as well as sludge and permeate withdrawal rates; which are all independent of one another. To simplify the mass balance the mass content of the MBR was assumed constant, as previous plant data has shown only small fluctuations in liquid level occurred during operation, ±0.1 m from day to day with a relative standard deviation of 1.5 %.

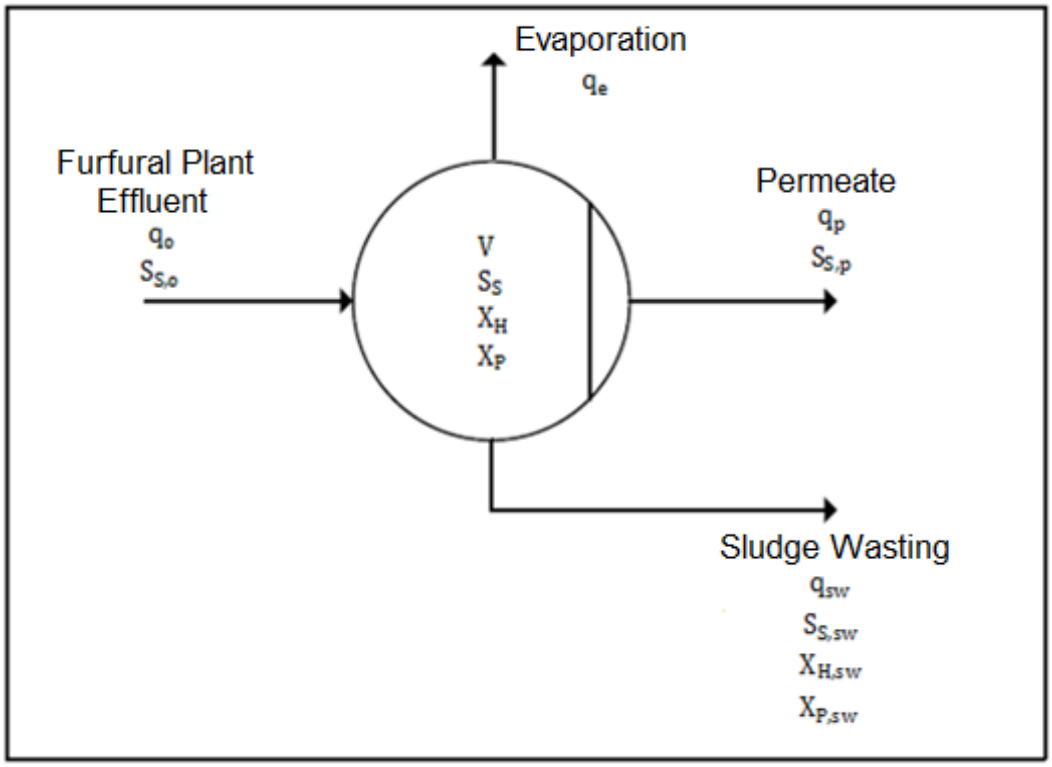

Figure 6.1. MBR mass balance (modified from Gent (2012)).

The overall mass balance was therefore represented as:

$$m_o = m_e + m_{sw} + m_p \qquad (6\text{-}1)$$

Where:

m_o is the mass flow rate of the furfural plant effluent fed into the MBR (kg.s^{-1}).
m_e is the mass flow rate of evaporation from the MBR (kg.s^{-1}).
m_{sw} is the mass flow rate of sludge wasting from the MBR (kg.s^{-1}).
m_p is the mass flow rate of the permeate from the MBR (kg.s^{-1}).

Assuming a uniform density throughout the reactor, equal to that of water (1 000 kg.m^{-3}), the mass balance may be written in volumetric terms as follows:

$$q_o = q_e + q_{sw} + q_p \qquad (6\text{-}2)$$

Where:

q_o is the volumetric flow rate of the furfural plant effluent fed into the MBR (m^3.s^{-1}).
q_e is the volumetric flow rate of evaporation from the MBR (m^3.s^{-1}).
q_{sw} is the volumetric flow rate of sludge wasting from the MBR (m^3.s^{-1}).
q_p is the volumetric flow rate of the permeate from the MBR (m^3.s^{-1}).

Although q_e is the flow rate of evaporation from the MBR it is modelled a liquid stream leaving the MBR to determine the effect it has on the overall mass balance. Under this assumption it has the same density as the liquid streams which allows the simplification to Eq. 6-2.

6.1.2. Component mass balances

Complete mixing has been assumed for the mass balance model, therefore the concentrations of each of the components in the exit streams (permeate and sludge wasting) are taken to be equal to the concentrations of each component within the MBR.

6.1.2.1. Readily biodegradable substrate

S_S enters the MBR with the feed, exits through the sludge wasting and permeate streams, and is consumed by reaction. It was assumed that S_S can pass through the membrane sheets with the permeate. As the furfural plant effluent to the MBR is primarily acetic acid (Table 3.1), S_S is assumed to consist entirely of acetic acid. Therefore all stoichiometric equations were written in terms of acetic acid. The mass balance for the substrate may be represented as follows:

$$\frac{d(VS_S)}{dt} = q_o S_{S,o} - q_{sw} S_{S,sw} - q_p S_{S,p} + r_{S_S} V \qquad (6\text{-}3)$$

Where:

$S_{S,o}$ is the concentration of the substrate in the furfural plant effluent stream (kg.m^{-3}).

$S_{S,sw}$ is the concentration of the substrate in the sludge wasting stream (equal to residual substrate concentration S_S) (kg.m^{-3}).

$S_{S,p}$ is the concentration of substrate in the permeate (equal to residual substrate concentration S_S) (kg.m^{-3}).

r_{S_S} is the rate of consumption of the substrate (kg.m^{-3}.s^{-1}).

V is the volume of the mixed liquor within the MBR (m^3).

6.1.2.2. Active heterotrophic biomass

The model assumes no biomass enters the MBR (sludge dosing from the neighbouring CAS plant is not considered); it is only generated from biodegradation of readily biodegradable substrate. The biomass is modelled with complete retention within the MBR; it is assumed it does not pass through the membrane sheets, and can only be removed through sludge wasting. For the particular system under study, illustrated in Fig. 6.1, the mass balance for active biomass is as follows:

$$\frac{d(VX_H)}{dt} = -q_{sw} X_{H,sw} + r_{X_H} V \qquad (6\text{-}4)$$

Where:

$X_{H,sw}$ is the concentration of the biomass in the sludge wasting stream (equal to residual biomass concentration X_H) (kg.m^{-3}).

r_{X_H} is the biomass growth rate (kg.m^{-3}.s^{-1}).

6.1.2.3. Inert organic matter from decay

X_P is generated during the decay of biomass and is retained within the MBR. It can only be removed through sludge wasting. The mass balance for X_P within the MBR may be written as follows:

$$\frac{d(VX_P)}{dt} = -q_{sw}X_{P,sw} + r_{X_P}V \qquad (6\text{-}5)$$

Where:

$X_{p,sw}$ is the concentration of inert organic matter from decay (equal to residual inert organic matter concentration X_P) (kg.m^{-3}).

r_{X_P} is the rate of inert organic matter from decay formation (kg.m^{-3}.s^{-1}).

6.1.2.4. Oxygen uptake by biological reaction

The oxygen that is consumed for the growth and decay of biomass may be represented solely by the reaction rate of the oxygen for biological means. This is not a mass balance on oxygen within the MBR, and therefore it is not an indication of the DO concentrations within the MBR, it is only representing the rate at which oxygen within the MBR is consumed. This is important in the modelling of the glass reactor vessel where the experimental work was performed, as it is directly linked to the OUR that is measured. However, this was not modelled for the continuous model of the MBR.

$$\frac{d(VS_o)}{dt} = -r_{S_o}V \qquad (6\text{-}6)$$

Where:

r_{S_o} is the rate at which oxygen is consumed (kg.m^{-3}.s^{-1}).

6.1.3. Process kinetics and stoichiometry

A modified form of the traditional modelling approach was used for the kinetic description of the MBR and glass reactor vessel. In the traditional modelling approach respiration is associated separately with the growth and decay of micro-organisms. A modification was made to the traditional modelling approach in that X_S was neglected, as the substrate entering the reactor with the feed is predominantly acetic and formic acid. The main processes that occur for heterotrophic growth and decay in the modified model are shown in Fig. 6.2.

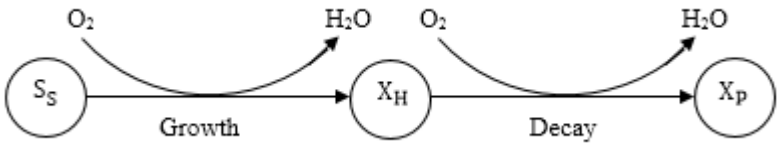

Figure 6.2. Modified traditional modelling approach, in which slowly biodegradable substrate is neglected. Adapted from Vanrolleghem (2002).

The two processes of growth and decay may be represented accordingly by their associated reactions, Eq. 2-2 and 2-1. The model kinetics and stoichiometry, following Fig. 6.2 are represented by the model's Gujer matrix in Table 6.1, with units of mg.L^{-1}. f_P is the fraction of biomass that becomes inert matter from decay of biomass, X_P.

Table 6.1. Gujer matrix for the traditional modelling approach.

i	Components →	1	2	3	4	
j	Processes ↓	S_S	X_H	X_P	S_O	
1	Aerobic growth of biomass	$-1/Y$	1		$(1-Y)/Y$	$\frac{\mu_m S_S X_H}{K_S + S_S}$
2	Biomass decay		-1	f_P	$(1-f_p)$	$k_d X_H$
		Readily biodegradable substrate	Active heterotrophic biomass	Inert organic matter from decay	Oxygen uptake	

Temperature dependency of kinetic parameters

The effect of temperature on the reaction rate of a biological process can be expressed, using a modification of the van't Hoff-Arrhenius relationship (Eddy *et al.*, 2003), as follows:

$$k_{T_k 2} = k_{T_k 1}\theta^{(T_k 1 - T_k 2)} \qquad (6\text{-}7)$$

Where:

$k_{T_k 2}$ is the coefficient at temperature $T_k 2$.

$k_{T_k 1}$ is the coefficient at temperature $T_k 1$.

θ is the temperature-activity coefficient.

$T_k 1$ and $T_k 2$ are the reference and actual temperatures, respectively (K).

6.1.4. Mass balance model calculated outputs

To compare model outputs to plant data and to literature several important calculated outputs are defined mathematically. Calculated outputs are variables calculated from state variables, or a combination of state variables and parameters.

6.1.4.1. Total VSS

The production of VSS within the MBR may be defined as the sum of X_H and X_P.

$$X_{VSS} = X_H + X_P \quad (6\text{-}8)$$

Where:

X_{VSS} is the concentration of VSS within the reactor (kg.m^{-3}).

6.1.4.2. Active biomass

The fraction of active biomass in the mixed liquor VSS (MLVSS) is the ratio of the active biomass produced divided by the total MLVSS production.

$$F_{x,act} = X_H / X_{VSS} \quad (6\text{-}9)$$

Where:

$F_{x,act}$ is the active fraction of biomass in MLVSS (kg.kg^{-1}).

6.1.4.3. Observed yield

The observed yield (Y_{obs}) accounts for the actual solids production that would be measured within the MBR divided by the substrate that has been fed, and is as follows:

$$Y_{obs} = \frac{q_{sw} X_{VSS}}{q_o S_S} \quad (6\text{-}10)$$

6.2.pH prediction

In this modelling approach, the total composition in terms of components at each point in time is fed to the speciation sub-routine of Brouckaert *et al.* (2010). The parameters of interest that the speciation routine outputs are the pH of the solution, the activity coefficients (γ), the concentrations of the species (c), as well as the dissolved CO_2 concentration. The driving force for CO_2 transfer depends on the dissolved $CO_{2(aq)}$ concentration and the partial pressure of $CO_{2(g)}$ in air. The rate of $CO_{2(g)}$ evolution controls the accumulation of dissolved $CO_{2(aq)}$ and therefore can strongly influence the system pH. This is illustrated in Fig. 6.3. The two right hand steps are effectively instantaneous, while the two left hand ones are substantially slower. Therefore if the biological system is producing more aqueous CO_2, it tends to distribute to the right of Fig. 6.3 while the accumulated CO_2 is transferred out of the system. This results in a transient H^+ and a lower pH.

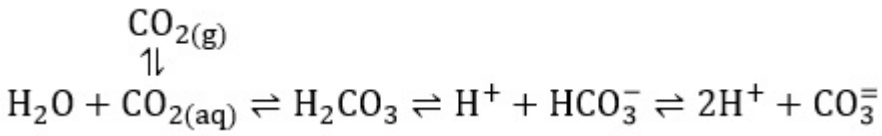

Figure 6.3. Different forms of carbonate.

6.2.1. CO_2 evolution rate

CO_2 is highly soluble in water, its transfer is a rate limited process which is usually modelled as a linear driving force process as follows (Brouckaert and Brouckaert, 2014a):

$$CO_2\ rate = K_{ev,CO_2} V \left(P_{CO_2,eq} - P_{CO_2}\right) \qquad (6\text{-}11)$$

Where:

K_{ev,CO_2} is the rate constant for CO_2 evolution per unit liquid based on the partial pressures (mol.Pa^{-1}.m^{-3}.s^{-1}).

$P_{CO_2,eq}$ is the partial pressure of CO_2 in equilibrium with the actual solution composition (Pa).

P_{CO_2} is the partial pressure of CO_2 in the gas contacting liquid (Pa).

$P_{CO_2,eq}$ can be calculated from Henry's law as follows (Brouckaert and Brouckaert, 2014a):

$$P_{CO_2,eq} = H_{CO_2} b_{H_2CO_3} \qquad (6\text{-}12)$$

Where:

H_{CO_2} is the Henry's law constant (Pa.kg.mol^{-1}).

$b_{H_2CO_3}$ is the molality of aqueous species H_2CO_3 (mol.kg^{-1}).

The Henry's law constant can be related to the formation constant for CO_2. The formation of CO_2 can be expressed in terms of the speciated components as follows:

$$2H^+ + CO_3^{2-} \rightarrow CO_{2(g)} + H_2O \qquad (6\text{-}13)$$

The formation constant can be expressed as a function of temperature (Brouckaert and Brouckaert, 2014a):

$$K_{f,CO_2} = 10^{\left(\left(18.147\times10^{4060}\left(\frac{1}{T_k}\right)-\frac{1}{298.15}\right)/(2.303\times8.314)\right)} \qquad (6\text{-}14)$$

Where:

K_{f,CO_2} is the formation constant for Eq. 6-13 (Pa.mol^3.kg^{-3}).

T_k is the temperature (K).

In this case the partial pressure of CO_2 can be calculated by (Brouckaert and Brouckaert, 2014a):

$$P_{CO_2,eq} = K_{f,CO_2}\gamma_{H^+}^2 {b_{H^+}}^2 \gamma_{CO_3^{2-}}\, b_{CO_3^{2-}} \qquad (6\text{-}15)$$

Where:

b_{H^+}, $b_{CO_3^{2-}}$ is the molality of H^+ and CO_2^{2-} (mol.kg^{-1}).

γ_{H^+}, $\gamma_{CO_3^{2-}}$ is the activity coefficients of H^+ and CO_2^{2-}.

The activity coefficients of charged species deviate significantly from unity and therefore cannot be neglected.

P_{CO_2} can be calculated by estimating the mole fraction of CO_2 in the aeration gas to the MBR as follows:

$$P_{CO_2} = \frac{CO_2\ rate}{n_a}.P = \frac{K_{ev,CO_2}V(P_{CO_2,eq}-P_{CO_2})}{n_a}.P \qquad (6\text{-}16)$$

Where:

n_a is the molar flow rate of air into the MBR (mol.s^{-1}).

Rearranging Eq. 6-16 and solving for P_{CO_2} yields:

$$P_{CO_2} = \frac{P.P_{CO_2,eq}K_{ev,CO_2}V}{n_a+P.K_{ev,CO_2}V} \qquad (6\text{-}17)$$

6.2.2. Component mass balance

The two processes that occur, aerobic growth of biomass and biomass decay (Eq. 2-2 and 2-1), can be represented by their associated reactions in molar form with CH_3COO^- as the carbon source:

Aerobic growth of biomass on acetate (macro-chemical reaction)

$$aCH_3COO^- + bNH_4^+ + cH^+ + dO_2 + eH_2O + 1C_5H_7O_2N + fHCO_3^- = 0 \qquad (6\text{-}18)$$

Biomass decay

$$C_5H_7O_2N + 5O_2 + 3H_2O \rightarrow 5HCO_3^- + NH_4^+ + 4H^+ \qquad (6\text{-}19)$$

To determine the stoichiometry of reaction 6-38, Y must be specified, the macro-chemical equation is a combination of the anabolic and catabolic reactions:

Catabolic reaction

$$CH_3COO^- + 2O_2 \rightarrow 2HCO_3^- + H^+ \qquad (6\text{-}20)$$

Anabolic reaction

$$CH_3COO^- + \frac{2}{5}NH_4^+ + \frac{3}{5}H^+ \rightarrow \frac{2}{5}C_5H_7O_2N + \frac{6}{5}H_2O \qquad (6\text{-}21)$$

The manner in which the anabolic and catabolic reactions are combined to form the macro-chemical equation is defined by Y (in COD units). The macro-chemical equation can be determined by the sum of the Y multiplied by the anabolic reaction and $(1-Y)$ multiplied by the catabolic reaction as follows:

$$CH_3COO^- + 2(1-Y)O_2 + \frac{2}{5}YNH_4^+ \rightarrow 2(1-Y)HCO_3^- + \left(\left(\frac{5}{2Y}\right) - 4\right)H^+ + \frac{2}{5}YC_5H_7O_2N + \frac{6}{5}YH_2O \qquad (6\text{-}22)$$

Rearranging the reaction and assigning biomass a stoichiometric coefficient of 1, yields:

$$\left(\frac{5}{2Y}\right)CH_3COO^- + \left(\frac{5(1-Y)}{Y}\right)O_2 + NH_4^+ \rightarrow \left(\frac{5(1-Y)}{Y}\right)HCO_3^- + \left(\left(\frac{5}{2Y}\right) - 4\right)H^+ + C_5H_7O_2N + 3H_2O \qquad (6\text{-}23)$$

The mass balance model was modified in order to accommodate for the speciation routine. The ions that were expected to have a significant effect on the pH were determined, acetate (CH_3COO^-) ammonium ion (NH_4^+), carbonate ion (CO_3^{2-}), phosphate ion (PO_4^{3-}), and the hydrogen ion (H^+).

At the expected pH of operation HCO_3^- will have a greater effect on the pH, however CO_3^{2-} is used in the speciation routine as a convention, similar to other packages (PHREEQC and MINTEQA2). It is an arbitrary choice, since stoichiometry only needs to account for the elemental balances, not the actual state of the solution.

Reactions 6-41 and 6-37 were converted into ionic form as follows:

Aerobic growth of biomass

$$\left(\frac{5}{2Y}\right)CH_3COO^- + \left(\frac{5(1-Y)}{Y}\right)O_2 + NH_4^+ \rightarrow \left(\frac{5(1-Y)}{Y}\right)CO_3^{2-} + \left(\frac{15-18Y}{2Y}\right)H^+ + C_5H_7O_2N + 3H_2O \qquad (6\text{-}24)$$

Biomass decay

$$C_5H_7O_2N + 5O_2 + 3H_2O \rightarrow 5CO_3^{2-} + NH_4^+ + 9H^+ \qquad (6\text{-}25)$$

The Gujer matrix in Table 6.1 can be modified to represent the reactions on a molar basis as a function of the process reaction rates (Table 6.2), all units are in $mol.L^{-1}$. The CO_2 rate is included in the model due to its effect on the pH, the associated reaction is Eq. 6-13.

Table 6.2. Modified Gujer matrix using ionic components.

i	Components →	1	2	3	4	5	
j	Processes ↓	CH_3COO^- (S_S)	H^+	NH_4^+	CO_3^{2-}	PO_4^{3-}	
1	Aerobic growth of biomass	$-\left(\frac{5}{2Y}\right)$	$\left(\frac{15-18Y}{2Y}\right)$	-1	$\left(\frac{5(1-Y)}{Y}\right)$	-	$\frac{\mu_m S_S X_H}{K_S + S_S}$
2	Biomass decay	-	9	1	5	-	$(1-f_P)k_d X_H$
3	CO_2 rate	-	-2	-	-1	-	$K_{ev,CO_2} V.$ $(P_{CO_2,eq} - P_{CO_2})$

The mass balance equations for each of the species follows that of the soluble species, in that it exits the MBR with the sludge wasting and permeate stream.

Hydrogen ion

$$\frac{dN_{H^+}}{dt} = n_{H^+,0} - n_{H^+,sw} - n_{H^+,p} + \dot{r_{H^+}} V \quad (6\text{-}26)$$

Ammonium ion

$$\frac{dN_{NH_4^+}}{dt} = n_{NH_4^+,0} - n_{NH_4^+,sw} - n_{NH_4^+,p} + \dot{r_{NH_4^+}} V \quad (6\text{-}27)$$

Carbonate ion

$$\frac{dN_{CO_3^{2-}}}{dt} = n_{CO_3^{2-},0} - n_{CO_3^{2-},sw} - n_{CO_3^{2-},p} + \dot{r_{CO_3^{2-}}} V \quad (6\text{-}28)$$

Phosphate ion

$$\frac{dN_{PO_4^{3-}}}{dt} = n_{PO_4^{3-},0} - n_{PO_4^{3-},sw} - n_{PO_4^{3-},p} + \dot{r_{PO_4^{3-}}} V \quad (6\text{-}29)$$

Where:

$n_{i,j}$ is the molar flow rate of component i in stream j (mol.s^{-1}).

$\dot{r_i}$ is the molar reaction rate of component i (mol.m^{-3}.s^{-1})

N_i is moles of component i (mol).

6.3.Energy balance model

The energy balance model of Sedory and Stenstrom (1995) was selected over a range of models due to its ability to give a complete breakdown of the heat exchange mechanisms occurring, and its extensive use by various authors ((LaPara and Alleman, 1999), (Gillot and Vanrolleghem, 2003), (Makinia *et al.*, 2005)). The model that is presented is applicable to a completely mixed

tank (lumped parameter) for modelling under non-steady state conditions. The assumption of complete mixing within the tank implies a uniform temperature, and an outlet stream temperature equal to that of the system.

The overall energy balance is represented by Eq. 2-13:

$$V\rho C_p \frac{dT}{dt} = Input(H_{liq}) - Output(H_{liq}) + Q$$

Where Q, is the sum of the various heat transfer terms illustrated in Fig. 6.4:

$$Q = Q_{SR} + Q_{AR} + Q_C + Q_{EV} + Q_A + Q_{TW,l} + Q_{RX} + Q_P \qquad (6\text{-}30)$$

Where:

Q_{SR} is the heat gain from solar radiation (W).
Q_{AR} is the heat loss from atmospheric radiation (W).
Q_C is the heat loss due to surface convection (W).
Q_{EV} is the heat loss due to surface evaporation (W).
Q_A is the heat loss due to aeration (W).
Q_{TW} is the heat loss due to convection from the tank sides and floor (W).
Q_{RX} is the heat gain from the exothermic reaction (W).
Q_P is the heat gain from the compressors (W).
$Input(H_{liq})/Output(H_{liq})$ is the enthalpy input/output terms respectively (W).

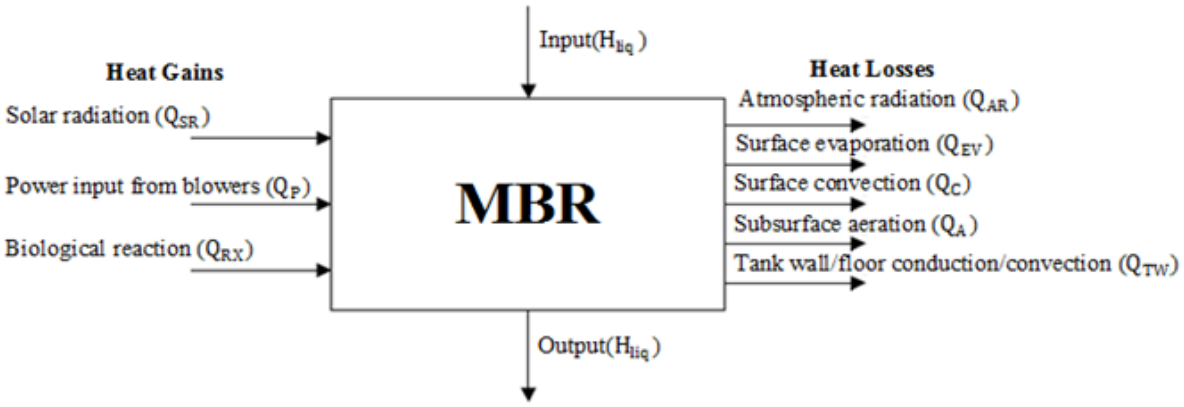

Figure 6.4. Aeration basin heat exchange components (Talati and Stenstrom, 1990).

6.3.1. Enthalpy

$Input(H_{liq})$ and $Output(H_{liq})$ is the heat provided or lost by the liquid streams entering the MBR (q_o) and the liquid streams exiting the MBR (q_{sw} & q_p), respectively. The enthalpy terms do not account for the enthalpy lost due to evaporation of water from the MBR, which is accounted for explicitly through the surface evaporation and aeration heat transfer terms.

The enthalpy terms are defined as follows:

$$Input(H_{liq}) = q_o \rho_l C_{p.l} T_i \quad (6\text{-}31)$$

$$Output(H_{liq}) = (q_{sw} + q_p)\rho_l C_{p.l} T \quad (6\text{-}32)$$

Where:

ρ_l is the density of water (kg.m^{-3}).
T_i is the influent temperature (°C).
T is the aeration basin temperature (°C).
$C_{p.l}$ is the specific heat of the reactor liquid contents (J.kg^{-1}.°C^{-1}).

6.3.2. Solar radiation

Energy from the Sun in the form of short wave radiation is an important factor for the heat balance of open surfaces. It is difficult to predict solar radiation as it depends on complex and unpredictable meteorological parameters which are further influenced by local environmental conditions.

A correlation was formed by Raphael (1962) to predict the contribution from solar radiation to the energy balance. The correlation is dependent on meteorological conditions, site latitude, and the day of the year.

$$Q_{SR} = H_{SR,0}(1 - 0.0071C_c^2)A_s \quad (6\text{-}33)$$

Where:

C_c is the cloud cover (tenths).
A_s is the surface area of the reactor contents in direct contact with the environment (m^2).
$H_{SR,0}$ is the average daily absorbed solar radiation for clear sky conditions (W.m^{-2}).

The solar radiation that is absorbed for clear skies depends on site latitude, season, and year; and should be estimated if meteorological data is not readily available. It may be calculated from a simplified form presented by Talati and Stenstrom (1990). Eq. 6-34 provides an averaged solar radiation over the entire day (night and day).

$$H_{SR,0} = a - b.sin\left(\frac{2\pi(d+183)}{366} + c\right) \quad (6\text{-}34)$$

Where:

d is the day of the year (out of 366).

The values for a, b and c are obtained from the following correlations:

$$a = (4.843 \times 10^{-5})(95.1892 - 0.3591l - 8.4537 \times 10^{-3} l^2)$$

$$b = (4.843 \times 10^{-5})(-6.2484 + 1.6645l - 1.1648 \times 10^{-2} l^2)$$

$$c = 1.4451 + 1.434 \times 10^{-2} l - 1.745 \times 10^{-4} l^2$$

Where:

l is the latitude of the reactor (°).

This correlation is valid between 26 ° and 46 ° latitude. Eq. 6-34 has a slight modification, the addition of 183 days, to adjust the equation for use in the Southern Hemisphere.

6.3.3. Atmospheric radiation

The heat exchange that results from atmospheric radiation is based on Stefan Boltzmann's fourth power radiation law. This is expressed as the difference between the incoming and back radiation, as follows:

$$Q_{AR} = [\epsilon\sigma(T_k)^4 A_s] - \left[(1-\lambda)\beta\sigma\left(T_{k,a}\right)^4 A_s\right] \quad (6\text{-}35)$$

Where:

ϵ is the water-surface emissivity.
σ is the Stefan Boltzman constant ($W.m^{-2}.K^{-4}$).
λ is the water-surface reflectivity.
β is the atmospheric radiation factor.
$T_{k,a}$ is the ambient temperature (°C).

The atmospheric radiation factor β ranges between 0.75 - 0.85 for most conditions. Most previous researchers have found that 0.97 and 0.03 are good estimates for the emissivity and reflectivity of water (ϵ and λ), respectively (Talati and Stenstrom, 1990).

6.3.4. Surface convection

The temperature difference between the air and the water surface provides the driving force for heat loss by surface convection. The following was obtained from Novotny and Krenkel (1973):

$$Q_C = \rho_g C_{p,g} h_v A_s (T - T_a) \quad (6\text{-}36)$$

Where:

ρ_g is the density of air (kg.m^{-3}).

$C_{p,g}$ is the specific heat of air at constant pressure (J.kg^{-1}.K^{-1}).

h_v is the convective transfer coefficient (m.s^{-1}).

The rate of convective heat loss is affected by the vapour transfer coefficient, which is a dependent on the wind velocity. The following equation was formed by Novotny and Krenkel (1973):

$$h_v = (4.537 \times 10^{-3}) A_s^{-0.05} W \qquad (6\text{-}37)$$

Where:

W is the wind velocity (m.s^{-1}).

6.3.5. Surface evaporation

The calculation of the heat loss due to evaporation is dependent on wind velocity, relative humidity, and temperature. Novotny and Krenkel (1973) correlated the following for evaporation, assuming that the heat and vapour transfer coefficients are similar:

$$Q_{EV} = \left[55.448\left(1 - \frac{r_h}{100}\right) + 3.322(T - T_a)\right] e^{0.0604 T_a} W A_s^{0.95} \qquad (6\text{-}38)$$

Where:

r_h is the relative humidity of ambient air (%).

6.3.6. Aeration

Aerobic biological wastewater systems are supplied with an additional amount of air to maintain sufficient DO concentrations. In the course of contact between air and water, evaporation of water to the air occurs. In the case of diffused aeration systems, the air bubbles are assumed to enter the MBR at ambient temperature and humidity, and leave the system with a temperature equal to the operating temperature of the MBR and saturated with water vapour (Novotny and Krenkel, 1973). The amount of water transferred depends on the air flow rate, tank temperature, ambient air temperature, and relative humidity.

Heat loss from aeration consists of two components: sensible and evaporative heat losses, it may be represented as:

$$Q_A = Q_{AS} + Q_{AL} \qquad (6\text{-}39)$$

Where:

Q_{AS} is the sensible heat loss due to aeration (W).

Q_{AL} is the evaporative heat loss due to aeration (W).

The driving force for sensible heat loss is the difference in temperature of air and water, and may be represented as:

$$Q_{AS} = q_g \rho_g C_{p,g}(T - T_a) \quad (6\text{-}40)$$

Where:

q_g is the mass flow rate of the air entering the MBR through aeration (kg.s^{-1}).

The second part of the aeration heat exchange is evaporation, and is dependent on the difference in the vapour pressure between the water and air. The equation was developed by Novotny and Krenkel (1973) and modified to this final form by Talati (1988):

$$Q_{AL} = \frac{MM_w q_g \Delta H_{vap}}{100R}\left\{\frac{v_w[r_h + h_f(100 - r_h)]}{(T+273.15)} - \frac{v_a r_h}{(T_a+273.15)}\right\} \quad (6\text{-}41)$$

Where:

R is the universal gas constant (8.314 J.mol^{-1}.K^{-1}).

v_a is the vapour pressure of water at air temperature (Pa).

v_w is the vapour pressure of water at reactor temperature (Pa).

h_f is the exit air humidity factor. It can be assumed to be 1, as air assumed to be saturated at exit.

MM_w is the molar mass of water (kg.mol^{-1}).

ΔH_{vap} is the latent heat of evaporation (J.kg^{-1}).

6.3.7. Tank wall and floor conduction/convection

Heat losses from the aeration tank walls and floor depend upon the material of construction, the heat transfer area, and its thickness. Heat transfer coefficients for the tank material to air and the tank material to earth are different. Therefore, this model has included two terms: one for the MBR wall area exposed to air and one for the MBR area exposed to the ground. The governing equation is as follows:

$$Q_{TW} = U_{a/g} A_l (T - T_{a/g}) \quad (6\text{-}42)$$

Where:

$U_{a/g}$ is the overall heat transfer coefficient for conduction from liquid phase through the reactor walls to air/ground (W.m^{-2}.K^{-1}).

A_l is the area of the reactor that surrounds the liquid phase (m^2).

$T_{a/g}$ is the temperature of the air/ground (K).

Determination of the overall heat transfer coefficient is as follows:

$$U = \frac{1}{\frac{1}{K_i}+\frac{x_1}{k_1}+\frac{x_2}{k_2}.....+\frac{1}{K_0}} \qquad (6\text{-}43)$$

Where:

x_i is the thickness of materials (m).

k_1 is the thermal conductivity of materials (W.m^{-1}.K^{-1}).

K_i is the surface conductance at the air-surface area inside the basin (W.m^{-2}.K^{-1}).

K_0 is the surface conductance at the air-surface area outside the basin (W.m^{-2}.K^{-1}).

The factor $1/K_i$ becomes zero if liquid is touching the surface of the wall. If the outside wall is in contact with air an approximate value of K_0 is taken as 33.90 W.m^{-2}.K^{-1}. If the wall is surrounded by an earth embankment greater than 3 m thick, K_0 becomes 0.285 W.m^{-2}.K^{-1} (Sedory and Stenstrom, 1995).

6.3.8. Heat of reaction

The heat released by the biological process depends on the heat of the reaction of the individual sub-processes and the amount of material that undergoes reaction. In a biological process, the exact process that takes place depends on the composition and concentration of the wastewater. The heat generated from reaction is calculated for the two principle reactions that occur within the system, the growth of biomass and the subsequent oxidation of decaying biomass (endogenous respiration). The first term in Eq. 6.44 is the heat released from the growth of biomass according to Eq. 6-18, while the second term is the fraction of biomass that is oxidised according to Eq. 6-19. The remaining fraction, defined by f_P, is the biomass which becomes inert organic matter from decay X_P.

$$Q_{RX} = \left[\frac{\mu_m S_S X_H}{K_S+S_S}\Delta H_{rxn,X_H} + (1-f_P)k_d X_H \Delta H_{rxn,d}\right]V \qquad (6\text{-}44)$$

Where:

$\Delta H_{rxn,X_H}$ is the heat of the macro-chemical reaction (6-18) (J.mol X^{-1}).

$\Delta H_{rxn,d}$ is the heat of endogenous respiration reaction (6-19) (J.mol X^{-1}).

The heats of reaction are assumed to be independent of temperature, and calculated at standard conditions following Eq. 2-8. The heat of reaction for growth ($\Delta H_{rxn,X_H}$) is dependent on the macro-chemical reaction and therefore Y.

6.3.9. Mechanical power

In diffused aeration systems, heat is supplied to the air stream through the process of compression. The heat input to the system is dependent upon the efficiency of the compressor. A fraction of the temperature increase during compression is lost as the bubbles expand when they rise through the medium. Only the efficiencies of the compressor can be converted into heat gain for the aeration system. Power losses in motors and gearboxes, which can be between 10 and 20 %, are neglected.

$$Q_P = B(1 - \eta/100) \qquad (6\text{-}45)$$

Where:

B is the power of the aerator/compressor (W).

η is the efficiency of the aerator/compressor (%).

6.4.Assumptions and limitations of the model

The assumptions and limitations of the combined mass and energy balance model are listed below:

- A lumped parameter model was to be used to describe the MBR and glass reactor vessel.
- The MBR model does not account for the dosing of WAS from the neighbouring CAS, and cannot predict the effects this would have on the operation of the MBR.
- The kinetic description of the temperature regimes was limited to one biomass population, in reality this may not be the case, further studies would be required.
- The model was designed for operation between 40 and 50 ºC, any temperatures below 40 ºC and above 50 ºC would require extrapolation of the model.
- The model accounts for the energy associated with aeration of the MBR, but assumes that the oxygen supply was not limiting, and so does not account for the effect of the DO concentration on biomass activity. Only the OUR of the biological system is modelled.
- It was assumed that the furfural plant effluent fed to the MBR consists entirely of acetic acid, and is a readily biodegradable substrate. The possible inhibitory effects of trace amounts of furfural contained within the feed are not considered.

6.5.MATLAB

The mass balance, energy balance, and speciation routine, as well as the kinetic regression was simulated on MATLAB R2010a. MATLAB's primary purpose is for numerical computing, it allows matrix manipulations, plotting of functions and data, and implementation of algorithms. MATLAB contains built in functions for ease of use and greater calculation speeds.

For the mass balance a batch system was modelled for the experimental work involving the respirometer, and a continuous system was modelled to describe the MBR. The energy balance and speciation routine were also modelled alongside the continuous mass balance. For the continuous mass balance Eq. 6-1 to 6-5 were used, with the kinetics of section 6.1.3. The batch system was similarly modelled, however with the addition of Eq. 6-6 and the flow rates into and out of the reactor neglected. The energy balance was simulated using the heat transfer terms described in section 6.3, and is linked to the mass balance primarily through the enthalpy terms and the heat of reaction. The speciation routine is a C++ code, termed 'IonicSpeciation', formulated by Brouckaert *et al.* (2010), that has been compiled into a binary MEX-file, which is callable from MATLAB. The MATLAB code for the MBR model can be found in Appendix H.

The mass balance, energy balance and speciation routine model forms a set of ODE's. Their solution was found through numerical methods which involve the calculation of the evolution of the state variables with time from a set of initial conditions, termed an initial value problem. The MATLAB function used for the integration of the model derivatives was 'ode23t' as well as 'ode45', they are used to solve initial value problems for ODE's. 'ode23t' is used for moderately stiff systems with a low order of accuracy and is an implementation of an implicit Runga-Kutta formula with a first stage that is a trapezoidal and a second stage that is a backward differentiation formula of order two, the same iteration matrix is used in evaluating both stages. 'ode45' is used for non-stiff systems with a medium order of accuracy. Its implementation is based on Runga-Kutta formula, the Dormand-Prince pair, and is a one-step solver (MATLAB, 2010).

The procedure that was followed in the simulation coding was to initially define all the mass balance, energy balance and speciation routine variables. The initial values for the integration were subsequently estimated, and the feed concentrations to the MBR were specified. The integration was then setup by initialising variables and defining the time step of the integration. The integration involved a loop whereby each time step was integrated, after each step the mass balance constraints were checked, the state variables stored for plotting, and the biomass viability with respect to pH updated. The integrator 'ode23t' calls up the integrand function 'Integrator_Integrated_Model_Final' which contains the ODE's, termed the 'rhs' (right hand side).

The integrand is setup as follows:

rhs (1,1) → Eq. 6-3
rhs (2,1) → Eq. 6-4
rhs (3,1) → Eq. 6-5
rhs (4,1) → Eq. 2-13
rhs (5,1) → Eq. 6-26
rhs (6,1) → Eq. 6-27
rhs (7,1) → Eq. 6-28
rhs (8,1) → Eq. 6-29

The integrand function calls up the MEX-file, 'IonicSpeciation', which is used as a black-box function to determine the CO_2 evolution rate, which allows the calculation of rhs (5,1) to rhs (8,1).

The kinetic parameter regressions of μ_m and K_S was performed on MATLAB R2010a, the MATLAB code can be found in Appendix I. The function used for the regression of kinetic parameters was a minimisation routine, 'fmincon'. It finds the minimum of a scalar function of several variables starting at an initial estimate for each of the variables; this is generally termed nonlinear optimisation. A Nelder-Mead simplex algorithm is used to search for the minimum (MATLAB, 2010). To calculate the 95 % confidence interval for the non-linear regression the 'nlinfit' and 'nlparci' functions were used. The 'nlinfit' function was intiallly used which outputs the Jacobian, residuals and coefficients of the regression. These values were then inputted to the 'nlparci' function which outputs the 95 % confidence interval for the regression.

In the kinetic parameter regression the respirometer was modelled as a batch system. In the primary function the experimentally determined OUR data was called up. Initial estimates of the kinetic parameters were defined, and initial S_S and X_H values obtained experimentally were stated. The minimisation routine was subsequently setup, and run, which called the minimisation function termed 'min_func'. The minimisation function sets up the integration with 'ode45' which in turn calls up the integrand 'integrator_kin'. The integrand contains the ODE's for the batch system, the ODE's describe S_O, X_H, and S_S. After the numerical integration the minimisation function compares the predicted OUR to the experimental OUR by calculating the sum of squared error (SSE), and adjusts the kinetic parameters accordingly until a best fit is obtained. When the SSE between the predicted and experimental OUR was found to be in the specified tolerance the routine was terminated. The 95 % confidence interval of the fitted parameters were then subsequently determined using MATLAB's built-in 'nlinfit' and 'nlparci' functions.

7. EXPERIMENTAL RESULTS

The experimental work performed involved obtaining the kinetic and stoichiometric parameters, detailed in section 5.5.4, through respirometric techniques. The tests were done at a mesophilic temperature of 40 ºC and a thermophilic temperature of 50 ºC. The Cyclic OUR Test was performed to obtain k_d, and the Dynamic Response Test was performed to determine Y. This then allowed for the regression of μ_m and K_S, by fitting the predicted OUR for the batch type model to the experimental data obtained from the Dynamic Response Test.

7.1.Specific death rate constant k_d

Grab samples were taken directly from the MBR tank, and placed into the respirometer's glass reactor vessel. To determine k_d for the heterotrophic biomass the samples were aerated until endogenous respiration was reached. This is indicated by the exponential decay of the OUR, evidenced after the initial drop in the OUR once external substrate has been depleted. The cyclic OUR mode of the respirometer was used to test for k_d. k_d is equal to the negative slope of the natural logarithm of the OUR versus time. The tests for k_d was performed at a mesophilic temperature of 40 °C and a thermophilic temperature of 50 °C, respectively.

7.1.1. Mesophilic k_d (40 °C)

Cyclic OUR Tests were performed on the BM-EVO respirometer at 40 °C for three separate samples. The results of the first sample are shown, the remaining two results that were generated by the experimental device are shown in Appendix G. The OUR profile generated by the respirometer is shown in Fig. 7.1. The test reached endogenous respiration relatively quickly, from which the OUR followed an exponential decline.

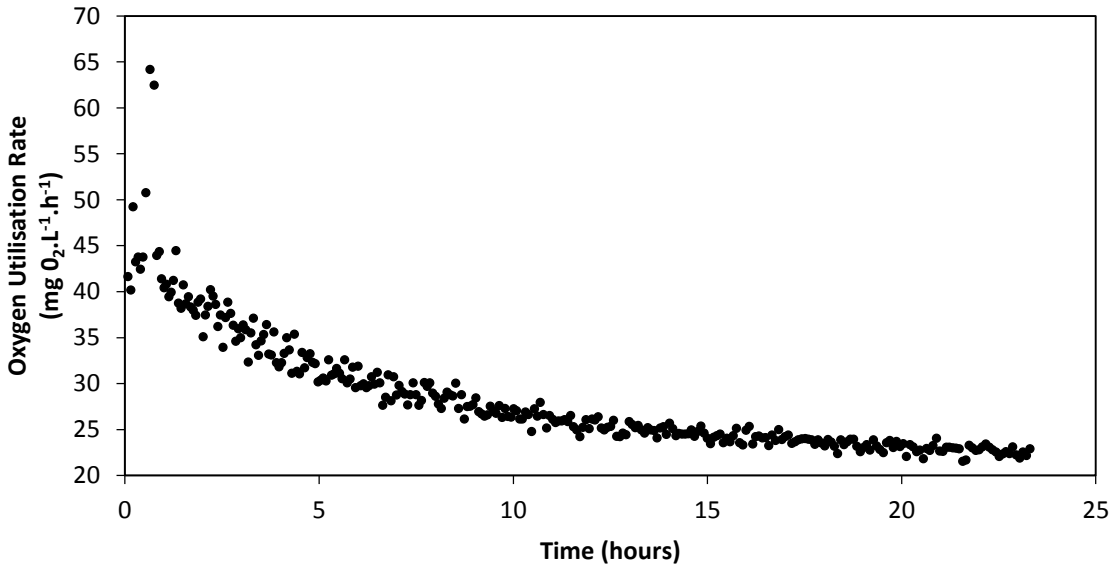

Figure 7.1. Oxygen utilisation rate generated by experimental OUR test at a mesophilic temperature.

The OUR verse time curve was plotted on semi-log axes in Fig. 7.2 over the entire experimental period.

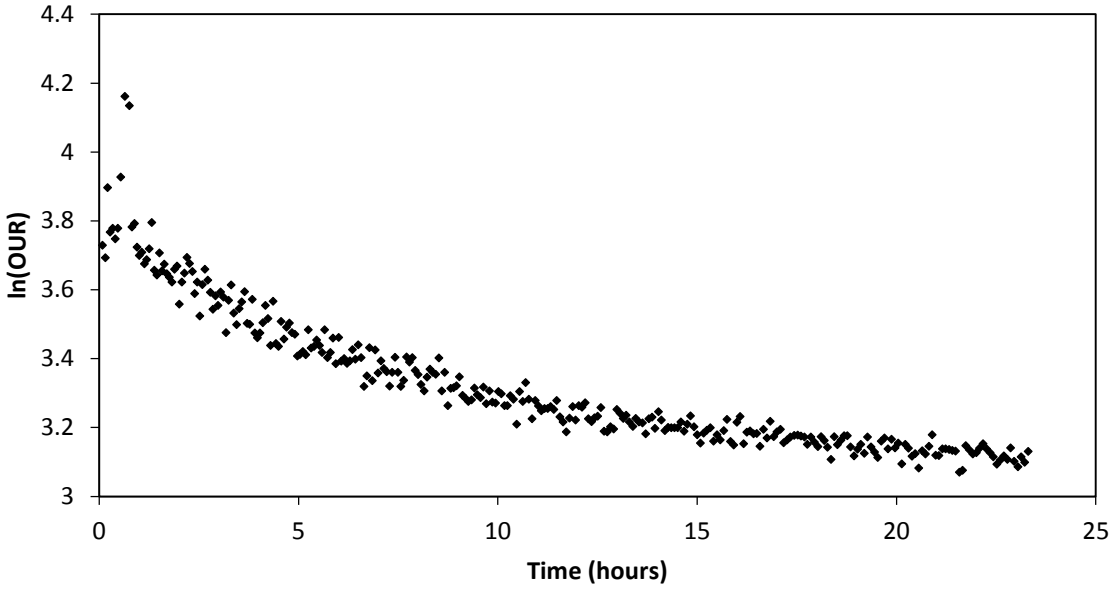

Figure 7.2. Natural logarithm of the oxygen utilisation rate versus time for the entire experimental period.

The data was regressed from just past the 12 hour mark where the linear section started. The data was analysed by statistical methods with the upper and lower 95 % prediction bounds for the fitted line determined for non-simultaneous bounds.

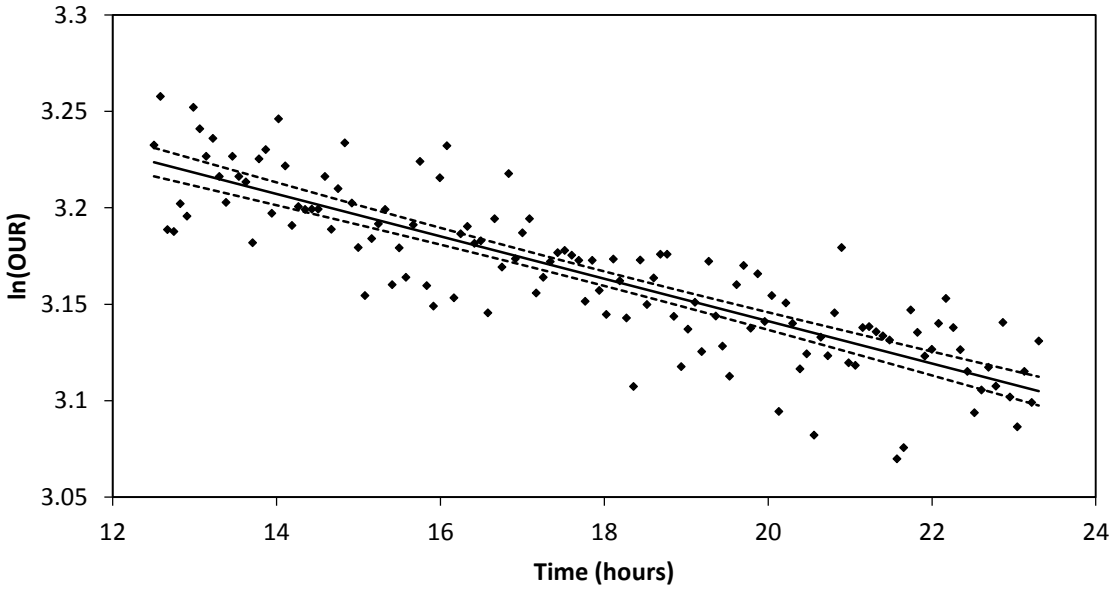

Figure 7.3. Natural logarithm of the oxygen utilisation rate versus time taken at endogenous respiration (R^2 = 0.725).

The negative slope of the regressed line is displayed in Table 7.1. The 95 % confidence interval shows a good fit to the experimental data.

Table 7.1. Oxygen utilisation rate test regression result.

Test T (°C)	k_d (h^{-1})
40	0.0110 ± 0.0012*

*95 % confidence interval

7.1.2. Thermophilic k_d (50 °C)

The Cyclic OUR Test was performed on the BM-EVO respirometer at 50 °C for two separate samples. The first test that was generated by the experimental device is shown in Fig.7.4, the second test may be found in Appendix G.

The activated sludge sample reached endogenous respiration rapidly for thermophilic operation. The generated OUR data shows irregular data around the 8 to 10 hour mark, this is a result of the DO probe being removed and cleaned, to remove the sludge which had accumulated around the probe which was affecting its measurement.

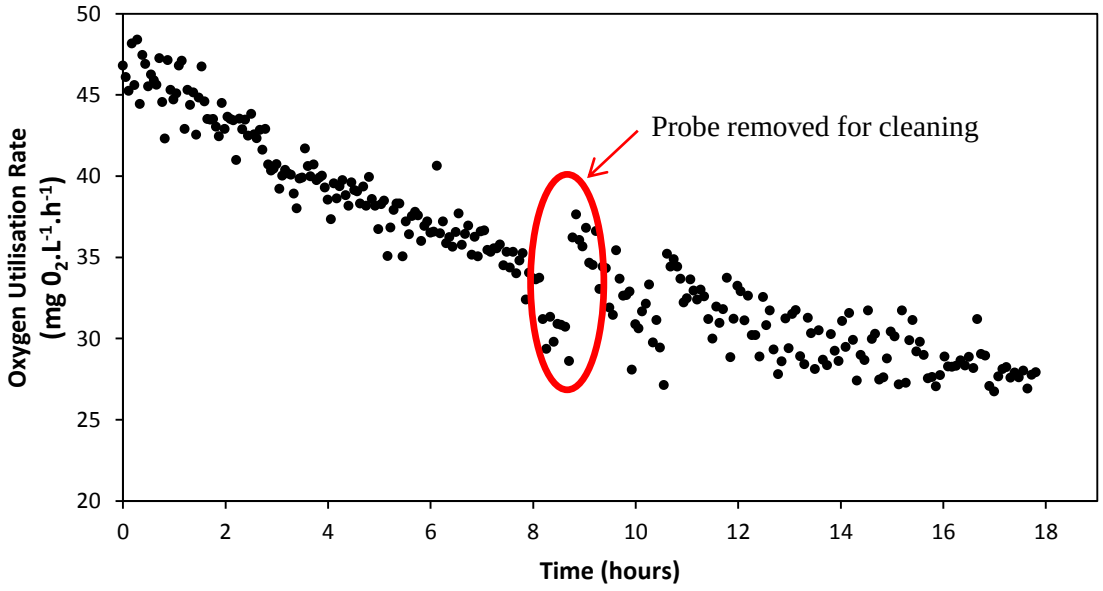

Figure 7.4. Oxygen utilisation rate generated by experimental OUR test at a thermophilic temperature.

As with the mesophilic test, the upper and lower 95 % prediction bounds for the fitted line were determined for non-simultaneous bounds. The natural logarithm of the OUR versus time is shown in Fig. 7.5. Even with the increased variance caused by cleaning of the probe a good fit was obtained, with an R^2 value of 0.901.

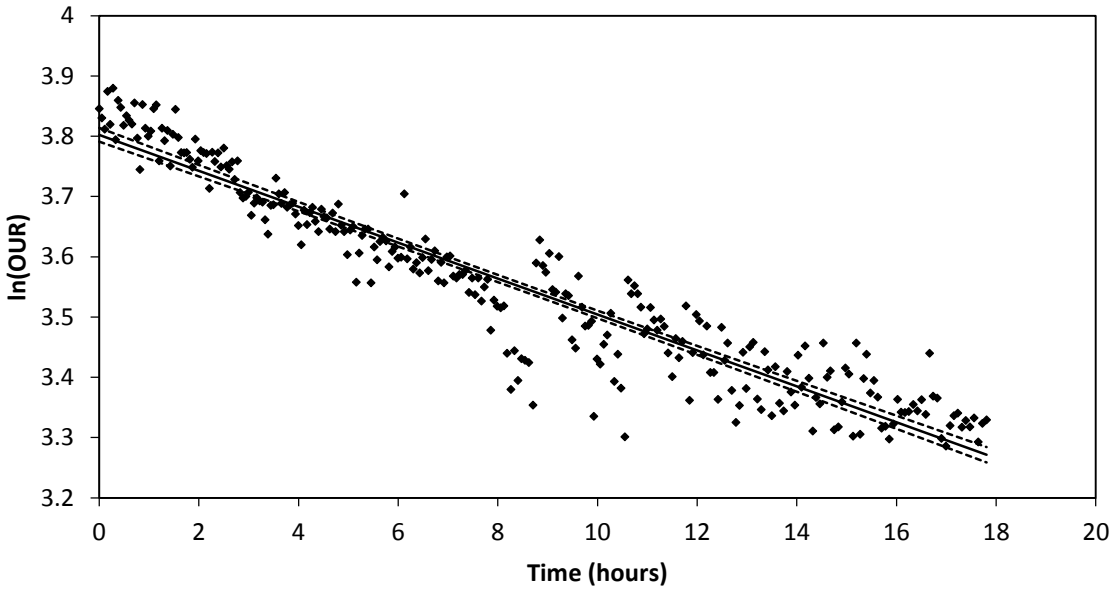

Figure 7.5. Natural logarithm of the oxygen utilisation rate versus time taken at endogenous respiration (R^2 = 0.901).

The negative slope of the regressed line is shown in Table 7.2, a good fit was obtained.

Table 7.2. Oxygen utilisation rate test regression result.

Test T (°C)	k_d (h^{-1})
50	0.0298 ± 0.0012*

*95 % confidence interval

7.1.3. Summary of k_d results

The results of the k_d tests are shown for all the replicate tests in Table 7.3, along with the averages for each temperature and their standard deviation.

There is a reasonable variance within the data of each of the individual semi-log plots, with 95 % confidence intervals between ±0.00045 and ±0.0013 h^{-1} for mesophilic and thermophilic regressions (Table 7.3). The small amount of variance within each of the tests is due to scatter around the average value, which arises due to the nature of the measurement and the non-homogenous nature of the reaction mixture. The non-homogeneity is caused by the imperfect distribution of the gas within the glass reactor vessel, imperfect mixing between the glass reactor vessel compartments, as well sludge build-up on the DO probe.

Table 7.3. Summary of specific death rate for mesophilic and thermophilic temperatures.

Test T (°C)	k_d (h^{-1})	Average k_d (h^{-1})
40	0.0110 ± 0.0012*	0.0123 ± 0.0053**
	0.0181 ± 0.0013	
	0.00776 ± 0.00045	
50	0.0298 ± 0.0012	0.0249 ± 0.0069
	0.200 ± 0.0010	

*95 % confidence interval, **standard deviation

However the k_d value between the individual Cyclic OUR Tests for mesophilic and thermophilic operation varies considerably more, with standard deviations between the individual death rates of 0.0053 and 0.0069 h^{-1} for mesophilic and thermophilic tests, respectively (Table 7.3). The variance that occurs between the tests is because the conditions are not replicated perfectly between the tests, so the sludge concentration and condition will not be the same. The sludge samples are highly heterogeneous and from different sources, with different histories, which results in the varying behaviour.

The variance between the samples is attributed to the MBR never completely operating at steady state, and therefore the conditions of the activated sludge differs for each of the samples that were taken from the MBR.

According to literature sources quoted in Table 2.2, k_d observed at thermophilic temperatures may be up to 10 times higher than those observed for mesophilic temperatures. Comparing the average k_d for the mesophilic temperature of 40 °C to the thermophilic temperature of 50 °C, there is a two-fold increase in k_d. Theoretical k_d predictions based on a thermodynamic correlation are presented in Appendix D, from which death rates of 0.005 and 0.0110 h^{-1} were obtained for 40 and 50 °C, respectively. The theoretically predicted k_d also show approximately a two fold increase between the two temperatures.

The data follows a similar trend to that of Abeynayaka (2009), where k_d was measured in a MBR, using sugar molasses as a carbon source (COD of 11 000 $mg.L^{-1}$). The death rates are presented in Table 2.3 for 30, 47 and 60 °C. Correlating this data to Eq. 6-7 predicts the temperature-activity coefficient (θ) to be 1.07 (Section 6.1.3). Correlating Eq. 6-7 to k_d obtained in this work for

mesophilic and thermophilic regimes gives an identical θ value of 1.07, confirming the trend observed with temperature.

7.2.Biological yield *Y*

Once the MBR sample within the respirometer had reached endogenous respiration, and directly after the Cyclic OUR Test had been performed for k_d, the Dynamic Response Tests were performed, and respirograms generated. *Y* and the kinetic parameters were determined from the resulting respirograms at the experimental temperatures. The Dynamic Response Test involved the injection of biodegradable substrate into the respirometer which generated a response, or increase in the OUR, with time. The substrate that was injected was the undiluted composite furfural plant effluent. The dosage of furfural plant effluent was varied until a suitable response was obtained which would allow for kinetic regression performed in section 7.3. The tests were performed at a mesophilic temperature of 40 °C and a thermophilic temperature of 50 °C.

7.2.1. Mesophilic *Y* (40 °C)

The Dynamic Response Tests were performed on an activated sludge sample at a mesophilic temperature of 40 °C. All testing was performed on the same activated sludge sample. The activated sludge was taken when the MBR was operating at a mesophilic temperature. In total 6 Dynamic Response Tests were performed for mesophilic operation, from which *Y* was calculated. The remaining results, which are repeats of substrate concentrations injected and therefore not illustrated, may be found in Appendix G.

The substrate was injected directly into the respirometer at the start of the test (Fig. 7.6). An initial lag phase was observed within the first five minutes, after which the maximum respiration rate was reached at between 40 and 45 (mg O_2).L^{-1}.h^{-1}. This trend was maintained until all the external substrate was depleted, causing the OUR to rapidly drop towards zero. The OUR did not reach a value of zero, after the rapid drop-off a gradual decline was observed towards an OUR of zero.

The eventual decline to an OUR of zero was not included, and the testing was stopped before zero was reached as its effect was deemed negligible on the *Y* calculation for the current model. Extrapolation of the decline and calculation of the consumed oxygen would yield at most an additional oxygen consumption of 0.4 mg O_2 or less, which would alter the calculated *Y* by no more than 1 % for each of the tests. As the effect of the growth of new biomass on the OUR was deemed to be negligible in Appendix B; it is expected that the cause of the gradual decline is a small amount of slowly biodegradable substrate being present in the injected wastewater. The effect of slowly biodegradable substrate is not modelled, and assumed negligible.

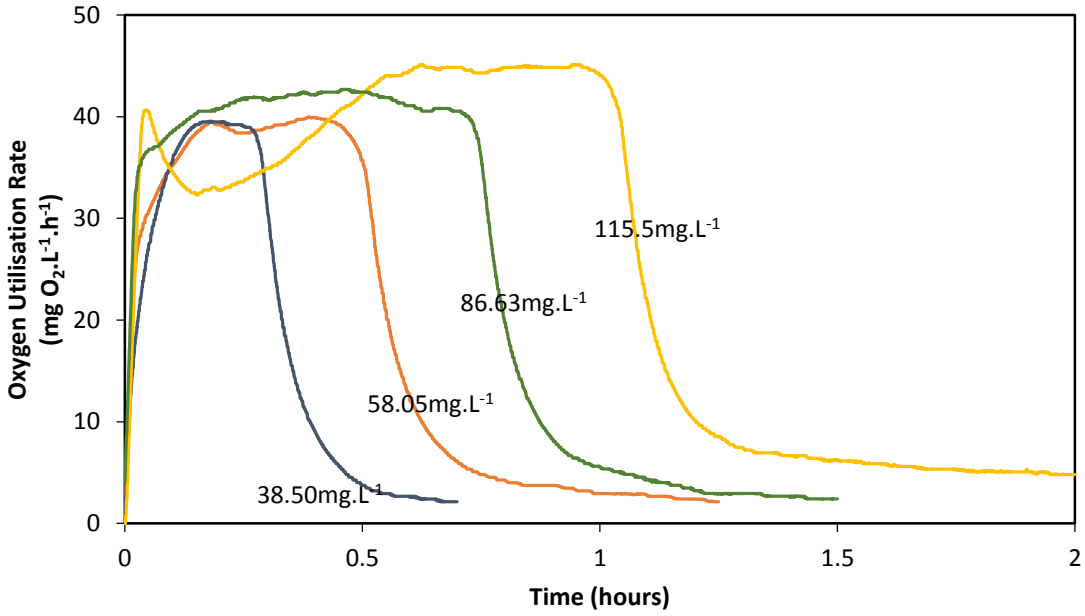

Figure 7.6. Summary of different types of OUR responses for a mesophilic temperature obtained for different COD concentrations.

Y was calculated from each of the respirograms in Fig. 7.6, as well as from those that are found in Appendix G. For the respirogram wherein 115.5 mg of COD was injected (Fig. 7.6), the maximum OUR was quickly reached followed by a dip and then an increase back to the maximum OUR. The cause of this phenomenon is not known, although it is expected that a type of inhibition occurred from the high concentration of substrate injected. This is not expected to have an effect on *Y*.

7.2.2. Thermophilic *Y* (50 °C)

The next set of Dynamic Response Tests were performed at a thermophilic temperature of 50 °C. A different sludge sample from mesophilic testing was used for the thermophilic tests; the mixed liquor sample was obtained when the MBR was operating at a thermophilic temperature. The Dynamic Response Test was performed when the sample had reached endogenous respiration, after the Cyclic OUR Test.

A summarised form of the Dynamic Response Tests are illustrated in Fig. 7.7. A total of four Dynamic Response Tests were performed for the thermophilic temperature. The yield was calculated from each of the respirograms in Fig. 7.7.

Y was calculated from the area under the graph, and compared to the substrate added (section 5.5.2). It was observed that the maximum respiration rate increased as the testing proceeded, with the first OUR at about 45 (mg O_2).L^{-1}.h^{-1} and the final OUR at 65 (mg O_2).L^{-1}.h^{-1}. An explanation for this phenomenon may be that either the growth of new biomass is substantial enough during the test to visibly and drastically increase the maximum observed OUR, or the

activated sludge reached a type of 'famine' induced dormancy, which was gradually overcome by the repeated addition of substrate. The idea that the OUR drastically increased from biomass growth due to substrate addition was ruled out, as the biomass concentration was estimated to be in the range of 1 000 (mg VSS).L^{-1} for the thermophilic Dynamic Response Tests (Appendix A). And therefore the amount of biomass growth from the added COD would not have significantly influenced the concentration.

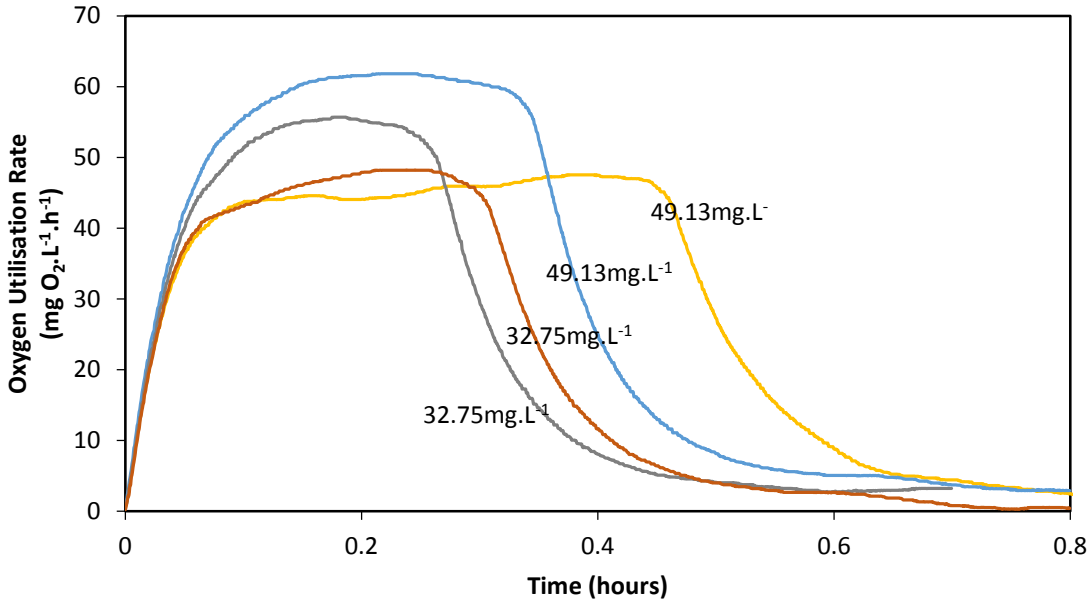

Figure 7.7. Summary of different types of OUR responses for a thermophilic temperature obtained for different COD concentrations.

The experiment was not repeated until the maximum OUR stopped changing between experiments, as the testing was halted before the OUR stabilised at a constant value. The maximum OUR that is achieved for each of the tests would not have an effect on *Y* calculation as it only depends on the total amount of oxygen consumed. However, the maximum OUR values does have an effect on the maximum growth rate (μ_m), casting some uncertainty on the estimation on this parameter for thermophilic temperatures, see Fig. 5.5.

7.2.3. Summary of *Y* results

A reliable value of *Y* was found for 40 and 50 °C, with standard deviations of 0.031 and 0.013 (mg COD biomass).(mg COD soluble)$^{-1}$, respectively.

The theoretical *Y* was calculated through the theoretical methods of Heijnen and Kleerebezem (2010) and Amy *et al.* (2011) in Appendix C, and was shown to be 0.625 and 0.585 (mg COD biomass).(mg COD soluble)$^{-1}$, respectively, at a temperature of 25 °C. This compares favourably with *Y* of 0.620 (mg COD biomass).(mg COD soluble)$^{-1}$ for 40 °C. *Y* for the thermophilic temperature of 50 °C is noticeably lower at 0.512 (mg COD biomass).

(mg COD soluble)$^{-1}$. Such a large change in *Y* was not expected in the results as only a small temperature dependence was expected, as illustrated by the data shown in Table 2.2 for Abeynayaka (2009).

Table 7.4. Summary of yield results for mesophilic and thermophilic temperature.

Test *T*	***Y***	**Average *Y***
(°C)	**((mg COD biomass). (mg COD soluble)$^{-1}$)**	**((mg COD biomass). (mg COD soluble)$^{-1}$)**
40	0.606	0.620 ± 0.031*
	0.574	
	0.665	
	0.630	
	0.634	
	0.613	
50	0.519	0.512 ± 0.013
	0.506	
	0.497	
	0.525	

*standard deviation

The amount of COD (furfural plant effluent) that was injected into the respirometer varied throughout the response tests. This was to determine the effect of the injection of a multitude of substrate concentrations into the respirometer. COD values between 32.8 mg and 86.6 mg produced respirograms for both mesophilic and thermophilic temperatures that were suitable for kinetic regression.

7.3.Kinetic regression

The kinetic regression was performed on the respirograms generated from the Dynamic Response Tests in section 7.2., neglecting the respirograms in which significant inhibition occurred. Only the portions of the respirograms suitable for the regression were used, as detailed in Fig. 5.5.

A batch type mass balance model was used, along with the kinetic description in section 6.1.3; the values of the two kinetic parameters that gave the best fit of the model formulation to the data were determined by regression. The respiration rate in the glass reactor was modelled in the

absence of endogenous respiration as only exogenous respiration is measured under the assumptions of the Dynamic Response Test. The total respiration rate is the sum of the endogenous and exogenous respiration rate. The MATLAB code that was used to estimate the kinetics can be found in Appendix I.

The 95 % confidence interval on the regressed parameters was calculated to determine uncertainty in the regression. This was found by using the MATLAB 'nlinfit' and 'nlparci' functions explained in section 6.5.

7.3.1. Mesophilic kinetic regression (40 °C)

The respirogram for 86.63 mg.L^{-1} COD was used for the illustrated regression, the excluded area was shown (Fig. 7.8). The remaining regressions that were performed for the Dynamic Response Test are found in Appendix G.

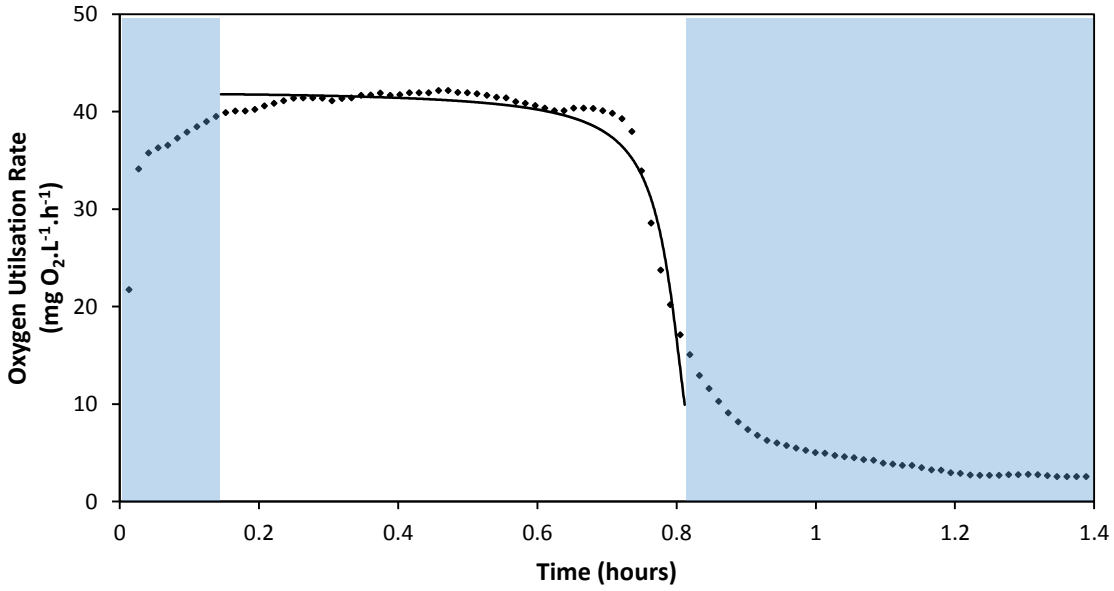

Figure 7.8. Regression of experimental data, enlarged view. —— Regressed model, • Experimental data (1 in 25 data points shown), ▭ excluded area in regression.

The portion of the respirogram that was used for the regression is shown in Fig. 7.9, the results of which can be found in Table 7.5.

Table 7.5. Mesophilic kinetic regression results.

μ_m (h^{-1})	K_S ($mg.L^{-1}$)
0.0230 ± 0.001*	1.11 ± 0.030*

*95 % confidence Interval

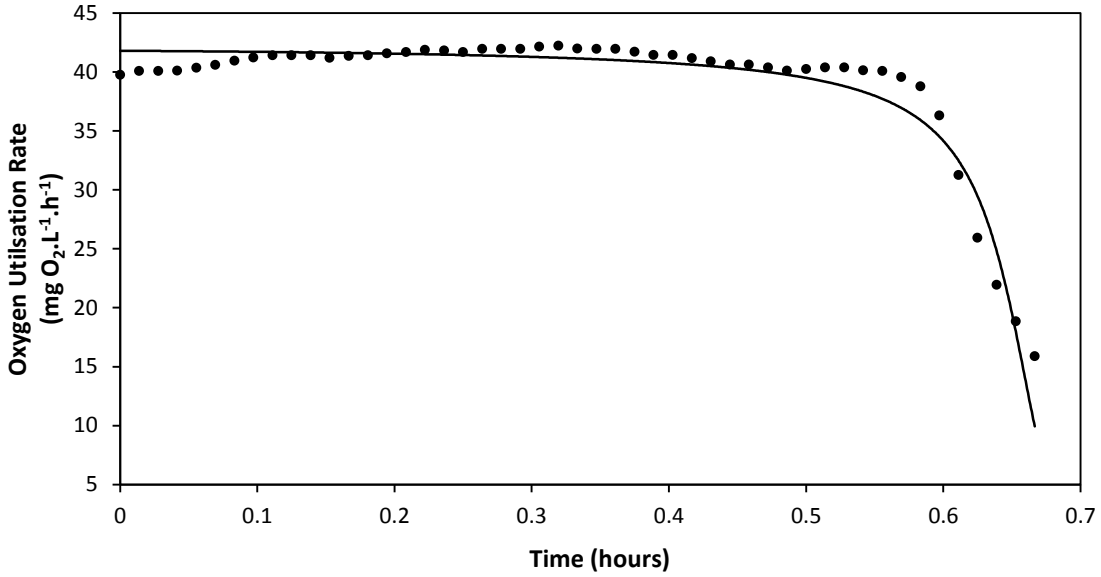

Figure 7.9. Regression of experimental data, zoomed view. —— Regressed model, • Experimental data.

7.3.2. Thermophilic kinetic regression (50 °C)

The process was repeated for the thermophilic respirogram for 49.13 mg.L^{-1} COD, where the area that was excluded has been shown (Fig. 7.10). The remaining regressions are shown in Appendix G.

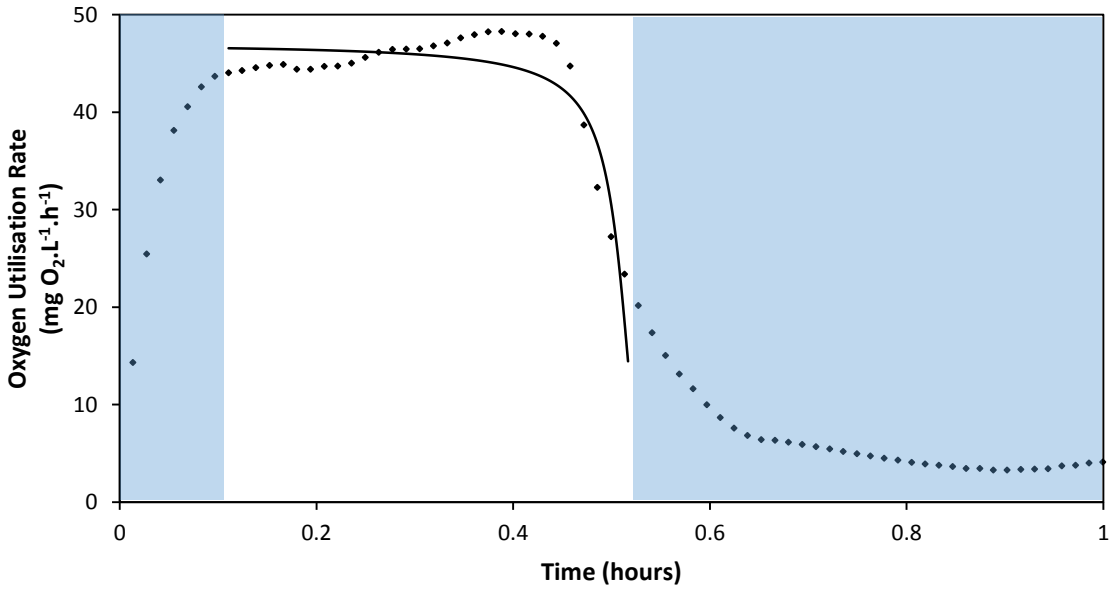

Figure 7.10. Regression of experimental data, enlarged view. —— Regressed model, • Experimental data (1 in 25 data points shown), ▭ excluded area in regression.

The area that was used in the regression is shown in Fig. 7.11, the results of which are in Table 7.6.

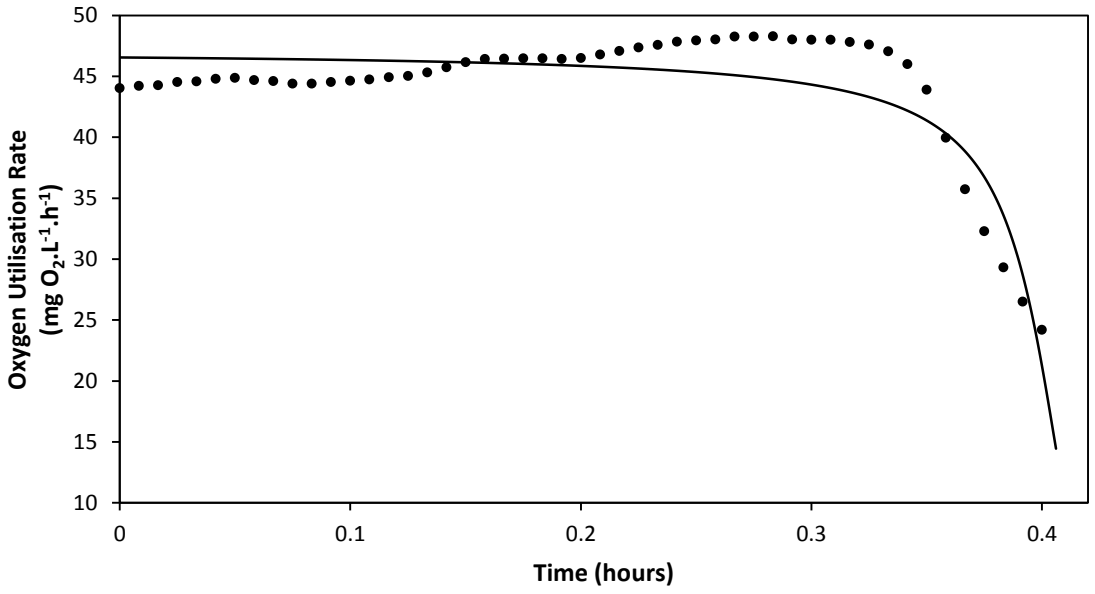

Figure 7.11. Regression of experimental data, zoomed view. —— Regressed model, • Experimental data.

Table 7.6. Thermophilic kinetic regression results.

μ_m	K_S
(h^{-1})	**($mg.L^{-1}$)**
0.0358 ± 0.002*	0.607 ± 0.034*

*95 %confidence Interval

7.3.3. Summary of kinetic regression results

The final values obtained for the kinetic parameters are shown in Table 7.7. A total of four and three respirograms were used for the mesophilic and thermophilic kinetic regression, respectively. The average parameter values for each of the temperatures were found and the standard deviation calculated.

An assumption was made that the COD is entirely biodegradable, and consists solely of a readily biodegradable substrate. As was evident from the respirograms there is a tail, caused by slowly biodegradable substrate/storage mechanisms. Data was therefore removed from the point at which the respirogram starts to level off. It is also evident from the experimentally generated respirograms that there is an acclimation phase, wherein an increasing number of micro-organism start to grow and consume substrate. As the acclimation phase was brief, occurring in the first 5 minutes of the test, thus it was neglected for the regression. It can be concluded that the model does not describe the data exactly, and therefore is not a complete mathematical description of the observations. The first hypothesis relies on a model that can describe the transition between

mesophilic and thermophilic operation, however the model does have certain limitations. Namely that it only considers readily biodegradable substrate, and that it does not account for the acclimation phase. The model that is required should be good enough that it is able to identify mechanisms and explain the major observations made during the transition from mesophilic and thermophilic operation; and therefore does not need to be a perfect mathematical description of the observations if it can fulfil this function. As a result the model was not modified further as it was seen as adequate in its current form.

Table 7.7. Summary of yield results for mesophilic and thermophilic temperature.

Test T (°C)	μ_m (h^{-1})	Average μ_m (h^{-1})	K_S ($g.L^{-1}$)	Average K_S ($g.L^{-1}$)
40	0.0230 ± 0.001*	0.0209 ± 0.0032**	1.11 ± 0.030	0.895 ± 0.187
	0.0225 ± 0.002		0.767 ± 0.036	
	0.0172 ± 0.001		0.808 ± 0.041	
50	0.0358 ± 0.002	0.0407 ± 0.0072	0.607 ± 0.034	1.00 ± 0.47
	0.0348 ± 0.003		0.582 ± 0.034	
	0.0418 ± 0.004		1.39 ± 0.059	
	0.0505 ± 0.004		1.44 ± 0.058	

*95 % confidence interval, ** standard deviation

In simulating the respirograms and regressing the kinetics, the estimation of the active biomass concentration was required. The active biomass concentration was estimated as a fraction of the MLSS concentration. A MLSS to MLVSS ratio of 0.75, and a MLVSS to active biomass concentration (X_H) ratio of 0.35 was used (Casey, 2006), (Ubisi *et al.*, 1997). There is a large amount of uncertainty associated with this method which is directly linked to the uncertainty involved with the estimate of μ_m. From the experimental work performed only a combination of μ_m and X_H can be determined. Therefore either an assumption of one of these values or additional measurements would allow the estimation of the other variable (in this case X_H was estimated which allowed the calculation of μ_m). No more information on the X_H and μ_m ratio was gathered from the batch test, but simulation and calibration of the full scale MBR was anticipated to offer further information for separating out these two variables.

The mesophilic respirograms that were generated, in Fig. 7.6, all reached a similar maximum growth rate, between 38 and 42 (mg O_2).L^{-1}.h^{-1} from which the growth rate plateaued until the

substrate was consumed. This trend was not observed for the thermophilic respirograms (Fig. 7.7), where each test reached a new maximum growth rate, starting at around 45 (mg O_2).L^{-1}.h^{-1} for the first test and ending just above 65 (mg O_2).L^{-1}.h^{-1} for the final test. This results in an uncertainty being associated with the estimation of μ_m at thermophilic temperatures, and resulted in an increased standard deviation in Table 7.7.

7.4.Stoichiometric and kinetic parameter temperature dependence

The temperature dependence of the parameters was modelled using Eq. 6-7, the temperature-activity coefficients were calculated in Table 7.8.

Table 7.8. Temperature dependence of mass balance parameters.

	μ_m	K_S	Y	k_d
θ	1.07	1.01	0.981	1.07

7.5.Summary of experimental results

Batch tests performed in the respirometer were used to obtain the four kinetic (μ_m, K_S and k_d) and stoichiometric (Y) parameters. The tests were done at mesophilic and thermophilic operation for separate sludge samples taken from the MBR, and tested at the same temperature at which they were sampled. Estimates of the temperature dependence of these parameter values were made by comparing the values at the two temperatures. These experimentally obtained parameters will be used as initial estimates in the calibration of the combined MBR model.

8. MODEL CALIBRATION

The calibration of the combined mass and energy balance model, as well as the calibration of the pH prediction routine is presented in this chapter. The mass balance model was firstly calibrated at steady state using the experimentally determined kinetic and stoichiometric parameters of chapter 7. After completing the steady state mass balance calibration, the pH routine and energy balance were calibrated at steady state. The model was first calibrated using steady state equations to ensure model outputs fell within range. The steady state calibration values were used as initial estimates for the calibration of the dynamic model. The final calibration, a dynamic calibration, was then carried out against measured plant data to test the steady state model's dynamic prediction capability, and parameters were modified accordingly with a minimisation routine to give the final model parameters. After the final model calibration was completed a sensitivity analysis was performed to find the effect of varying inputs on the predicted MBR operating temperature. The calibration procedure followed in this chapter is illustrated in Fig. 8.1.

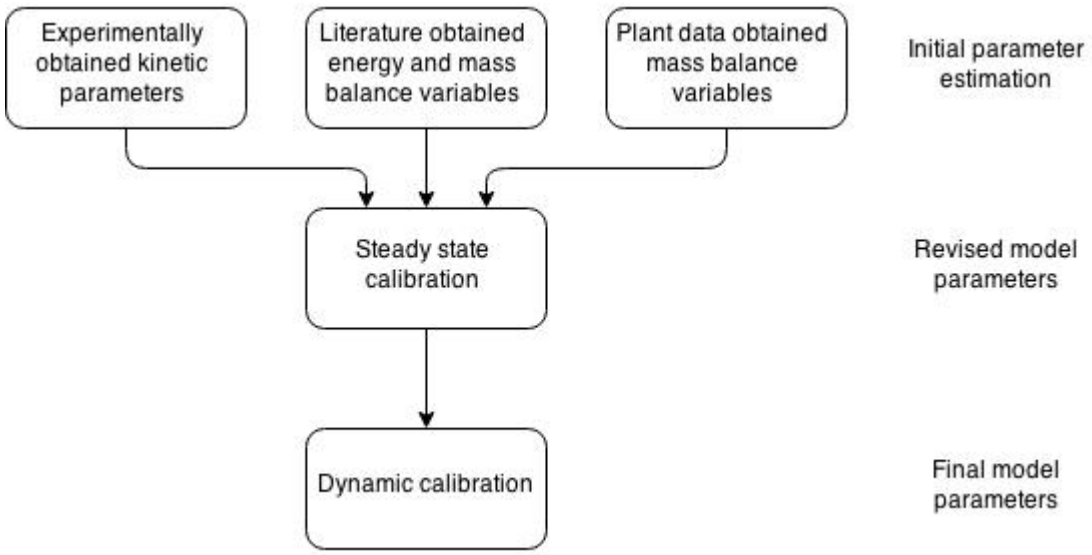

Figure 8.1. Flow diagram for the calibration procedure for the final model.

8.1. Steady state calibration

8.1.1. Mass balance

From the mass balances formed in section 6.1.2 the steady state concentrations were able to be determined. This was achieved by setting the derivatives in Eqs. 6-3 to 6-5 equal to zero and solving for the state variables. The state variables of the mass balance are the readily biodegradable substrate concentration (S_S), the heterotrophic biomass concentration (X_H), and the organic matter from decay concentration (X_P). The calibration was performed at steady state for these parameters. The mass balance is once again shown graphically in Fig. 8.2.

8.1.1.1. Steady state mass balance

Readily biodegradable substrate S_S

The steady state equations were determined for each of the state variables. The steady state concentration of readily biodegradable substrate can be calculated by manipulation of the mass balance over heterotrophic biomass, which is defined by Eq. 6-4, as follows:

$$\frac{d(VX_H)}{dt} = -q_{sw}X_{H,sw} + r_{X_H}V$$

With the substitution of the kinetics from the Gujer matrix (Table 6.1), and at steady state this simplifies to:

$$0 = -q_{sw}X_{H,sw} + \left(\frac{\mu_m S_S X_H}{K_S + S_S} - k_d X_H\right)V$$

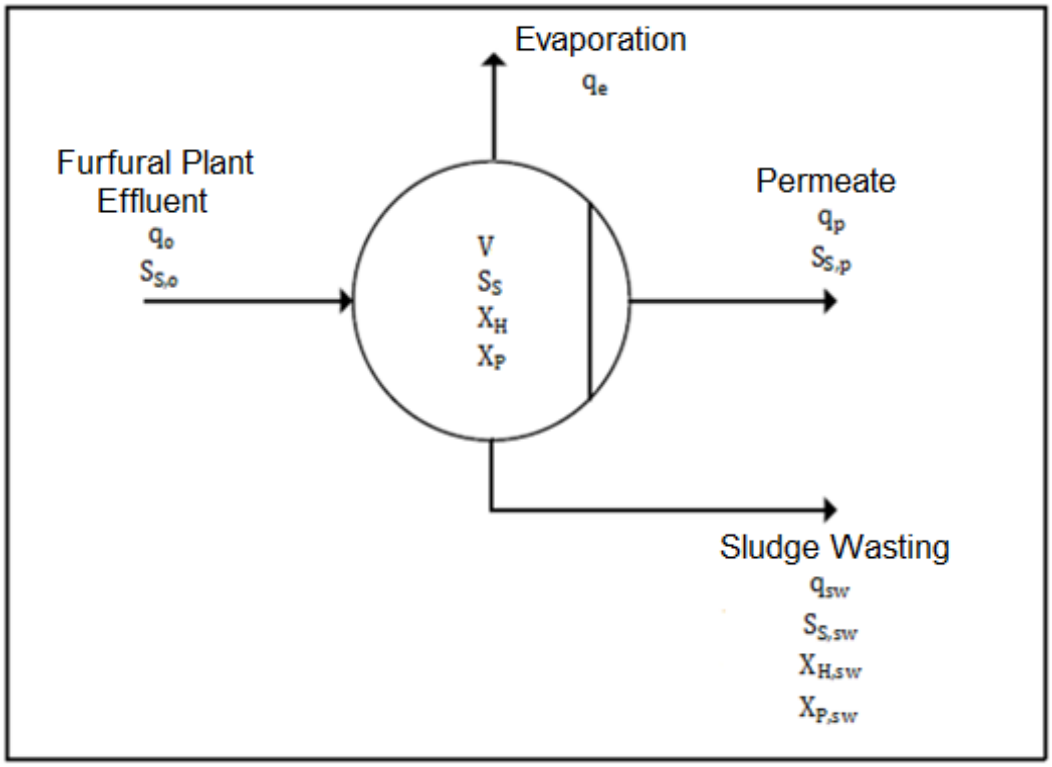

Figure 8.2. MBR mass balance (modified from Gent (2012)).

Under the assumption that the biomass concentration of the sludge wasting stream is the same as bulk biomass concentration within the MBR (lumped parameter), the equation simplifies to:

$$0 = -\left(\frac{q_{sw}}{V}\right) + \left(\frac{\mu_m S_S}{K_S + S_S} - k_d\right)$$

Rearranging, the steady state substrate concentration within the MBR may be calculated from:

$$\boldsymbol{S_S} = \frac{\left[\left(\frac{q_{sw}}{V} + k_d\right)K_S\right]}{\left[-\left(\frac{q_{sw}}{V} + k_d\right) + \mu_m\right]} \qquad (8\text{-}1)$$

It is of interest to note that steady state residual S_S concentration within the MBR is independent of the feed rate to the MBR, as well as the S_S concentration of the feed. Under the assumptions of the model, the only operational parameter that the substrate concentration is dependent upon is the inverse of the sludge age (q_{sw}/V).

Heterotrophic biomass concentration X_H

X_H within the MBR can be calculated through manipulation of the mass balance over readily biodegradable substrate, represented by Eq. 6-3:

$$\frac{d(VS_S)}{dt} = q_o S_{S,o} - q_{sw} S_{S,sw} - q_p S_{S,p} + r_{S_S} V$$

Which with the assumption of steady state, and substituting the kinetics simplifies to:

$$q_o S_{S,o} - q_{sw} S_{S,sw} - q_p S_{S,p} + \left(\frac{1}{Y}\frac{\mu_m S_S X_H}{K_S + S_S}\right) V = 0$$

The assumption that the S_S concentration in the sludge wasting stream and the permeate stream is the same as the bulk concentration within the MBR, yields the following relationship:

$$X_H = \left(\frac{Y}{\mu_m V}\right)\left[-(q_{sw} + q_p)S_S + \frac{(K_S q_o S_{S,o})}{S_S} - (q_{sw}K_S + q_p K_S - q_o S_{S,o})\right]$$

Substituting Eq. 8-1 yields:

$$\boldsymbol{X_H = \left(\frac{Y}{\mu_m V}\right)\left[\frac{(q_{sw}+q_p)\left[\left(\frac{q_{sw}}{V}+k_d\right)K_S\right]}{\left[\left(\frac{q_{sw}}{V}+k_d\right)-\mu_m\right]} + \frac{\left[-\left(\frac{q_{sw}}{V}+k_d\right)+\mu_m\right](K_S q_o S_{S,o})}{\left[\left(\frac{q_{sw}}{V}+k_d\right)K_S\right]} + \left(q_o S_{S,o} - q_{sw}K_S - q_p K_S\right)\right]} \quad (8\text{-}2)$$

Organic matter from decay X_p

The mass balance equation for X_P is defined by Eq. 6-5:

$$\frac{d(VX_P)}{dt} = -q_{sw} X_{P,sw} + r_{X_P} V$$

At steady state and substituting the kinetics gives:

$$0 = -q_{sw} X_P + f_P k_d X_H V$$

Rearranging yields:

$$X_P = \frac{f_P k_d X_H V}{q_{sw}}$$

Substituting Eq. 8-2 gives:

$$\boldsymbol{X_P = \left(\frac{f_P k_d Y}{q_{sw}\mu_m}\right)\left[\frac{(q_{sw}+q_p)\left[\left(\frac{q_{sw}}{V}+k_d\right)K_S\right]}{\left[\left(\frac{q_{sw}}{V}+k_d\right)-\mu_m\right]} + \frac{\left[-\left(\frac{q_{sw}}{V}+k_d\right)+\mu_m\right](q_o S_{S,o})}{\left[\left(\frac{q_{sw}}{V}+k_d\right)\right]} + \left(q_o S_{S,o} - q_{sw}K_S - q_p K_S\right)\right]} \quad (8\text{-}3)$$

It is preferred to perform the calibration of X_P in terms of VSS concentration, as it is a directly measurable quantity. The VSS concentration is defined as:

$$X_{VSS} = X_H + X_P$$

The VSS concentration can therefore be calculated from Eq. 8-2 and 8-3:

$$\boldsymbol{X_{VSS}} = \left[\left(\frac{Y}{\mu_m V}\right) + \left(\frac{f_P k_d Y}{q_{sw}\mu_m}\right)\right]\left[\frac{(q_{sw}+q_p)\left[\left(\frac{q_{sw}}{V}+k_d\right)K_S\right]}{\left[\left(\frac{q_{sw}}{V}+k_d\right)-\mu_m\right]} + \frac{\left[-\left(\frac{q_{sw}}{V}+k_d\right)+\mu_m\right](q_o S_{S,o})}{\left[\left(\frac{q_{sw}}{V}+k_d\right)\right]} + \left(\boldsymbol{q_o S_{S,o} - q_{sw}K_S - q_p K_S}\right)\right] \quad (8\text{-}4)$$

8.1.1.2. Variable estimation

The steady state mass balance calibration was performed by comparison with averages of plant data measured by Illovo. The data (records of daily measurements) is from historical operation of the MBR. The typical feed rates to the MBR were estimated from previous plant data ranging between a mesophilic temperature of 40 °C and the thermophilic temperature of 50 °C. The expected operational ranges of the S_S and MLSS concentration (X_{MLSS}) were also estimated from the plant data. From X_{MLSS} the expected X_H and the expected X_P concentrations were estimated, using assumed ratios. The height of the working fluid within the MBR did not vary by a significant degree, and therefore a constant height was assumed during the calibration, from which the working volume was determined. A working height of 6.5 m was assumed for the MBR which was estimated from plant data measurements.

Feed rate and sludge wasting estimation

To determine the furfural plant effluent feed rates to the MBR at various temperatures, stable MBR operating regions were located through historical plant data, and average flow rates and temperatures throughout the region of stability were calculated. This was done for five periods of stable operation to obtain a full spectrum of the operating feed rates and their associated temperatures (Fig 8.3). A linear relationship was assumed for the temperature versus feed rate plot for temperatures between 41.0 and 50.5 °C. A 95 % prediction interval was included, the prediction interval shows that for a given feed rate to the MBR the temperature can vary between 2.2 and 3.8 °C. It is emphasised that this method is only used to provide an estimation of the feed rate to the MBR for the mesophilic and thermophilic temperatures, and that in reality many other factors (sludge dosing, weather conditions, feed COD, etc.) will also affect the temperature.

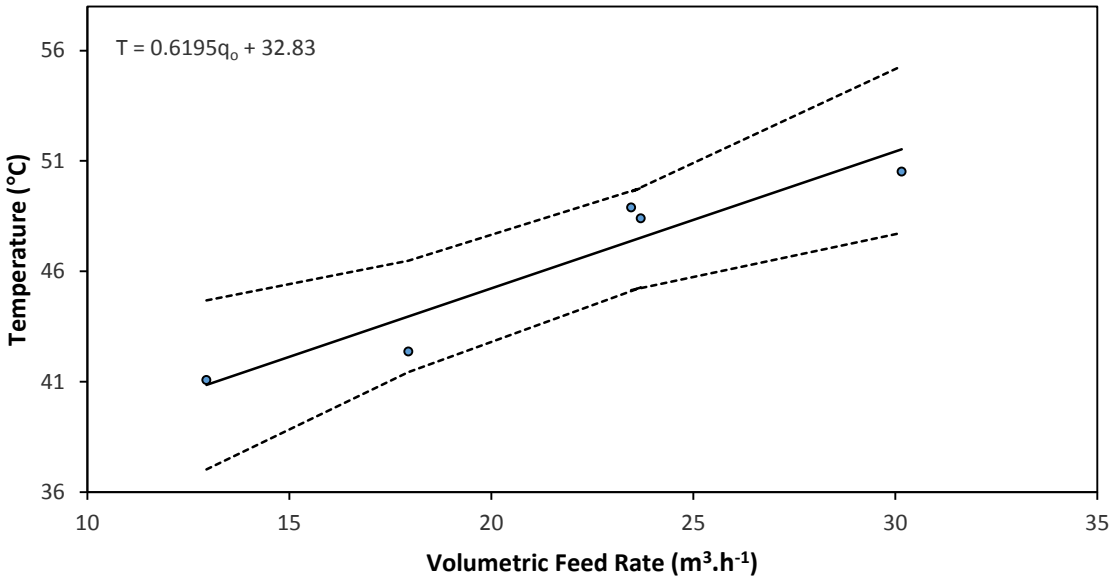

Figure 8.3. Plant data feed rate verse temperature for stable regions of operation, (R^2 = 0.907).

The regressed line was extrapolated to estimate the feed rate at 40 ºC and interpolated for the feed rate at 50 ºC (Table 8.1).

Table 8.1. Feed rate estimates for mesophilic and thermophilic operation.

T **(ºC)**	***q$_o$*** **(m^3.h^{-1})**
40	11.6
50	27.7

The sludge wasting rate is used to maintain the MLSS concentration within the MBR, and could not be accurately predicted due to its high day-to-day variance, and the counter effect of sludge dosing from the CAS plant on the MLSS concentration. From plant data it was estimated that the average sludge wasting rates range between 2 m^3.h^{-1} for mesophilic operation and 4 m^3.h^{-1} for thermophilic operation. Due to the high variance in the plant data for the sludge wasting rates, these values were taken only as indicative of the range in which sludge wasting rates occur. These estimates were taken from the plant data where a limited amount of sludge dosing from the CAS process had occurred. As the model does not account for the sludge dosing into the MBR, it was expected that the sludge wasting rates may be overestimated.

S_S, X_H, and X_P ranges within MBR plant data

The operating ranges for the measured variables (S_S and X_{MLSS}) were estimated from 2013 plant data. An average was taken over a number of stable time periods, and the standard deviation associated with each variable was also calculated.

S_S in the permeate from the MBR was measured, in terms of COD, by the laboratory located within Illovo. However X_H and X_{VSS} could only be inferred through the MLSS concentration that was measured. These concentrations were inferred through the X_{VSS} to X_{MLSS} ratio and the X_H to X_{VSS} ratio which were discussed in chapter 7.3.3. The concentration ranges that were determined from plant data are illustrated in Table 8.2:

Table 8.2. Estimation of operating readily biodegradable substrate and MLSS concentration from plant data.

Variable	Operating Concentration ($g.L^{-1}$)	Standard Deviation ($g.L^{-1}$)
S_S	0.83	0.21
X_{MLSS}	13.50	1.40

Using a X_{VSS} to X_{MLSS} ratio between 0.65 to 0.85 and a X_H to X_{VSS} ratio of 0.35 yields the expected operating ranges in Table 8.3.

Table 8.3. Estimation of operating active heterotrophic biomass and volatile suspended solids concentration from plant data.

Variable	Operating Concentration ($g.L^{-1}$)
X_H	3.0 – 4.0
X_{VSS}	8.8 – 11.5

It should be noted that the furfural plant effluent COD measured by Illovo, detailed in section 5.4.1, measures the total COD of the sample, while the feed to the MBR and therefore the residual substrate concentration is assumed in the model to consist entirely of completely and readily biodegradable substrate. In reality it is expected that there is a small unidentified portion of the feed which may be unbiodegradable.

8.1.1.3. Calibration procedure

By inputting the parameters into Eqs. 8-1, 8-2 and 8-4 the state variables can be calculated at steady state, and compared to their expected ranges in Table 8.2 and 8.3. The input parameters may then be adjusted accordingly to ensure the state variables fall within the specified ranges. The experimentally obtained kinetic and stoichiometric parameters (μ_m, K_S, k_d, and Y); the expected operating concentrations in Tables 8.2 and 8.3; the expected furfural plant effluent feed (Table 8.1) and sludge wasting rates; the furfural plant effluent feed COD concentration; the working volume estimation of the MBR of 4 060 m^3; and the residual inert material from decay of biomass parameter (f_P) of 0.125, estimated from Eddy *et al.* (2003); were all inputted into Eqs. 8-1, 8-2 and 8-4. For the purpose of the calibration, the amount of water evaporated from the MBR was neglected, simplifying the steady state mass balance to $q_o = q_{sw} + q_p$. The assumption that the liquid evaporated was small in comparison to the feed flow was to have been checked against the predicted evaporation using the final calibrated dynamic simulation model. The initial parameters that were used for the steady state calibration are shown in Table 8.4.

The state variable steady state operating concentrations for the input parameters of Table. 8.4 are calculated in Table 8.5 using Eqs. 8-1, 8-2, and 8-4.

Table 8.4. Parameter values used in the calculation of the state variables using the steady state model equations.

Parameter	Mesophilic (40 ºC)	Thermophilic (50 ºC)
q_0 ($m^3.h^{-1}$)	11.6	27.7
q_{sw} ($m^3.h^{-1}$)	2	4
μ_m (h^{-1})	0.0209	0.0407
K_S ($g.L^{-1}$)	0.895	1.00
k_d (h^{-1})	0.0123	0.0249
f_P	0.125	0.125
$S_{S,o}$ ($g.L^{-1}$)	17.8	17.8
Y (mg COD biomass). (mg COD soluble)$^{-1}$	0.512	0.620
V (m^3)	4 060	4 060

Table 8.5. Calculated state variables from steady state model equations using parameter values.

T (ºC)	S_S (g COD.L^{-1})	X_H (g VSS.L^{-1})	X_{VSS} (g VSS.L^{-1})
40	1.41	1.74	7.15
50	1.75	1.69	7.04

The estimated operating concentration predictions in Table 8.5 lie out of the expected MBR operating range for 2013 plant data (Table 8.2 and 8.3). The X_P value is calculated as the difference between X_{VSS} and the X_H using Eq. 6-8. To adjust the state variables to within the expected MBR operating range, alteration of the parameters was required. The parameters that were expected to have a large amount of uncertainty were the specific death rate constant (k_d); the sludge wasting rates (q_{sw}), which are dependent on the MLSS concentration; and the fraction of biomass that becomes residual inert material from decay of biomass, the f_p value, which was estimated from literature. It was found that by altering these three values within a reasonable range, a satisfactory estimate of the state variables was obtained (Table 8.6).

Table 8.6. Modified estimation of state variables.

T (ºC)	S_S (g COD.L^{-1})	X_H (g VSS.L^{-1})	X_P (g VSS.L^{-1})	X_{VSS} (g VSS.L^{-1})
40	0.731	2.267	7.765	10.032
50	0.874	2.193	7.851	10.044

The modified k_d, sludge wasting rates and f_p used to obtain the values in Table 8.6 are shown in Table 8.7. The change in the variables in relation to their values in Table 8.4 are provided.

Table 8.7. Modified estimates for mass balance.

Parameter	Mesophilic (40 ºC)	Relative change (%)	Thermophilic (50 ºC)	Relative change (%)
q_{sw} (m^3.h^{-1})	1.6	20	3.1	23
k_d (h^{-1})	0.009	27	0.0182	27
f_p	0.15	20	0.15	20

For the steady state calibration S_S lies within the expected range (Table 8.2 and 8.3), however X_H and X_{VSS} do not.

- The calculated X_H value depends on the parameters in Eq. 8-2, there is a high amount of interaction between the parameters in calculating the state variables. The expected range for X_H and X_{VSS} are reliant on assumed ratios. It was therefore decided to not spend considerable effort in making the prediction meet the target range; especially as the calibrated parameters obtained were only to be used as starting estimates for the dynamic simulation calibration in section 8.2, where they can be tested more rigorously. This is maintained due to the large uncertainty associated with the prediction of X_H.
- The k_d value was lowered to 0.009 h^{-1} for mesophilic operation and 0.0182 h^{-1} for thermophilic operation. These values lie within the standard deviations that were calculated in chapter 7. The temperature dependence of k_d was maintained by keeping the θ value of 1.07 (section 7.4), thus any change to the parameter at 40 °C would automatically adjust the parameter for 50 °C.

8.1.2. pH prediction

For the pH prediction routine, the concentration of species entering the MBR was estimated as part of the calibration. The concentration of hydrogen ions entering the MBR was assumed equal, on a molar basis, to the concentration of the COD, as the COD is assumed to consist entirely of acetic acid which is monoprotic. It is expected that the acetic acid should be almost completely dissociated upon entering the MBR which has an operating pH of 6 or above. Urea and phosphoric acid are dosed daily into the MBR to maintain a healthy microbial community. A nutrient dosing ratio of nitrogen and phosphorus was assumed from literature, for COD:N:P of 100:11:2 on a mass basis (1:0.25:0.021 on a molar basis) (Milenko and Vrtovsek, 2004). To fine tune the pH to that recorded by plant data the feed carbonate concentration was altered, as a small amount of CO_2 was expected to enter the MBR through aeration.

8.1.2.1. Calibration procedure

The COD concentration of the feed was taken as 17.8 g $COD.L^{-1}$ (Table 8.4). The pH of the MBR recorded in the Illovo plant data is always maintained above 6 but rarely goes above a value of 7.

The feed concentrations for each of the species is shown in Table 8.8. It was modelled that the nutrient concentrations enter the MBR with the furfural plant effluent feed stream as a basis ($mol.m^{-3}$ of furfural plant effluent feed).

Table 8.8. Species feed concentrations to the MBR.

Species	Molar Feed Concentration ($mol.m^{-3}$)
$c_{CH_3COO^-,o}$	278.1
$c_{H^+,o}$	278.1
$c_{CO_3^{2-},o}$	5.5
$c_{PO_4^{3-},o}$	7.2
$c_{NH_4^+,o}$	64.0

8.1.2.2. Effect of pH on biomass activity

A study was previously performed by Sasol Pty (Ltd) on the Illovo MBR to investigate the activity of the sludge at various pH values (Kennedy and Young, 2006). The effect of the pH on the biomass activity was incorporated into the model to simulate a realistic effect of lowered pH values on the MBR system. The biomass activities were normalised as percentages, and a simple linear interpolation between the values was performed (Table 8.9). The model can therefore output a pH value, from which a suitable linear equation is selected, and the biomass activity factor calculated (Fig. 8.4). The biomass activity factor affected the model through multiplication with μ_m.

Table 8.9. Effect of pH on biomass activity (Kennedy and Young, 2006).

pH	Biomass Activity (%)	Normalised Biomass Activity (%)
7	80	100
6	80	100
5.5	75	93.8
5	5	6.3
4.5	0	0

The effect of pH on the biomass was incorporated into the model to simulate the effect of lowered pH values on the system, and give a realistic limitation to the model.

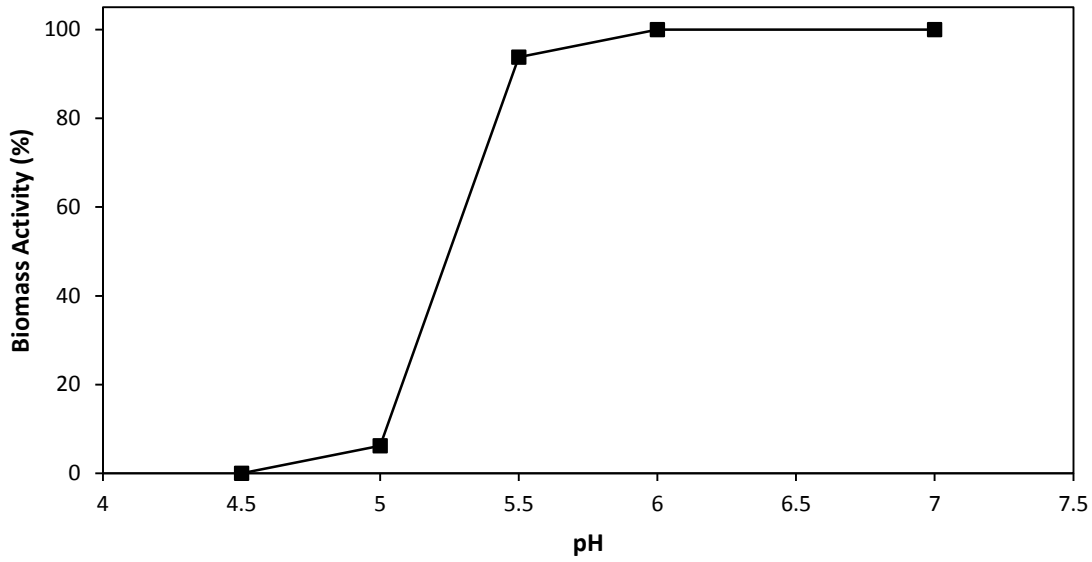

Figure 8.4. Proposed linear interpolation to describe biomass activity within the model as a function of pH.

8.1.3. Energy balance

Once the mass balance had been calibrated at steady state, the calculation of the heat of reaction and aeration terms could be calculated, and therefore the energy balance completed. The energy balance also requires the estimation of parameters, which are dependent on the external factors and environmental conditions.

8.1.3.1. Calibration procedure

The permissible ranges of the parameters were obtained from literature, historical databases and through estimation. The calibration of the energy balance has been performed by varying these parameters within their permissible ranges. The parameters were altered so that a mesophilic and thermophilic flow rate, in Table 8.4, would give a steady state operating temperature of 40 and 50 °C, respectively. The parameters with their estimations are shown in Table 8.10. During the daily operation of the MBR generally only the membrane scourer and one of the large blowers are operational. The power consumption of the blowers was discussed in section 3.4.

With the values of Table 8.10, the combined mass and energy balance model predicts a temperature of 40 °C for a mesophilic feed rate, and a temperature of 50 °C for a thermophilic feed rate stated in Table 8.1.

Table 8.10. Energy balance parameter estimation.

Parameter	Parameter Range	Estimate	Source
C_C (tenths)	0-10	4	(holiday-weather, 2014)*
r_h (%)	70 – 80	80	(holiday-weather, 2014)
W (m.s^{-1})	4 – 6	4	(holiday-weather, 2014)
T_a (°C)	18-27	25	(holiday-weather, 2014)
d (days)	1-366	180	(holiday-weather, 2014)
T_e (°C)	-	25	estimate
T_f (°C)	36-40	38.3	(Gent, 2012),(Judd, 2011)
Blowers Operational	Membrane scourer, Blower 1 & Blower 2	Membrane Blower & Blower 1	(Judd, 2011)
Blower Power	Membrane scourer: 61.5kW Blower 1 & 2: 224kW	Membrane scourer: 61.5kW Blower 1 & 2: 224kW	(Judd, 2011)

*All weather estimations are performed for Durban, South Africa.

8.2. Dynamic simulations with steady state calibration

To test the validity of the steady state model calibration, recorded furfural plant effluent feed rates (q_o), and sludge wasting rates (q_{sw}) obtained from historical plant data for 2012 and 2013 were used in dynamic simulations. Stable periods of operation were selected from each of the years. All other input variables were assumed constant (feed temperature, feed COD concentration, weather conditions, etc.). The input parameters from Table 8.10 were used. The substrate concentration entering the reactor was assumed constant throughout the simulation at 17.8 g COD.L^{-1} as there is only a small variation experienced during normal operation of the plant. The effect of sludge dosing from the neighbouring CAS plant was completely neglected. The nutrient dosing rate (PO_4^{3-} and NH_4^+) to the MBR was also assumed constant throughout the simulation, as quantified in Table 8.8.

The model is capable of predicting S_S, X_{VSS}, T and pH, however the prediction of X_{VSS} by the model was excluded from the comparison as its prediction was complicated by the fairly regular sludge dosing into the MBR from the CAS plant neighbouring the MBR, and therefore was considered unreliable at this stage. Additionally, Illovo measure the MLSS concentration of the MBR, and the model predicts the VSS concentration; the ratio of these values, which was estimated for the kinetic regression, is uncertain.

The prediction of residual S_S concentration within the MBR was included, however, the permeate is complicated by the fact that the model assumes that the furfural plant effluent feed entering the MBR is completely and readily biodegradable. It is expected that there may be a small and varying very slowly biodegradable or unbiodegradable fraction of the COD present, estimated to be around 0.5 $g.L^{-1}$ (out of a total COD of ~17.8 $g.L^{-1}$), that is unaccounted for within the feed. The unknown fraction was detailed in section 5.4.1. An added effect is the sludge dosing from the CAS plant, which likely contains an unquantified unbiodegradable soluble fraction, which is not accounted for by the model. The plant data measures the total COD of the permeate, and does not distinguish between unbiodegradable and biodegradable substrate. Therefore for the simulations and comparison, the variables that were of primary importance are the MBR temperature of operation, and the MBR pH. S_S plots are included for comparison purposes and to show the link between S_S and pH.

The primary model outputs were compared to the measured plant data. As plant data was recorded as daily averages, the model simulation was altered to calculate an average of the model outputs over a 24 h period, so that the comparison can be performed on the same time basis. Regions from 2013 and 2012 were selected that exhibited the most stability, that is an operating temperature for the MBR that is between 40 and 50 °C, and where minimal sludge dosing has occurred that could skew the measured data.

For the dynamic simulation the effect of the pH on biomass activity was neglected at first to avoid reactor shutdown, this was reactivated for the final calibration. Reactor shutdown occurs when the operating pH of the MBR drops below 6 and the biomass becomes less active (Fig. 8.4). This leads to a vicious circle type effect, where the reduced biomass activity leads to lower substrate consumption rates resulting in higher residual substrate concentrations within the MBR; which further decreases the pH, the pH reduction once again decreases the biomass activity. This cycle continues until the pH drops below 4.5 and the biomass becomes completely inactive, leading to reactor shutdown. The results of the 2012 and 2013 calibrations are presented in sections 8.2.1 - 8.2.3.

8.2.1. Temperature simulation

From the comparison of the dynamic simulations to plant data the temperature predictions have a root mean square deviation (RMSD) between 1.66 and 1.82 °C (Fig. 8.5 and 8.6). This results in a reasonable accuracy for dynamic temperature prediction of the MBR. All that is required is the q_o and q_{sw} for the MBR. These results suggest that the main factors controlling the temperature in the MBR is q_o and q_{sw}. More accurate prediction is likely possible if more detailed information is used, such as the concentration of the furfural plant effluent and external conditions (ambient temperature, cloud cover, relative humidity, etc.).

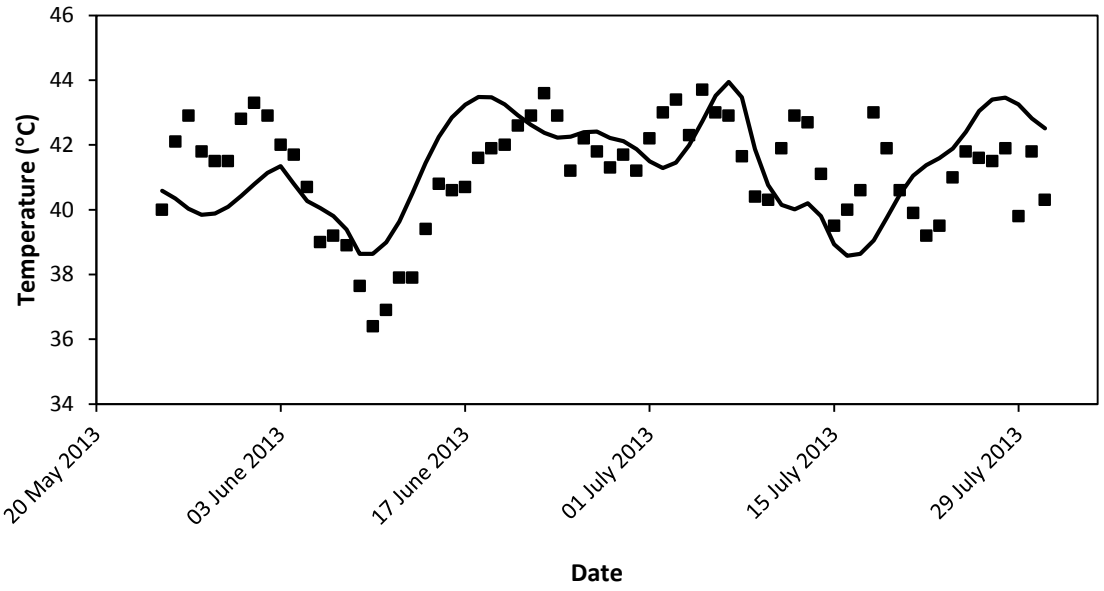

Figure 8.5. Temperature comparison for 2013 period, ▪ plant data, ── model, RMSD 1.66 °C.

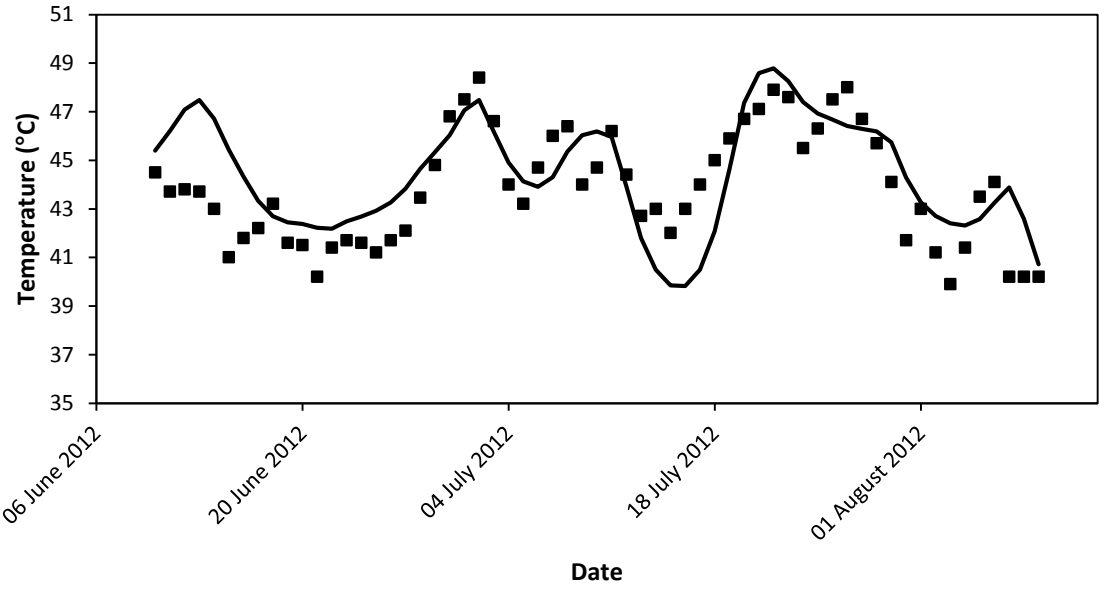

Figure 8.6. Temperature comparison for 2012 period, ▪ plant data, ── model, RMSD 1.82 °C.

8.2.2. pH simulation

For both the 2013 and 2012 pH comparisons, there were large fluctuations that occured in the simulated predictions, as compared to the measured plant data (Fig 8.7 and 8.8). The pH is related to the residual S_S concentration within the MBR, as it is assumed for simulation purposes to be entirely composed of acetic acid. Therefore a fluctuating residual COD concentration results in a similar but inversely fluctuating pH (Fig. 8.9 and 8.10).

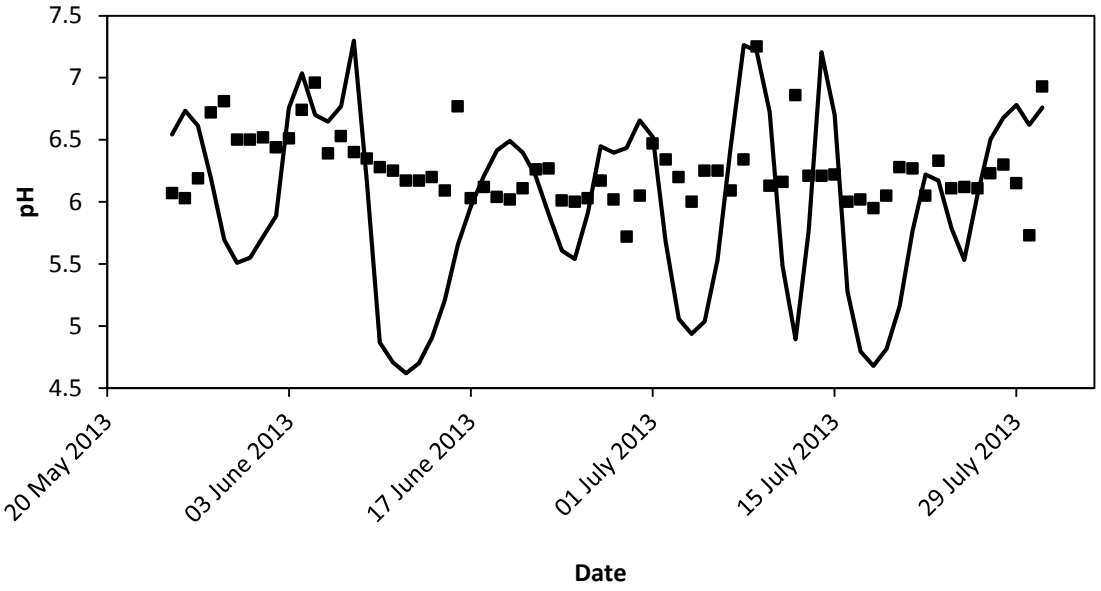

Figure 8.7. pH comparison for 2013 period, ▪ plant data, ── model, RMSD 0.78.

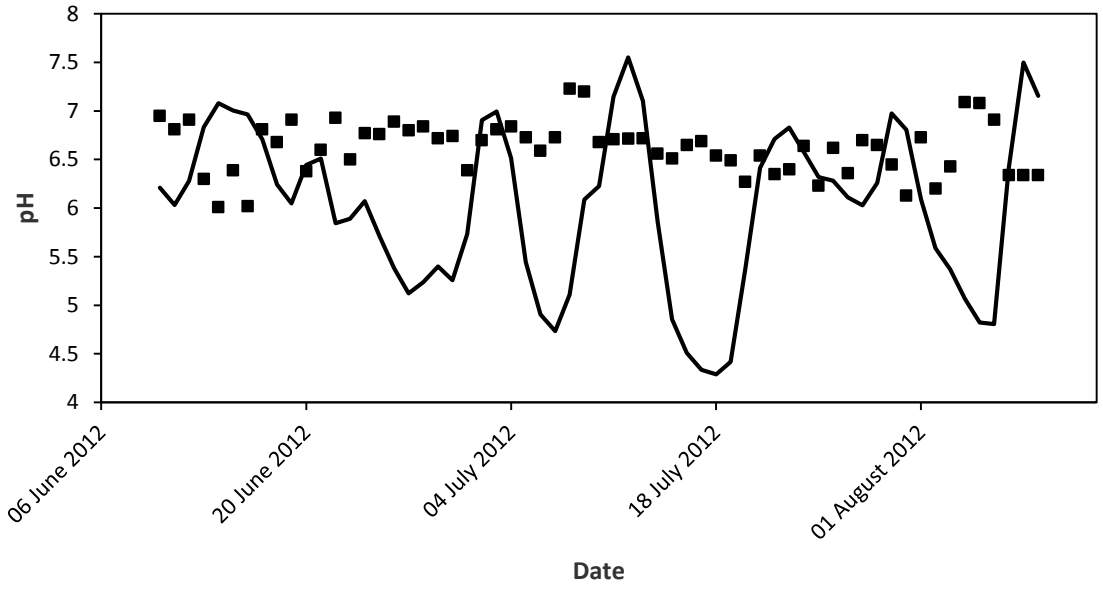

Figure 8.8. pH comparison for 2012 period, ▪ plant data, ── model, RMSD 1.14.

It could be concluded that the error therefore lies in the S_S concentration prediction, which the pH is dependent upon. It may be theorised that by increasing μ_m, which was dependent on the uncertain estimation of X_H (Appendix A), S_S may become more stable, with less severe fluctuations. The more stable COD prediction in turn could lead to a more stable pH prediction. This is further analysed in section 8.3.

8.2.3. Residual S_S concentration simulation

The residual S_S concentration within the MBR, generated by the simulation, is shown in Fig. 8.9 and 8.10. The S_S concentration follows the opposite trend to the pH, in that an increase in the COD concentration will lead to a decrease in the pH.

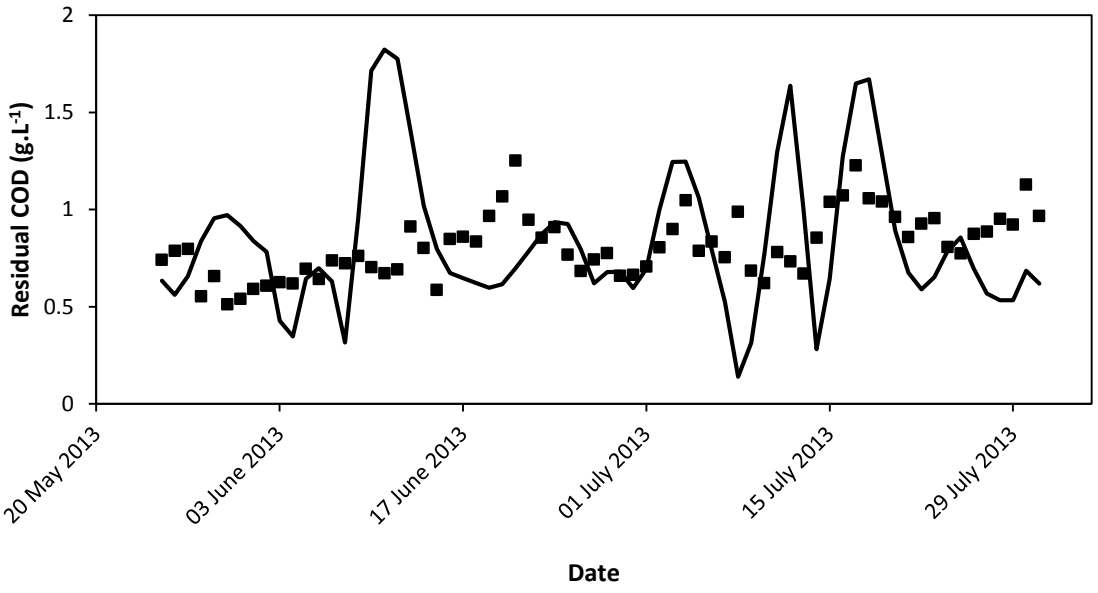

Figure 8.9. Residual COD comparison for 2013 period, ▪ plant data, ── model, RMSD 0.39 g.L^{-1}.

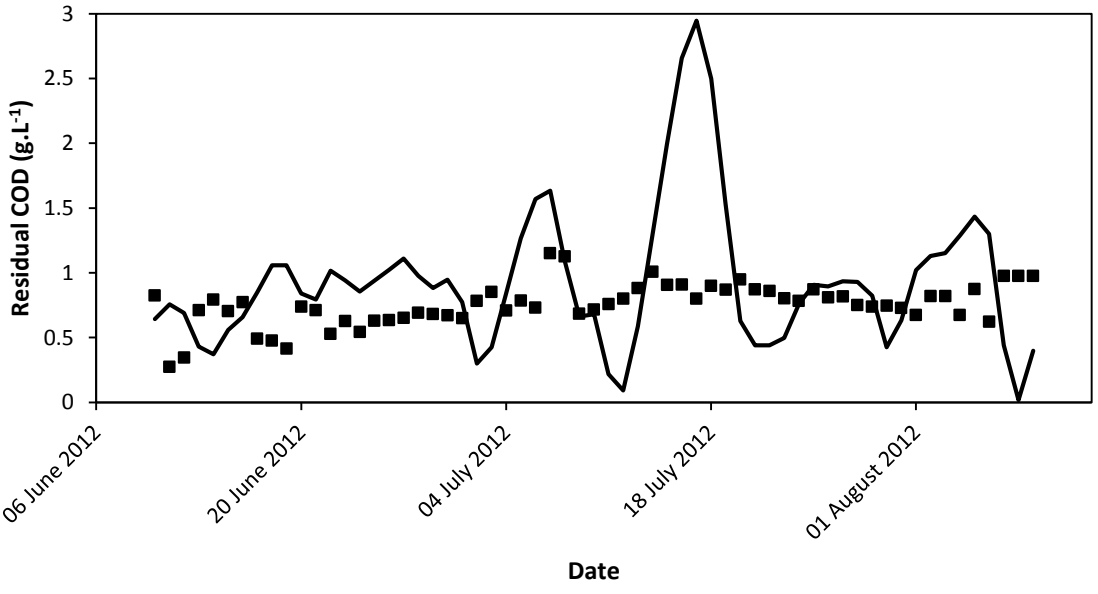

Figure 8.10. Residual COD comparison for 2012 period, ▪ plant data, ── model, RMSD 0.58 g.L^{-1}.

To obtain a more accurate COD and pH prediction a dynamic calibration was performed, in which an objective function was formulated to minimise the error between the measured plant data and model outputs, by altering relevant parameters.

8.3. Dynamic calibration with minimisation routine

The minimisation routine was carried out on MATLAB R2010a using the built-in 'fmincon' function which was formed around the existing batch model. The minimisation was performed by altering preselected parameters associated with the mass and energy balance. The effect of the pH on the biomass activity in section 8.1.2.2 was initiated for the simulation. The calibration was carried out in two-stages, firstly by setting the temperature in the minimisation routine to that measured on the plant data for 2012 and calibrating only the mass balance with the attached speciation routine. The parameters that were altered for the mass balance were the maximum specific growth rate (μ_m), and the molar flow rate of CO_2 into the MBR in the form of carbonate ($c_{CO_3^{2-},o}$). By altering μ_m the pH fluctuations that occurred in Fig. 8.7 and 8.8 were dampened, and by altering $c_{CO_3^{2-},o}$ entering the MBR the pH was recalibrated to the plant data pH values. The RMSD for the difference in plant and predicted pH was the objective function to be minimised for the mass balance.

The temperature was subsequently calibrated using the new mass balance parameters. The parameters altered for the energy balance were the wind speed (W), the cloud cover (C_c), and the relative humidity (r_h). The RMSD for the difference between the plant and predicted temperature was the objective function to be minimised during the calibration. Once the minimum was obtained and new values for the mass and energy balance model determined, the furfural plant effluent feed rates of table 8.1 were no longer applicable due to the altered parameters; the new furfural plant effluent feed rates to the MBR were found for a temperature of 40 and 50 °C. The parameters and flow rates obtained from this calibration were taken as the final calibrated model parameters, resulting in the final calibrated model.

8.3.1. Mass balance recalibration

The minimisation was carried out with respect to the 2012 plant data as the time period had both mesophilic and thermophilic operational temperatures, unlike the 2013 period. The data from 2013 was used as validation of the dynamic model calibration in section 8.4. The parameters that were altered during the mass balance calibration were μ_m(40 °C) and $c_{CO_3^{2-},o}$, the temperature dependence of μ_m (Table 7.8) was maintained the same throughout the calibration, thus μ_m(50 °C) is dependent on μ_m(40 °C). μ_m showed a drastic increase, almost 3 times the previous value, while the molar feed rate of CO_2 was halved from the original estimate from the calibration (Table 8.11). The increase in μ_m implies that X_H was overestimated in Appendix A, leading to lower μ_m values obtained from the kinetic regression. As stated in section 7.3.3 only the

combination of μ_m and X_H could be accurately found from the experimental work, however the combination was initially estimated through X_H for the kinetic regression. There is no significance in the alteration of $c_{CO_3^{2-},o}$ as it was originally intended only as a calibration factor for the pH.

Table 8.11. Modified mass balance parameters from the dynamic calibration.

	μ_m(40°C) (h^{-1})	$c_{CO_3^{2-},o}$ ($mol.m^{-3}$)
Steady State calibration	0.0202	5.5
Dynamic calibration	0.0589	2.28

8.3.2. Energy balance recalibration

In the second part of the calibration, the temperature was recalibrated using the modified parameters of Table 8.11. The parameters that were altered were the W, C_c and r_h. The modified parameters that were obtained are presented in Table 8.12.

Table 8.12. Modified energy balance parameters from dynamic calibration.

	W ($m.s^{-1}$)	C_c (tenths)	r_h (%)
Steady State calibration	4	4	80
Dynamic calibration	5	4.5	83

The flow rates for mesophilic operation at 40 °C and thermophilic operation at 50 °C (Table 8.1), have been altered by the recalibration to those in Table 8.13.

Table 8.13. Modified flow rates for mesophilic and thermophilic operation.

T (ºC)	q_o ($m^3.h^{-1}$)
40	12.9
50	29.3

8.3.3. Calibration simulation

8.3.3.1. Temperature simulation

The recalibrated simulation shows an improvement at a higher μ_m value. The temperature comparison has an RMSD of 1.34 °C, a slight improvement compared to the previous calibration with an RMSD of 1.82 °C for the 2012 data (Fig. 8.11).

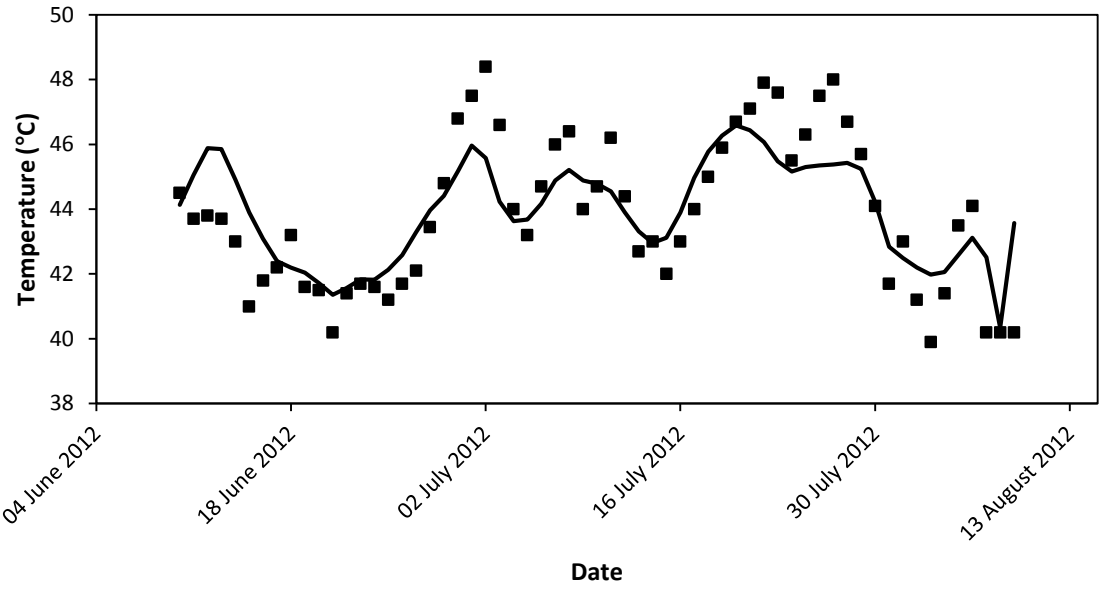

Figure 8.11. Temperature comparison for 2012 period, ▪ plant data, ── model, RMSD 1.34 °C.

8.3.3.2. pH simulation

The pH prediction shows a substantial improvement with an RMSD of 0.47, compared to an RMSD for the previous calibration of 1.14 for 2012 (Fig. 8.12). The decreased fluctuations are a direct result of the increased μ_m value.

8.3.3.3. Residual S_S concentration simulation

The residual S_S concentration predicted by the model accounts only for the readily biodegradable substrate, and therefore the S_S prediction is far below the total COD measured by Illovo Laboratory. By the addition of an assumed unbiodegradable COD (uCOD) of 0.65 $g.L^{-1}$, slightly higher than that estimated in section 5.4.1, however still within the standard deviation, the S_S prediction is greatly improved. However more analyses are required in quantifying the furfural plant effluent feed to fully confirm this.

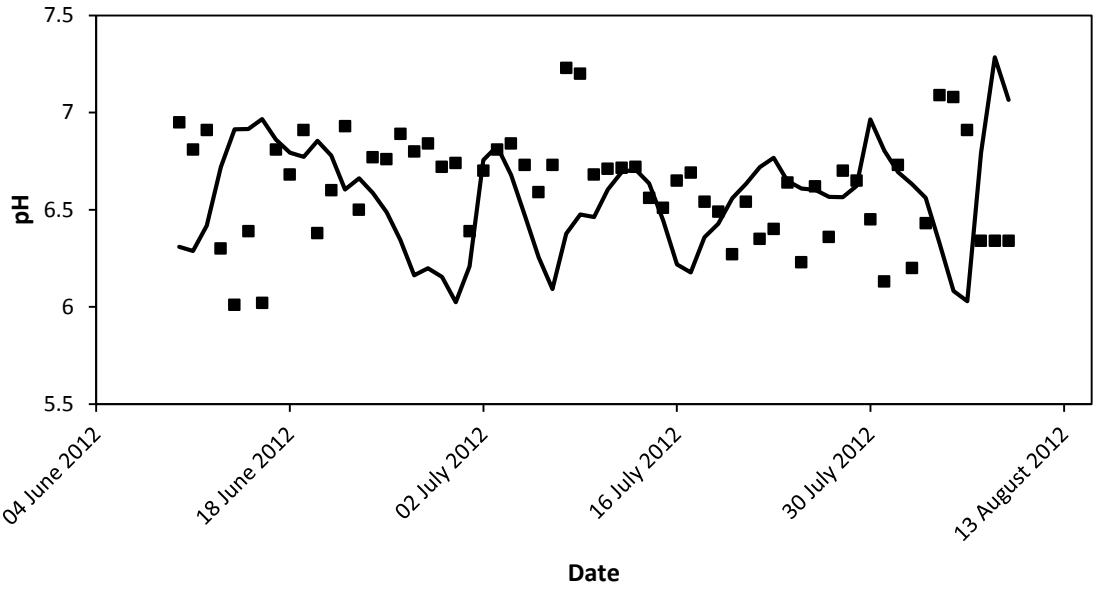

Figure 8.12. pH comparison for 2012 period, ▪ plant data, ── model, RMSD 0.47.

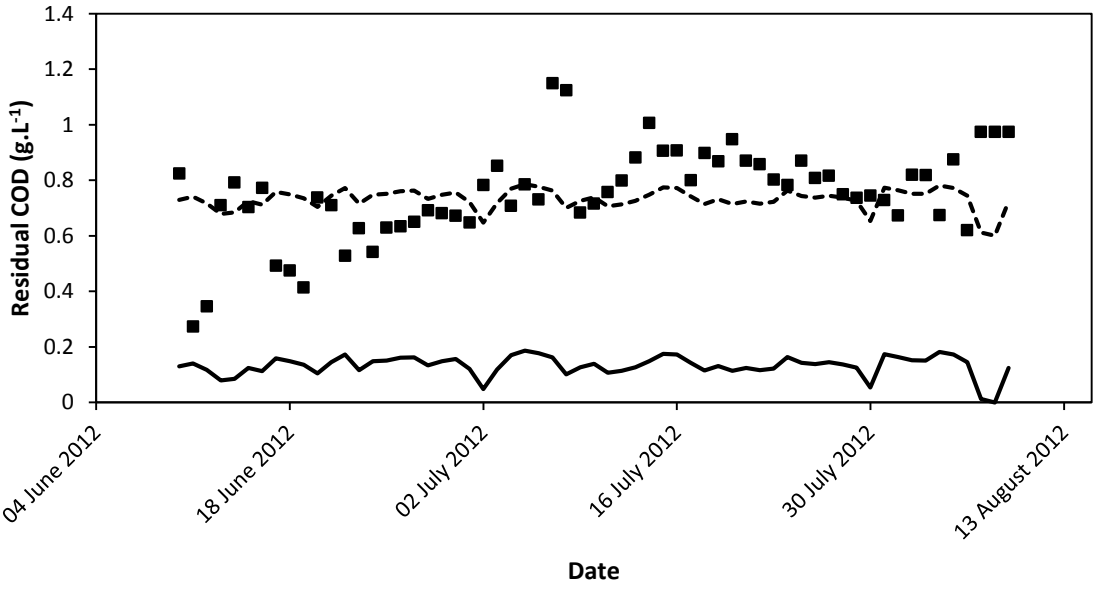

Figure 8.13. Residual COD comparison for 2012 period, ▪ plant data, ┅ uCOD model, ── model, RMSD 0.18 g.L^{-1} (0.65 g.L^{-1} uCOD).

From the final model calibration X_H was more accurately determined, lower than that estimated from the assumed ratio in Table 8.3. X_H was found by operating at mesophilic and thermophilic temperatures of 40 and 50 °C, respectively, and finding the steady state active biomass concentration. For the simulation the steady state X_H values that were observed were 2.6 and 2.4 g.L^{-1} for mesophilic and thermophilic operation, respectively. This is substantially lower than the initial X_H estimate of 3.7 g.L^{-1} obtained in Appendix A, and used for the kinetic regression.

This was responsible for the underestimation of μ_m that was obtained from the kinetic regression in section 7.3.

8.4. Model validation

8.4.1. Validation simulation

The validation of the final model calibration was carried out against 2013 plant data. Only q_o and q_{sw} were used as model inputs, and the effect of the pH on the biomass activity in section 8.1.2.2 was initiated for the simulation.

8.4.1.1. Temperature simulations

The validation simulation shows an improvement for the 2013 data. The temperature comparison has a RMSD of 1.61 °C, a slight improvement compared to the steady state calibration with a RMSD of 1.66 °C for the 2013 data (Fig. 8.5).

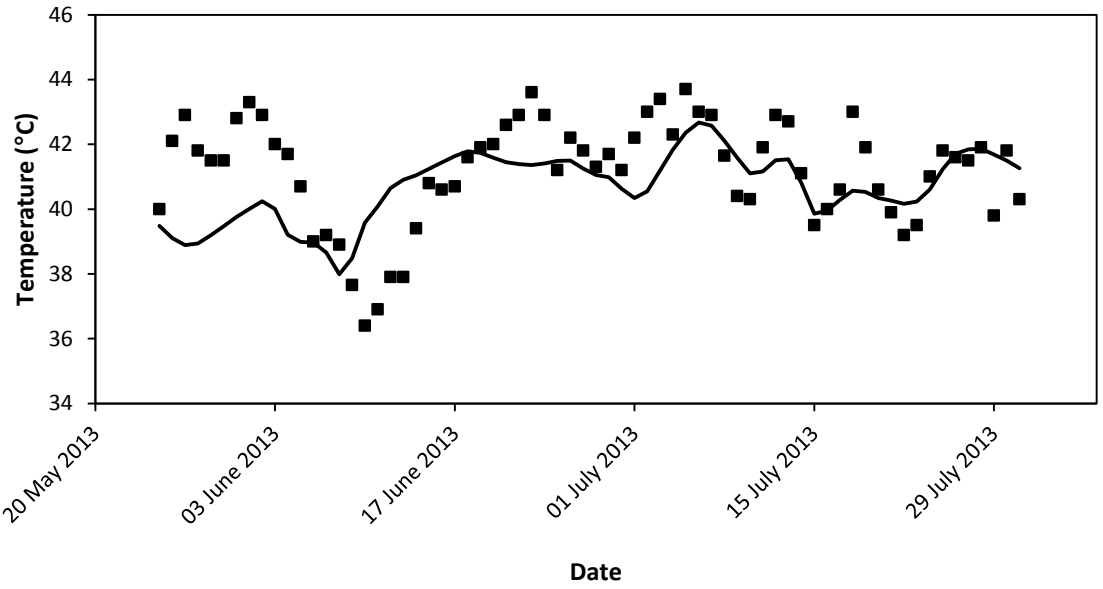

Figure 8.14. Temperature comparison for 2013 period, ▪ plant data, ── model, RMSD 1.61 °C.

8.4.1.2. pH simulation

The pH prediction in Fig. 8.15 again shows a substantial improvement with a RMSD of 0.36, compared to a RMSD for the previous calibration of 0.78 for 2013 (Fig. 8.7).

8.4.1.3. Residual S_S concentration simulation

Once again, by the addition of an assumed unbiodegradable fraction of 0.65 g.L^{-1} the S_S prediction is greatly improved (Fig. 8.16). The plot is only illustrative of potential substrate concentration estimation if the furfural plant effluent were fully characterised, and the assumption of an unbiodegradable fraction confirmed.

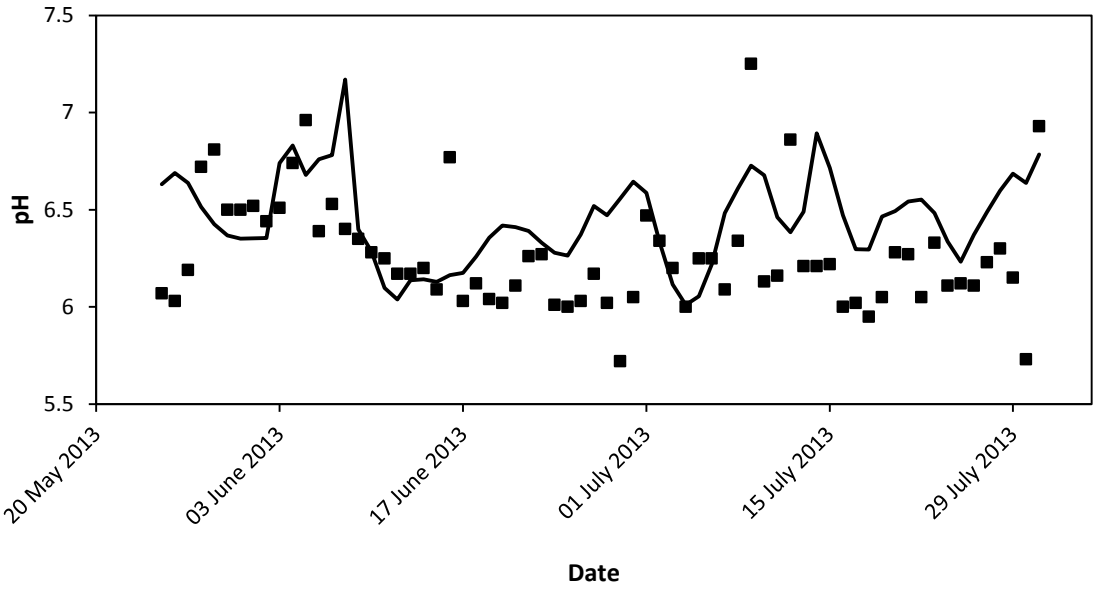

Figure 8.15. pH comparison for 2013 period, ▪ plant data, ── model, RMSD 0.36.

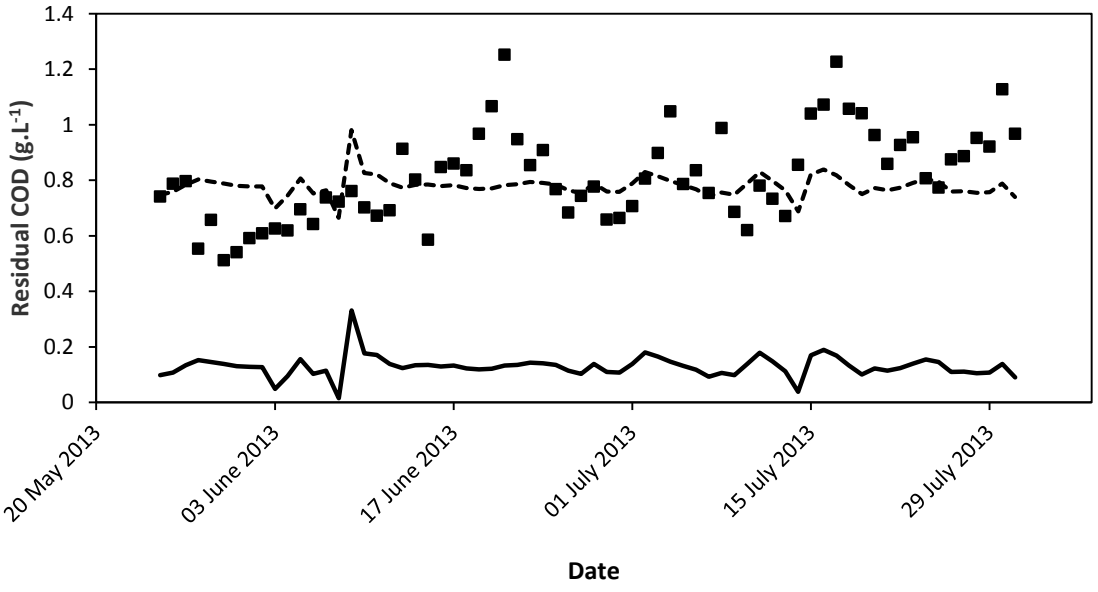

Figure 8.16. Residual COD comparison for 2013 period, ▪ plant data, ┅ uCOD model, ── model, RMSD 0.36 g.L^{-1} (0.65 g.L^{-1} uCOD).

8.4.2. Validation of mesophilic-thermophilic temperature transition

The overall objective of the model was the ability to simulate the mesophilic to thermophilic temperature transition. To validate that the model is capable of describing the transition, a clear transition from a mesophilic temperature of 40 to 50 °C was located from the historical plant data. A period of data was found for the year 2010 which showed a clear transition from under 40 °C to above 50 °C, with no process upsets and minimal sludge dosing occurring during the transition. The final calibrated model that was validated against 2013 data was used in the simulation of the

transition. Only q_o, and q_{sw} obtained from the plant data was used as model inputs. The effect of pH on the biomass activity was activated for the simulation (Fig. 8.17).

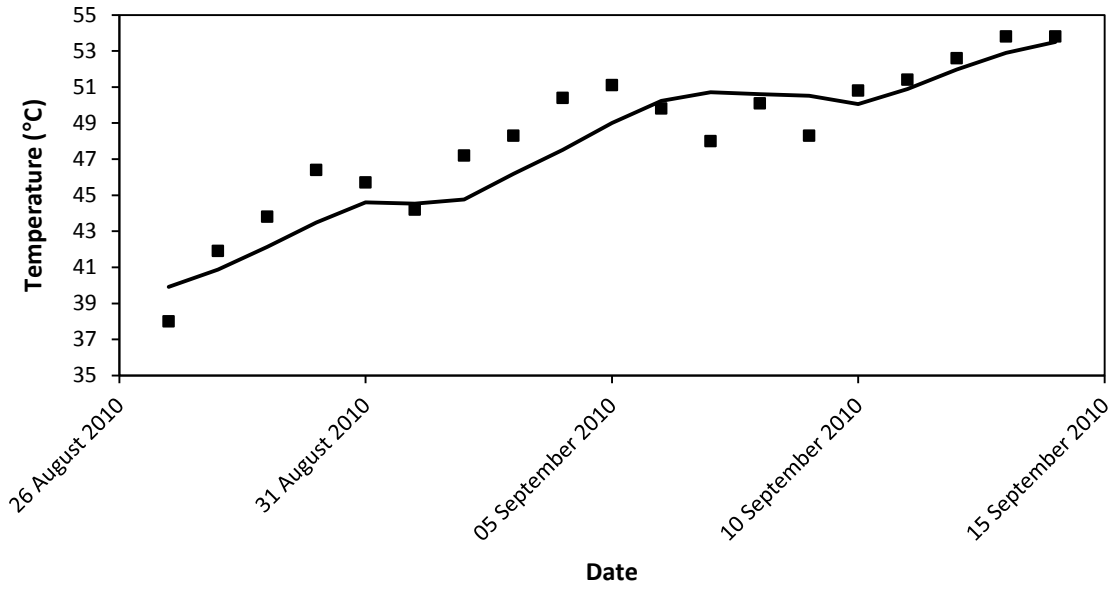

Figure 8.17. Mesophilic to thermophilic temperature transition for 2010 period, ▪ plant data, ── model, RMSD 1.70°C.

The primary objective of the model is that it is able to represent the transition from mesophilic to thermophilic operation. From Fig. 8.17 it can be observed that the model is able to describe the temperature transition between mesophilic and thermophilic regimes, with a RMSD of 1.70 °C, and is able to follow the trends observed by the plant data during the temperature increase, validating the primary objective of the model. The specific trends that were followed are the rates at which the temperature increases throughout the simulation. Therefore the model is able to simulate with reasonable success, the temperature profile with time as a result of changes in the feeding rate of the furfural plant effluent. The effect of the rate of chemical energy addition with the feed and how this controls (in part) the operating temperature of the reactor is clearly demonstrated in Fig. 8.17.

8.5. Sensitivity analysis

A sensitivity analysis was performed on the final calibrated model to determine the parameters that had the most significant effect on the MBR temperature, and may be a likely cause of any error in the model temperature prediction. For the sensitivity analysis the combined final model was simulated with the energy balance parameters being varied one at a time. The steady state temperature was determined for both a mesophilic and thermophilic feed rate (Table 8.13) for each of the parameters. The energy balance parameters that were altered are from Table 8.10, as well as the blowers that are operational, and additionally the parameters that were altered in Table 8.12. The baseline temperature for mesophilic and thermophilic operation following in the

trend of the study is 40 and 50 °C, respectively. A time indication is included to demonstrate the time that it took for the MBR temperature to reach a steady state temperature. The time taken for steady state to be reached does not always have a direct relationship with the change in MBR temperature; a larger temperature change can occur quicker when altering the same parameters. This is due to temperature oscillations which sometimes occur during temperature changes, and delay the temperature transition time.

8.5.1. Feed temperature

The furfural plant effluent enters the MBR from the DAF unit at a temperature between 36 and 40 °C. The influence of the furfural plant effluent temperature on the MBR temperature was investigated for a range of temperatures between 20 and 45 °C. Low temperatures, from 20 °C were selected to give an indication of how a possible buffer tank before the MBR would affect the operating temperature; it is assumed that the buffer tank would be at a temperature slightly above the ambient temperature, depending on the design.

As shown in Table 8.14 there was a small effect on the MBR temperature for the current feed temperature range of 36 to 40 °C for the furfural plant effluent fed to the MBR. The MBR temperature ranged between 39.3 and 40.3 °C for a mesophilic feed rate and 48.8 and 50.6 °C for a thermophilic feed rate, for a furfural plant effluent feed temperature between 35 and 40 °C. The effect of the lower furfural plant effluent temperatures has a somewhat more significant effect on the MBR temperature, specifically for thermophilic operation where the temperature retreats below 45 °C and into the mesophilic range.

Table 8.14. Steady state MBR temperature achieved at different feed temperature values at lower (mesophilic) and higher (thermophilic) feed rates.

MBR feed *T*	**MBR *T***	
(ºC)	**(ºC)**	
	Mesophilic feed rate	**Thermophilic feed rate**
20	36.4 (20 days)	43.3 (21days)
25	37.4 (17 days)	45.2 (16 days)
30	38.4 (14 days)	47.0 (11 days)
35	39.3 (14 days)	48.8 (10 days)
40	40.3 (10 days)	50.6 (11 days)
45	41.3 (14 days)	52.3 (10 days)

8.5.2. Aerators

The effect of the blowers on the operating temperature of the MBR was found by activating and deactivating the 2 blowers and 1 membrane scourer in different simulations, and finding the steady state temperature. The evaporation rate of water from the MBR was also calculated for each of the simulations. This is illustrated in Table 8.15 for both of the temperatures of operation.

Table 8.15. Steady state MBR temperature and evaporation rate achieved at different operational blowers at lower (mesophilic) and higher (thermophilic) feed rates.

MBR Blower	**MBR *T* (°C)**		**Evaporation Rate ($kg.s^{-1}$)**	
	Mesophilic Feed rate	**Thermophilic Feed Rate**	**Mesophilic Feed Rate**	**Thermophilic Feed Rate**
Blower 1	40.2	50.6	0.32	0.54
Blower 1 & Membrane Scourer	40.0	50.0	0.34	0.57
Blower 1 & Blower 2	40.0	49.5	0.38	0.63
Blower 1, Blower 2 & Membrane Scourer	39.8	49.0	0.40	0.67

The operation of blowers did not have a significant effect on the MBR temperature, with temperature changes of no more than 1 °C. The total quantity of water that is evaporated was calculated by dividing the total energy lost to evaporation, due to evaporative heat loss from aeration and surface evaporation, by the latent heat of evaporation at the temperature of operation. The evaporation rate from the MBR almost doubled for thermophilic operation. The evaporation from the MBR is approximately 11 % of the mesophilic feed to the MBR, and 5 % of the thermophilic feed to the MBR. Thus although evaporation rates are lower for mesophilic operation, a much larger portion of the feed is evaporated.

8.5.3. Wind speed

The wind speed has an effect on the surface evaporation and surface convection from the MBR. Low and high wind speeds can have an equally significant effect on the MBR temperature as shown in Table 8.16. A wind speed of 0 $m.s^{-1}$ increases the MBR temperature by around 10 °C for mesophilic and thermophilic operation, while a wind speed of 8 $m.s^{-1}$ reduces the temperature by around 4 °C for both thermophilic and mesophilic operation, respectively. As the MBR is

situated along the coast, and does not have substantial wind protection it is expected that the wind speed is a large factor associated with temperature fluctuations.

Table 8.16. Steady state MBR temperature achieved at different wind speed values at lower (mesophilic) and higher (thermophilic) feed rates.

Wind Speed ($m.s^{-1}$)	**MBR *T*** (^oC)	
	Mesophilic Feed Rate	**Thermophilic Feed Rate**
0	49.4 (18 days)	60.4 (11 days)
1	46.8 (19 days)	57.9 (10 days)
2	44.7 (17 days)	55.5 (12 days)
3	42.9 (14 days)	53.5 (12 days)
4	41.3 (17 days)	51.6 (9days)
5	40.0	50.0
6	38.8 (18 days)	48.5 (12days)
7	37.8 (15 days)	47.1 (12 days)
8	36.9 (18 days)	45.8 (12 days)

8.5.4. Relative humidity

The relative humidity of the incoming air is an important factor to evaporative aeration and surface evaporation (Eq. 6-41 and 6-38), and is directly linked to how much water is evaporated from the MBR. The effect of the relative humidity on the operating temperature and evaporation rate is shown in Table 8.17.

8.5.5. Ambient temperature

The ambient temperature affects the temperature driving force upon which the power loss terms are dependent. The MBR operating temperature is highly sensitive to changes in the ambient temperature (Table 8.18). Mesophilic operation is more sensitive, with temperatures fluctuating by around ± 9 °C while thermophilic temperatures fluctuate by around ± 6 °C. The steady state temperatures for each of the simulations was reached between 9 and 22 days.

Table 8.17. Steady state MBR temperature achieved at different relative humidity values at lower (mesophilic) and higher (thermophilic) feed rates.

Relative Humidity (%)	MBR *T* (ºC)		Evaporation Rate ($kg.s^{-1}$)	
	Mesophilic Feed Rate	Thermophilic Feed Rate	Mesophilic Feed Rate	Thermophilic Feed Rate
50	38.3 (20 days)	47.8 (11 days)	0.47	0.74
60	38.7 (16 days)	48.1 (12 days)	0.45	0.72
70	39.2 (17 days)	48.5 (10 days)	0.43	0.70
80	39.6 (4 days)	48.8 (6 days)	0.40	0.67
90	40.1 (5 days)	49.2 (7 days)	0.38	0.65
100	40.5 (14 days)	49.5 (9 days)	0.36	0.63

Table 8.18. Steady state MBR temperature achieved at different ambient temperature values at lower (mesophilic) and higher (thermophilic) feed rates.

Ambient T_a (ºC)	MBR *T* (ºC)	
	Mesophilic Feed Rate	Thermophilic Feed Rate
10	31.0 (22 days)	44.0 (15 days)
15	34.1 (20 days)	46.1 (14 weeks)
20	37.1 (16 days)	48.1 (14 days)
25	40.0	50.0
30	42.8 (10 days)	51.8 (9 days)
35	45.7 (10 days)	53.6 (9 days)
40	48.6 (13 days)	55.5 (10 days)

8.5.6. Rainfall

The effect of rainfall on the MBR temperature was investigated. Rainfall figures were used from historical data for Durban, wherein a roughly 800 mm of rain falls every year. There are around 90 days throughout the year wherein rainfall occurs, leading to an estimated average rainfall of

approximately 10 mm per day of rain. Therefore rainfall between 5 and 20 mm was simulated to determine the effect on MBR temperature, it was estimated that the rainfall occurred over a 6 hour period.

To simulate the rainfall an additional input stream to the MBR mass balance was modelled, consisting of water. The temperature of this stream is equal to the temperature of the rainfall, and was estimated at 20 °C. The flow rate of the stream entering the reactor was averaged over the time interval by dividing the total amount of rainfall (1 mm rainfall = 1 $L.m^{-2}$), by the interval over which the rainfall occurred (Table. 8.19).

Table 8.19. Steady state MBR temperature achieved at different rainfall values at lower (mesophilic) and higher (thermophilic) feed rates.

Rainfall (mm) (6 h interval)	**MBR *T* (°C)**	
	Mesophilic Feed Rate	**Thermophilic Feed Rate**
5	39.8	49.8
10	39.7	49.6
15	39.5	49.4
20	39.4	49.2

The parameters that the rainfall directly affected were the space time of the MBR and the enthalpy difference between the inlet and outlet streams. The effect of the rainfall on the MBR temperature was determined to be minimal, with a maximum temperature drop between 0.6 and 0.8 °C for mesophilic and thermophilic temperatures respectively.

It is expected that the high wind speeds and low ambient temperatures that often accompany rainfall would have a more significant effect.

8.5.7. Cloud cover

The effect of cloud cover on the MBR operating temperature was determined for thermophilic and mesophilic operation. The amount of solar radiation that the MBR receives is dependent on the cloud cover, which is measured in tenths. The maximum temperature drop over the range of cloud cover for mesophilic and thermophilic operation is 1.9 and 1.6 °C respectively. Thus solar radiation has a small effect on the temperature of operation.

The influence of night time on the MBR was simulated by equating the solar radiation to zero. The MBR temperature dropped by 0.7 °C for mesophilic and thermophilic operation, within the

first 12 hours after solar radiation was deactivated. The steady state temperatures, in the absence of solar radiation, are 37.0 and 47.6 °C; the steady state temperatures were reached in approximately 1 000 hours. The results of the simulations are shown in Table 8.20.

Table 8.20. Steady state MBR temperature achieved at different cloud cover values at lower (mesophilic) and higher (thermophilic) feed rates.

Cloud Cover (tenths)	**MBR *T* (ºC)**	
	Mesophilic Feed Rate	**Thermophilic Feed Rate**
0	40.5 (13 days)	50.4 (10 days)
2	40.4 (5 days)	50.3 (3 days)
4	40.1 (1 days)	50.0 (0 days)
6	39.6 (10 days)	49.7 (11 days)
8	38.9 (16 days)	49.1 (13 days)
10	38.1 (19 days)	48.4 (12 days)
Night	39.3 (37.0)*	49.3 (47.6)

*steady state values, 1000 hours after upset

8.5.8. Summary of results of sensitivity analysis

From the sensitivity analysis it can be observed that the MBR temperature is highly sensitive to wind speed and ambient temperature. The MBR temperature is also slightly less sensitive to the furfural plant effluent feed temperature, however the feed temperature generally does not vary to a large degree throughout the operation of the MBR. The assumption of an average wind speed and the ambient temperature throughout the energy balance calibration are therefore likely to cause a certain degree of error; it is expected that these parameters have a high variance in reality. Rainfall does not have a significant effect on the steady state MBR temperature, however, it is the conditions that tend to come with rainfall, i.e. high wind speeds and low ambient temperatures, which affect the MBR temperature.

The aeration rate and the relative humidity have a significant effect on the evaporation rate from the MBR. As expected the evaporation rate increases with an increase in aeration, and increases with a decrease in relative humidity. The evaporation rate is always greater at a higher temperature, however a greater amount of water is evaporated per volume of furfural plant effluent for mesophilic temperatures, approximately double that for thermophilic operation. This is due to the longer HRT experienced for mesophilic operation.

9. DISCUSSION AND MODEL OUTCOMES

This chapter firstly investigates the scientific significance of the model in its final calibrated form, and its outcome in relation to the hypotheses outlined in chapter 4. The analysis of the model is presented primarily in terms of its ability to predict the plant performance, as well as the accuracy of the model prediction.

The remaining sections in the chapter, 9.2 to 9.4, analyse the engineering significance of the model, in terms of the power distribution of the various heat transfer mechanisms, design outcomes, and operational outcomes. The outcomes and analyses are primarily in terms of mesophilic versus thermophilic operation, investigating the advantages and disadvantages of each temperature regime.

9.1.Discussion of scientific outcomes

The hypotheses upon which the thesis is based are restated:

Hypothesis 1:

A mass and energy balance model of the MBR that explicitly considers the interactions of temperature and pH on the kinetics and stoichiometry of the furfural plant effluent degradation, will be able to simulate the key variables to agree with plant observations during transition from mesophilic to thermophilic conditions.

Hypothesis 2:

The transition from a mesophilic to thermophilic regime, or thermophilic to mesophilic regime, can be described by modelling a single biomass population, as opposed to separate biomass populations representing each temperature regime.

The hypotheses are answered through the formulation of a dynamic mass and energy balance model, and an attached speciation routine for pH prediction. The model has been formulated in chapter 6, and the model calibrated in chapter 8.

It can be concluded that the model is capable of steady state and dynamic prediction for temperature and pH within the required range for the design and operational model predictions. It has also been shown in Fig. 8.17 that one of the primary outcomes of the model has been validated, i.e. that it can predict the temperature transition from mesophilic operation at 40 °C to thermophilic operation at 50 °C. The temperature can be accurately predicted to less than 2 °C during a dynamic simulation over an extended period of time (over 60 days), with only the furfural plant effluent feed rate (q_o) and the sludge wasting rate (q_{sw}) required. The model is also capable of pH predictions to within a RMSD of less than 0.5 pH units.

As illustrated in Fig. 8.14 the model is able to predict the general trend of the temperature over the simulation time period. The same can be said, although to a lesser extent for the pH prediction in Fig. 8.15. It is expected that a cause of uncertainty in the prediction is that the pH is dependent on the day to day nutrient dosing to the MBR, for which plant data is not available. Urea and phosphoric acid are dosed to the MBR to maintain a healthy microbial population. A typical nutrient rate was been estimated for the simulation purposes. There is also an unquantified amount of nutrients that enter the MBR through WAS dosing from the neighbouring CAS which further complicates the pH prediction.

The model is also capable in theory of predicting X_{VSS} within the MBR, as well as S_S. But due to assumptions made by the model, i.e. the sludge dosing from the neighbouring CAS plant not being accounted for, the uncertain ratio between the MLSS and MLVSS concentration, as well as the feed being entirely and readily biodegradable; the predictions of the aforementioned parameters are uncertain. Therefore until further quantification has been performed in this area the model is not capable of reliable prediction of X_{VSS} and S_S within the MBR.

By including a temperature dependence factor in the kinetic parameters the MBR can be successfully modelled using a single biomass concentration for both mesophilic and thermophilic temperatures; in addition the temperature transition can be modelled. Whether or not there actually is a single micro-organism population or more present within the MBR is uncertain; what has been shown is that both temperature regimes may be adequately represented by the single biomass concentration. It is believed that the upsets which occur and the lengthy recovery times are partially a result of the drop in X_H resulting from a high k_d value.

It is believed that the best predictive ability has been obtained for the current model for the assumptions and simplifications that have been made. To achieve a more accurate model prediction a more in-depth calibration of the model is required, one in which all the parameters (external environmental factors, etc.) have been measured over a suitable time interval, and a minimisation routine performed again. Questions may also be raised over the comparison of the plant data measurements, since they are calculated as an average over the day (the temperature and pH are measured every 8 hours at Illovo), whereas the model simulation calculates an average temperature and pH over a 24 hour period using a time step of 1 hour. In addition to this, an assumption of the model is that the MBR temperature is uniform throughout the reactor (lumped parameter), whereas in reality, temperature gradients are present which affect the temperature measurement. The temperature is measured in the permeate withdrawal line, which may lead to an underestimation of the actual MBR temperature. The model also assumes that the feed and sludge wasting rates are constant throughout the day, however during daily operation of the MBR

the furfural plant effluent feed is not constant throughout the day, and fluctuations regularly occur.

The latter part of the chapter will deal with the engineering significance of the results and the differences between the two temperature regimes.

9.2.Power distribution

The distribution of the different power outputs and inputs to the MBR have been determined for operation at the mesophilic and thermophilic flow rates, respectively (Fig. 9.1 and 9.2). The effect of each of the heat transfer mechanisms can be assessed for each of the temperature regimes. The mechanisms are all included in the pie charts, both power losses and gains. Power of reaction, blowers and solar radiation is always positive (gains), while surface evaporation, surface convection, atmospheric radiation and aeration are always negative (losses). The enthalpy is dependent on the inlet and outlet stream temperatures and the temperature of operation, and therefore can be either positive or negative.

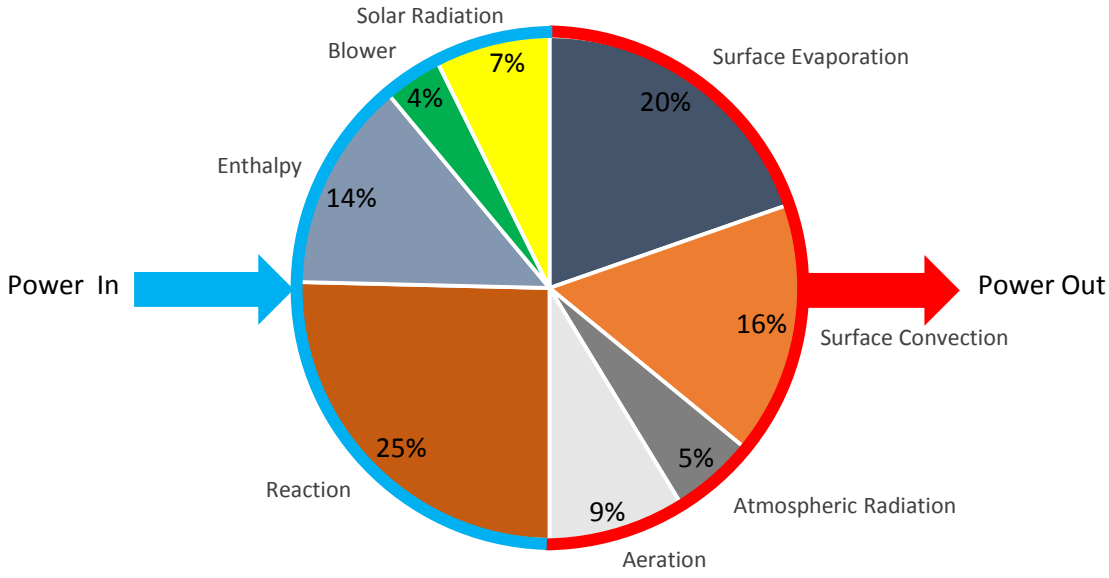

Figure 9.1. Power distribution for mesophilic operation at steady state.

The power generated by reaction is the dominant source of power for both modes of operation, with 25 and 36 % for mesophilic and thermophilic regimes, respectively. There is a large difference between the heat of reaction for the regimes, as at thermophilic operation higher k_d values are experienced, leading to higher power generation from the exothermic reaction of biomass decay Eq. 6-19. In addition to this μ_m is increased, leading to greater substrate consumption rates and increased power generated from the exothermic macro-chemical reaction Eq. 6-18. Other considerable factors that play a significant role in the energy balance are surface convection, surface evaporation and enthalpy.

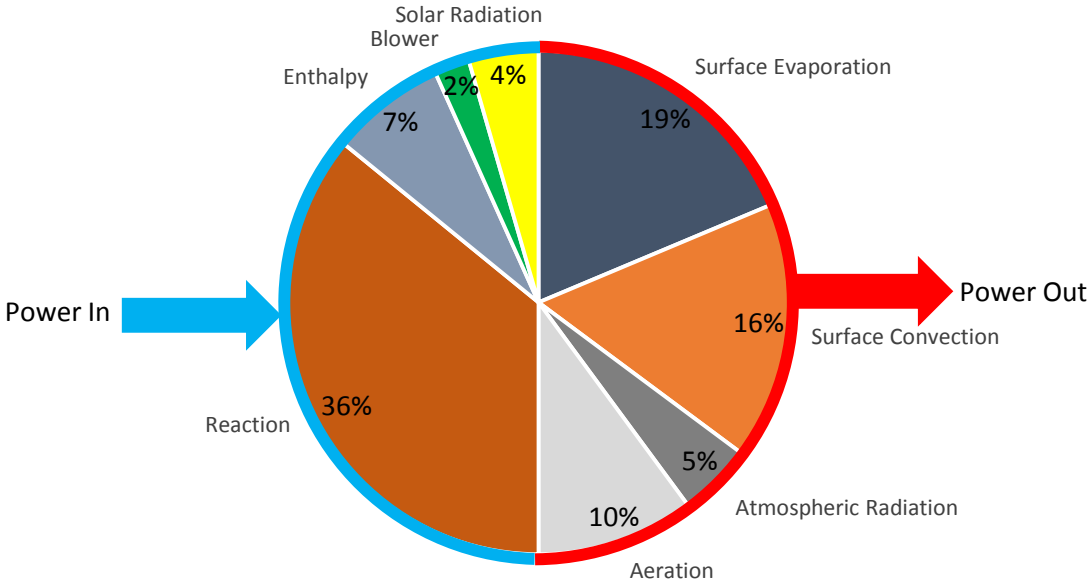

Figure 9.2. Power distribution for thermophilic operation at steady state.

Initially it was expected that the enthalpy difference of the streams flowing into and out of the MBR would have a negative effect on the MBR temperature, as the furfural plant effluent feed to the MBR is at a lower temperature (38 °C) than the MBR operating temperature during mesophilic and thermophilic operation. The outcome of the overall enthalpy balance was that it had a positive contribution to the energy balance, this is as the enthalpy loss resulting from evaporated water from the MBR is explicitly calculated through the evaporation and aeration power loss terms (Eq. 6-38 and 6-41). Therefore the enthalpy as represented in Fig. 9.1 and 9.2 only accounts for liquid inlet and outlet streams, and is not balanced in terms of mass as there is a greater flow into the reactor than out of it because of evaporative losses.

Solar radiation and atmospheric radiation have a minor contribution to the overall energy balance for both mesophilic and thermophilic operation; they are the two smallest heat transfer terms for both operational regimes. This is further diminished by the fact that solar radiation and atmospheric radiation have counteracting effects on the energy balance. Therefore the radiation terms tend to cancel each other out; the net effect of radiation is a 2 % contribution for mesophilic operation and a 1 % contribution for thermophilic operation. Thus the overall effect of radiation can be assumed to be very nearly negligible to the overall energy balance.

9.3.Design outcomes

The design outcomes pertains to the reactor space time that is associated with each of the different temperature regimes. Very simply this is the feed rate for each temperature of operation, from Table 8.13, divided by the estimated reactor volume of 4 060m^3.

Table 9.1. Reactor space time for mesophilic (40 ºC) and thermophilic (50 ºC) operation.

T **(ºC)**	**Space Time (h)**
40	315
50	139

Thus for the same furfural plant effluent feed rate to the MBR, the mesophilic regime would require a reactor working volume that is 2.2 times larger than that required for the thermophilic regime.

9.4.Operational outcomes

The operational outcomes from the model involve the simulation of the MBR at unsteady state, for a number of 'process upset' scenarios that the Illovo MBR would typically encounter during an operational season. The scenarios that were simulated relate to furfural plant effluent feed rate upsets that occur during operation of the MBR, caused by a fluctuating feed rate. Identical simulations were performed for both mesophilic and thermophilic temperatures. The comparison of the regimes was performed on the basis of which would be more costly, in terms of energy required to be added/removed during a process upset to maintain stable operation, as well as which regime provides more operational stability through the process upset. The final calibrated model was used with the effect of the pH on the biomass activity for the scenario simulations.

9.4.1. Thermophilic-mesophilic/mesophilic-thermophilic process transitions

The furfural plant effluent feed rate to the MBR was altered during steady state operation to cause the operating regime transition for both mesophilic to thermophilic, and thermophilic to mesophilic operation. The energy loss/gain required to maintain the MBR at the selected temperature of operation (mesophilic or thermophilic) during a feed increase/decrease was also determined through simulation of the model. For mesophilic operation the energy to be removed was calculated for when the feed rate to the MBR increases to a thermophilic feed rate (29.3 $m^3.h^{-1}$). For thermophilic operation a feed reduction to a mesophilic rate (12.9 $m^3.h^{-1}$) was simulated and the amount of heating required to maintain thermophilic operation was calculated.

9.4.1.1. Thermophilic-mesophilic process transitions

A simple switching function was used. At a set time of 100 hours, the feed rate to the MBR was decreased from a thermophilic flow rate of 29.3 $m^3.h^{-1}$ to a mesophilic feed rate of 12.9 $m^3.h^{-1}$. In addition to this, the sludge wasting flow rate was altered from thermophilic to that used for mesophilic operation (Table 8.7).

The temperature versus time plot generated by the model simulation is shown in Fig. 9.3. The temperature initially decreases at a rate of around 0.08 °C per hour, before the temperature begins to level off at 40 °C. Steady state is reached in approximately 200 hours (8.3 days) from the initial process change.

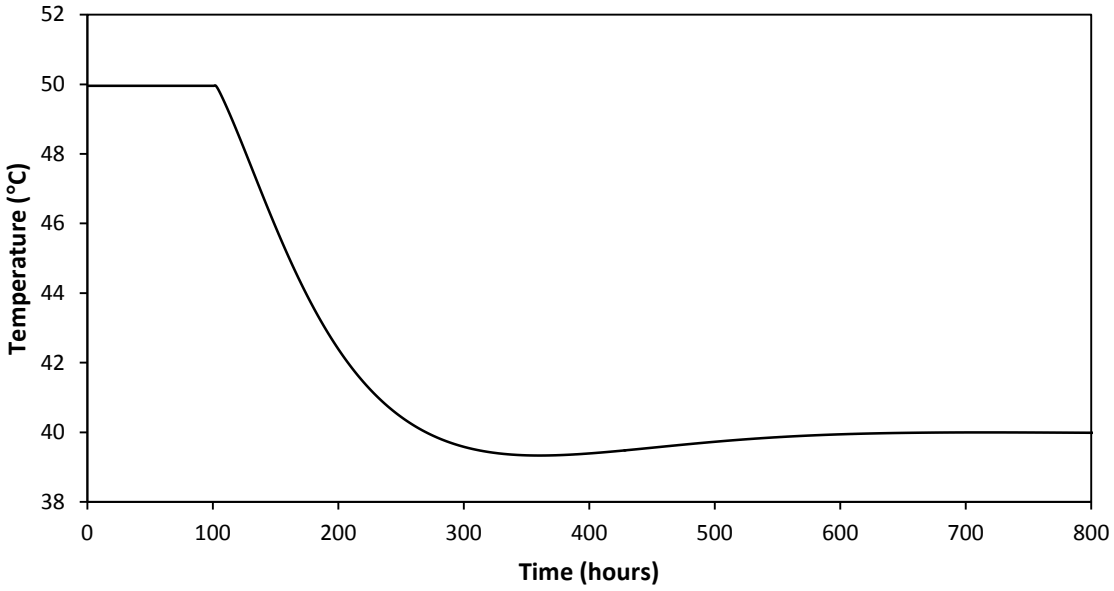

Figure 9.3. Simulated temperature response for thermophilic-mesophilic process transition.

The related pH and X_H simulations are shown in Fig. 9.4 and 9.5. As the furfural plant effluent is cut the pH of the MBR rapidly rises as a result of the rapid consumption of substrate at a lower feed rate. The lower S_S leads to lower X_H growth rates and lead to a decrease in X_H. As the temperature decreases X_H growth rates decrease, as well as X_H death rates, which leads to an increase in X_H.

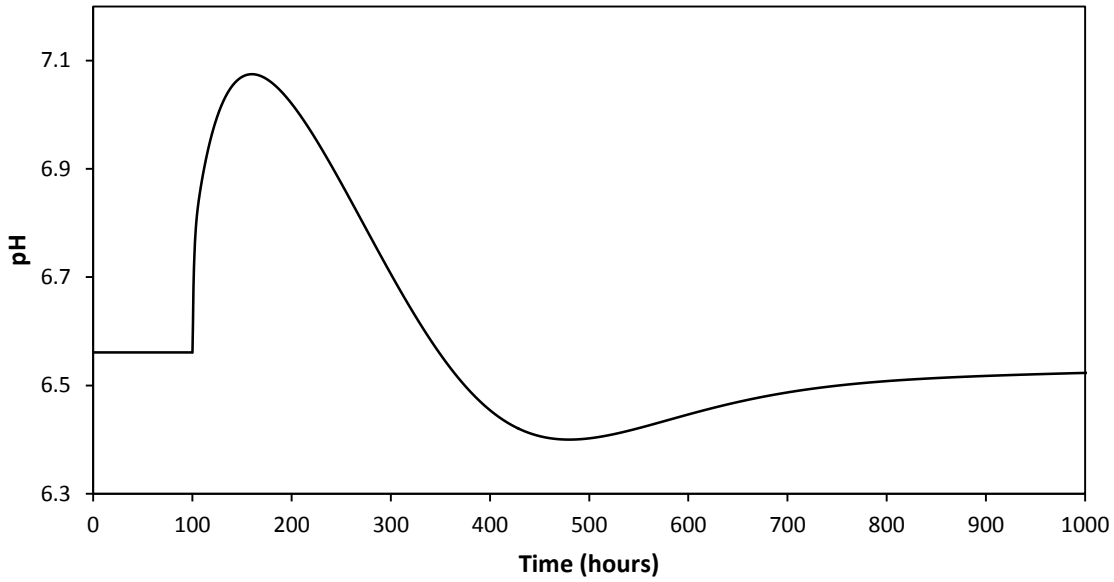

Figure 9.4. Simulated pH response for thermophilic-mesophilic process transition.

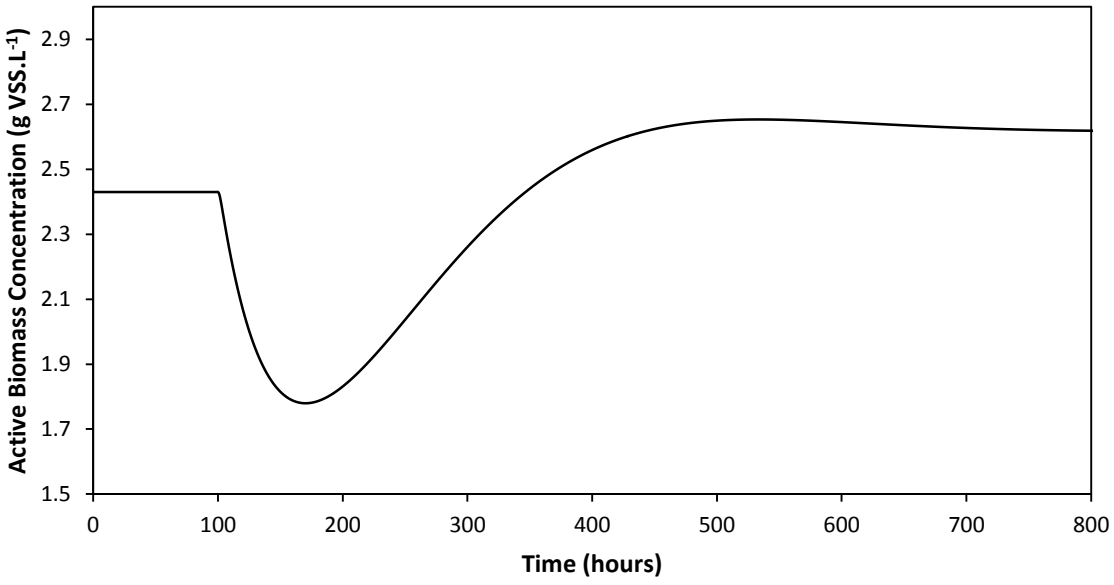

Figure 9.5. Simulated active biomass response for thermophilic-mesophilic process transition.

The power distribution has been generated for the process upset, and plotted as a percentage of total power gains and total power losses versus time. There are only minor changes in the power loss distribution for the duration of the upset (Fig. 9.6). The contribution of aeration to the total power losses drops from 20.2 to 17.3 %, due to a lower temperature driving force between the reactor and ambient air. There is also very slight decrease in the contribution of surface convection. On the other hand the effect of evaporation and atmospheric radiation increase.

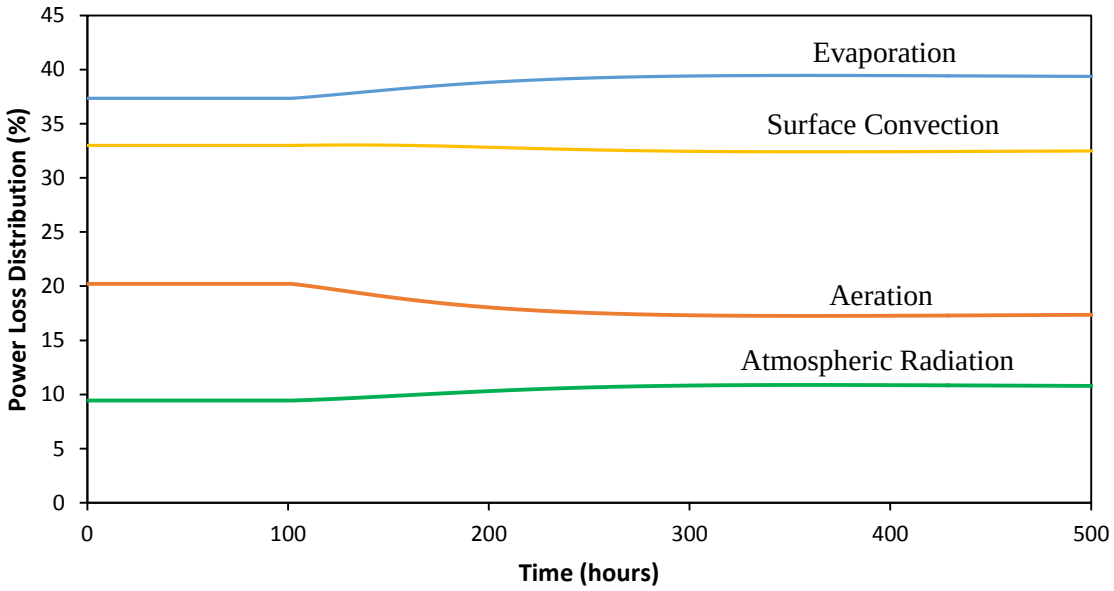

Figure 9.6. Distribution of the power lost from the MBR during the simulation.

The distribution of the power gained by the MBR is shown in Fig. 9.7. Due to the lower feed rate to the MBR the power generated by reaction decreases considerably, and this is subsequently offset by the enthalpy contribution. The enthalpy contribution is sharply increased, due to the altered enthalpy balance caused by the decreased feed and withdrawal rates. The percentage contribution of solar radiation and the compressors increases slightly. Solar radiation and the power from the compressors is independent of the MBR temperature, and therefore do not change in the absolute value of power contributed, they only increase in their proportion of energy contributed.

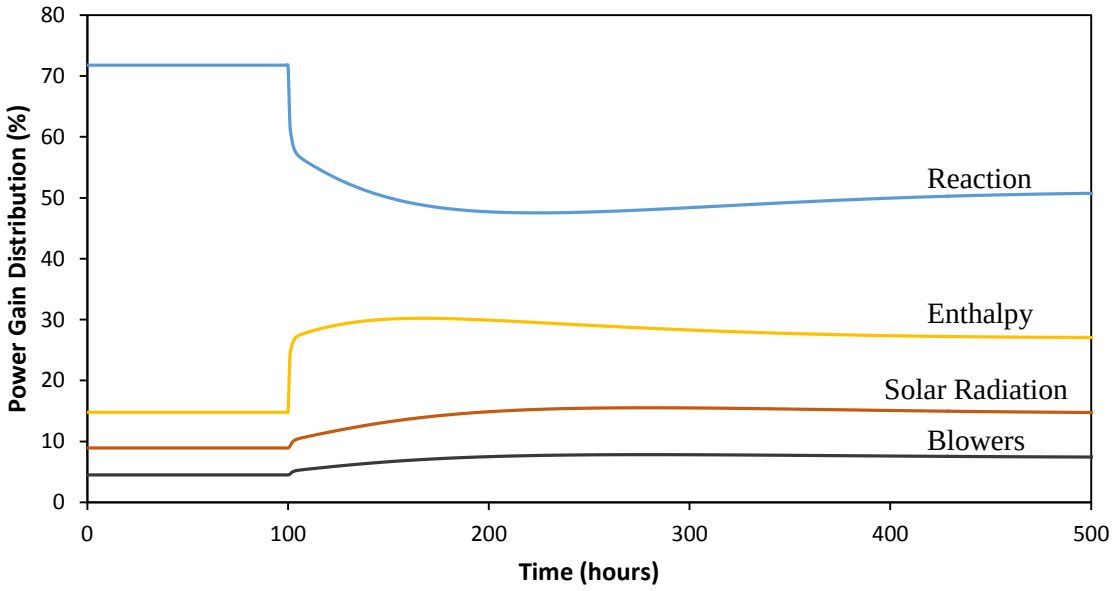

Figure 9.7. Distribution of the power gained from the MBR during the simulation.

The power input/output over the process transition is illustrated in Fig. 9.8, at steady state the power input and output to the MBR are equal, but when the temperature is unsteady the values differ. The sharp decrease in the power input to the MBR is a result of the enthalpy balance being altered by the decrease in feed rate.

An iteration was performed to determine the quantity of heating required to maintain thermophilic operation, by selecting a heating amount that would increase the temperature back to 50 °C. The amount of power required to maintain thermophilic operation for a mesophilic feed rate was determined to be 790 kW.

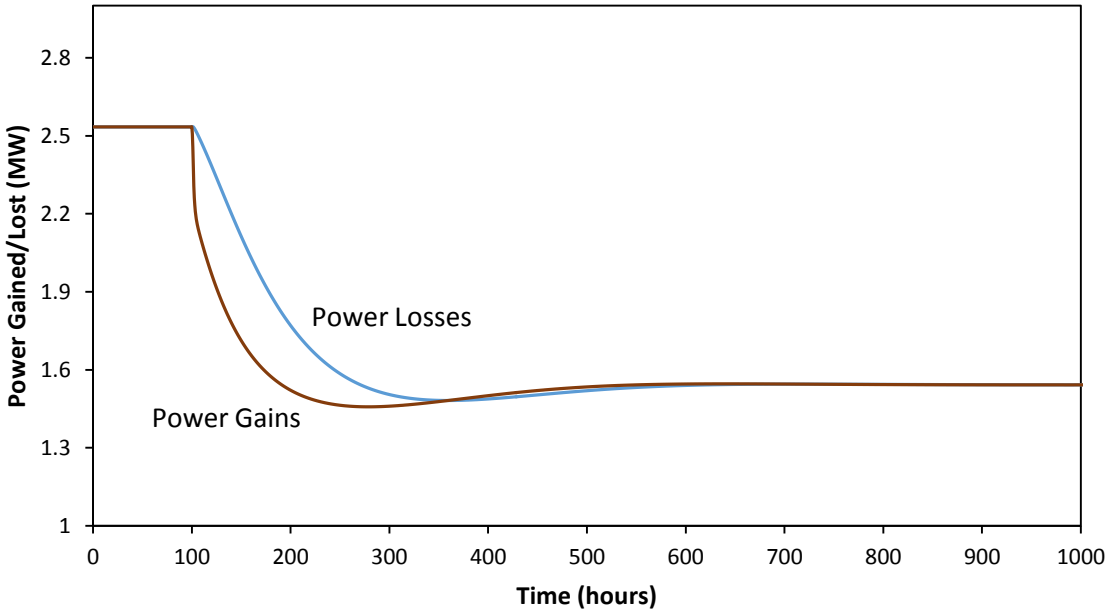

Figure 9.8. Power lost/gained from the MBR during the simulation.

9.4.1.2. Mesophilic-thermophilic process transitions

The alternate simulation was performed where the MBR is operating at steady state at a mesophilic temperature, and a process transition occurs, whereby the feed to the MBR is increased to a thermophilic feed rate. It was found through the simulation that the instantaneous feed rate increase to the MBR had an adverse effect on the MBR, as the pH rapidly dropped to values below 5 due to increased S_S concentrations within the MBR. The drop in the pH led to a vicious circle type scenario which had a detrimental effect on the biomass population which became inactive, and operation of the MBR collapsed, as illustrated by Fig. 9.9 – 9.11. The vicious circle type scenario is where a decrease in biomass activity lowers the pH, and a low pH decreases the biomass activity until MBR activity collapses. This scenario can be avoided by controlling the furfural plant effluent feed rate (q_o) so as to maintain the MBR pH above 6.

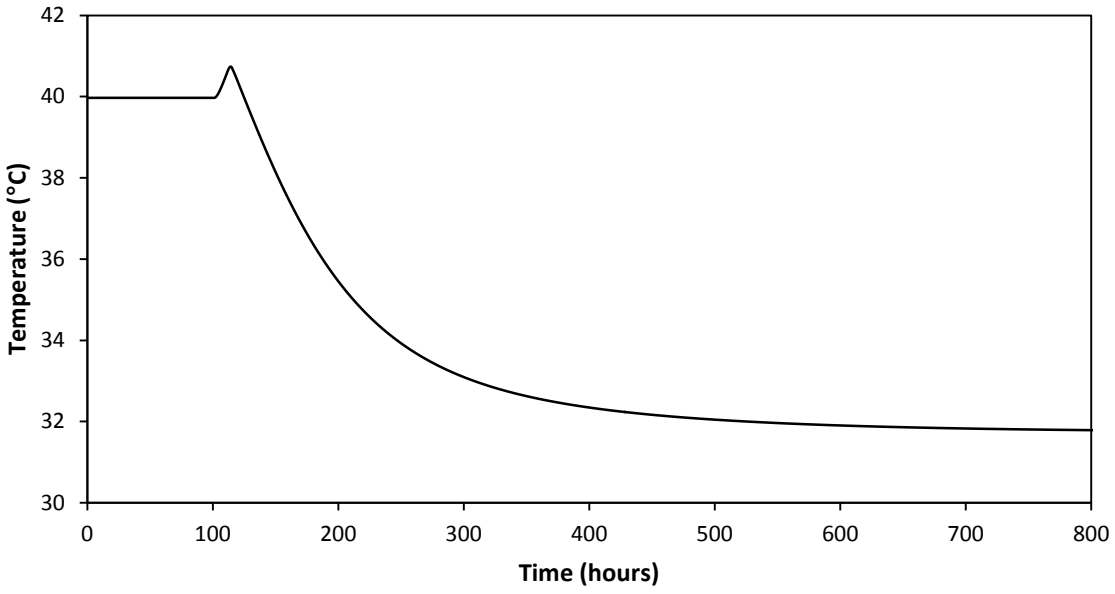

Figure 9.9. Simulated temperature response to a mesophilic-thermophilic process transition.

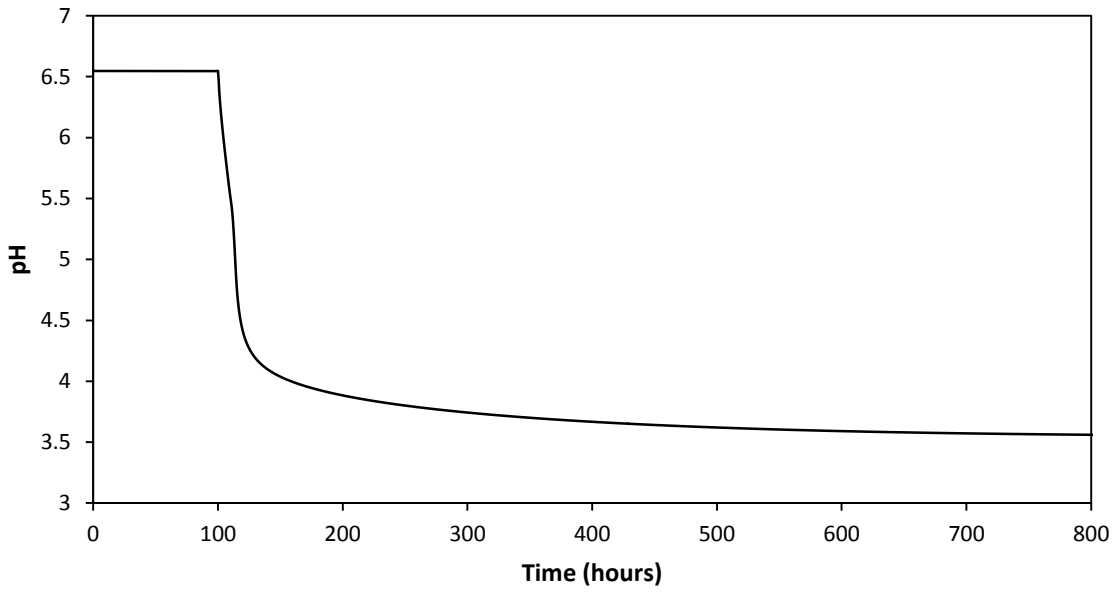

Figure 9.10. Simulated pH response to a mesophilic-thermophilic process transition.

To avoid the sharp pH drop a control mechanism was employed to gradually increase the feed to the MBR up to a thermophilic flow rate. The feed is pH controlled using the algorithm in Table 9.2.

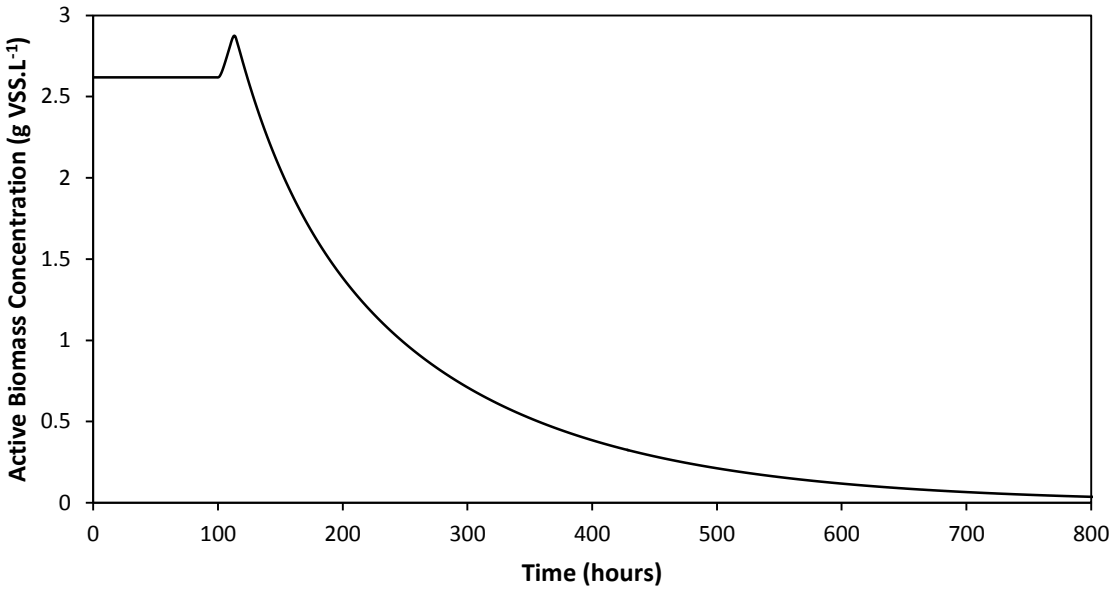

Figure 9.11. Active heterotrophic biomass concentration from a mesophilic-thermophilic process transition.

Table 9.2. Feed rate control mechanism.

	q_o ($m^3.h^{-1}$)	q_{sw} ($m^3.h^{-1}$)
pH ≤ 6.05	12.9	1.6
pH ≥ 6.20	29.3	3.1

Using this method the feed is increased quickly without inactivating the micro-organism population due to a drastic pH drop. It was observed that a transition from mesophilic to thermophilic operation takes in excess of 300 hours (12.5 days) (Fig. 9.12.). The temperature increases initially at a gradual rate of 0.029 °C per hour. The pH throughout the simulation is shown in Fig. 9.13 and X_H is shown in Fig 9.14. X_H initially increases due to an increased S_S at mesophilic conditions, leading to increased X_H growth rates. An increase in temperature leads to an increase in k_d which decreases X_H, as well as an increase in μ_m which decreases S_S back to a steady state value.

To overcome the long transition time from mesophilic to thermophilic operation Illovo tend to feed activated sludge from a neighbouring CAS plant to increase biomass activity. By feeding sludge from the neighbouring CAS plant, it has the effect of increasing the X_H concentration within the MBR which leads to increased S_S consumption rates and therefore increased power generated from the exothermic reaction, which in turn leads to decreased temperature increase

times. The higher S_S consumption rates also maintain the pH above 6. An alternative solution may be to increase the pH through the addition of NaOH.

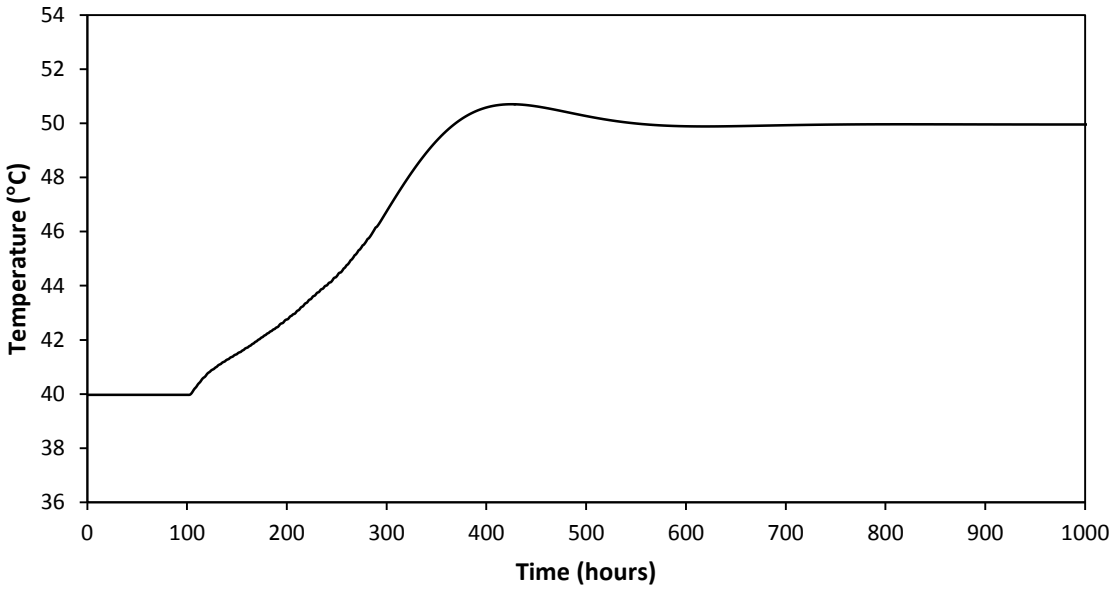

Figure 9.12. Simulated temperature response to a mesophilic-thermophilic process transition, with control mechanism.

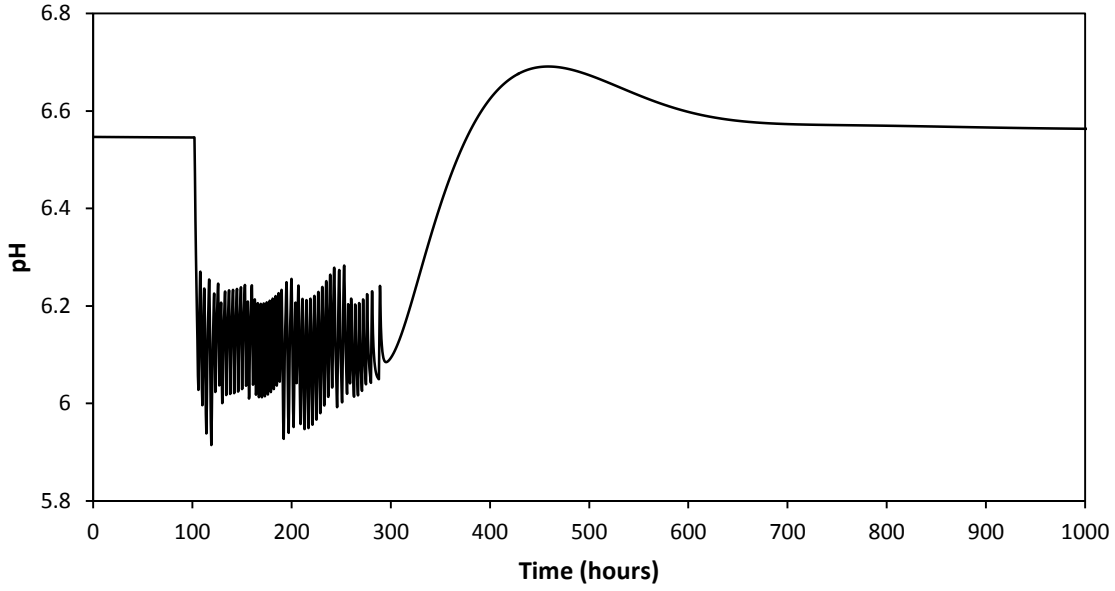

Figure 9.13. Simulated pH response to a mesophilic-thermophilic process transition, with control mechanism.

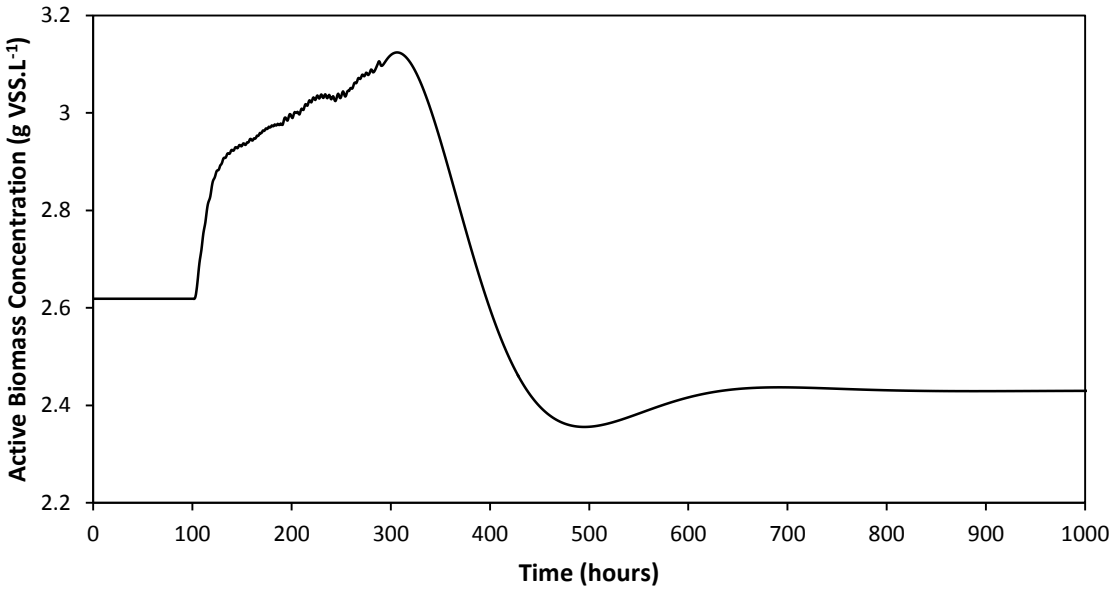

Figure 9.14. Active biomass response to a mesophilic-thermophilic process transition, with control mechanism.

To determine the amount of cooling required to maintain mesophilic operation for a thermophilic feed rate, cooling was applied. It was found that 920 kW of cooling is required to maintain a mesophilic temperature for a thermophilic feed rate. More cooling is required to maintain mesophilic operation, than heating (790 kW) to maintain thermophilic operation. The difference in values is due to the temperature dependence of the kinetics, which has different values at different temperatures, which the heat of reaction is reliant on.

However, it was found during the cooling simulation that in order to accommodate the increase in the feed rate higher S_S consumption rates were required. The only manner in which the model can achieve this is through increasing X_H, the concentration increased to a value of 5.05 g.L^{-1}. The model has not been validated for these conditions, and the effects are uncertain on the operation of the MBR.

9.4.1.3. Summary of results of temperature transitions

From this analysis it can be observed that it may be a time consuming process to increase the operating temperature due to the low pH of the feed to the MBR, however temperature drops can occur slightly faster as the pH limitation does not play a role. It is critical to maintain the MBR pH above 6 to maintain biomass activity. What this translates to in terms of thermophilic operability is that it would be a time consuming process during reactor startup to increase the temperature to the higher operating temperature. For mesophilic operability the feed rate is very much limited, any sudden increases in the feed would quickly result in a detrimental effect on the MBR caused by a drop in the pH.

9.4.2. MBR instability (feed – no feed – feed)

If the furfural plant effluent feed to the MBR is cut for a significant amount of time, after which the feed to MBR is resumed, a disturbance in the operation of the MBR is caused. The disturbance occurs as there is a drop in X_H due to lack of S_S which is rapidly depleted, leading to lower X_H growth rates. Once the feed to the MBR is resumed X_H rapidly reaches the maximum growth rate, although at the lower X_H the substrate cannot be consumed fast enough, leading to lower S_S consumption rates. This results in a sharp increase in the S_S concentration (acetic acid), which results in a pH drop, and as the environment within the MBR becomes increasingly intolerable, the biomass activity drops further (Table 8.9), and a vicious circle scenario is thus created.

The purpose of these simulations is to compare the MBR recovery times for each of the upsets for both the mesophilic and the thermophilic regime.

9.4.2.1. Mesophilic instability

For the mesophilic upset, the feed is cut for a set time after which the mesophilic feed rate resumes. The maximum time that the feed cut can occur without causing instability within the reactor was found through iteration to be 98 hours (4.1 days). Instability in this case is defined as the vicious circle scenario.

A simulation was performed where the feed was cut for 99 hours, so as to cause instability. The control mechanism of Table 9.3 was used for the temperature response back to mesophilic operation (Fig. 9.15). The control mechanism is only employed after the feed cut, of 99 hours.

Table 9.3. Mesophilic upset feed control algorithm.

	q_o ($m^3.h^{-1}$)	q_{sw} ($m^3.h^{-1}$)
pH ≤ 6.05	6	0.8
pH ≥ 6.25	12.9	1.6

The temperature, shown in Fig. 9.15, falls at a steep rate when the feed has been cut, almost reaching 30 ºC within 96 hours (4 days). The feed is resumed at the 199 hour mark and gradually begins its pH limited climb back to a mesophilic temperature of 40 °C. It takes slightly over 300 hours (12.5 days) to fully recover back to a mesophilic temperature of 40 °C.

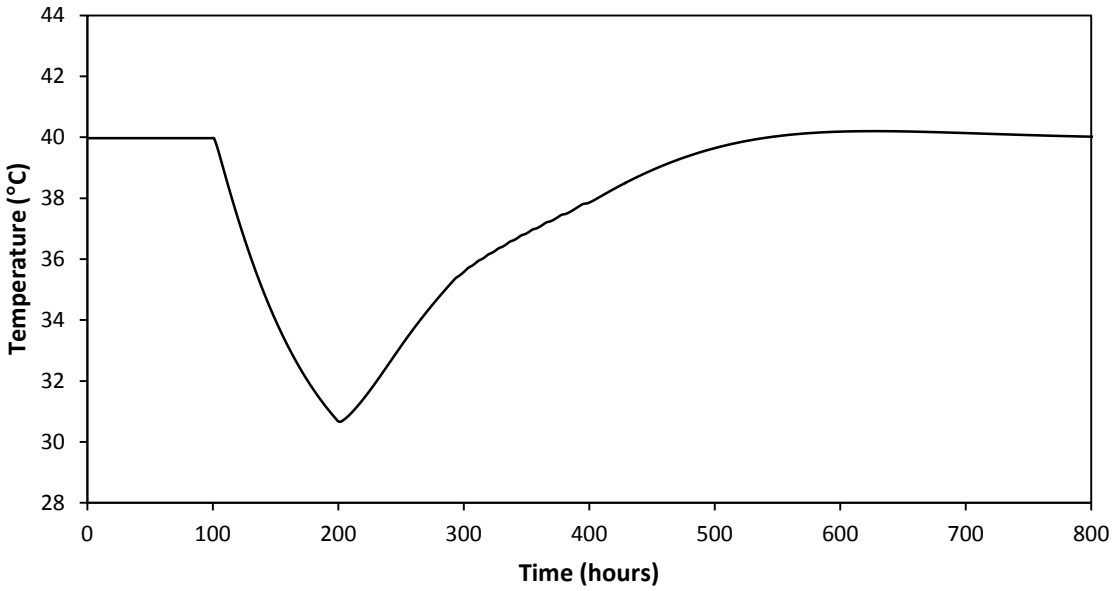

Figure 9.15. Simulated mesophilic temperature response to temperature upset and recovery.

The pH plot generated by the simulation is shown in Fig. 9.16, it can be seen where the control scheme starts just before the 300 hour mark. The X_H concentration in Fig. 9.17 decreases until the feed is resumed, until it rapidly increases back to mesophilic concentrations.

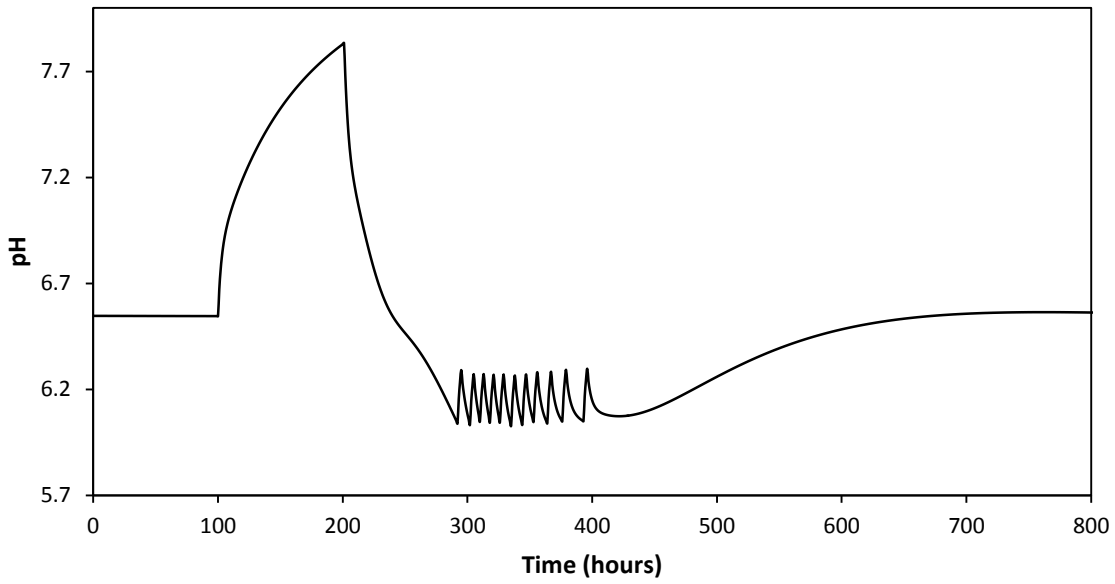

Figure 9.16. Simulated mesophilic pH response to temperature upset and recovery.

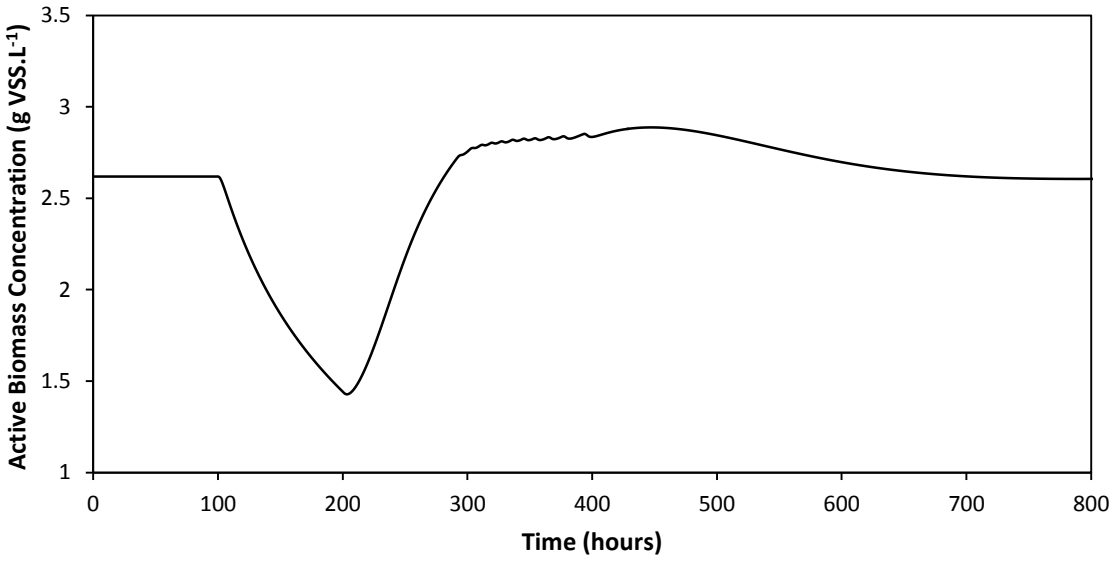

Figure 9.17. Simulated mesophilic active biomass response to temperature upset and recovery.

9.4.2.2. Thermophilic instability

In the thermophilic simulation the MBR receives a complete feed cut for a set amount of time, after which the thermophilic feed rate resumes. It was found that the maximum amount of time in which a feed cut could occur for thermophilic operation was 30 hours, at a time longer than this the pH would significantly drop. The effect of a feed cut is shown for 31 hours, with the control mechanism of Table 9.2. The temperature drops to below 42 °C within 44 hours before it starts to increase again (Fig. 9.18). The total recovery time back to a thermophilic temperature of 50 °C is approximately 300 hours (12.5 days).

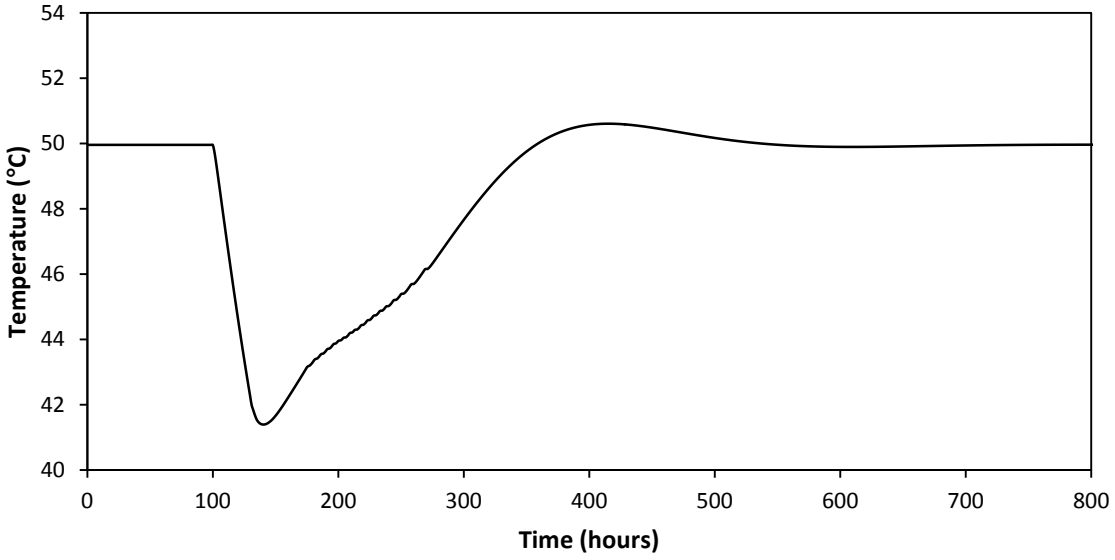

Figure 9.18. Simulated thermophilic temperature response to temperature upset and recovery.

The pH plot is illustrated in Fig. 9.19. The control mechanism begins about 50 hours after the feed is resumed. The X_H concentration is illustrated in Fig. 9.20.

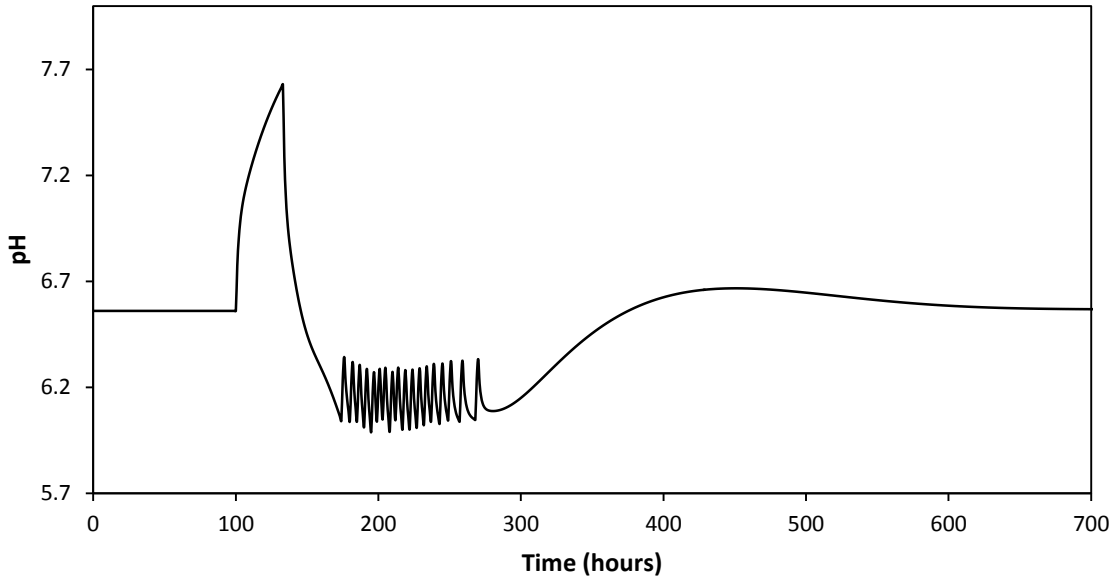

Figure 9.19. Simulated thermophilic pH response to temperature upset and recovery.

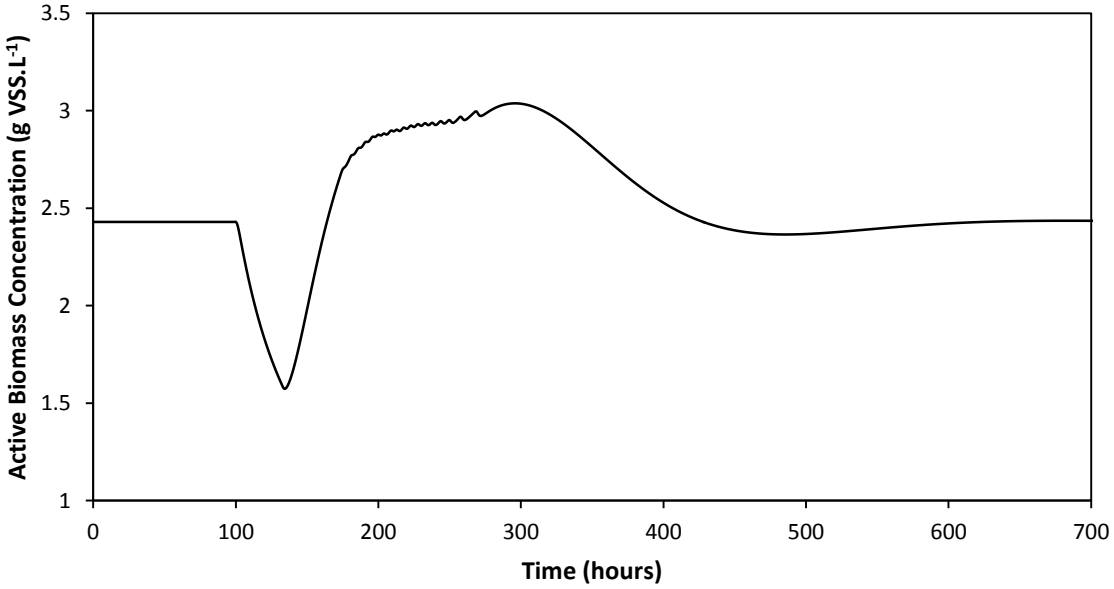

Figure 9.20. Simulated thermophilic active biomass response to temperature upset and recovery.

9.4.2.3. Summary of results of feed upset

A feed cut for a period of time, followed by the resumption of the feed rate to the MBR would be representative of typical plant operation, where feed cuts often occur due to maintenance of equipment or upstream production stoppages. It can be seen that feed upsets to the MBR can have a significant impact on the operation of the MBR, and result in time consuming recoveries back

to stable operation. The feed upsets are further exacerbated by the pH limitation on feed increases. It was found that mesophilic operation is more resistant to the feed upsets to the MBR, and is able to withstand a feed upset for approximately 3.3 times longer than thermophilic operation.

9.5.Final outcomes

In summary, the comparison of mesophilic to thermophilic operation of the MBR results in the following:

Power distribution	The radiation terms tend to cancel each other out, and have a negligible effect on the overall energy balance. The heat of reaction is the dominant source of heat transfer. Its overall contribution increases by 10 % for thermophilic operation as compared to mesophilic operation.
Design outcomes	Mesophilic operation would require an MBR volume that is 2.2 times larger than that required for thermophilic operation, for the same feed rate.
Operational outcomes	Startup to thermophilic operation is a time consuming process as compared to mesophilic operation. Due to the acidic nature of the furfural plant effluent only limited increases in the feed rate can be achieved to maintain pH levels. Mesophilic operation is better suited to handling feed reductions, and provides overall more stable operation. The amount of heat removal required to maintain mesophilic operation for a thermophilic feed rate is slightly higher, by 130 kW, than the power required to heat the MBR and maintain thermophilic operation for a mesophilic feed rate. However it is uncertain what effect heat removal would have on the operation of the MBR as it would necessitate to a substantial increase in the biomass concentration. To decrease the temperature transition times during feed increases, the active biomass concentration may be increased by dosing active sludge, or possibly by increasing the pH by the addition of NaOH.
Miscellaneous	It has been found through simulations that for thermophilic operation more evaporation occurs, up to double the rate for mesophilic operation. However, the percentage of the feed that is evaporated is 6 % higher for mesophilic operation.

In conclusion, there is no clear cut answer as to which temperature regime to design for, and a full economic analysis, taking into account the nature and frequency of process upsets that the process will be subject to, would be required to provide a comprehensive solution. Thermophilic operation can handle substantially larger feed rates. If identical MBRs were constructed to treat the entire furfural plant effluent, with a total flow rate estimated at 125 $m^3.h^{-1}$ (Table 3.1) it would require approximately 5 MBRs to successfully treat the stream for thermophilic operation. For mesophilic operation it would require approximately 11 MBRs to treat the entire furfural plant effluent, which would result in a substantial increase in capital expenditure, as well as operational costs for aeration and maintenance for each of the MBRs. If a method were found to reduce instability within the MBR for thermophilic operation then it would be the clear selection. The primary cause of the instability is the frequent feed reductions that occur, and the timely recovery back to normal operation.

One of the possible solutions to reduce feed fluctuations to the MBR may be a buffer tank. This would increase the capital costs involved with thermophilic operation, but would likely be less than the capital costs involved with constructing the extra MBRs required for mesophilic operation. An added benefit of a buffer tank is that the temperature of the furfural plant effluent to the MBR would be reduced, which would decrease the operating temperature of the MBR. The result of this is that the MBR would be able to achieve even higher feed rates to reach an operating temperature of 50 °C. It has been found through model simulations that if the feed temperature of the furfural plant effluent were reduced to 30 °C, as a result of a buffer tank, a feed rate of 36 $m^3.h^{-1}$ would be required to maintain operation at 50 °C. Resulting in approximately four MBRs being required to fully treat the furfural plant effluent, and even lower capital and operational costs involved for thermophilic operation.

10.CONCLUSIONS AND RECOMMENDATIONS

10.1. Conclusions

It has been concluded from this study that:

- The dynamic mass and energy balance model provides an accurate method for steady state prediction, and unsteady-state prediction for the MBR operating temperature and pH. The temperature can be predicted within 2 °C, and the pH within 0.5 units for a period greater than 60 days, using only the daily furfural plant effluent feed rates and sludge wasting rates as model inputs. The model is capable in theory of predicting the VSS concentration and the residual substrate concentration within the MBR, although more work is required to quantify the link between the VSS and MLSS concentration, as well as the biodegradability of the furfural plant effluent.

- A single biomass population can be used to model the MBR by including a temperature dependency in the kinetic and stoichiometric parameters.

- The model does not account for sludge dosing from the neighbouring CAS plant. When high sludge dosing occurs the model cannot accurately predict operation, and may overestimate the temperature of operation.

- There are advantages and disadvantages associated with both mesophilic and thermophilic operation of the MBR. A detailed economic analysis would be required to determine which regime is optimal. Comparison of model simulations and plant data leans toward indicating thermophilic operation is advantageous in terms of handling feed rates 2.2 times higher than mesophilic operation. However, thermophilic operation is more unstable than mesophilic operation and constant feed disruptions can have detrimental effects on MBR operation.

- The specific death rate constant for thermophilic operation is double that for mesophilic operation. The temperature dependency of the specific death rate constant closely follows the trends reported in literature.

- The biological yield is lower for thermophilic operation as opposed to mesophilic operation, resulting in less biomass synthesis per mass of substrate consumed.

- As a result of the higher specific death rate constant and lower biological yield, the observed yield for thermophilic operation is lower than that of mesophilic operation.

- The maximum specific growth rate increases with temperature, and in accordance with literature, substrate consumption rates increase with temperature.

10.2. Recommendations

Based on the work conducted in this study, the following is recommended:

- The sludge from the neighbouring CAS plant be characterised, and the model altered to account for the sludge dosing to the MBR.

- Find a more precise method to estimate the active biomass concentration during batch laboratory testing, to allow for a more accurate estimate of the maximum specific growth rate.

- Fully test the model dynamic prediction capability by measuring input parameters over a period of time (relative humidity, cloud cover, wind speed, day of the year, nutrient dosing) to perform a more robust calibration on the combined model.

- Quantify the unbiodegradable fraction of the furfural plant effluent to determine the true residual readily biodegradable substrate concentration measured by Illovo laboratory within the reactor, allowing for a better prediction of the mass balance model to be achieved.

- Include the DO concentration as a state variable in the mass balance, as opposed to only the OUR, and include a DO limitation factor within the kinetics. The DO concentration should be linked to the aerators.

11.REFERENCES

Abeynayaka, A. 2009. *Thermophilic Aerobic Membrane Bioreactor for Industrial Wastewater Treatment.* Master of Engineering, Asian Institute of Technology.

Amy, G., Brdjanovic, D., Comeau, Y., Ekama, G. A., Garcia, J. H., Gerba, C. P., Henze, M., Hooijmans, C. M., Judd, S. K., B., van Lier, J. B., Mahmoud, N., Martins, A. M., Morgenroth, E. F., Olsson, G., Rosso, D., Stenstrom, M. K., Takacs, I., van Loosdrecht, M. C. M., Wentzel, M. C. & Zeeman, G. 2011. *Biological Wastewater Treatment: Principles, Modelling and Design,* London, UK, IWA Publishing.

Argaman, Y. & Adams, C. E. 1977. Comprehensive temperature model for aerated biological systems. *Prog. Wat. Technol.,* 9**,** 397 - 409.

Bérube, P. 2010. Membrane Bioreactors: Theory and Applications to Water Reuse. *Sustainable Water for the Future: Water Recycling versus Desalination.* Elsevier.

Boogerd, F. C., Bos, P., Kuenen, J. G., Heinen, J. J. & van der Lans, R. G. J. M. 1989. Oxygen and Carbon Dioxide Mass Transfer and Aerobic, Autotrophic cultivation of Moderate and Extreme Thermophiles: A Case Study Related to the Microbial Desulfization of Coal. *Biotechnology and Bioengineering,* 35**,** 1111 - 1119.

Brouckaert, B. & Brouckaert, C. J. 2014a. Bioreactor Model Case Study. Available: http://www.iwawaterwiki.org/xwiki/bin/download/WorkGroup_Integration+of+Physico-chemical+and+Bio-process+Modelling+Course/BioreactorModel/BioreactorModelCaseStudy.pdf [Accessed 20 October 2014].

Brouckaert, C. J. & Brouckaert, B. 2014b. The Aquatic Chemistry Framework For Biochemical Modelling Available: http://www.iwawaterwiki.org/xwiki/bin/download/WorkGroup_Integration+of+Physico-chemical+and+Bio-process+Modelling+Course/AquaticChemistryFramework/PhysicochemicalFramework.pdf [Accessed 20 October 2014].

Brouckaert, C. J., Ikumi, D. & Ekama, G. A. 2010. Modelling of Anaerobic Digestion for incorporation into a plant-wide wastewater treatment model. Available: http://www.ewisa.co.za/literature/files/249_198%20Brouckaert.pdf [Accessed 22 September 2013].

Brown, E. V. & Enzminger, J. D. 1991. Temperature profile and heat transfer model for a chemical wastewater treatment plant. *Environ. Prog.,* 10**,** 159 - 168.

Cameron, I. T. & Hangos, K. 2001. Dynamic Models - Lumped Parameter Systems. *Process Modelling and Model Analysis.* London: Academic Press.

Campbell, H. J. & Rocheleau, R. F. 1976. Waste treatment at a complex plastics manufacturing plant. *J. Wat. Pollut. Control Fed.,* 48**,** 256-273.

Casey, T. J. 2006. *Unit Treatment Processes in Water and Wastewater Engineering,* Blackrock, Dublin, Aquavarra Research Limited.

Cicek, N. 2003. A review of membrane bioreactors and their potential application in the treatment of agricultural wastewater. *Canadian Biosystems Engineering,* 45, 637-649.

Couillard, D., Gariepy, S. & Tran, F. T. 1989. Slaughterhouse effluent treatment by thermophilic aerobic process. *Wat. Res.,* 23**,** 573-579.

Couillard, D. & Zhu, S. 1993. Thermophilic aerobic process for the treatment of slaughterhouse effluents with protein recovery. *Environ. Pollut.* , 79.

Davies, P. S. 2005. *The biological basis of wastewater treatment,* Scotland, Strathkelvin Instruments Ltd.

Eddy, M. a., Tchobanoglous, G., Burton, F. L. & Stensel, H. D. 2003. *Wastewater Engineering: Treatment and Reuse*, McGraw Hill Education.

Gent, R. D. 2012. Experimental Effluent Treatment at Sezela. *Proc. S. Afr. Technol. Ass.*, 85**,** 267 - 277.

Gillot, S. & Vanrolleghem, P. A. 2003. Equilibrium temperature in aerated basins—comparison of two prediction models. *Water Research,* 37**,** 3742-3748.

Heijnen, J. J. & Kleerebezem, R. 2010. Bioenergetics of microbial growth. *Encyclopedia of Industrial Biotechnology.* Netherlands: John Wiley & Sons, Inc.

Henze, M., Gujer, W., Mino, T. & van Loosdrecht, M. 2000. Activated sludge models ASM1, ASM2, ASM2d, and ASM3. *In:* TREATMENT, I. T. O. M. M. F. D. A. O. O. B. W. (ed.) *Scientific and Technical Report Series.* London.

holiday-weather. 2014. *Holiday Weather for Durban - Averages* [Online]. Available: http://www.holiday-weather.com/durban/averages/ [Accessed 10 March 2014].

Illovo. 2014. *Illovo Sugar Homepage* [Online]. Available: www.illovosugar.co.za/home [Accessed 8th October 2013].

Jackson, M. L. Thermophilic treatment of a high biochemical oxygen demand wastewater: Laboratory, pilot-plant and design. *In:* BELL, J. M., ed. Proceedings of the 37th Purdue Industrial Waste Conference, 1983 Purdue University. Ann Arbor Science Publishers.

Jamniczky-Kaszas, D. 2010. *Energy efficiency improvement of wastewater treatment - Case study of an autothermal thermophilic aerobic digestion process*. M. Sc. , University of Limerick

Jewell, W. J. & Kabrick, R. M. 1980. Autoheated aerobic thermophilic digestion with aeration. *Water Pollution Control Federation,* 52**,** 512 - 523.

Judd, S. 2011. *The MBR Book: Principles and applications of Membrane Bioreactors for water and wastewater treatment,* Oxford, UK, Elsevier Ltd.

Kennedy, S. & Young, T. 2006. Membrane bioreactors for water re-use in Southern Africa. Available: http://www.kubotafreeair.com/files/S_%20Kennedy%20&%20T_%20Young%20(2007)_%20Membrane%20Bioreactors%20for%20Water%20ReUse%20in%20Southern%20Africa.pdf [Accessed 22 March 2013].

Khambu, K. & Andrews, J. F. 1968. Aerobic thermophilic process for the biological treatment of wastes: Simulation Studies. *Water Pollution Control Federation,* 41**,** R127 - R141.

Kim, B. R., Podsiadlik, D. H., Yeh, D. H., Salmeen, I. T. & Briggs, L. M. 1997. Evaluating the conversion of an automative paint spray-booth scrubber to an activated-sludge system for removing paint volatile organic compounds from air. *Wat. Environ. Res.*, 69**,** 1211-1221.

Kono, T. 1968. Kinetics of microbial cell growth. *Biotechnology and Bioengineering,* 10**,** 105-131.

LaPara, T. M. & Alleman, J. E. 1999. Thermophilic Aerobic Biological Wastewater Treatment *Wat. Res.,* 33**,** 895 - 908.

Makinia, J., Wells, S. A. & Zima, P. 2005. Temperature Modeling in Activated Sludge Systems: A Case Study. *Water Environment Research,* 77**,** 8.

MATLAB. 2010. Computer Software.

Matsch, L. C. & Drnevich, R. F. 1977. Autothermal aerobic digestion. *Water Pollution Control Federation,* 49**,** 296 - 310.

Messenger, J. R., de Villiers, H. A. & Ekama, G. A. 1990. Oxygen utilization as a control parameter for the aerobic stage in dual digestion. *Wat. Sci. Technol.,* 22**,** 217 - 227.

Milenko, R. & Vrtovsek, J. 2004. The study of nutrient balance in sequencing batch reactor wastewater treatment. *Act Chim. Slov.,* 51**,** 779-785.

Novotny, V. & Krenkel, P. A. 1973. Simplified Mathematical Model of Temperature Changes in Rivers. *Water Pollution Control Federation,* 45**,** 240 - 248.

Ponti, C., Sonnleitner, B. & Fiechter, A. 1995. Aerobic thermophilic treatment of sewage sludge at pilot plant scale. 1. operating conditions. *Journal of Biotechnology,* 38**,** 173 - 182.

Prescott, L. M., Harkey, J. P. & Klein, D. A. 2002. *Microbiology,* McGraw-Hill.

Raphael, J. M. 1962. Prediction of Temperature in Rivers and Reservoirs. *Journal of the Power Division,* 88**,** 157-188.

Rice, E. W. 2012. Standard Methods for the Examination of Water and Wastewater. *In:* RICE, E. W. B., R. B.; EATON, A. D.; CLESCERI, L. S. (ed.) 22 ed. USA: American Public Health Association; AWWA; Water Environment Federation.

Rittman, B. E. & McCarty, P. L. 2001. *Environmental Biotechnology: Principles and Applications,* Boston, Mass., USA, McGraw-Hill

Rozich, A. F. & Colvin, R. J. 1. Design and operational considerations for thermophilic aerobic reactors treating high strength wastes and sludges. 52nd Purdue Industrial Waste Conference, 1997 USA. Ann Arbor Press.

Sedory, P. E. & Stenstrom, M. K. 1995. Dynamic Prediction of Wastewater Aeration Basin Temperature. *Journal of Environmental Engineering,* 121**,** 609 - 618.

Smith, J. M., Van Ness, H. C. & Abbott, M. M. 2005. *Introduction to Chemical Engineering Thermodynamics,* New York, NY, USA, McGraw-Hill International.

Staton, K. L., Alleman, J. E., Pressly, R. L. & Eloff, J. 2001. 2nd Generation Autothermal Thermophilic Aerobic Digestion: Conceptual Issues and Process Advancements. *WEF/AWWA/CWEA Joint Residuals and Biosolids Management Conference, Biosolids 2001: "Building Public Support".* . USA: Water Environment Federation

Sürücü, G. A., Chan, E. S. K. & Engelbrecht, R. S. 1976. Aerobic thermophilic treatment of high strength wastewaters. *Water Pollution Control Federation,* 48**,** 669 - 679.

Talati, S. N. 1988. *Heat Loss in Aeration Tanks.* M. Sc. Civil Engineering, University of California.

Talati, S. N. & Stenstrom, M. K. 1990. Aeration-Basin Heat Loss. *J. Environ. Eng,* 116**,** 70 - 86.

Tchobanoglous, G. & Burton, F. L. 1991. *Wastewater Engineering: Treatment, Disposal, and Reuse, 3rd Ed.,* New York, NY, USA, McGraw-Hill.

Tripathi, C. S. & Allen, D. G. 1999. Comparison of mesophilic and thermophilic aerobic biological treatment in sequencing batch reactors treating bleached kraft pulp mill effluent. *Wat. Res.,* 33**,** 836 - 846.

Ubisi, M. F., Jood, T. W., Wentzel, M. C. & Ekama, G. A. 1997. Activated sludge mixed liquor heterotrophic active biomass. *Water SA,* 23**,** 239 - 248.

USEPA 1990. Autothermal thermophilic aerobic digestion of municipal wastewater sludge. *In:* AGENCY, E. P. (ed.). USA.

Vanrolleghem, P. 2002. Principles of Respirometry in activated sludge wastewater treatment. Belgium: Universiteit Gent.

Vismara, R. 1985. A model for the autothermic aerobic digestion. *Wat. Res.,* 19**,** 441 - 447.

Vogelaar, J. C., Klapwijk, B., Temmink, H. & van Lier, J. B. 2003. Kinetic comparisons of mesophilic and thermophilic aerobic biomass. *J Ind Microbiol Biotechnol,* 30**,** 81-8.

Vogelaar, J. C. T., Klapwijk, A., van Lier, J. B. & Rulkens, W. H. 2000. Temperature effects on the oxygen transfer rate between 20 and 55°C. *Wat. Res.,* 34**,** 1037 - 1041.

Weast, R. C. 1981. *Handbook of Chemistry and Physics,* Boca Raton, FL, CRC Press.

Wynn, B. F., Linden, W. V. & Backman, R. C. Evaluation of the oxygen transfer characteristics of aeration systems operating in thermophilic temperature ranges. 52nd Purdue Industrial Waste Conference, 1997 USA. Ann Arbor Press, 7 - 15.

12.APPENDICES

Appendix A: Active biomass concentration estimation

An estimate of the active heterotrophic biomass concentration (X_H) for the experimental work was required for the regression of the kinetic parameters.

The MLSS concentration for the tests were measured by the Sezela laboratory, detailed in section 5.4.2. From the MLSS concentration an active fraction is estimated using data from literature. A ratio of the MLSS to MLVSS has been estimated to be between 0.65 and 0.85, a value of 0.75 was assumed (Casey, 2006). An estimate of the ratio of the MLVSS to X_H has been estimated from literature to be 0.35 (Ubisi *et al.*, 1997). The MLSS of the activated sludge for both the thermophilic and mesophilic round of experimental work, as determined by the laboratory tests was equal to 13.9 g.L^{-1} and 14.0 g.L^{-1}, an MLSS of 14.0 g.L^{-1} was used. The active biomass concentration was estimated as:

$X_H = 0.75 \times 0.35 \times 14 = 3.7$ g.L^{-1}

This is the estimated X_H fraction at the time of sampling the mixed liquor for the experimental work from the MBR. The next step was to estimate X_H at the beginning of the Dynamic Response Tests, after 48hours of respiration during the Cyclic OUR Test. This could be done with the use of the differential equation for biomass in the absence of substrate:

$$\frac{dX_H}{dt} = -k_d X_H \qquad (12\text{-}1)$$

The integration of Eq. 12-1 yields:

$$X_H = X_{H,0} e^{-k_d t} \qquad (12\text{-}2)$$

The active biomass concentration after 48 hours of endogenous respiration may be calculated as 2.1 g.L^{-1} and 1.1 g.L^{-1} for mesophilic and thermophilic operation, respectively, using the average specific death rate constant (k_d) from section 7.1.3. These were rounded off to 2 g.L^{-1} and 1 g.L^{-1} for X_H during the respiratory testing for mesophilic and thermophilic operation, respectively.

Appendix B: Corrected biological yield

The methodology to determine Y was detailed in chapter 5. The respirometer generated the respirogram in Fig. 12.1 for mesophilic Dynamic Response Test in which 86.63 g of COD is injected.

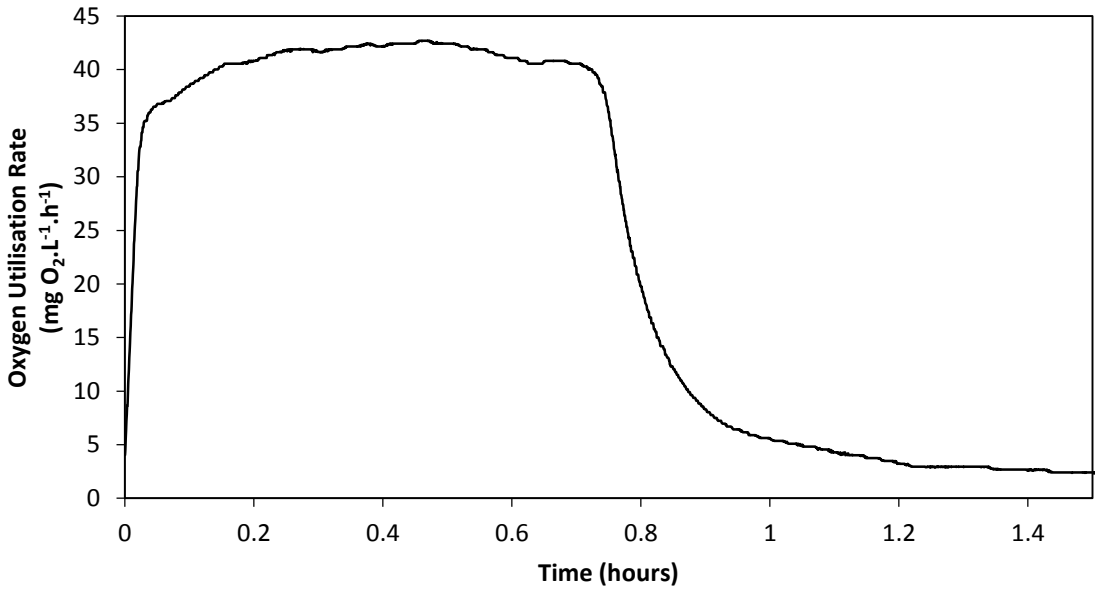

Figure 12.1. Respirogram generated from the Dynamic Response Test for 86.63 mg COD of substrate.

The area under the respirograms was found from the Trapezoidal Rule to be 34.13 mg O_2. Y was estimated from the area under the respirogram, as follows:

$Y = 1 - 34.13/86.63 = 0.606$ (mg COD biomass).(mg COD soluble)$^{-1}$

To undo the assumption of a constant X_H concentration the fraction of oxygen that is consumed for endogenous respiration for old and newly formed X_H was be estimated. This was achieved through the simulation of the Dynamic Response Test, and the subsequent estimation of the oxygen utilised for endogenous respiration. The simulation involved two procedures, the first to determine the effect of endogenous respiration of pre-existing biomass on the respirogram, the second procedure was to determine the effect of the endogenous respiration rate from newly formed biomass due to the addition of substrate.

To find the effect of pre-existing biomass in the absence of substrate on the respirogram, the respiration rate was simulated from:

$$r_{o,end1} = (1 - f_p) k_d X_H \qquad (12\text{-}3)$$

Where the initial value for X_H is the concentration at the beginning of the Dynamic Response Test. The initial X_H value for the mesophilic Dynamic Response Test was estimated to be 2 g.L^{-1}

(Appendix A). In integrating Eq. 12-3 the average k_d from section 7.1.3 was used. X_H can be modelled according to Eq. 12-2. Simulating Eq. 12-3 on MATLAB, yielded the modified respirogram accounting oxygen consumption due to death of pre-existing biomass (Fig 12.2).

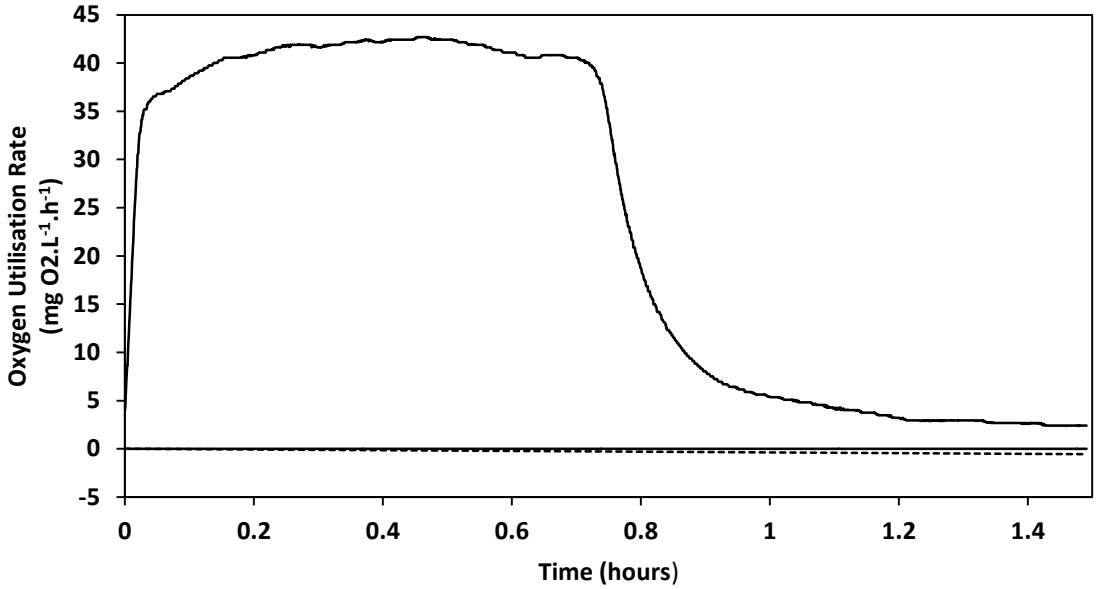

Figure 12.2. Modified respirogram with a corrected OUR.

It was observed from Fig. 12.2 that the effects of endogenous respiration of pre-existing biomass only had a small effect on the respirogram. The area under the curve was altered from 34.132 mg O_2 to 34.547 mg O_2.

The second step was to determine the effect of endogenous respiration from newly formed biomass. This was done by simulating the Dynamic Response Test, and using a minimisation routine to find Y. The reason for the minimisation routine was that the endogenous respiration rate due to newly formed biomass is dependent on Y, and in turn Y is dependent on the endogenous respiration rate. The kinetics for the simulation were estimated by regression using Y from the unmodified respirogram. The kinetics only have a minor effect on Y, and therefore only an estimate was required. The methodology in Fig. 12.3 was used for the routine.

The OUR due to endogenous respiration from newly formed biomass was described by:

$$r_{o,end2} = (1 - f_p)k_d(X_H - X_{H,0}) \qquad (12\text{-}4)$$

Similarly the active biomass concentration was described by:

$$r_X = \frac{\mu_m S_S X_H}{K_S + S_S} - k_d(X_H - X_{H,0}) \qquad (12\text{-}5)$$

The final modified respirogram, solely responsible for exogenous respiration was formed, yielding Fig. 12.4.

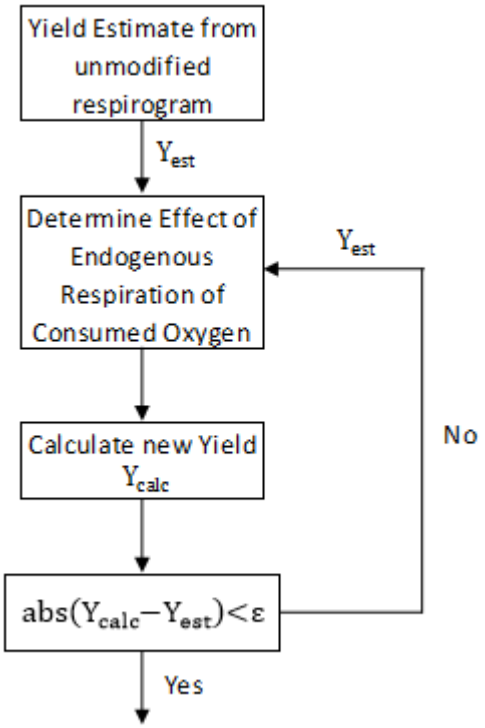

Figure 12.3. Yield correction estimation flow diagram.

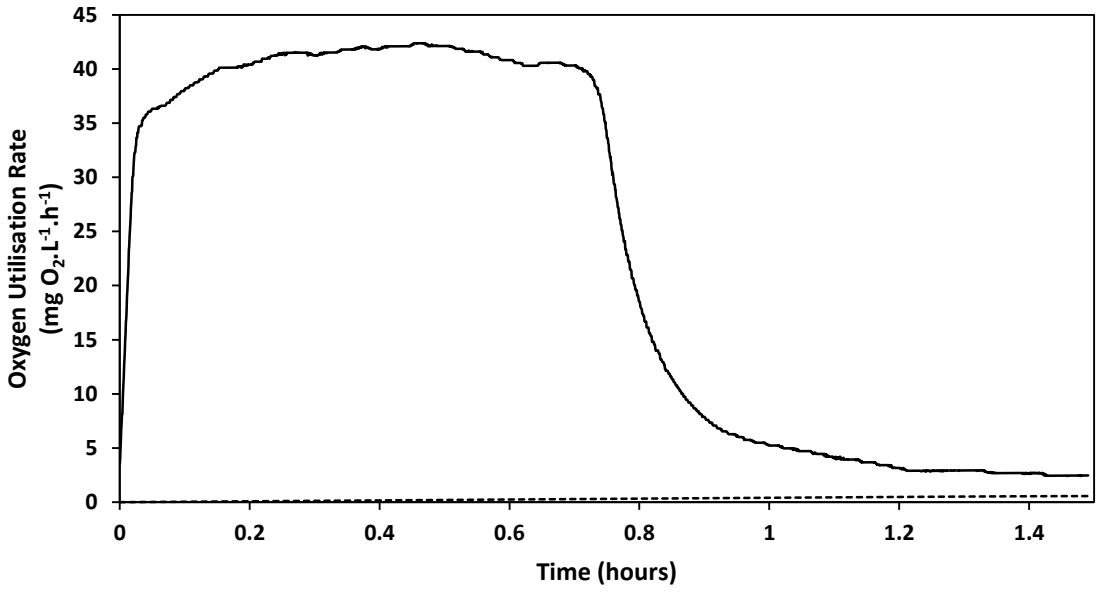

Figure 12.4. Modified respirogram, with varying biomass concentrations.

The area under the respirogram was modified to account for the endogenous respiration of newly formed biomass, the final area was further modified from 34.547 mg O_2 to 34.522 mg O_2. The final Y was found to be:

$Y_{mod} = 1 - 34.522/86.625 = 0.602$ (mg COD biomass).(mg COD soluble)$^{-1}$

The modified yield had a 0.7 % difference to the initial estimate under the assumption of constant X_H concentration. This procedure was repeated for the Dynamic Response Test for a thermophilic respirogram and the difference was found to be 0.9 %. It could therefore be confidently stated that the assumption of a constant X_H concentration is justified for this experimental work, and will have a negligible effect on the yield calculation.

Appendix C: Thermodynamic methods for growth stoichiometry and kinetics

A method is presented to estimate Y and kinetic parameters from thermodynamic principles. Chemical reactions, which involve changes in energy, can be described thermodynamically by the change in Gibbs free energy (Eddy *et al.*, 2003).

C.1. Thermodynamic estimation of biological yield *Y*

Method 1

The approach presented has been formed by Amy *et al.* (2011), which is an adaptation from that of Eddy *et al.* (2003), which is a simplification of Rittman and McCarty (2001). The procedure can be broken down into three steps, (i) the energy provided for catabolism knowing the electron donor, the electron acceptor and the source of nitrogen for growth; (ii) the energy needed for cell synthesis (anabolism); (iii) the energy needed for the overall growth reaction and the subsequent determination of Y.

A portion of the electron donor substrate is used for cell synthesis (f_s^0: true synthesis fraction) and the rest for energy production (f_e^0: true energy fraction). On an electron equivalent basis, the sum of f_s^0 plus f_e^0 equals 1. The electron balance and thus the COD balance are maintained. The active bacterial cells generated by growth using the initial electron donor then undergo decay due to maintenance, predation and cell lysis. During decay, a portion of the active bacterial cells become the electron donor to generate more energy and more reaction products (endogenous respiration) (Amy *et al.*, 2011).

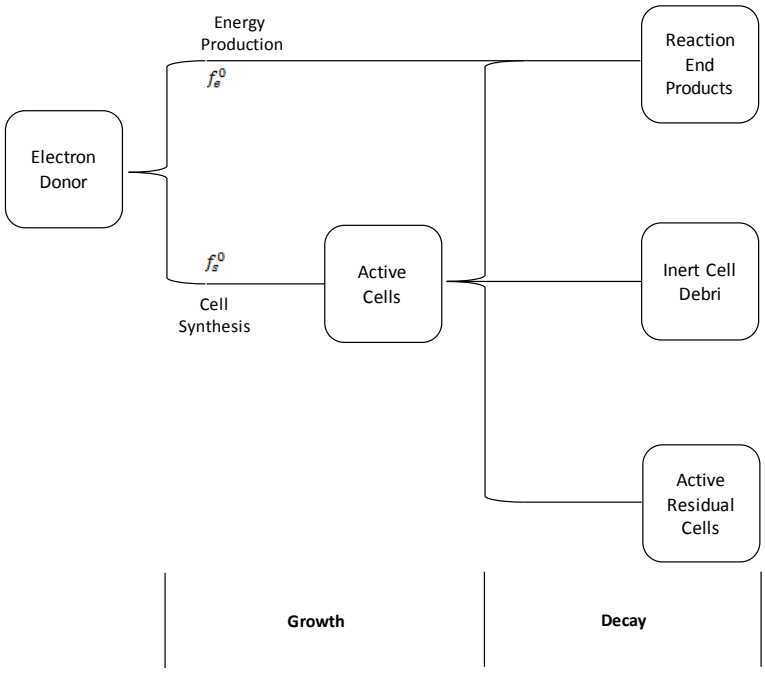

Figure 12.5. Use of electron donor for energy production or cell synthesis (Amy et al., 2011).

The fraction f_s^0 can be expressed in mass units rather than on an electron equivalent basis, which gives Y.

Under the assumption that $C_5H_7O_2N$ is the empirical formula for cells, the fraction f_s^0 can be used to estimate Y:

$$Y = \frac{f_s^0}{1.42 gCOD/gCells} \quad (12\text{-}6)$$

(i)

The Gibbs energy that is available for catabolism is determined from:

$$\Delta G_{cata} = E\Delta G_R \quad (12\text{-}7)$$

Where:

ΔG_{cata} is the Gibbs energy available for catabolism per electron equivalent (eeq) of electron donor (ED) ($J.eeq^{-1}$).

E is the fraction of energy transfer captured and typically has a value of 0.6.

ΔG_R is the Gibbs energy released from 1 eeq of ED ($J.eeq^{-1}$).

(ii)

The energy that is needed for the synthesis of heterotrophic biomass from an electron donor is estimated by considering pyruvate as a central metabolic intermediate, and a source of nitrogen for biomass synthesis:

$$\Delta G_{ana} = \frac{\Delta G_p}{E^m} + \Delta G_c + \frac{\Delta G_N}{E} \quad (12\text{-}8)$$

Where:

ΔG_{ana} is the Gibbs energy required for anabolism from 1 eeq of ED ($J.eeq^{-1}$).

ΔG_p is the Gibbs energy required to convert 1eeq of ED to pyruvate ($J.eeq^{-1}$).

m is a constant: +1 if ΔG_p is positive (endergonic) and -1 if ΔG_p is negative (exergonic).

ΔG_c is the Gibbs energy required to convert pyruvate to cells (31.41 $J.(eeq\ Cells)^{-1}$).

ΔG_N is the Gibbs energy required to reduce nitrogen to ammonia ($J.(eeq\ Cells)^{-1}$ = 17.46, 13.61, 15.85, 0.00 for NO_3^-, NO_2^-, N_2 and NH_4^+, respectively).

(iii)

Two mass balance equations can be written, one that was already presented for the electron donor for which its electrons are used for energy and synthesis:

$$f_e^0 + f_s^0 = 1 \quad (12\text{-}9)$$

The other one is for the energy where as much energy is consumed for anabolism as provided by catabolism. The negative sign accounts for the fact that anabolism consumes rather than produces energy:

$$-f_s^0 \Delta G_{ana} = f_e^0 \Delta G_{cata} \qquad (12\text{-}10)$$

The two unknowns (f_e^0 and f_s^0) can then be solved for from Eqs. 12-9 and 12-10, from which Y may be estimated from Eq. 12-6.

Method 2

A second method has been proposed (Heijnen and Kleerebezem, 2010), which is applicable to all chemotrophic systems. This method differs from that of Amy *et al.* (2011) primarily in its estimation of the anabolic energy required by using an energy dissipation function instead of an efficiency factor. No detailed knowledge is required; only the identity of the electron donor, carbon source, and electron acceptor. The method relates directly to the second law of thermodynamics.

The Gibbs energy required for the macro-chemical equation is estimated, from which Y can be determined. The calculation of the Gibbs energy for the macro-chemical equation would provide an additional conservation equation, and allow for the solution of the macro-chemical equation.

The Gibbs energy required to produce biomass may be divided into two parts:

1. A growth-related part
2. A maintenance-related part

This can be expressed mathematically as:

$$\Delta G_x = \Delta G_x^m + \frac{m_G}{\mu} \qquad (12\text{-}11)$$

Where:

ΔG_x is the total Gibbs energy required for biomass production (kJ.(mol biomass^{1})).
ΔG_x^m is the Gibbs energy required for new biomass (kJ.(mol biomass^{-1})).
m_G is the Gibbs energy required for biomass maintenance (kJ.(mol biomass^{-1}).h^{-1}).
μ is the biomass specific growth rate (h^{-1}).

Eq. 12-11 shows that in order to calculate ΔG_x as a function of growth rate μ, information about ΔG_x^m and m_G is required. Correlations have been established to estimate these parameters using a very large set of experimental growth yields, including many different micro-organisms, carbon sources and electron acceptors (aerobic, anaerobic, denitrifying).

The data for m_G has been correlated with an Arrhenius type of equation:

$$m_G = 4.5exp\left[\frac{-69000}{R}\left(\frac{1}{T}-\frac{1}{298}\right)\right] \quad (12\text{-}12)$$

Where:

R is the universal gas constant (8.314 J.mol^{-1}.K^{-1}).

The correlation holds with a ± 40 % accuracy for a very wide variety of organisms, electron donors, for aerobic and anaerobic conditions, and for a temperature range of 5 to 75 ºC. The equation is highly dependent on temperature, which is expected from an Arrhenius type equation. m_G can be neglected from Eq. 12-11 at lower to moderate temperatures, although at higher temperatures, such as 50 ºC, m_G should be taken into account. If m_G is neglected, Y that is obtained will be the maximal biological yield, Y_t^m (maximum attainable yield, purely due to growth of biomass).

The data for ΔG_x^m has been correlated to:

$$\Delta G_x^m = 200 + 18(6-C)^{1.8} + exp[((3.8-\gamma)^2)^{0.16}(3.6+0.4C)] \quad (12\text{-}13)$$

Where:

C is the number of carbon atoms in the ED.

γ is the degree of reduction. It is a stoichiometric number of a chemical compound that represents the number of electrons in the compound.

The predictive accuracy of this correlation for chemotrophic growth has been shown to have 10 to 20 % relative error in a yield range of nearly two orders of magnitude of 0.01 to 0.70 (mol biomass).(mol substrate)$^{-1}$.

C.2. Thermodynamic estimation of the kinetic parameters

C.2.1. Thermodynamic relation for the estimation of the specific death rate constant k_d

k_d can be estimated from thermodynamic data as follows (Heijnen and Kleerebezem, 2010):

$$k_d = m_D Y_t^m \quad (12\text{-}14)$$

Where:

m_D is the rate of consumption of ED (substrate) that is catabolised to generate the necessary Gibbs energy flow for maintenance ((mol subtrate).(mol biomass^{-1}).h^{-1}).

Y_t^m is the maximal biological yield ((mol biomass).(mol substrate)$^{-1}$).

The maintenance term m_D is stoichiometrically linked to m_G through the catabolic reaction:

$$m_D = \frac{m_G}{(-\Delta G_{cata})} \quad (12\text{-}15)$$

Where:

$-\Delta G_{cata}$ is the Gibbs energy of the catabolic reaction (kJ.mol^{-1}).

m_G can be calculated through Eq. 12-12. It is recommended to calculate Y_t^m by relating it to the Gibbs energy required for new biomass ΔG_x^m, through the macro-chemical equation. Therefore, once ΔG_x^m has been estimated through Eq. 12-13, the macro-chemical equation may be solved and Y_t^m determined.

C.2.2.Thermodynamic correlation for the maximum specific growth rate constant μ_m

The value of μ_m is the result of a limiting factor within the metabolism (Heijnen and Kleerebezem, 2010).

The three possible bottlenecks are identified as:

1. Uptake rate of substrate.
2. Rate of synthesis of biomass, as related to the ribosomal capacity to synthesize biomass protein.
3. The rate of making Gibbs energy available to enable growth and maintenance.

Heijnen and Kleerebezem (2010) presented a method to determine μ_m in which it is assumed that the rate of making Gibbs energy available for micro-organisms is limited by the maximum rate of electron transport in the catabolic energy production.

A correlation has been proposed for the maximal electron-transport capacity in the microbial electron transport as a function of temperature:

$$maximal\ electron - transport\ capacity = 3exp\left[\frac{-69000}{R}\left(\frac{1}{T} - \frac{1}{298}\right)\right] \quad (12\text{-}16)$$

For a given electron donor/acceptor combination, the maximal rate of Gibbs energy made available per unit biomass follows as:

$$q_G^m = 3[(-\Delta G_{cata})/\gamma_D]exp\left[\frac{-69000}{R}\left(\frac{1}{T} - \frac{1}{298}\right)\right] \quad (12\text{-}17)$$

Where:

q_G^m is the maximal rate of Gibbs energy made available per unit biomass (J.mol^{-1}.h^{-1}).

$(-\Delta G_{cata})/\gamma_D$ is the Gibbs energy made available per mole electron transported between donor and acceptor by the electron transport chain (J.(mol electron)$^{-1}$).

Following Eq. 12.11, the Gibbs energy spent for growth and maintenance can be written under the maximum growth condition:

$$q_G^m = \Delta G_x^m \mu_m + m_G \qquad (12\text{-}18)$$

By eliminating q_G^m with Eq. 12-17, and rearranging gives μ_m as a function of temperature:

$$\mu_m = \frac{3[(-\Delta G_{cat})/\gamma_D - 4.5]}{\Delta G_x^m} exp\left[\frac{-69000}{R}\left(\frac{1}{T} - \frac{1}{298}\right)\right] \qquad (12\text{-}19)$$

C.2.3. Half saturation constant of electron donor K_S

Values of K_S have been reported over a wide range, even for the same organism. The wide range is likely due to systematic errors in the determination of K_S. It is therefore not possible to give, from a thermodynamic point of view, a generalisation about the value of K_S for different microbial growth systems (Heijnen and Kleerebezem, 2010).

Appendix D: Theoretical stoichiometric and kinetic parameter estimation

D.1. Biological yield estimation

Method 1

Firstly the Gibbs energy required for catabolism was found. The catabolic reaction is represented by:

$$\frac{1}{8}CH_3COO^- + \frac{1}{4}O_2 \rightarrow \frac{1}{8}HCO_3^- + \frac{1}{8}CO_2 + \frac{1}{8}H_2O \qquad (12\text{-}20)$$

Where the energy released was determined from literature as -105.82 kJ.(eeq acetate)$^{-1}$ (Amy *et al.*, 2011). The energy required for the catabolic reaction was determined from:

$$\Delta G_{cata} = 0.6 \times -105.82 = -63.49 \text{kJ.(eeq acetate)}^{-1}$$

Where E is equal to 0.6 (Amy *et al.*, 2011). Secondly the Gibbs energy required for anabolism was estimated. The reaction and Gibbs energy required to convert one eeq of acetate to pyruvate is:

$$\frac{1}{8}CH_3COO^- + \frac{3}{40}CO_2 \rightarrow \frac{1}{40}HCO_3^- + \frac{1}{10}CH_3COCOO^- + \frac{1}{40}H_2O \qquad (12\text{-}21)$$

Where:

ΔG_p = 8.1 kJ.(eeq acetate)$^{-1}$

The Gibbs energy for anabolism is calculated from Eq. 12-8, where m = +1, ΔG_c = 31.41 kJ.(eeq Cells)$^{-1}$, and ΔG_N = 0 for ammonia:

$$\Delta G_{ana} = \frac{8.1}{0.6^1} + 31.41 + \frac{0}{0.6} = 44.91 \text{ kJ.(eeq acetate)}^{-1}$$

Y may then be calculated using Eq. 12-9 and 12-10:

$$\frac{f_s^0}{f_e^0} = -\left(\frac{44.91}{63.49}\right) = 0.707$$

Therefore:

f_s^0 = 0.585 (mg COD biomass).(mg COD soluble)$^{-1}$

Using Eq. 2-6 gives:

Y = 0.412 (mg VSS).(mg COD soluble)$^{-1}$

Method 2

Firstly the Gibbs energy required to produce biomass, which consists of a growth related part and a maintenance related part, was determined from Eq. 12-11:

$$\Delta G_x = \Delta G_x^m + \frac{m_G}{\mu}$$

As the specific biomass growth rate (μ) is unknown the maintenance part was neglected. The maintenance term becomes prevalent at higher temperatures such as 50 °C (Heijnen and Kleerebezem, 2010). The Gibbs energy can be determined from Eq. 12-13, where for acetate, C = 2 and γ = 4 electrons per Carbon-mol. Therefore:

$\Delta G_x^m = 200 + 218 + 14 = 432$ kJ.(Carbon-mol Biomass)$^{-1}$.

With biomass represented by $C_5H_7O_2N$,

$\Delta G_x^m = 5 \times 1441 = 2160$ kJ.(mol Biomass)$^{-1}$

The conservation equations can now be written for C, H, O, N, electric charge, and the Gibbs energy balance using Eq. 6-18:

$$a\mathrm{CH_3COO^-} + b\mathrm{NH_4^+} + c\mathrm{H^+} + d\mathrm{O_2} + e\mathrm{H_2O} + 1\mathrm{C_5H_7O_2N} + f\mathrm{HCO_3^-}$$

C Balance: $2a + 5 + f = 0$

H Balance: $3a + 4b + c + 2e + 7 + f = 0$

O Balance: $2a + 2d + e + 2 + 3f = 0$

N Balance: $b + 1 = 0$

Charge Balance: $-a + b - f = 0$

Gibbs Energy Balance: $(-369.41)a + (-79.37)b + (-39.87)c + (-237.18)e + (-335) + (-586.85)f$

$+2160 = 0$

Solving these six equations gives, for *a* to *f:*

$a = -4$, $b = -1$, $c = 34.8$, $d = 5.7$, $e = 14.4$, and $f = 3$

The yield was be calculated as 1/4 = 0.25 (mol biomass).(mol acetate)$^{-1}$. Converting to mass units leads to:

$Y = 0.44$ (mg VSS).(mg COD soluble)$^{-1}$

(The molar mass of biomass ($C_5H_7O_2N$) is 113 (g VSS).(mol biomass)$^{-1}$, and 2 moles O_2 is required to oxidise 1 mole of acetate (64 (g COD).(mol acetate)$^{-1}$)).

D.2. Specific death rate constant k_d

k_d was estimated through the procedure presented by Heijnen and Kleerebezem (2010), Appendix C.2. To calculate k_d the maintenance term m_D was calculated through Eq. 12-15. The Gibbs energy required for biomass maintenance m_G was determined through Eq. 12-12, at a temperature of 40 and 50 ºC:

$m_G(40°C) = 4.5exp\left[\frac{-69000}{8.314}\left(\frac{1}{313}-\frac{1}{298}\right)\right]$ = 17.07 kJ.(mol biomass^{-1}).h^{-1}

$m_G(50°C) = 4.5exp\left[\frac{-69000}{8.314}\left(\frac{1}{323}-\frac{1}{298}\right)\right]$ = 38.76 kJ.(mol biomass^{-1}).h^{-1}

The Gibbs energy for the catabolic reaction $(-\Delta G_{cata})$ has been calculated in Appendix D.1, as 846.56 kJ.(mol acetate)$^{-1}$.

The maintenance can thus be calculated as:

$m_D(40°C) = \frac{17.07}{846.56}$ = 0.02016 (mol acetate).(mol biomass^{-1}).h^{-1}

$m_D(50°C) = \frac{38.76}{846.56}$ = 0.04579 (mol acetate).(mol biomass^{-1}).h^{-1}

To calculate the maximal biomass yield Y_t^m, ΔG_x^m is required. ΔG_x^m was previously calculated in Appendix D.1, where the yield was estimated (0.25 (mol biomass).(mol acetate)$^{-1}$), which happens to be Y_t^m due to maintenance being neglected. k_d can therefore be estimated as:

$k_d(40°C) = 0.02016 \times 0.25 =$ 0.005 h^{-1}

$k_d(50°C) = 0.04579 \times 0.25 =$ 0.011 h^{-1}

D.3. Maximum specific growth rate constant, μ_m

μ_m can be estimated by the method of Heijnen and Kleerebezem (2010), using Eq. 12-19. The Gibbs energy made available per electron transported between donor and acceptor by the electron transport chain $[(-\Delta G_{cat})/\gamma_D]$ is equal to 105.5 kJ.(mol electron)$^{-1}$ for an aerobic system where acetate is the electron donor (Heijnen and Kleerebezem, 2010). ΔG_x^m has been previously calculated, Appendix D.1.

$\mu_m(40°C) = \frac{3[105.5-4.5]}{432}\exp\left[\frac{-69000}{8.314}\left(\frac{1}{313}-\frac{1}{298}\right)\right]$ = 2.66 h^{-1}

$\mu_m(50°C) = \frac{3[105.5-4.5]}{432}\exp\left[\frac{-69000}{8.314}\left(\frac{1}{323}-\frac{1}{298}\right)\right]$ = 6.04 h^{-1}

Appendix E: Respirometer calibration

The calibration of the respirometric device was carried out following the procedure of section 5.3.3. A known amount of sodium sulphite was injected into distilled water, and the OUR was measured, from which the total amount of oxygen was calculated through numerical methods (trapezoidal rule). The calibration factor was then automatically calculated from Eq. 5-3, and a calibration factor of 0.262 was obtained. To verify the calibration the sodium sulphite test was repeated under normal response test conditions, the results of which are shown in Table 12.1.

Table 12.1. Verification of BM-EVO respirometer calibration with Sodium Sulphite addition.

Mass of sodium sulphite injected (mg)	**Theoretical oxygen demand (mg O_2)**	**Experimental oxygen demand (mg O_2)**	**Experimental error (%)**
100	12.7	12.2	96.1

The experimental data generated by the respirometer is shown in Fig. 12.6.

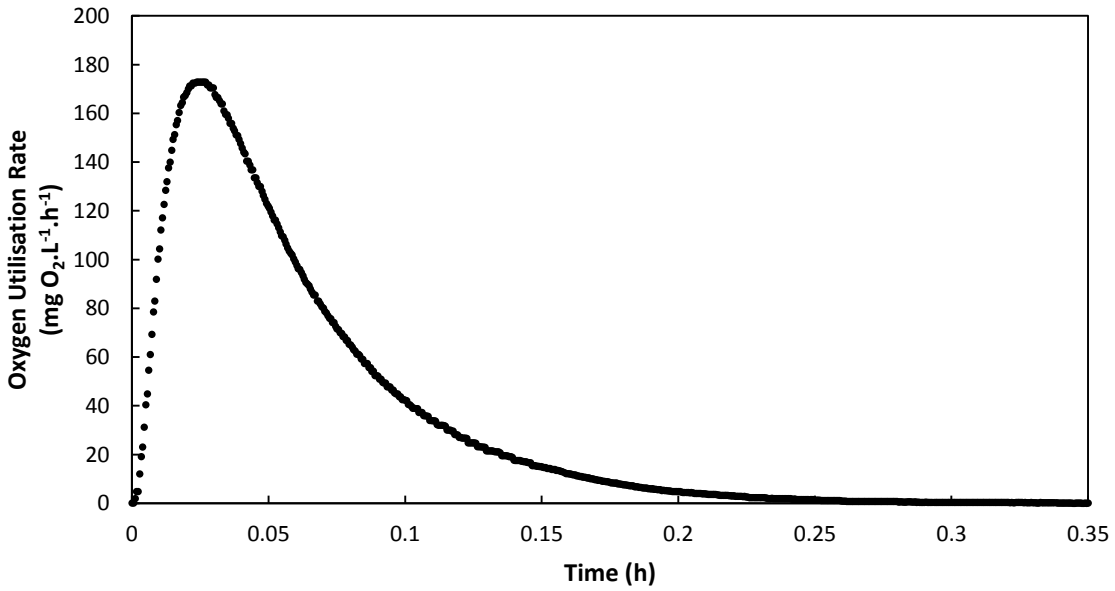

Figure 12.6. Respirogram generated for sodium sulphite addition.

Appendix F: Experimental procedure

The experimental procedure that was followed for the experimental work regarding the respirometer is detailed as follows:

OUR Test

The OUR test was used to determine k_d, the procedure is listed:

1. A 1 L sample of the mixed liquor from the MBR was placed into the glass reactor vessel; the temperature of the MBR was recorded during sampling.
2. The OUR test was selected and the test parameters were inputted to the GUI, namely: the minimum DO and maximum DO concentration of 4 and 5 $mg.L^{-1}$, respectively; the test temperature of either 40 or 50 ºC depending on the regime being tested (the MBR was sampled when the operational temperature was less than 2 ºC to the selected test temperature); the peristaltic pump speed setting of 3; and the aeration rate between 55 and 80 %, depending on the rate at which the oxygen is consumed (generally a higher aeration rate was required for thermophilic operation).
3. The test was left to run for an extended period of time, between 2 and 3 days allowing endogenous respiration to be reached, and sufficient data points for the regression for k_d.
4. During the test evaporation of the water from the mixed liquor occurred, between 20 and 40 $mL.day^{-1}$, the respirometer was refilled with distilled water once a day. For the thermophilic tests there was a build-up of sludge around the DO probe which at times may skew the measurements, this was cleaned with distilled water when required.

Dynamic Response Test

The Dynamic Response Test was performed directly after the OUR test, on the same sample. The Dynamic Response Test generated the respirograms which allowed the estimation of Y and the regression of the kinetic parameters. The procedure is detailed:

1. The mixed liquor sample volume was maintained at 1 L within the glass reactor vessel.
2. The Dynamic Response Test was selected and the test parameters were inputted, namely: the test temperature at either 40 or 50 ºC; the peristaltic pump speed setting at 2; and the aeration rate at 55 %. The pumps speed and aeration rate were set to the values at which the calibration was performed.
3. The temperature control, peristaltic pump, stirrer, and aerator were activated on the respirometer, a minimum of 50 minutes was allowed for the temperature and DO readings to stabilise.
4. A known volume of composite furfural plant effluent, between 2 and 8 mL, was injected directly into the respirometer, and the test immediately started.

5. Once the Dynamic Response Test had completed, after 25 to 120 minutes when the OUR was nearing the baseline, the test was stopped.

Appendix G: Additional experimental data

The experimental data that was used to estimate the stoichiometric and kinetic coefficients, and not included in chapter 7, is illustrated. The order is the same as that observed in chapter 7, OUR tests to determine k_d, and Dynamic Response Tests to determine Y and kinetic regression.

G.1. Specific death rate tests k_d

G1.1. Mesophilic k_d tests

Cyclic OUR Test 2

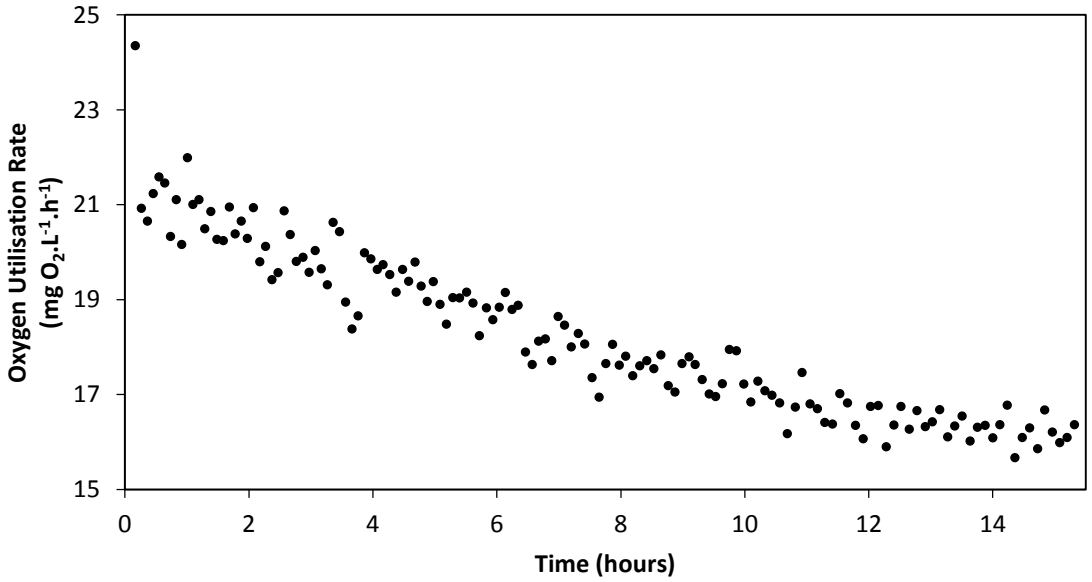

Figure 12.7. Oxygen utilisation rate generated by experimental test at a mesophilic temperature.

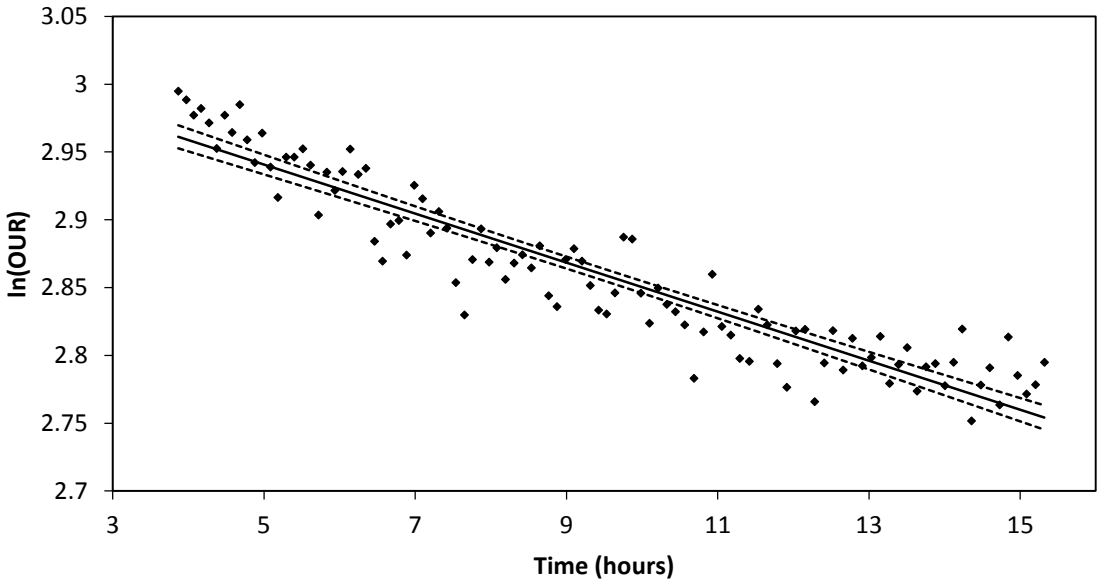

Figure 12.8. Natural logarithm of the oxygen utilisation rate versus time taken at endogenous respiration (R^2 = 0.880).

Table 12.2. Oxygen utilisation rate test regression result.

Test T (ºC)	k_d (h^{-1})
40	0.0181 ± 0.0013*

*95 % confidence interval

Cyclic OUR Test 3

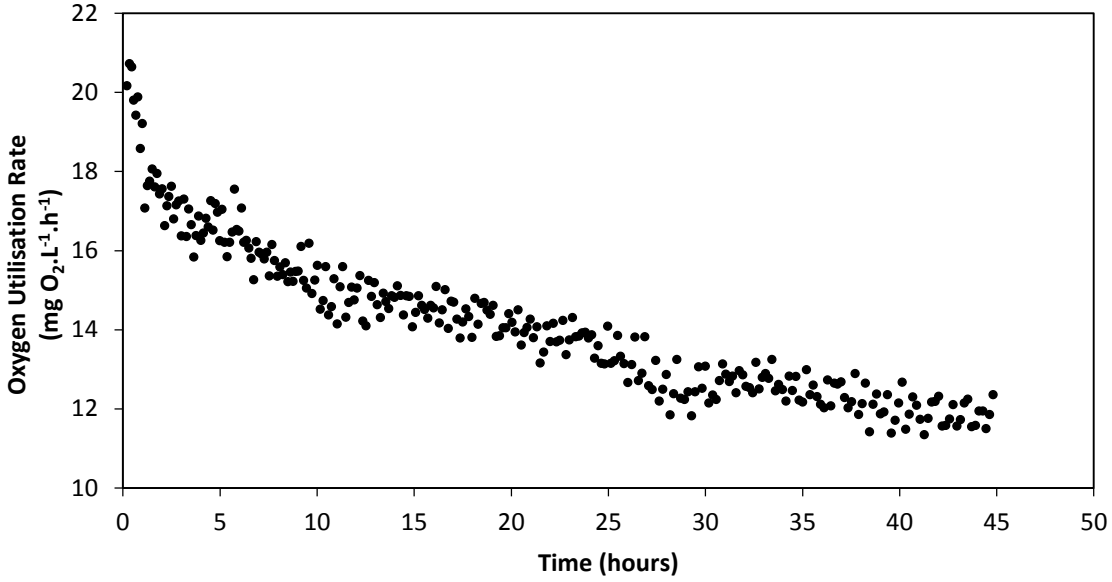

Figure 12.9. Oxygen utilisation rate generated by experimental test at a mesophilic temperature.

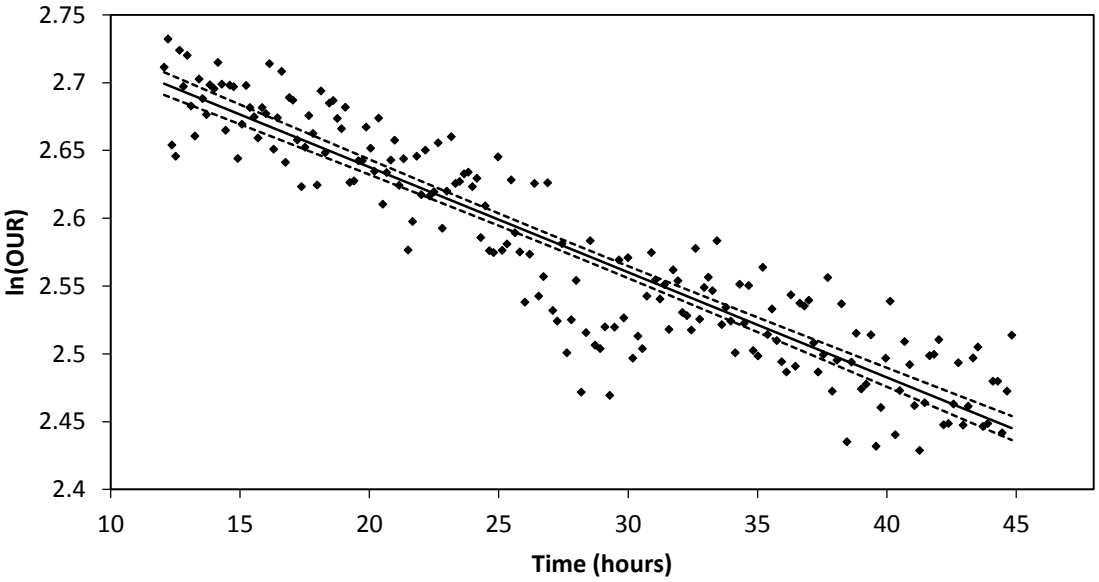

Figure 12.10. Natural logarithm of the oxygen utilisation rate versus time taken at endogenous respiration (R^2 = 0.856).

Table 12.3. Oxygen utilisation rate test regression result.

Test T (ºC)	k_d (h^{-1})
40	0.00776 ± 0.00045*

*95 % confidence interval

G.1.2. Thermophilic k_d tests

Cyclic OUR Test 2:

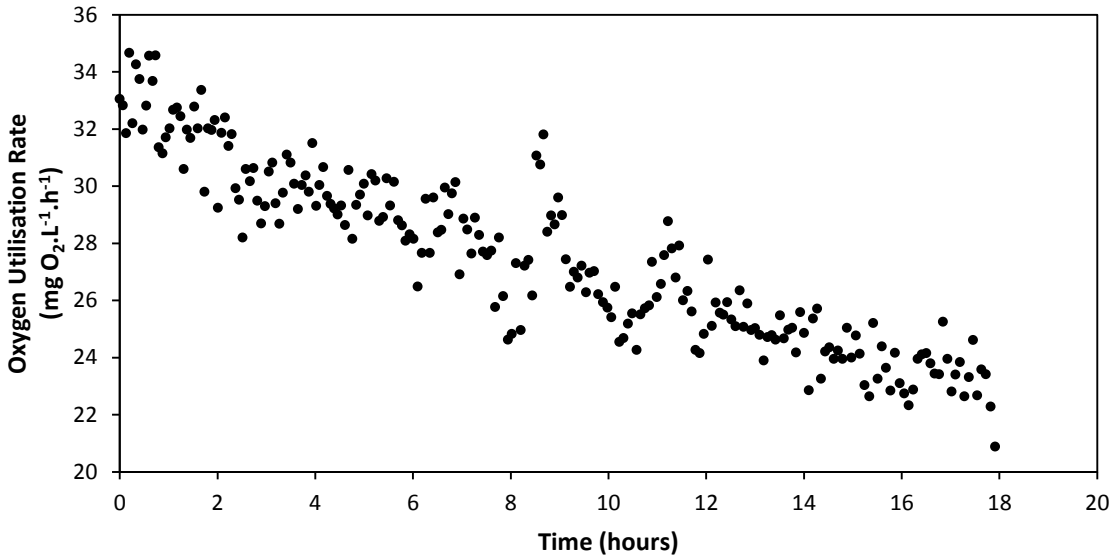

Figure 12.11. Oxygen utilisation rate generated by experimental test at a thermophilic temperature.

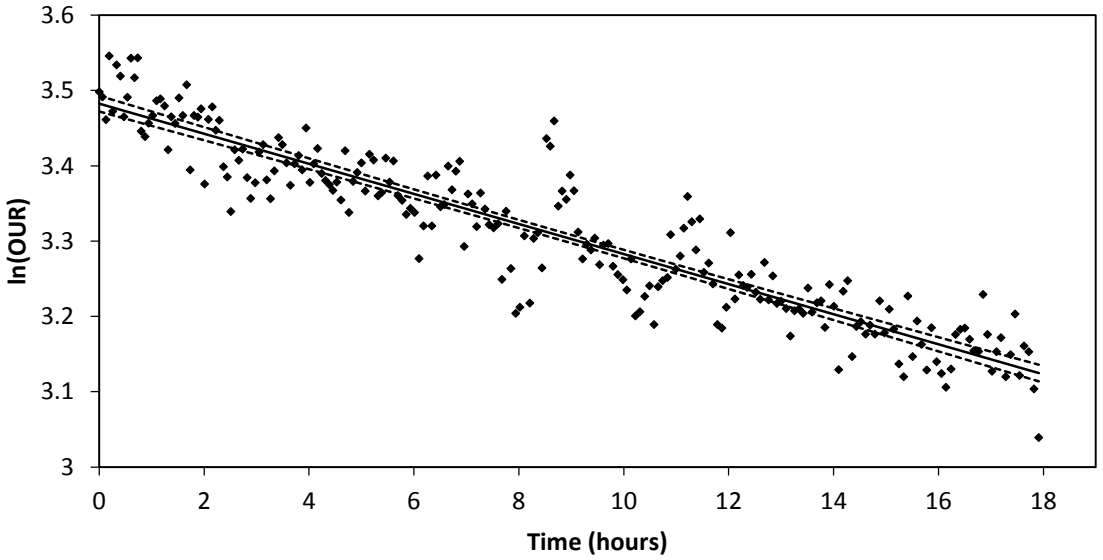

Figure 12.12. Natural logarithm of the oxygen utilisation rate versus time taken at endogenous respiration (R^2 = 0.867).

Table 12.4. Oxygen utilisation rate test regression result.

Test T (ºC)	k_d (h^{-1})
50	0.0200 ± 0.0010*

*95 % confidence interval

G.2. Biological yield *Y*

G.2.1. Mesophilic *Y*

Dynamic Response Test 5

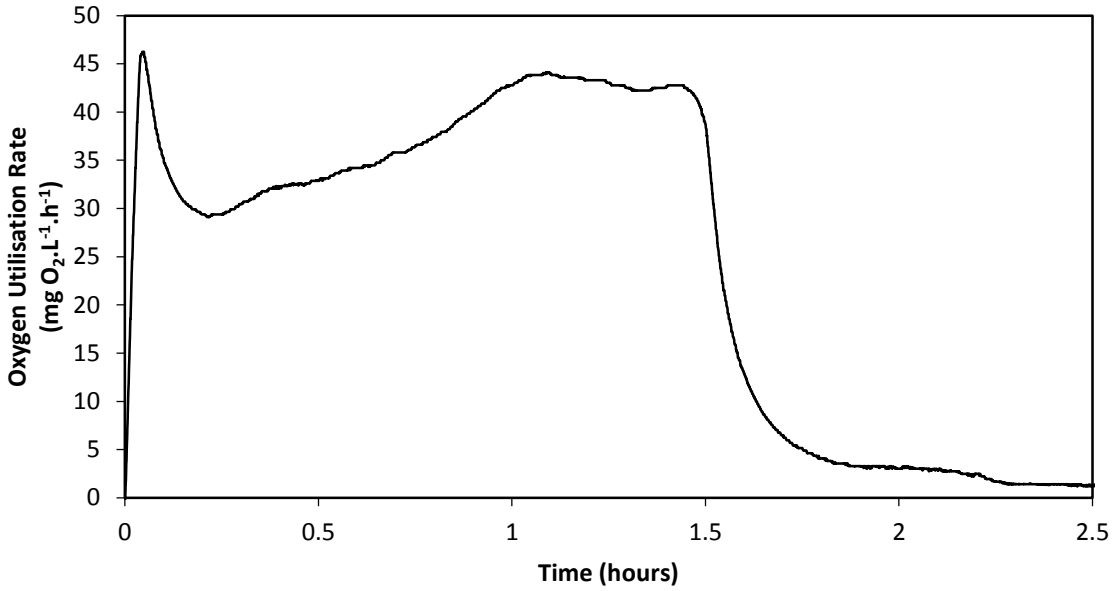

Figure 12.13. Generated respirogram from BM-EVO respirometric device for 114.3mg.L^{-1} COD.

Table 12.5. Results from the generated respirogram for 114.3mg.L^{-1} COD.

COD injected (mg COD)	Mass Of oxygen consumed via substrate degradation (mg O_2)	Y ((mg COD biomass). (mg COD soluble)$^{-1}$)
114.3	61.50	0.574

Dynamic Response Test 6

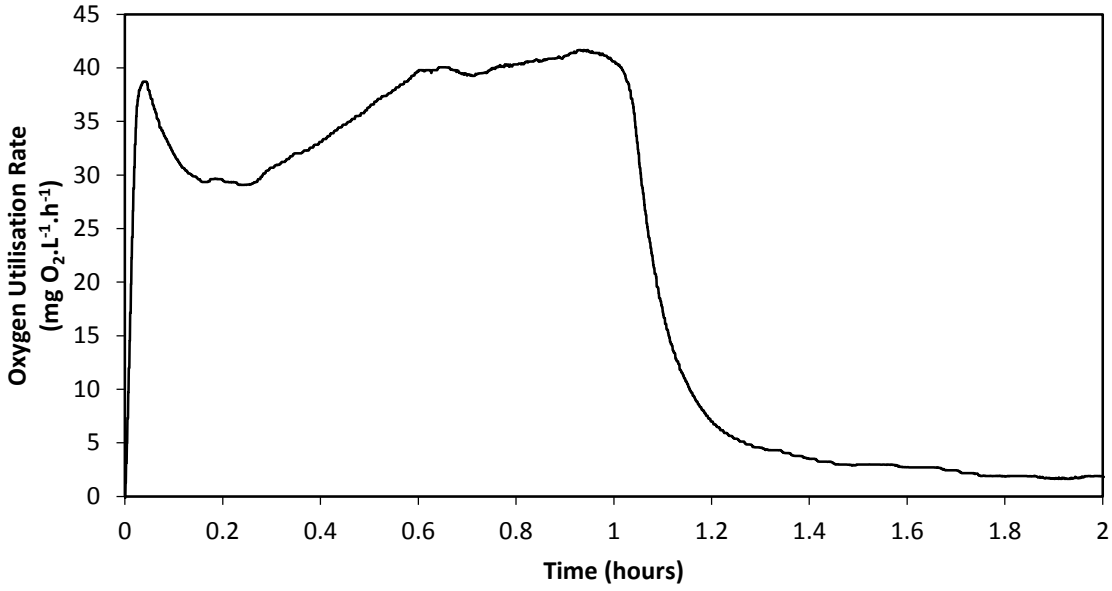

Figure 12.14. Generated respirogram from BM-EVO respirometric device for 115.5mg.L^{-1}.

Table 12.6. Results from the generated respirogram for 115.5mg.L^{-1}.

COD injected (mg COD)	**Mass Of oxygen consumed via substrate degradation (mg O_2)**	***Y*** **((mg COD biomass). (mg COD soluble)$^{-1}$)**
115.5	41.88	0.634

G.3. Kinetic regression

G.3.1. Mesophilic kinetic regression

Kinetic regression 2:

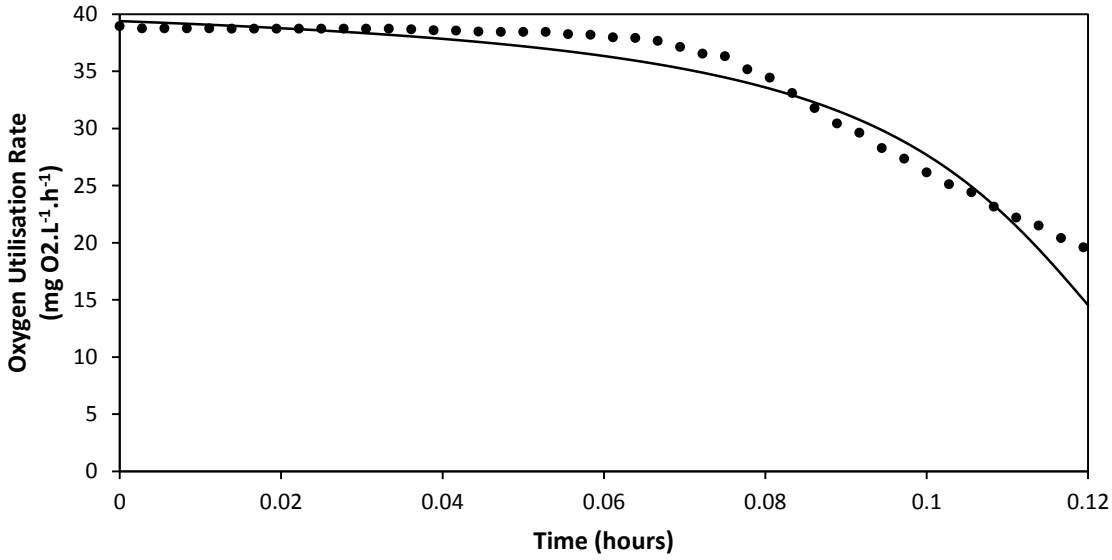

Figure 12.15. Regression of experimental data, zoomed view for 38.50 mg.L^{-1} COD. —— Regressed model, • Experimental data.

Table 12.7. Kinetic regression results for 38.50 mg.L^{-1} COD.

μ_m (h^{-1})	K_S (mg.L^{-1})
0.0225 ± 0.002*	0.767 ± 0.036*

*95 % confidence Interval

Kinetic regression 3:

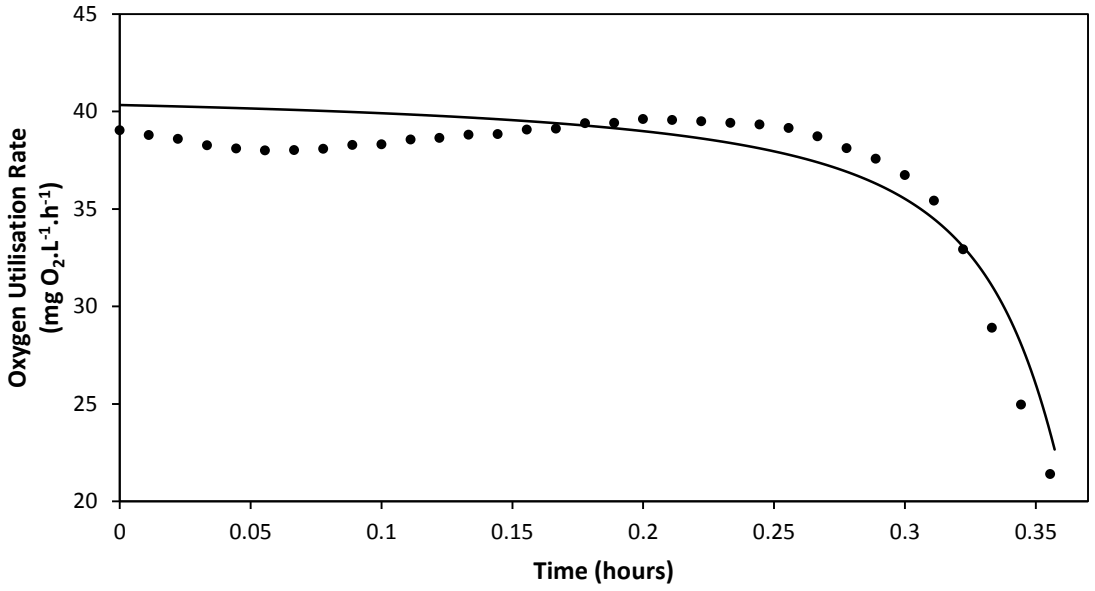

Figure 12.16. Regression of experimental data for 58.05 mg.L^{-1} COD, zoomed view. —— Regressed model, • Experimental data.

Table 12.8. Kinetic regression results for 58.05 mg.L^{-1} COD.

μ_m (h^{-1})	K_S (mg.L^{-1})
0.0172 ± 0.001*	0.808 ± 0.041*

*95 %confidence Interval

G.3.2. Thermophilic kinetic regression

Kinetic regression 2:

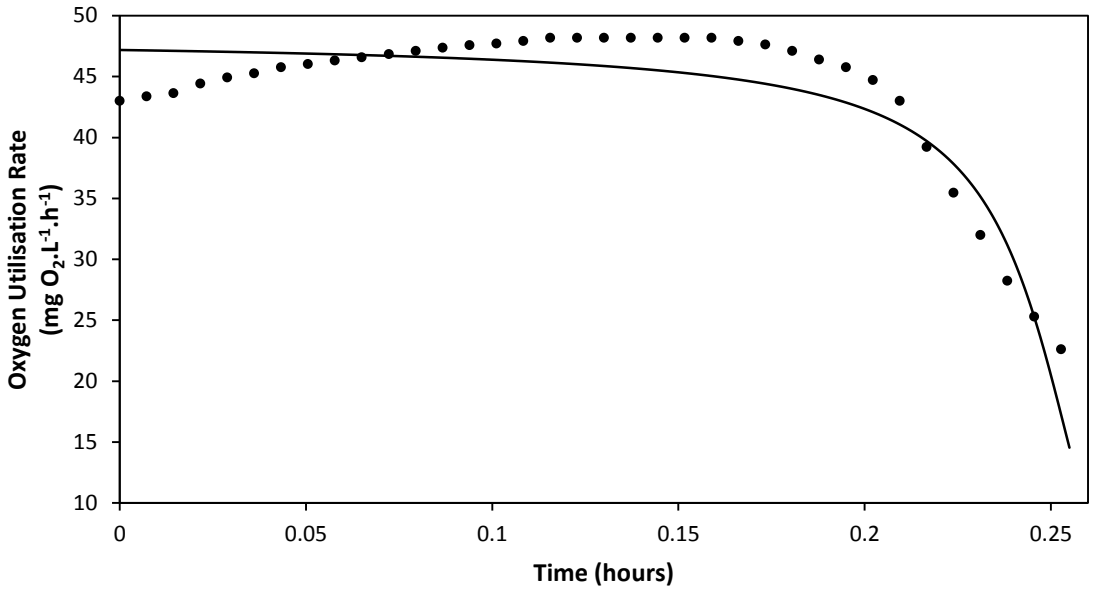

Figure 12.17. Regression of experimental data, zoomed view for 32.75 mg.L^{-1} COD. —— Regressed model, • Experimental data.

Table 12.9. Kinetic regression results 32.75 mg.L^{-1} COD.

μ_m (h^{-1})	K_S ($mg.L^{-1}$)
0.0348 ± 0.003*	0.582 ± 0.034*

*95 %confidence Interval

Kinetic regression 3:

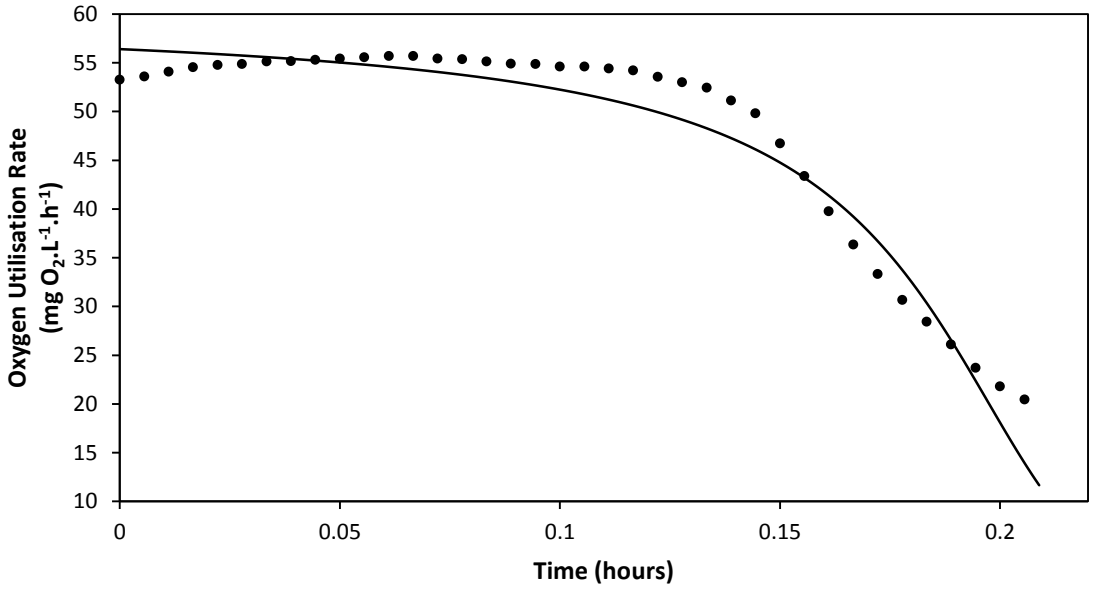

Figure 12.18. Regression of experimental data, zoomed view for 32.75 mg.L^{-1} COD. Regressed model, • Experimental data.

Table 12.10. Kinetic regression results 32.75 mg.L^{-1} COD.

μ_m (h^{-1})	K_S ($mg.L^{-1}$)
0.0418 ± 0.004*	1.39 ± 0.059*

*95 %confidence Interval

Kinetic regression 4:

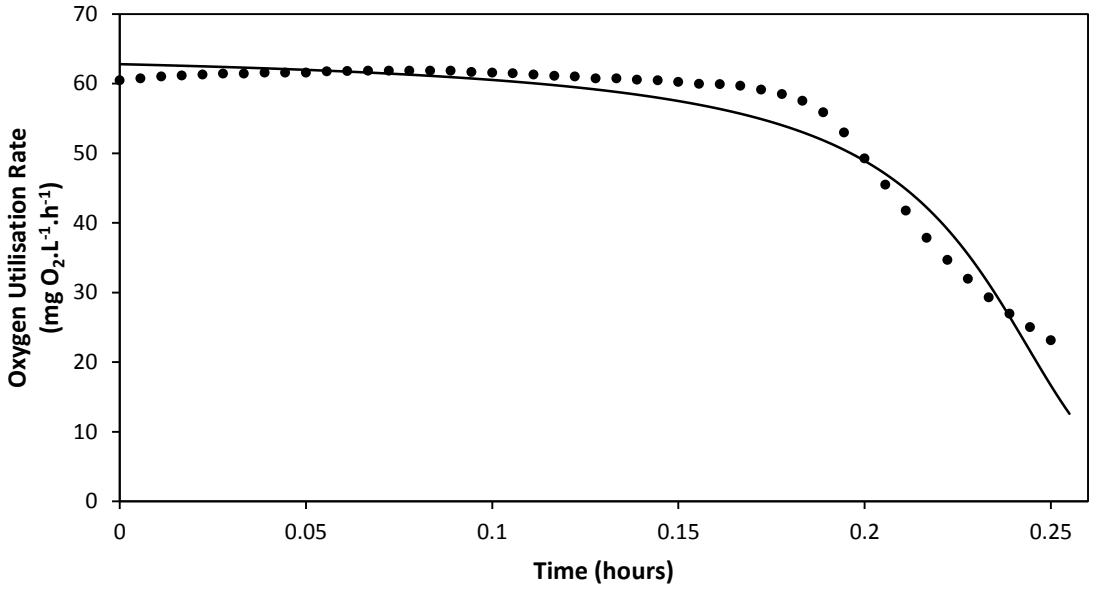

Figure 12.19. Regression of experimental data, zoomed view for 49.13 mg.L^{-1} COD. Regressed model, • Experimental data.

Table 12.11. Kinetic regression results 49.13 mg.L^{-1} COD.

μ_m (h^{-1})	K_S (mg.L^{-1})
0.0505 ± 0.004*	1.44 ± 0.058*

*95 %confidence Interval

Appendix H: Model MATLAB code

Primary function

```
clear
clc

global kd Y mu_max Ks  V_l C_Ss_0 fp m_i m_H2O m_sw rho_t...
       A B C rho_air Cp_air h_v T_amb MM_X Pb  C_Xh_0 Ks ...
       UA_air UA_earth  rh v_tr Cp_i Cp_o m_o Hsr0 Cc E_s ...
       boltz q_air_total T_air_in MM_W R v_a  Cp_t  T_i ...
       lambda_w lambda_s beta E_w q_i q_sw  VL KfCO2 KevCO2...
       m_o q_o Wall_SA Surf_SA  Y_40 Ks_40 mu_max_40 kd_40...
       C_NH4_0 C_CO3_0 n_air C_PO4_0  P_total NE pH_pred...
       T_r m_i m_sw  N_X Q_heat_cool delH_X delH_AA ...
       delH_HCO3 delH_H2O delH_NH4 m_H2O m_r Tref_f c ...
       gamma Tk k I pH aw lastTk Adh TotalIt test1 ...
       test2 C_H_0

SetupSpeciation ;

%%%notation%%%
%Readily biodegradable substrate - Ss
%Heterotrophic biomass - Xh
%Particulate organic matter - Xp
%Mass flow rate - m
%Mass of component present - M
%Molar flow rate - n
%Molar amount of component present - N
%Temperature - T
%Volumetric flow rate - q


%%%%%%%%%%%%%%%%%%%%%%%%%Input Variables%%%%%%%%%%%%%%%%%%%%%%%%%%%%%
height = 6.5;                               %m
T_i = 38.25;                                %˚C, Influent wastewater
T_amb = 25;                                 %˚C, Ambient air
T_air_in = T_amb;                           %˚C  Blower inlet
T_earth = 25;                               %˚C, Ground contact with MBR
%Thermophilic 29.3, 3.1    Mesophilic  12.9, 1.6
q_i = 12.9/3600;                            %m^3/s, Wastewater influent
q_sw = 1.6/3600;                            %m^3/s, Sludge wasting
q_air_FBDA1 = 7060/3600;                    %m^3/s, Blower 1
q_air_FBDA2 = 7060/3600;                    %m^3/s, Blower 2
q_air_mb = 2880/3600;                       %m^3/s, Membrane blower
P_FBDA1 = 224000;                           %W, Blower 1
P_FBDA2 = 224000;                           %W, Blower 2
P_mb = 61500;                               %W, Membrane blower
v_tr = 5;                                   %m/s, Wind velocity
Cc = 4.5;                                   %Cloud cover (1-10)
day = 180;                                  %Day of the year
rh = 83;                                    %relative humidity percentage
hf = 1;                                     %humidity factor
rainfall_mm = 0;                            %mm, rainfall, (L/m^2)
rainfall_time = 6;                          %h, hours of rainfall
T_r = 20;                                   %˚C, rain
int_time = 4000;                            %h
int_interval = 2000;                        %h

%%%%%%%%%%%%%%%%%%%%%%%%%%%%Reactor parameters%%%%%%%%%%%%%%%%%%%%%%%%%%
```

```
%MBR dimensions (volume assumed constant)
R = 14.1;                                   %m, radius
Surf_SA = 3.1416*(R^2);                     %m², top surface area
Wall_SA = 2*3.1416*R*height;                %m², wall surface area
V_l = Surf_SA*height;                       %m³, volume
VL = V_l*1000;                              %L

%%%%%%%%%%%%%%%%%%%%%%%%%%Kinetic Parameters%%%%%%%%%%%%%%%%%%%%%%%%
%Kinetic parameter
Tref = 298.15;                              %K, General reference
Tref_f = 40;                                %˚C, kinetics reference
T0 = 45;                                    %˚C, Initial MBR
%Reference kinetics
Y_40 = 0.62/1.42;                           %kg VSS/kg COD, Biological
Yield
Ks_40 = 0.895;                              %kg/m³ Half saturation constant
mu_max_40 = 0.0763/3600;                    %1/s maximum specific growth
rate
kd_40 = 0.009/3600;                         %1/s specific death rate
constant
%Biomass death split
fp = 0.15;                                  %fraction of cell debri

%%%%%%%%%%%%%%%%%%%%%%%%Energy balance Parameters%%%%%%%%%%%%%%%%%%%%%%%%
%Temperatures
T_i_K = T_i + 273.15;                       %K
%Species properties
rho_t = 1000;                               %kg/m³, Tank density
rho_air = 1.34;                             %kg/m³, Air density
Cp_t = 4170;                                %J/kg.K, Tank heat capacity
Cp_o = 4170;                                %J/kg.K, Outlet heat capacity
Cp_air = 1006;                              %J/kg.K, Air heat capacity
Cp_i = 4170;                                %J/kg.K, Inlet heat capacity
MM_AA = 60.05;                              %g/mol, Acetic acid
MM_X = 113;                                 %g/mol, Biomass
MM_W = 18;                                  %g/mol, Water
%Stream flow rates
q_r = (((Surf_SA*rainfall_mm)/1000)/rainfall_time)/3600;    %m³/s
rainfall
m_r = q_r*rho_t;                            %kg/s, Rainfall
m_i = q_i*rho_t;                            %kg/s, Inlet
m_sw = q_sw*rho_t;                          %kg/s, Sludge wasting
q_air_total = q_air_FBDA1 + q_air_FBDA2 + q_air_mb;  %m³/s, Blower
total
m_air_total = q_air_total*rho_air;          %kg/s, Blower total
m_H2O = 0.08*m_i;                           %kg/s, Evaporation initial
estimate
m_o = m_i + m_r - m_H2O - m_sw;             %kg/s, Outlet (const. mass)
q_o = m_o/rho_t;                            %m³/s, Outlet
P_total = P_FBDA1 + P_FBDA2 + P_mb;         %W, Blower total
NE = 0.6;                                   %Blower Efficiency

%%%%%%%%%%%%%%%%%%%%%%%%Energy Balance Variables%%%%%%%%%%%%%%%%%%%%%%%%
%Atmospheric Radiation
E_s = 0.97;                                 %Emissivity of surface
lambda_s = 0.03;                            %Water reflectivity
lambda_w = 0.3;                             %Wall reflectivity
beta = 0.85;                                %Atmospheric radiation factor
E_w = 0.7;                                  %Emissivity of wall
boltz = 5.6704*(10^-8);                     %W/m².K⁴, Boltzmann Constant
%Convection
```

```
h_v = (392*(Surf_SA^-0.05)*v_tr)/(3600*24);  %m/s, Transfer
coefficient
%Solar radiation
lat = 30;                                    %˚, Latitude
aa = 95.1892 - 0.359*lat - (8.4537*(10^-3))*(lat^2);
ba = -6.2484 + 1.6645*lat - (1.1648*(10^-2))*(lat^2);
ca = 1.4451 + (1.434*(10^-2))*lat - (1.745*(10^-4));
Hsr0 = (aa - ba*sin((2*pi*day +183)/366 + ca))*4.18;  %W/m2, clear sky
%Aeration
A = 16.3872;                                 %Antoine constant
B = 3885.70;                                 %Antoine constant
C = 230.170;                                 %Antoine constant
v_a = (exp(A - B./(T_amb + C)))*1000;    %Pa, VP water T_amb
R = 8.314;                                   %J/mol.K, Gas constant
%Conduction
Ko_air = 33.91;                              %J/m2.˚C.s, Air-tank surface
Ko_earth = 0.285;                            %J/m2.˚C.s, Earth-tank surface
x1 = 0.005;                                  %m, Wall thickness
k1 = 79;                                     %J/m.s.˚C, Tank wall
UA_air = (1/((x1/k1) + (1/Ko_air))).*Wall_SA;          %J/s, tank-air
UA_earth = (1/((x1/k1) + (1/Ko_earth))).*Surf_SA;      %J/s.K, tank-
earth
%Enthalpy of Formation
delH_X = -5*91000;                           %J/mol, Enthalpy biomass
delH_AA = -486000;                           %J/mol, Enthalpy acetate
delH_O2 = 0;                                 %J/mol, Enthalpy oxygen
delH_HCO3 = -692000;                         %J/mol, Enthalpy bicarbonate
delH_H2O = -286000;                          %J/mol, Enthalpy water
delH_NH4 = -133000;                          %J/mol, Enthalpy ammonium
delH_H = 0;                                  %J/mol, Enthalpy hydrogen ion

%%%%%%%%%%%%%%%%%%%%%%pH variables%%%%%%%%%%%%%%%%%%%%%%%%%%%%%%%%%%%%
P = 101325;                                  %Pa, Atmospheric
Pb = P/100000;                               %bar, Atmospheric
n_air = (q_air_total*P)/(R*T_i_K);           %mol/s, Blower air
KfCO2 = 10^(18.147+4060*(1/T_i_K - 1/298.15)/(2.303*8.314));  %Form.
Const.
KevCO2 = 0.08 ;                              % mol/L.bar.h, rate constant

%%%%%%%%%%%%%%%%%%%%%%Integration Initial Estimates%%%%%%%%%%%%%%%%%%%%
%Mass balance initial values
M_Xh_ss = 2.5*V_l;                           %kg VSS, Biomass
M_Xp_ss = 9*V_l;                             %kg VSS, Cell Debri
M_Ss_ss = 0.2*V_l;                           %kg COD, Substrate

%Temperature initial values
T_ss = T0;                                   %˚C, MBR temperature
%pH initial values
N_H_ss = 35*V_l;                             %mol, Hydrogen ion
N_NH4_ss = 80*V_l;                           %mol, Ammonium ion
N_CO3_ss = 15*V_l;                           %mol, Carbonate ion
N_PO4_ss = 10*V_l;                           %mol, Phosphate ion

%%%%%%%%%%%%%%%%%%%%%%MBR feed concentrations%%%%%%%%%%%%%%%%%%%%%%%%%%
C_Ss_0 = 17.8;                               %kg/m3, Feed concentration
C_Xh_0 = 0;                                  %kg/m3, Feed concentration
C_H_0 = ((C_Ss_0*1000)/64);                  %mol/m3, Feed concentration
C_NH4_0 = 0.23*C_H_0;                        %mol/m3, Feed concentration
C_CO3_0 = 2.28;                              %mol/m3, Feed concentration
C_PO4_0 = 0.026*C_H_0;                       %mol/m3, Feed concentration
```

```
%Storing Initial Values in a vector
C0 = [M_Ss_ss M_Xh_ss M_Xp_ss T_ss N_H_ss N_NH4_ss N_CO3_ss N_PO4_ss];

%Initialising Vectors
M_Ss_r = [];
M_Xh_r = [];
M_Xp_r = [];
M_VSS = [];
q_i_stor = [];
T_t_r = [];
N_H_r = [];
N_NH4_r = [];
N_Ac_r = [];
N_CO3_r = [];
N_PO4_r = [];
pH_pred_r = [];
ts = [];

%time of integration
t = 0;
t_l = int_time*3600;                        %s, Integration length, hour
to sec
t_i = t_l/int_interval;                     %time intervals
n = t_l./t_i;                               %number of integration steps

%Integration loop
for i = 1:n

options = odeset('RelTol',1e-6, 'AbsTol',1e-6);    %Integration
settings

[tau, y] = ode23t('Integrator_Integrated_Model_Final', [t, t + t_i],
C0);     %Integrator function

%Model Constraints for the mass balance
if y(end,1) < 0                             %M_Ss >= 0
    y(end,1) = 0;
end
if y(end,2) < 0                             %M_Xh >= 0
    y(end,2) = 0;
end
if y(end,3) < 0                             %M_Xp >= 0
    y(end,3) = 0;
end

%Storing integrated state variables, etc (Used for plotting)
q_i_stor = [q_i_stor q_i];
M_Ss_r = [M_Ss_r y(end,1)];
M_Xh_r = [M_Xh_r y(end,2)];
M_Xp_r = [M_Xp_r y(end,3)];
M_VSS = [M_VSS (y(end,2) + y(end,3))];
T_t_r = [T_t_r y(end,4)];
N_H_r = [N_H_r y(end,5)];
N_NH4_r = [N_NH4_r y(end,6)];
N_CO3_r = [N_CO3_r y(end,7)];
N_PO4_r = [N_PO4_r y(end,8)];
pH_pred_r = [pH_pred_r pH_pred];
ts = [ts t];
```

```
%%%%biomass viability wrt to pH%%%%%
if t > 300*3600                          %Waiting for integration
stability
if pH_pred < 6 && pH_pred >= 5.5
    N_X = 12.5*pH_pred + 25;
elseif pH_pred < 5.5 && pH_pred >= 5
    N_X = 175*pH_pred - 868.75;
elseif pH_pred < 5 && pH_pred >= 4.5
    N_X = 12.5*pH_pred - 56.25;
elseif pH_pred < 4.5
    N_X = 0;
else N_X = 100;
end
else
end

%%%%%displays loading perc%%%%
clc
Loading = round((t/t_l)*100)


t = t + t_i;                             %Next time step

C0 = y(end,:);

end

%Converting to concentrations for plotting
C_Ss = M_Ss_r/V_l;                      %kg/m3
C_Xh = M_Xh_r/V_l;                      %kg/m3
C_Xp = M_Xp_r/V_l;                      %kg/m3
C_VSS = M_VSS/V_l;                      %kg/m3

% Plotting Integration Results
th = ts/3600;                           %seconds to hours
figure(1)
plot(th, C_Ss, 'r')
xlabel('time,h')
ylabel('Cs_f, kg/m3')
figure(3)
plot(th, C_Xh, 'b')
xlabel('time,h')
ylabel('C_x(active), kg VSS/m3')
figure(4)
plot(th, C_VSS, 'b')
xlabel('time,h')
ylabel('C_V_S_S, kg/m3')
figure(5)
plot(th, pH_pred_r, 'b')
xlabel('time,h')
ylabel('pH')
figure(6)
plot(th, T_t_r, 'b')
xlabel('time,h')
ylabel('Temperature, C')
```

Integrand

```
function rhs = Integrator_Integrated_Model_Final(t, y)

global kd Y mu_max Ks  V_l C_Ss_0 fp m_i m_H2O m_sw rho_t...
          A B C rho_air Cp_air h_v T_amb MM_X Pb  C_Xh_0 Ks ...
          UA_air UA_earth  rh v_tr Cp_i Cp_o m_o Hsr0 Cc E_s ...
          boltz q_air_total T_air_in MM_W R v_a  Cp_t  T_i ...
          lambda_w lambda_s beta E_w q_i q_sw  VL KfCO2 KevCO2...
          m_o q_o Wall_SA Surf_SA  Y_40 Ks_40 mu_max_40 kd_40...
          C_NH4_0 C_CO3_0 n_air C_PO4_0  P_total NE pH_pred...
          T_r m_i m_sw  N_X Q_heat_cool delH_X delH_AA ...
          delH_HCO3 delH_H2O delH_NH4 m_H2O m_r Tref_f c ...
          gamma Tk k I pH aw lastTk Adh TotalIt test1 ...
          test2 C_H_0


%Restating state variables
M_Ss = y(1);                            %kg
M_Xh = y(2);                            %kg
M_Xp = y(3);                            %kg
T_t = y(4);                             %°C
N_H = y(5);                             %mol
N_NH4 = y(6);                           %mol
N_CO3 = y(7);                           %mol
N_PO4 = y(8);                           %mol

%calculating concentrations for Monod
C_Ss = M_Ss/V_l;                        %kg/m3
C_Xh = M_Xh/V_l;                        %kg/m3

%updating the flow rates
m_i = q_i*rho_t;                        %kg/s
m_sw = q_sw*rho_t;                      %kg/s
m_o = m_i + m_r - m_H2O - m_sw;         %kg/s
q_o = m_o/rho_t;                        %m3/s

%%%%%%%%%%%%%%%Kinetics and Mass Balance%%%%%%%%%%%%%%%%%%%%%%%%%%%%%%%%
%Estimating kinetics at temperature of operation
Y = Y_40*(0.981^(T_t - Tref_f));        %kg VSS/kg COD
fs = Y*1.42;                            %synthesis energy fraction
Ks = Ks_40*(1.011^(T_t - Tref_f));      %kg/m3
mu_max = mu_max_40*(1.069^(T_t - Tref_f));    %1/s
kd = kd_40*(1.07307^(T_t - Tref_f));    %1/s

%Substrate Utilisation of soluble COD
r_su = -(N_X/100)*(1./Y).*(mu_max.*C_Ss.*C_Xh)./(Ks + C_Ss); %kg
COD/m3.s
%Rate at which biomass is oxidised
r_er =  (1-fp)*kd.*C_Xh;                %kg VSS/m3.s
%Growth of biomass
r_g = (N_X/100)*(mu_max.*C_Ss.*C_Xh)./(Ks + C_Ss);
r_d = kd.*C_Xh;
r_x = r_g - r_d;                        %kg VSS/m3.s, Biomass net growth
r_p = fp*kd.*C_Xh;                      %kg VSS/m3.s, Inert organic
matter

%%%%%%%%%%%%%%%%%%%%%%%%%%Mass balance%%%%%%%%%%%%%%%%%%%%%%%%%%%%%%%%%%
%Mass Balance for soluble COD (kg/s)
```

```
rhs(1,1) = q_i.*C_Ss_0 - (q_sw./V_l).*M_Ss - (q_o./V_l).*M_Ss +
r_su*V_l;
%Mass Balance for biomass (kg/s)
rhs(2,1) = q_i.*C_Xh_0 -(q_sw/V_l)*M_Xh + r_x*V_l;
%Mass Balance for inert organic matter (kg/s)
rhs(3,1) = -(q_sw/V_l)*M_Xp + r_p*V_l;

%%%%%%%%%%%%%%%%%%%%%%%Energy Balance%%%%%%%%%%%%%%%%%%%%%%%%%%%%%%%%
%Convection from the surface of the tank (W)
Q_conv_surf = rho_air*Cp_air*Surf_SA*h_v*(T_t - T_amb);
%Convection from the tank walls (W)
Q_conv_wall = UA_air*(T_t - T_amb);
%Convection from the tank bottom (W)
Q_conv_bott = UA_earth*(T_t - T_amb);
%Overalll convection loss (W)
Q_conv = Q_conv_surf + Q_conv_wall + Q_conv_bott;

%Evaporation from the surface of the tank (W)
Q_evap = (((1.145*(10^6))*(1 - rh/100) + (6.86*(10^4))*(T_t -
T_amb))*(exp(0.0604*T_amb))*v_tr*(Surf_SA^0.95))*(4.1858/(24*3600));

%Power gain/loss from enthalpy difference between liquid streams(W)
Q_enth = (m_i*Cp_i*(T_i + 273.15) + (m_r*Cp_i*(T_r + 273.15)) -
(m_o+m_sw)*Cp_o*(T_t + 273.15));

%Power gain from solar radiation (W)
Q_rad_solar = (Hsr0.*(1-0.007*(Cc^2))*Surf_SA);
%Radiation loss from the surface of the tank to the atmosphere (W)
Q_rad_atmos_surf = E_s*boltz*((T_t + 273.15)^4)*Surf_SA - (1-
lambda_s)*beta*boltz*((T_amb+273.15)^4)*Surf_SA;
%Radiation loss from the tank wall to the atmosphere (W)
Q_rad_atmos_wall = E_w*boltz*((T_t + 273.15)^4)*Wall_SA - (1-
lambda_w)*beta*boltz*((T_amb+273.15)^4)*Wall_SA;
Q_rad_atmos = Q_rad_atmos_surf + Q_rad_atmos_wall;
Q_rad = Q_rad_solar - Q_rad_atmos;

%Sensible heat loss from aeration (W)
Q_as = q_air_total*rho_air*Cp_air*(T_t - T_air_in);
%Latent heat loss from aeration (W)
v_wa = (exp(A - B./(T_t + C)))*1000;  %Pa, Vapour pressure
H_lat = (2501-2.361*T_t)*1000;        %J/kg, Latent heat
Q_al =
((MM_W*q_air_total*(H_lat/1000))/(100*R))*((100*v_wa)/(T_t+273.15) -
(v_a*rh)/(T_amb+273.15));
Q_aer = Q_as + Q_al;

%Heat generated from exothermic reaction (W)
delHrxn_macro = ((3*delH_H2O + delH_X + ((5*(1-fs))/fs)*delH_HCO3 -
delH_NH4 - (5/(2*fs))*delH_AA)*1000)/MM_X;     %J/kg X produced
delHrxn_er = ((delH_NH4 + 5*delH_HCO3 - 3*delH_H2O ...
 - delH_X)*1000)/MM_X;                %J/kg X decayed
Q_macro = (delHrxn_macro)*r_g*V_l;    %W, Macrochemical Reaction
Q_er = (delHrxn_er)*r_er*V_l;         %W, Endogenous Respiration
Q_rxn = -(Q_macro + Q_er);            %W, Heat of Reaction

%Heat generated via blowers (W)
Q_com = P_total*(1 - NE);

%Energy Balance differential equation
```

```
rhs(4,1) =  (Q_enth - Q_aer - Q_evap + Q_rxn - Q_conv + Q_rad + Q_com
+ Q_heat_cool)/(rho_t*V_l*Cp_t);

%Amount of water evaporated from MBR (kg/s)
m_H2O = (Q_evap + Q_al)/(H_lat);

%%%%%%%%%%%%%%%%%%%%%%%%%%%%%%%%pH Balance%%%%%%%%%%%%%%%%%%%%%%%%%%%%%%%%
%Mass to moles
r_g_m = (r_g*1000*V_l)/113;          %mol Xh/s
r_er_m = (r_er*1000*V_l)/113;        %mol Xh/s
N_Ac = M_Ss*1000/64;                 %mol Ac- (64 g O2:mol Ac-)


%%%%%%%%%%%Calculation of pH using speciation%%%%%%%%%%%%%%%%%%%%%%%%%
%  H+   Na   K   Ca    Mg   NH4   Cl    Ac   Pr   CO3c   SO4    PO4
%  1    2    3   4     5    6     7     8    9    10     11     12
N = [N_H 0 0 0 0 N_NH4 0 N_Ac 0 N_CO3 0 N_PO4];
tot_m = N/VL ;                       %Ionic molalities
Tk = T_t + 273.15;
%call speciation subroutine
resid =
IonicSpeciation(Tk,tot_m,c,gamma,k,I,pH,aw,lastTk,Adh,TotalIt,test1,te
st2)
%Equilibrium partial pressure of CO2 (bar)
PCO2eq = KfCO2*c(1)*c(1)*c(19)*gamma(1)*gamma(1)*gamma(19);
%CO₂ partial pressure (bar)
PCO2 = (Pb*PCO2eq*KevCO2*VL)/(3600*n_air + Pb*KevCO2*VL);
%CO2 transfer rate (mol/s)
CO2rate = (((PCO2eq - PCO2)*KevCO2*VL)/3600);

%%%%differential molar balance for ions %%%%%%
%Hydrogen ion molar balance (mol/s)
rhs(5,1) = q_i.*C_H_0 - (q_sw./V_l).*N_H - (q_o./V_l).*N_H + ((15-
18*fs)/(2*fs))*r_g_m + 9*r_er_m + (-2)*CO2rate;
%Ammonium ion molar balance (mol/s)
rhs(6,1) = q_i.*C_NH4_0 - (q_sw./V_l).*N_NH4 - (q_o./V_l).*N_NH4 -
r_g_m  + r_er_m;
%Carbonate ion molar balance (mol/s)
rhs(7,1) = q_i.*C_CO3_0 - (q_sw./V_l).*N_CO3 - (q_o./V_l).*N_CO3 +
((5*(1-fs))/fs)*r_g_m + 5*r_er_m + (-1)*CO2rate;
%Phosphate ion molar balance (mol/s)
rhs(8,1) = q_i.*C_PO4_0 - (q_sw./V_l).*N_PO4 - (q_o./V_l).*N_PO4;

pH_pred = pH;                                   %Storing pH value

end
```

Setup speciation

```
H = 1  ;Na = 2  ;K = 3  ;Ca = 4  ;Mg = 5  ;NH4 = 6  ;Cl = 7  ;Ac = 8
;Pr = 9  ; CO3c = 10 ; SO4 = 11 ; PO4c = 12 ; % ionic components
HCO3 = 10  ;SO4 =  11 ;HPO4 = 12  ; OH =  13 ; H2CO3 = 14  ; CaCO3 = 15
;
MgCO3 = 16  ;CaHCO3 = 17  ;MgHCO3 = 18  ; CO3 = 19  ; H2PO4 = 20 ; MgPO4
= 21  ;
CaPO4 = 22   ;MgHPO4 = 23  ;CaHPO4 = 24  ;PO4 = 25  ;HAc = 26  ;HPr =
27 ;NH3 = 28  ;
CaSO4 = 29  ;MgSO4 = 30  ;CaOH = 31  ;MgOH = 32  ;NH4SO4 = 33  ;NaHPO4
= 34;
```

```
NaCO3 =  35 ;NaHCO3 =36   ;MgH2PO4 = 37  ;CaAc = 38  ;NaAc = 39  ;MgAc
= 40;
CaPr =  41 ;MgPr = 42  ;NaSO4 = 43  ;
gamma = zeros(1,43) ;
k = zeros(1,43) ;
c = zeros(1,43) ;
I= 1e-11;
pH=7.88;
act=1.111;
test1 = 2.12 ; test2 = 4.03 ;
Tk = 273.15 +40 ;
lastTk = -1.03 ;
aw=-0.99 ; conduct=4.4 ; Adh=0.511 ;
TotalIt = 1e-13 ;
Alkalinity = [] ; BufferCap = [] ;
```

Appendix I: Kinetic estimation MATLAB code

Primary function

```
clear
clc

global kd Y mu_max Ks fd Xh_0 Ro_exp T Ss_0

Ro_exp = [“Experimentally generated data”];

%%%%%%%%%%%%%%%%%%%%%%Regressing for Kinetics%%%%%%%%%%%%%%%%%%%%%%%%%%
x(1) = “Initial Estimate”;            %1/h
x(2) = “Initial Estimate;             %mg COD/L

Y = “predetermined from Dynamic Response Test”
Xh_0 = 2000.*1.42;                    %mg COD/L, biomass estimate
Ss_0 = 30.73;                         %mg COD/L, experimentally
determined

T = linspace(0, (2./3600).*(length(Ro_exp)-1), length(Ro_exp)); %h,
time

lb(1:2) = [0.0001, 0.8];              %Lower bounds
ub(1:2) = [0.1, 5];                   %Upper bounds

options = optimset('Algorithm','sqp','MaxIter', 1e20, 'TolX', 1e-20,
'MaxFunEvals', 1e20, 'TolFun', 1e-20, 'Display', 'final');

x = fmincon('min_func', x, [], [], [], [], lb, ub); %min. function

mu_max = x(1);                        %1/h, regressed parameter
Ks = x(2);                            %mg COD/L, regressed parameter

%%%%%%%%%%%%%%%%%%%%%%95% confidence interval%%%%%%%%%%%%%%%%%%%%%%%%
kd = 0.012;                           %1/h
So_0 = 0;                             %mg/L, Initial Oxygen consumption
fd = 0.125;

%Integration vector
C0 = [So_0 Xh_0 Ss_0];

%Initialising variables
So_r = [];
Ro_1 = [];
Xh_r = [];
Ss_r = [];

%Integration time
t = 0;
t_i = 2/3600;                         %h, Integration interval
n = length(T);                        %number of integration steps

%Integration loop
for i = 1:n

options = odeset('RelTol',1e-6, 'AbsTol',1e-6);       %Integration
settings
```

```
[tau, y] = ode45('integrator_kin', [t, t + t_i], C0); %Integrator
function


Ro_i = ((1-Y)/Y).*(mu_max.*y(end,3).*y(end,2))./(Ks + y(end,3));
So_i = y(end,1);
Ro_1 = [Ro_1 Ro_i];
So_r = [So_r So_i];
Xh_r = [Xh_r y(end,2)];
Ss_r = [Ss_r y(end,3)];

t = t + t_i;

C0 = y(end,:);

end

figure(2)
plot(T, Ro_1, 'g', T, Ro_exp, 'k')
ylabel('OUR, mg O2/(L.h)')
xlabel('time, h')

%Determining 95% confidence interval
x = [Ss_r' Xh_r'];

% the proposed functionality (fh is a handle to the function)
fh=@(b,x) ((1-Y)./Y).*(b(1).*x(:,1).*x(:,2))./(b(2) + x(:,1));
% guess values for parameters (beta0)
b0=[mu_max, Ks];
% determine best fit values for coefficient (bhat)
[bhat,resid,J,Sigma] =nlinfit(x,Ro_exp,fh,b0);

bhat(1)
bhat(2)

ci = nlparci(bhat,resid,'jacobian',J)
```

Minimisation function

```
function sse = sse(x)

global kd Y mu_max Ks fd Xh_0 Ro_exp T Ss_0

kd = 0.012;                             %1/h
So_0 = 0;                               %mg COD/L
fd = 0.125;

mu_max = x(1);                          %1/h
Ks = x(2);                              %mg COD/L

C0 = [So_0 Xh_0 Ss_0];

Ro_1 = [];

t = 0;
t_i = 2/3600;
n = length(T);
```

```
for i = 1:n                              %Integration Loop

options = odeset('RelTol',1e-6, 'AbsTol',1e-6);       %Integration
settings

[tau, y] = ode45('integrator_kin', [t, t + t_i], C0);  %Integrator
function

Ro_i = ((1-Y)/Y).*(mu_max.*y(end,3).*y(end,2))./(Ks + y(end,3));

Ro_1 = [Ro_1 Ro_i];

t = t + t_i;

C0 = y(end,:);

end


sse = sum((Ro_exp' - Ro_1).^2);      %sum squared error, function to
be minimised

end
```

Integrand

```
function rhs = integrator_kin(t, y)  %y0 = [So_0 Xh_0 Ss_0];

global kd Y mu_max Ks fd Xh_0

Xh = y(2);
Ss = y(3);

rhs(1,1) = ((1-Y)/Y).*(mu_max.*Ss.*Xh)./(Ks + Ss);
rhs(2,1) = (mu_max.*Ss.*Xh)./(Ks + Ss) - kd.*Xh;
rhs(3,1) = -(1/Y).*(mu_max.*Ss.*Xh)./(Ks + Ss);


end
```